The University of Southern Mississippi
The Aquila Digital Community

Dissertations

Summer 8-2012

Coastal Hurricane Damage Assessment via Wavelet Transform of Remotely Sensed Imagery

Ricky Carl Crowsey
University of Southern Mississippi

Follow this and additional works at: https://aquila.usm.edu/dissertations

Part of the Atmospheric Sciences Commons, Climate Commons, and the Meteorology Commons

Recommended Citation

Crowsey, Ricky Carl, "Coastal Hurricane Damage Assessment via Wavelet Transform of Remotely Sensed Imagery" (2012). *Dissertations*. 839.
https://aquila.usm.edu/dissertations/839

This Dissertation is brought to you for free and open access by The Aquila Digital Community. It has been accepted for inclusion in Dissertations by an authorized administrator of The Aquila Digital Community. For more information, please contact Joshua.Cromwell@usm.edu.

The University of Southern Mississippi

COASTAL HURRICANE DAMAGE ASSESSMENT

VIA WAVELET TRANSFORM OF REMOTELY SENSED IMAGERY

by

Ricky Carl Crowsey

Abstract of a Dissertation
Submitted to the Graduate School
of The University of Southern Mississippi
in Partial Fulfillment of the Requirements
for the Degree of Doctor of Philosophy

August 2012

ABSTRACT

COASTAL HURRICANE DAMAGE ASSESSMENT

VIA WAVELET TRANSFORM OF REMOTELY SENSED IMAGERY

by Ricky Carl Crowsey

August 2012

This dissertation uses post storm imagery processed using wavelet transforms to investigate the capability of wavelet transform-based methods to classify post storm damage of residential areas. Five level Haar, Meyer, Symlets, and Coiflets wavelet transform decompositions of the post storm imagery are inputs to damage classification models of post hurricane and tornado damage. Hurricanes Ike, Rita, Katrina, and Ivan are examined as are the 2011 Joplin and Tuscaloosa tornadoes.

Wavelet transform-based classification methods yielded varying classification accuracies for the four hurricanes examined, ranging from 67 percent to 89 percent classification accuracy for classification models informed by samples from the storms classified. Classification accuracies fall when the samples being classified are from a hurricane not informing the classification model, from 17 percent for Rita classified with an Ike-based model, 41 percent for Rita classified with an Ike-Katrina-based model, to 69 percent for Rita classified with an Ike-Katrina-Ivan-based model.

The variability within and poor classification accuracy of these models can be attributed to the large variations in the four hurricane events studied and the significant differences in impacted land cover for each of these storms.

Classification accuracies improved when these variations were limited via examination of residential areas impacted by 2011 Joplin and Tuscaloosa tornadoes. Damage classification models required as few as nineteen to as many as fifty nine wavelet coefficients to explain the variability in the hurricane storm data samples, and included all four wavelet functions studied. A similar analysis of the tornado damaged areas resulted in a damage classification model with only six wavelet coefficients, four Meyer-based, one Symlets-based and one Haar-based. Classification accuracies ranged from 96 percent for samples included in the model formation to 85 percent for samples not included in the model formation.

The damage classification accuracies found for tornado storms suggests this model is suitable for operational implementation. The damage classification accuracies found for the hurricane storms suggests further investigation into methods that will reduce the variability attributable to land cover and storm variability.

COPYRIGHT BY

RICKY CARL CROWSEY

2012

The University of Southern Mississippi

COASTAL HURRICANE DAMAGE ASSESSMENT

VIA WAVELET TRANSFORM OF REMOTELY SENSED IMAGERY

by

Ricky Carl Crowsey

A Dissertation
Submitted to the Graduate School
of The University of Southern Mississippi
in Partial Fulfillment of the Requirements
for the Degree of Doctor of Philosophy

Approved:

Carl A. Reese
Director

Bandana Kar

George T. Raber

David M. Cochran, Jr.

Gregory A. Carter

Susan A. Siltanen
Dean of the Graduate School

August 2012

DEDICATION

To Rhonda and Sarah, without your support, encouragement and love this wouldn’t have been possible.

ACKNOWLEDGMENTS

Thank you to the United States Geospatial Intelligence Foundation for their encouragement and scholarship supporting this research. Thanks to Brenda Jones who tirelessly responded to questions about post hurricane imagery and FEMA damage maps. Dr. Bandana Kar provided valuable and helpful GIS expertise, guidance and support throughout my research efforts to which I am grateful. Thanks to Dr. Carl ‘Andy’ Reese who taught me that in academia, as in the law, what’s important is what you can prove, not what you know. Thank you to those in the Geography and Geology Department at The University of Southern Mississippi who provided helpful feedback, encouragement and guidance as I focused on research questions outside the box, particularly my committee who continued to enthusiastically encourage and support my work in the face of more than the usual number of distractions.

TABLE OF CONTENTS

ABSTRACT ii

DEDICATION iv

ACKNOWLEDGMENTS v

LIST OF TABLES viii

LIST OF ILLUSTRATIONS ix

LIST OF ABBREVIATIONS xii

CHAPTER

I. INTRODUCTION 1

Research Objectives and Significance
Study Areas

II. LITERATURE REVIEW 9

III. METHODS 24

Problem Statement
Hypotheses
Selection of Hurricanes
Selection of Tornadoes
Storms Examined – Similarities, Differences, and Challenges
Differences and Similarities
Challenges
Data and Processing
Wavelet Transforms

IV. RESULTS AND DISCUSSION 71

Statistical Analysis
Hurricane Combination Discriminant Analysis Performance
Tornado Storm Damage Classification

V. CONCLUSIONS AND RECOMENDATIONS 118

Conclusions
Spectral Limitations
Recommendations

APPENDIXES 136

REFERENCES 250

LIST OF TABLES

Table

1. Hurricane characteristics for Ike, Rita, Katrina & Ivan 30

2. Hurricane combination DF classification accuracy 74

3. Hurricane Ike Wilk's Lambda analysis 79

4. Hurricane Ike discriminant analysis classification results 82

5. Hurricane Rita discriminant analysis classification results 89

6. Hurricane Katrina discriminant analysis classification results 94

7. Hurricane Ivan discriminant analysis classification results 98

8. Hurricane combinations discriminant function accuracies 101

9. Hurricanes Ike, Rita, and Katrina discriminant analysis classification results 103

10. Hurricanes Rita classified with Ike, Ike & Katrina, and Ike, Katrina, and Rita discriminant functions accuracies 109

11. Joplin tornado discriminant analysis classification results 113

12. Hurricane combinations classification accuracies sorted by percent cross-validated cases correctly classified 120

LIST OF ILLUSTRATIONS

Figure

1. Typical FEMA post hurricane landfall damage assessment map 3

2. Fourier transform of centered and offset block 11

3. Post-Katrina image low and high pass filtering 13

4. Meyer wavelet transform of centered and offset block..... 15

5. Best Tracks of Hurricanes Ike, Rita, Katrina and Ivan 28

6. Cat 1 winds areas affected for hurricanes Ike, Rita, Katrina and Ivan 34

7. Land cover distribution for category 1 winds areas affected 37

8. Ike sampling areas..... 43

9. Ike sample blocks filtered for residential filtering 45

10. Data processing/analysis block diagram..... 46

11. Katrina sampling areas 47

12. Katrina image sample blocks for residential filtering 48

13. Rita sampling areas 49

14. Rita catastrophic damage sampling area..... 50

15. Ivan sampling area 51

16. Ivan moderate and extreme sampling areas..... 52

17. Joplin tornado DF and test sampling areas 54

18. Tuscaloosa tornado sampling area..... 55

19. Test target image for illustrating wavelet transform operations 57

20. Five level Haar wavelet transform decomposition of test target 58

21. First level Haar diagonal detail image of test target 59

22. Wavelet mother functions Investigated 60

23. Five level Meyer wavelet transform decomposition of test target 61

24. First level Meyer diagonal detail image of test target 62

25. Five level Coiflets wavelet transform decomposition of test target 64

26. First level Coiflets diagonal detail image of test target 65

27. Five level Symlets wavelet transform decomposition of test target 67

28. First level Symlets diagonal detail image of test target 68

29. Ike canonical discriminant functions 1 and 2 plot 76

30. Ideal classification accuracy bar chart 83

31. Ike classification accuracy bar chart 84

32. Rita canonical discriminant functions 1 and 2 plot 86

33. Rita classification accuracy bar chart 90

34. Katrina canonical discriminant functions 1 and 2 plot 91

35. Katrina classification accuracy bar chart 95

36. Ivan canonical discriminant functions 1 and 2 plot 96

37. Ivan classification accuracy bar chart 99

38. Histogram of top 18 independent variables in discriminant functions 107

39. Joplin tornado canonical discriminant functions 1 and 2 plot 111

40. Joplin tornado classification accuracy bar chart 114

41. Joplin comparison area classification accuracy bar chart 116

42. Joplin tornado classification accuracy bar chart collapsed to two groups 125

43. Joplin tornado test area two group classification accuracy bar chart 126

44. Tuscaloosa tornado two group classification accuracy bar chart 127

LIST OF ABBREVIATIONS

ATLAS	Advanced Thermal and Land Applications Sensor
FEMA	Federal Emergency Management Agency
GIS	Geographic Information System
GLCM	Grey Level Cooccurrence Matrix
GPS	Global Positioning System
NGA	National Geospatial-Intelligence Agency
PDF	Portable Document Format
RADAR	Radio Detection and Ranging
SAR	Synthetic Aperture RADAR
USACE	United States Army Corps of Engineers
WT	Wavelet Transform
DF	Discriminant Function
DA	Discriminant Analysis

CHAPTER I

INTRODUCTION

Hurricanes on average make landfall on U.S. soil 1.2 (for El Niño years) to 2.1 times per year (for La Niña years) resulting in normalized mean damage of $7.7 (El Niño years) to $9.2 billion (La Niña years) per year (Pielke 2009). Since the 1990s tornadoes have impacted the U.S. approximately 1,000 times per year causing severe localized damage (Boruff et al. 2003).These disasters raise immediate questions about the extent and severity of damage, which can be answered by image-based damage assessments to aid in the response and recovery phases. Image based damage assessments can meet the response and recovery information needs only if they are collected soon after the event and over the correct location, contain sufficient geographic detail, and are evaluated by skilled interpreters (Clarke et al. 2007). The National Academy's Committee on Planning for Catastrophe has suggested that processes which can reduce the time between image acquisition and delivery to responders to twenty four to forty eight hours are of particular interest (Clarke et al. 2007).

Such a methodology with an analytical component can also be used by the United States Federal Courts, which according to the Daubert decision (Blackmun 1993) are require to consider several factors when evaluating the suitability of scientific evidence, including the scientific validity, acceptability and accuracy of the methodology, and acceptability of the methodology. An algorithmic methodology would more easily allow an analytical assessment of

offered damage assessment evidence against the Daubert falsifiability, and potential error rates factors.

FEMA currently produces image-based damage assessments (Figure 1 is an example from Hurricane Katrina) using skilled visual interpretations of post event imagery. These damage assessments are usually performed by interpreters of varying skills working with an evolving set of rules, requirements, and tools. For example, prior to the availability of now commonly available remote sensing, geographic information systems (GIS) and global positioning systems (GPS) tools, NOAA collected post Hurricane Camille imagery for simple visual damage extent evaluations. Hurricane Andrew in 1993, the World Trade Center attack in September 2001and Hurricane Katrina in August 2005 accelerated the collection and use of high resolution imagery use with these advanced tools for response, recovery and study of U.S. disasters. These three major events and others which followed have precipitated the routine use of remotely sensed imagery, GIS and GPS tools to assess the extent and severity of damage after most disasters.

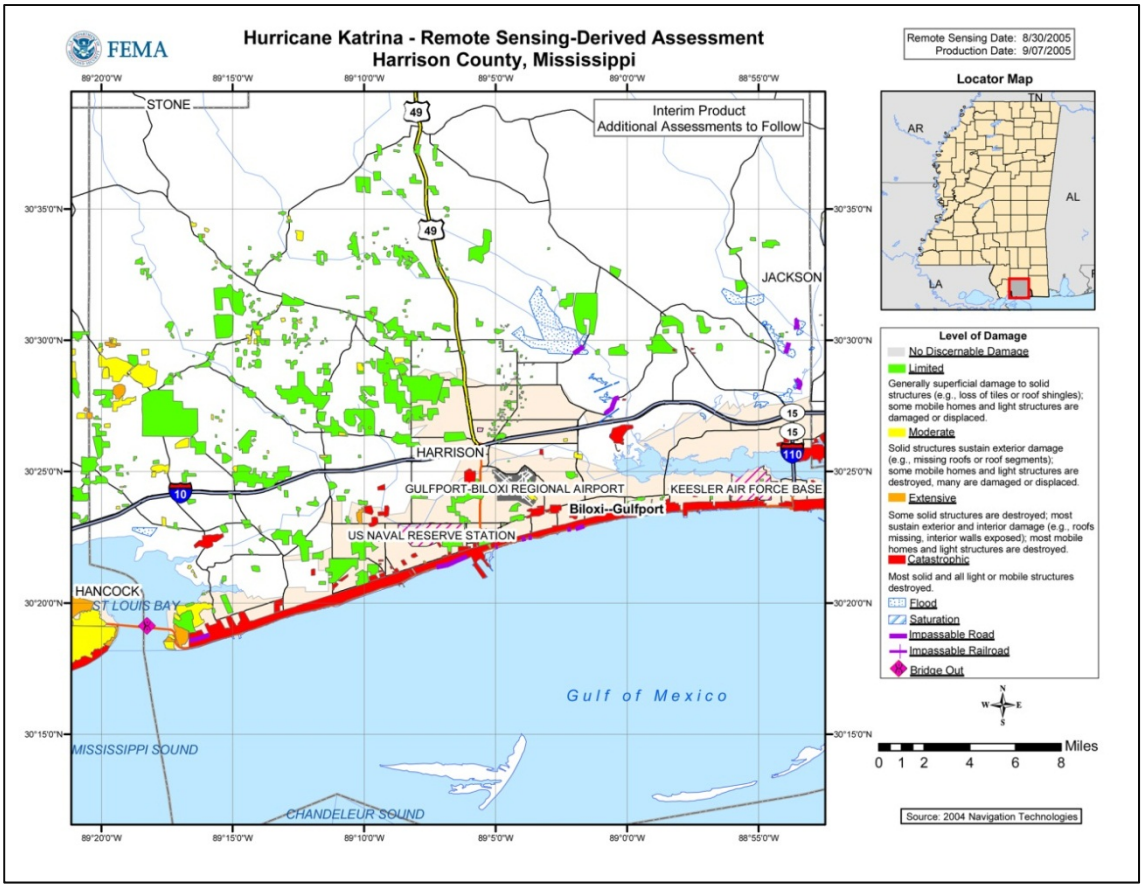

Figure 1. Typical FEMA distributed post hurricane landfall damage assessment map. This post hurricane Katrina Harrison County, Mississippi damage assessment is based on visual interpretation of overhead imagery acquired August 30, 2005 and was made available to the public shortly after the September 7, 2005 production date.

There are several potential issues with a visual interpretation based damage assessment approach. (1) Rapid response visual interpretation of overhead imagery requires significant human and infrastructure resources. Hurricanes typically cause wide areas of damage resulting in large volumes of imagery. Many skilled interpreters working concurrently on this large volume of imagery requires access to at least a workstation with image processing and geographic information system (GIS) software running on relatively robust, multi-

monitor workstations. (2) Damaging hurricanes make landfall at unpredictable times and with uncertain periodicity. This sporadic and unpredictable nature of hurricane landfall hinders the development and maintenance of a dedicated, trained, ongoing human capability for visual damage assessment. The result is that visual interpretation teams are pulled together at the last minute from where ever they are available. This ad hoc human capability makes it difficult for damage assessments to be performed consistently across large storms and from storm to storm. (3) Visual interpretation also poses the problem of validation. The lack of a set of uniformly implemented rule or guidelines applied for all events over time exacerbates the challenges of ad hoc commercial or government visual interpretation teams. This research focuses on developing an analytical damage assessment methodology building on wavelet transformation and change detection techniques to address the need for faster delivery of image-based damage assessments to responders.

The results found to date indicate that the proposed approach works as well as visual interpretation methods based on comparison with published FEMA damage assessments for hurricanes Ike, Rita, Katrina and Ivan. More promising results have been found with the same methodology when classifying tornado damaged areas. If implemented, this approach has the potential to reduce the time and resources required by visual interpretation. Additionally, this methodology is structured in a way that allows calibration and maintenance of performance metric improvements across and among damage events. This methodology also easily supports two of the Daubert scientific evidence

guidelines (falsifiability and error rates), which provides benefit for application in legal application uses.

This research focuses exclusively on damage classification from the spatial frequency content within immediate response imagery. Samples were collected from existing imagery collected by NOAA and the National Weather Service as part of their normal immediate response activities. This imagery is natural color RGB imagery. This limited the ability to explore the impacts of image enhancement methods that rely on spectral bands outside the visible range. While many of the areas impacted by hurricanes experienced flooding and storm surge damage, this research does not consider water damage, focusing on damage caused by hurricane and tornado wind fields.

Research Objectives and Significance

For the purposes of information extraction, the scattered and reflected radiation captured by overhead image sensors exists in five domains: spectral, spatial, temporal, geometrical, and polarization. Until recently, little attention has been paid to the spatial domain because of the difficulty in extracting this information quantitatively from remotely sensed imagery (Curran 2001). This research focuses on information extraction from the spatial domain of remotely sensed imagery using wavelet transformation.

The objective of this research is to examine the effectiveness and accuracy of wavelet transform informed post storm (hurricane and tornado) high resolution imagery for identification of storm damaged areas.

The specific questions addressed by this research include:

1. Can wavelet processed post storm overhead imagery identify areas of residential damage?
2. What wavelet mother functions and levels identify damage in remotely sensed imagery?
3. How accurately does a wavelet transform-based discriminant function classify damage in imagery not used to inform the discriminant function?

In addition to adding to the limited but growing body of geoscience in the area of information extraction from imagery using the spatial domain, two application areas may benefit from this research. FEMA currently uses visual interpretation for preliminary damage assessments and could realize improved effectiveness (speed of damage assessments to responders) and increased accuracy (consistent damage assessments based on methodologies that can be calibrated) if the wavelet transform-based methodology developed in this research substituted for visual interpretation. U.S. Courts may experience added value in confidence and speed of adjudication of disputes that hinge on a valid residential damage assessment method suitable for use in trials. U.S. Federal Courts look to the 1993 Daubert (Blackmun 1993) decision to assess the suitability of expert testimony for use in a legal proceeding. This decision offers guidelines for assessing scientific information (including geographic information). These guidelines are simpler to apply to quantitative methods, therefore the courts will find it easier to evaluate this algorithmic damage assessment

methodology compared to a subjective visual interpretation approach to determine damage.

Study Areas

This research focuses primarily on coastal areas of the U.S. Gulf of Mexico where high spatial resolution pre- and post-storm imagery is available. Hurricanes were selected for study where post storm high resolution imagery is available, a damage assessment was made and is available and where enough damage extent is documented to support analysis of adequate samples for each category of damage. Four hurricane events (from west to east, Ike (13 September 2008), Rita (24 September 2005), Katrina (29 August 2005), and Ivan (16 September 2004) shown in Figure 5) met all the selection constraints. Table 1 summarizes some of the characteristics of these storms.

Secondary areas of focus are the areas damaged by the April 2011 Tuscaloosa, Alabama and May 2011 Joplin, Missouri tornado outbreaks. The hurricane areas examined revealed significant variability within and among storms which appeared to be in part the cause of some of the variability in the classification results within and among hurricane areas. Tornadoes were added to the research in an effort to minimize these variations so as to emphasize the accuracy of the wavelet transform analysis on less variable samples, as might be expected with the smaller areas of tornadoes and the more homogenous damage seen in tornado damaged areas.

The remainder of this manuscript is organized as follows. Chapter II, Literature Review, examines the development of wavelet transform and spatial

information extraction from overhead imagery. Chapter III, Methods, documents the data used in this research, the methodology employed to examine the success of wavelet transform based spatial information extraction to assess post hurricane and post tornado damage, and Chapter IV, Results and Discussion, presents the statistical analysis employed and performance of damage classification models among the four studied hurricanes and two tornado events. Chapter V offers conclusions and recommendations for future research.

CHAPTER II

LITERATURE REVIEW

Wavelet transform analysis of signals, including imagery, is a natural extension of Fourier analysis. Fourier was the first to explain (Fourier 1878) that almost any periodic function can be described as the sum of a series of sines and cosines (commonly known as a Fourier series).

Fourier analysis works well for linear problems and problems with long periodic signals that are relatively stable. It is poorly suited for problems with short signals or signals that change suddenly or unpredictably. In this context, a signal can be whatever is recorded in one or more dimensions. An analog recording of a musical instrument and an image of a portion of the earth with a digital camera are examples of signals that are often processed using Fourier analysis. In fact, while Fourier analysis easily reveals the frequencies of periodic signals, it hides information about time (or space). In other words, a local characteristic of the signal becomes a global characteristic of the Fourier transform (see Figure 2). This means that the Fourier transform is vulnerable to errors in the signal or abrupt, brief signal changes (e.g., a sixty-fourth note in musical recording or a narrow road in an otherwise forest covered area in an image). The Fourier transform of music, for example, reveals what notes (frequencies) is played, but it cannot reveal when during the performance of the music that the notes are played (Richards and Jia 2006).

Figure 2 illustrates this shortcoming of Fourier transform-based analysis with two images and their respective Fourier transform. The top image is of a

black square centered within a white field. The Fourier transform to the right of this image shows that most of the frequencies in this image are near the origin, decreasing substantially with distance away from the origin along the vertical and horizontal axis. While this is a complete description of the frequencies within the image, there is no information about where these frequencies occur in the image. The lower image and Fourier transform pair illustrate this short-coming dramatically. The lower image contains the same size black square within the same field of white, except that the location of the square is in the lower right of the image. The Fourier transform of the lower image is the same as the Fourier transform of the upper image. While Fourier transform analysis reveals what frequencies are present in an image, it does not provide information about the location of the square within the image.

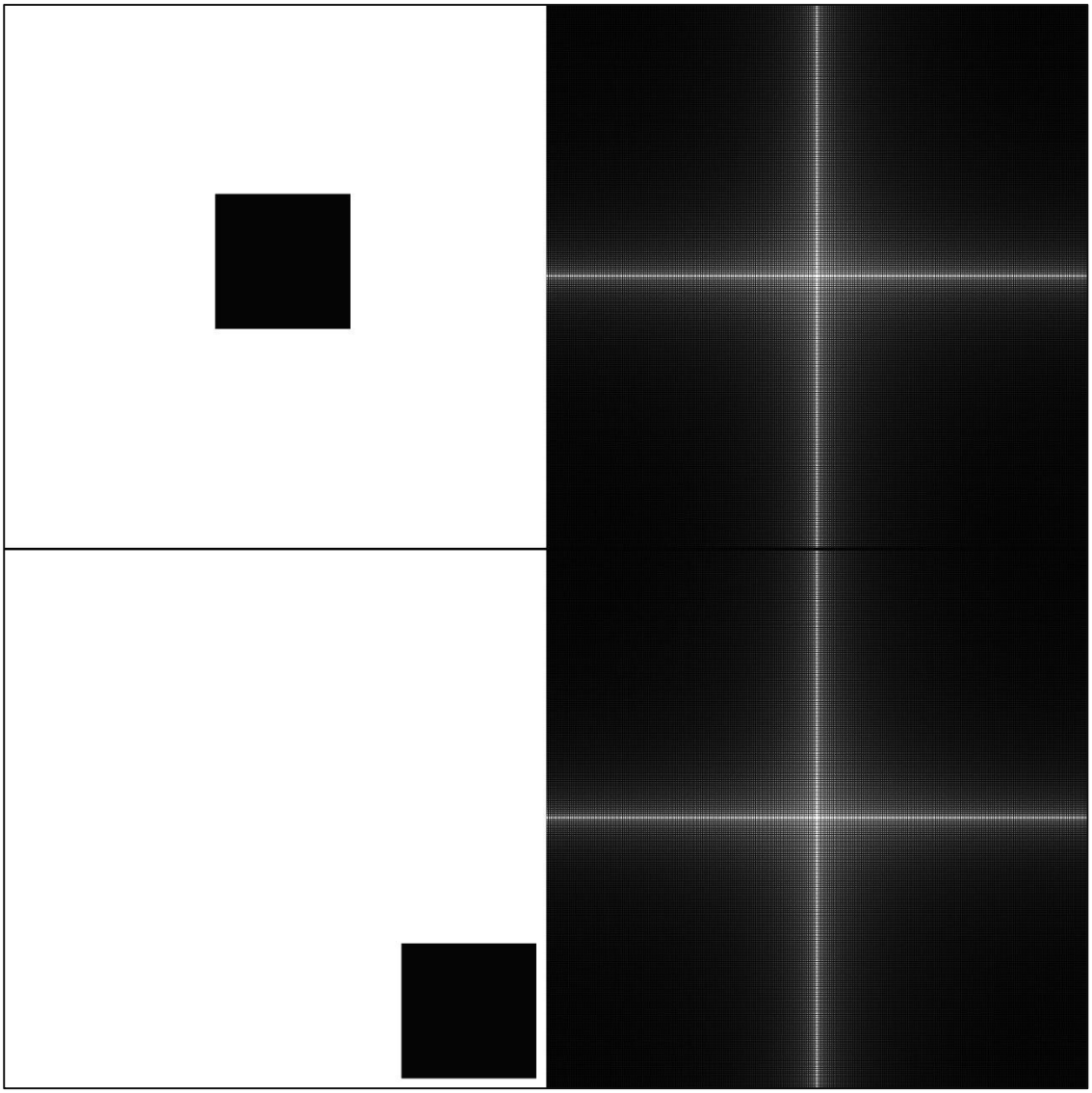

Figure 2. The Fourier transform (upper right) of an image of a centered black block (upper left) is the same as the Fourier transform (lower right) of an image of a black block in the lower right of an image. Fourier transforms reveal the frequencies in an image but not their location as illustrated above.

Several operations commonly used on remotely sensed imagery, or three dimensional (3-D) functions, rely on Fourier transforms and theory. For example, low and high pass filters commonly found in image processing software such as ERDAS Imagine (Smith, Pyden, and Cole 1995), rely on Fourier theory and transformation. To carry out a high pass filter operation (e.g., remove speckle

noise from an image), the image is transformed from space domain (often referred to as time domain for 2-D signals) to the frequency domain, then the high frequencies associated primarily with the noise are removed by multiplying the frequency function with a notch function to eliminate the high frequencies associated with the noise. The resultant frequency domain signal is Fourier transformed back to the space domain, with the result that the image no longer contains the high frequency noise (see Figure 3 for high pass and low pass Fourier filtering examples). A Fourier transformed and filtered image is also missing any high frequency target signal at the same frequencies as the noise. Low pass filtering is another common filter found in most image processing software and often relies on Fourier theory and operations (Jensen 1986). Figure 3 shows, at left, a post-Katrina aerial photo of the Port of Gulfport, at center, the aerial photo high pass filtered, and at right, the aerial photo low pass filtered. While this type of analysis and filtering has benefit, for example, in edge detection and noise reduction, the effects of Fourier-based filtering apply throughout an image without regard for location.

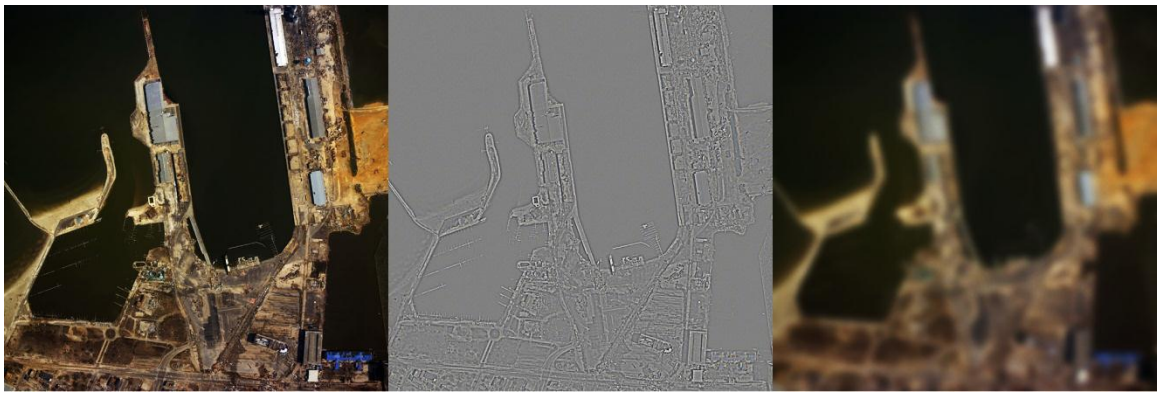

Figure 3. The post-Katrina image collected by NOAA of the Port of Gulfport (far left) has undergone high pass filtering (center) and low pass filtering (far right). High pass filters leave the high frequency (e.g., edges) while eliminating the low frequency information detail. Low pass filters leave the low frequency information while eliminating the high frequency information. These Fourier transform based filters operate on frequency information throughout the image.

A partial solution to this shortcoming of Fourier analysis is windowed Fourier analysis, first introduced by Gabor (1946). The windowed Fourier analysis is a special case of the short-time Fourier transform and begins with multiplying the signal by a Gaussian window then Fourier transforming the signal to determine the time-frequency content. While this approach moves closer to revealing both frequency and time (or space) information about the signal of interest, it does so at the expense of lost information at lower frequencies.

The solution to the lack of both frequency and location problems with Fourier transform-based analysis is wavelet transformation (WT). Wavelet transform analysis was developed at approximately the same time by several researchers in several locations and disciplines (Hubbard 1998). Wavelet transform analysis keeps the number of oscillations in a window constant and varies the width of the window instead of keeping the size of the window constant

and filing it with different frequencies as is done with windowed Fourier transform analysis.

Wavelet transform analysis extracts image information at different positions and scales. A continuous wavelet transform is essentially the convolution of a wavelet mother function with an image, or signal, at multiple scales (Watson 1999). The value of the convolution of the wavelet mother function with the image function indicates the interaction between the two functions. For example, if an overhead image is being examined for tree crowns a Mexican hat wavelet mother function can be convolved with the image. The resultant wavelet transformed image will show high values at the location of tree crowns in the image that best match the shape of the Mexican hat function (Falkowski et al. 2006).

Figure 4 shows a five-level discrete Meyer WT of the centered block and lower right located block images (previously Fourier transformed in Figure 2). On the left are the original images. The center figures show an image visualization of the five levels of discrete Meyer WT of each image on the left. On the right are enlarged views of the diagonal transform of the third level discrete Meyer WT. These are outlined in blue in the center figures. Unlike Fourier transforms, WT provides information about both the frequency and the location of features within the image (Watson 1999). Notice that the third level discrete Meyer WT of the centered block (shown top right) indicates the block's corners are centered in the image. The third level discrete Meyer WT of the lower right block image (shown lower right in Figure 4) illustrates WT's capability to provide information about the

location in addition to the frequency information. The corners of the lower right block are clearly indicated in the lower right of the WT.

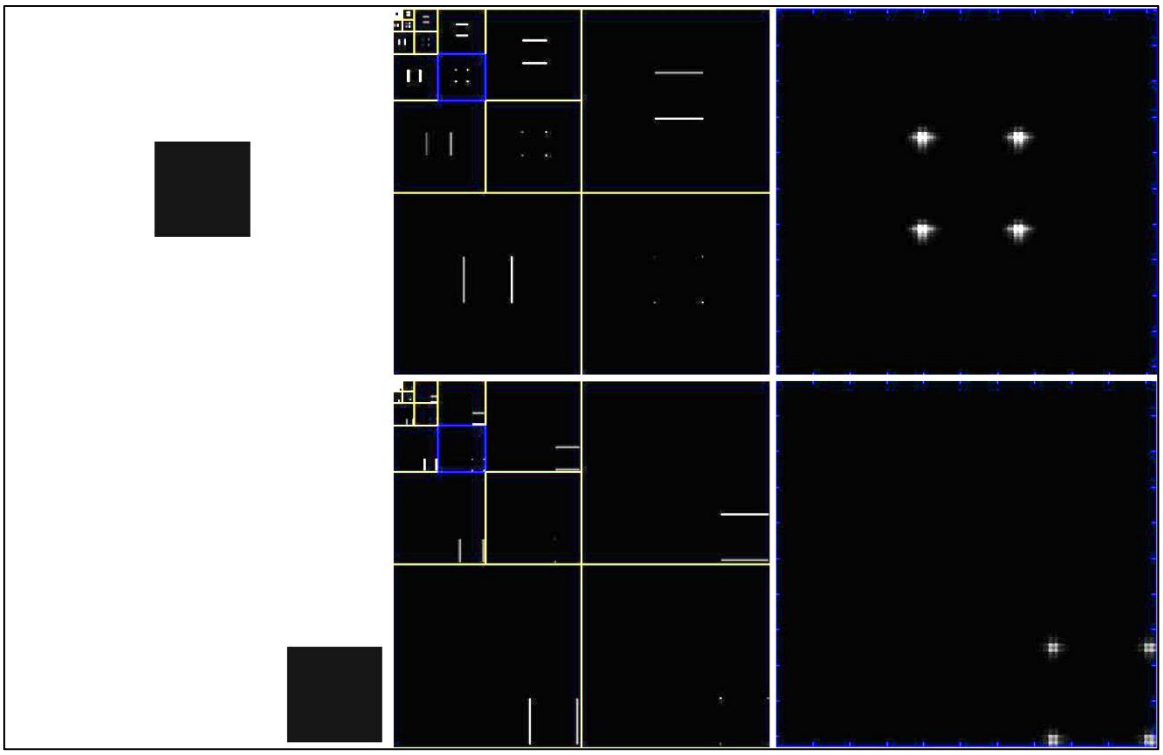

Figure 4. Original centered and lower right block images are in the left column above. Visualizations of a 5 level discrete Meyer WT are in the center column. The 3rd level discrete Meyer wavelet transform visualizations are in the right column. Where the Fourier transforms in Figure 2 do not provide location information of the frequency components in the image, wavelet transformation does provide this information.

Grossman and Morlet's collaborative wavelet transform work in the early 1980's (Hubbard 1998) is often cited (Rao and Bopardikar 1998) as one of the first in wavelet transformations. Their work was motivated by a desire to better understand seismic signals in both time and location. In addition to their work, original work with wavelets appeared at approximately the same time in several disciplines, by several different researchers working on different problems (e.g.,

Marcelja suggested that human vision could be best modeled using Gabor's scheme (Marcelja 1980), quadrature mirror filters and subband filtering developed by Croisier, Esteban, and Galand (1977) for use in electrical engineering discipline, Zweig's (1976) discovery of continuous wavelet transform while studying transduction of sound into nerve impulses in the ear). Morlet developed wavelets as a tool for oil prospecting as a geophysicist with the French oil company Elf-Aquitaine. A typical approach for oil prospecting in the 1960's was to send vibrations underground and analyze the echoes. This methodology indicates how deep and how thick various underground layers are. After developing an empirical method for decomposing and reconstructing a signal, he met with Grossman who worked in phase space quantum mechanics, which intensively uses Fourier transform analysis. Working together Grossman and Morlet validated the oil exploration-based empirical work begun by Morlet (Hubbard 1998).

Mallat (1989) first suggested wavelet transformation for imagery texture analysis. Ingrid Debauchies' "Ten Lectures on Wavelets" (Daubechies 1992) is widely regarded as the foundational paper on wavelet transformation analysis (Hubbard 1998). A novel set of invariant Fourier-Wavelet descriptors for recognizing complex patterns (e.g., Chinese characters) is described by Chen and Bui (1999).

Curran (2001) is one of the first to emphasize the paucity of exploitation of spatial content of remotely sensed imagery. He suggested that this is likely due to how well the human visual system processes spatial image content combined

with the difficulty until recently of extracting quantitative spatial content from remotely sensed imagery.

Myint (2001) began looking at wavelet analysis for classification of urban environments using high resolution imagery with his dissertation. The subsequent 2002 paper (Myint, Lam, and Tyler 2002) evaluated four different wavelet procedures for spatial feature discrimination in urban areas, finding that the additional levels of combination improves classification accuracy. In a 2003 paper (Myint 2003) examining fractal approaches (isarithm, triangular prism and variogram) in texture analysis and classification of remotely sensed data, 2.5 meter spatial resolution ATLAS (Advanced Thermal and Land Applications Sensor) data was used to compare fractal, spatial autocorrelation and spatial co-occurrence approaches (Myint, Lam, and Tyler 2004). Myint, Lam, and Tyler (2002) found that wavelet transformation increases classification accuracy. In 2006 Myint (2006) offered a new framework for multiscale analysis and classification to identify urban classes. In this manuscript he confirmed that traditional approaches are poor for urban mapping from high resolution imagery and that wavelet approaches are more accurate. Most recently, Myint (2010) authored further wavelet research based on IKONOS imagery looking at window size variation, finding that the intrinsic scale of the most complex feature among the classes might be the optimal local window size for best accuracy. Overall, Myint has the longest and broadest body of work examining wavelet transformation approaches focused on urban classification from high resolution imagery.

Though not as recent or long standing, others have looked at classification of urban environments. Zhou's (2006) Ph.D. dissertation examines the detection of socioeconomic conditions of urban neighborhoods through wavelet analysis of remotely sensed imagery, finding that wavelet analysis in combination with artificial neural networks support detection of socioeconomic conditions of urban neighborhoods.

Ecology has seen the longest interest in the use of wavelet transformation. Dale and Mah (1998) examined the use of wavelets for spatial pattern analysis in ecology, finding several advantages to wavelet analysis as compared to paired quadrat or blocked quadrat variance calculations. Mi and colleagues (Mi et al. 2005) examined Mexican hat and Morlet wavelets for detection of ecological patterns, finding the Morlet wavelet transform providing better scale detection and location than the Mexican Hat wavelet transform. Keitt and Urban (2005) found that wavelet transform and wavelet-coefficient regression performs well in characterizing scale-specific patterns in ecological data. Keitt and Fischer (2006) examine wavelet transformation to partition patterns of synchrony and compensation by time scale, finding that wavelet transforms provide insight into time scales to facilitate understanding ecological community patterns.

Wavelet analysis was successfully used by Strand (Strand et al. 2006) as a repeatable background invariant technique for quantifying ecological patterns. Falkowski (Falkowski et al. 2006) demonstrated the ability to automatically estimate location, height, and crown diameter of individual trees within a mixed conifer open canopy stand using wavelet-based analysis. Forest stand density

estimation from high resolution imagery using wavelet texture measures is demonstrated by Verbeke (Verbeke, Van Coillie, and De Wulf 2006), where they use wavelet analysis to characterize local texture using wavelet coefficient statistics and found significantly better performance compared to a local maximum-based method. Chou, Chen, and Yeh (2007) demonstrate crop identification using wavelet analysis combined with weighted Bayesian distance based on crop texture and leaf features.

Zhu and Yang (1998) describe their wavelet-based approach to characterize different scales of texture, finding that texture classifications for twenty five types are accomplished with few errors when using wavelet transforms. Wang and Liu (1999) propose multiresolution Markov Random Field modeling to describe textures and retain highpass information normally lost with other approaches. Acharyya and Kundu (2001) describe a successful application of automated M-band wavelets for identifying defects in textiles. Ruiz, Fdez-Sarria, and Recio (2004) analyze and compare grey level coocurrence matrix (GLCM), energy filters and edgeness, Gabor filters and wavelet transforms for classifying textures in Mediterranean forested areas and growing urban areas, finding no approach works best in all the applications they studied. Arivazhagan and Ganesan (2003b) found that discrete wavelet transformation works better than other approaches and is expected to perform well in computer vision and pattern recognition applications. Texture classification using wavelet analysis is addressed by several researchers in the early 2000s (e.g., Arivazhagan and Ganesan 2003a, Ruiz et al. 2004, and Kim and Kang 2007).

Three additional general areas seeing significant use of wavelet analysis include target, pattern, signal detection and recognition, image fusion, and miscellaneous applications.

He's (1996) dissertation focused on pattern recognition and image processing of infrared astronomical satellite images, including wavelet analysis. Bailey and colleagues (Bailey et al. 1998) found plausible results on real data when using wavelet analysis to detect transient feature in noisy sound recordings. Tang and Stewart (2000) employed a multichannel texture classification algorithm based on wavelet and Fourier transforms for optical and sidescan sonar image classification. They found that wavelet transform methods perform more accurate feature extraction on seafloor data but less accurate results on Arctic ice canopy data. Li (2004) shows improvement of spectral unmixing using discrete wavelet transform analysis of hyperspectral signals. Arivazhagan and Ganesan (2004) presented an algorithm for detecting specific targets within noise based on comparison of wavelet coocurrence features. Tello, Lopez-Martinez, and Mallorqui (2005) demonstrate a wavelet transform-based ship detection algorithm from synthetic aperture RADAR (SAR) data, finding that performance on both simulated and real SAR images confirmed the robustness of this method. Elsayed (2007) used wavelet analysis to detect the dispersion and groupings of waves during a mistral event (cold northerly wind that descends the Rhone Valley). Chen and Wang (2009) show with their transform correlator experiments the potential of edge extraction using wavelet analysis as part of a successful approach to detect small targets and targets in

clutter scene. Ghazvini et al. (2009) demonstrate a method to classify normal and defective tiles using wavelet analysis and artificial neural networks, showing a 90 percent validity for the cases tested. Pokhriyal and Lehri (2010) combine wavelet analysis and pseudo Zernike moments for fingerprint comparison and verification, finding this approach better than others and best results are achieved when the Symmlet wavelet of eighth order is used.

One of the first publications describing the application of spatial frequency signatures to image matching was by Dunlop et al. (1989). Prior to this image matching was accomplished using correlation or feature matching, both of which have problems with certain image content types. Ulfarsson, Benediktsson, and Sveinsson (2003) found success using wavelet transform methods for data fusion and feature extraction. Hong and Zhang (2004) examine the effects of different types of wavelets on image fusion, finding the best results when wavelet transformation and IHS (intensity hue saturation) transformation are used together. The wavelet-based image fusion tutorial by Pajares and de la Cruz (2004) provides a clear wavelet transform tutorial and earth observation and medical imaging data fusion examples.

In addition to the coherent streams of research featuring wavelet analysis, there has been a potpourri of applications that are interesting and potentially significant but do not yet have a well-developed body of research. Huang and Wechsler (1999) used wavelet packet for eye detection and radial basis functions for classification. Paul Arellano's (2003) geoinformatics Master of Science thesis focuses on a wavelet-based approach to detecting and removing clouds and their

shadows. Bruce, Mathur, and Byrd (2006) examined denoising followed by feature extraction methods, comparing Fourier and wavelet methods, finding that noise affected wavelet analysis, but that in spite of that the wavelet based analysis performed significantly better for discriminating vegetative classes. Cai's (2007) dissertation focused on wavelet based transformation for hiding and recovering information from image data and identifying unique features in genetic microarray data. Osicka's (2008) dissertation examines analysis and classification of lung nodules on CT scans using wavelet based methodologies.

This research is significantly informed by Myint's wavelet transform-based classification work, beginning with his dissertation (Myint 2001) research focused on classification of urban environments using wavelet analysis of high resolution multispectral image data. His evaluation (Myint 2010) of Shannon's index, energy and log energy texture coefficients showed significantly better performance by the energy texture measure, informing the use of the energy texture measure in combination with wavelet transforms for this research. Myint's examination of local window size with wavelet transformed high resolution imagery (Myint 2010) showed high accuracy with square windows of 63 and 95 meters on a side for residential areas, however he found considerable variability based on class, pointing out that there appears to be no ideal window for all applications (Myint 2010). He observed that overall accuracy decreases with increasing window sizes. However, this is countered by the potential misclassification of small regions of classes that can be lost in large window sizes. The best window size computationally is the smallest window that produces the highest accuracy

(Hodgson 1998). This research focuses on hurricane and tornado damage of residential areas. The choice of 78 x 78 meter image subsample sizes was informed by Myint's work on optimal residential classification performance and the utility of maximizing the information extraction from dyadic deconstruction of the wavelet transform process. A 78 x 78 meter window falls between the two most accurate residential windows examined by Myint and has the added benefit of supporting five level wavelet decompositions.

CHAPTER III

METHODS

Problem statement

Can wavelet transform-based methodology identify storm (hurricane or tornado) damage to residential areas? Post event damage assessment is currently accomplished by acquisition and visual interpretation of remotely sensed imagery. Post hurricane landfall damage assessments have been performed and released by FEMA a few days to more than a week after imagery acquisition (e.g., Figure 1 is a FEMA damage assessment of Harrison County, Mississippi where the imagery was acquired on August 30, 2005 and the production is dated September 7, 2005). This delay, in part, is due to the process of visual interpretation of overhead imagery. Visual interpretation by different interpreters can produce unacceptable variability in damage assessments. Ad hoc visual interpretation of imagery to determine damage is difficult to reliably calibrate, making it difficult to systematically apply corrections and assess their impact on classification accuracy.

Hypotheses

The specific questions and associated hypotheses addressed include:

- Question 1 - Can wavelet processed post storm (hurricane or tornado) overhead imagery identify areas of residential damage?
- Null Hypothesis 1 - Wavelet transform processed post event imagery does not discriminate damage conditions (FEMA categories for hurricanes, F

level for tornadoes) at the 95 percent confidence level. All statistical tests are performed at the 95 percent confidence level.

- Question 2 – What wavelet mother functions and levels identify damage in remotely sensed imagery?
- Null Hypothesis 2a - Damage condition is not discriminated when informed by Haar, Myer, Coiflets, or Symlets wavelet function based classification.
- Null Hypothesis 2b - Damage condition is not discriminated when informed by first, second, third, fourth, or fifth level wavelet transform decompositions.
- Question 3 - How accurately does a wavelet transform-based discriminant function classify damage in imagery not used to inform the discriminant function
- Null Hypothesis 3 - Damage condition is not discriminated in events not sampled to inform the discriminant function (e.g., hurricane Rita image samples are not discriminated with respect to damage level when evaluated with a discriminant function informed by hurricane Ike image samples).

Selection of Hurricanes

Three criteria guided the selection of hurricanes for study. First, a Gulf Coast land falling hurricane must have caused enough damage to coastal, residential areas so that at fifty to one hundred samples from each category can be extracted from the imagery. Congalton suggested that for large areas or more than 12 categories the minimum number of samples per category should be

increased from a good rule of thumb minimum of fifty to 75-100 samples per category (Congalton 1991). Second, high resolution overhead imagery must have been collected and be available from civil or commercial sources. Third, a remote sensing based damage assessment must have been performed and this assessment must be currently available.

Selection of Tornadoes

Two well documented tornadoes were selected in an effort to eliminate the variability found within and between hurricane data sets, allowing an examination of wavelet transform classification apart from hurricane variability. The same three criteria were used to select tornadoes for analysis as was applied to hurricanes. The tornado must have caused enough damage so that approximately fifty or more image samples of damaged area could be extracted from the imagery. A damage assessment must have been performed and be available. High resolution imagery of the damaged areas must be publically available. The April 2011 Tuscaloosa and May 2011 Joplin tornadoes were flown by NOAA NGS and high resolution imagery similar to Hurricanes Ike, Rita, Katrina, and Ivan was posted for emergency response and research use shortly after the storms. While much smaller than hurricanes, these two tornadoes were unusually large, large enough to support collecting enough samples to meet Congalton's sample size metric. Damage assessments were available from the National Weather Service and the University of Alabama's Center for Advanced Public Safety. These two tornadoes also offered the benefit of their imagery

being collected and archived by the same organization (NOAA NGS) as for the hurricane imagery.

Storms Examined - Similarities, Differences, and Challenges

The research focus began with hurricanes on coastal areas of the U.S. Gulf of Mexico by acquiring the National Hurricane Center's historical storm track data set (Franklin 2011) and selecting all Gulf of Mexico hurricanes making U.S. landfall from 1993 to 2010. There were 134 Atlantic basin hurricanes during this period. To qualify as a candidate for examination in this research, three factors were used to guide hurricane selection. First, high resolution (approximately 0.3 meter [1 foot] spatial resolution), post storm overhead imagery must have been collected and be currently available from civil or commercial sources. Second, FEMA must have performed a remote sensing-based damage assessment and this assessment must be currently available. Third, the hurricane must have caused enough residential damage so that approximately 100 or more subsamples can be obtained from the high resolution overhead imagery. Four hurricane events met all three constraints (high resolution imagery available, FEMA damage assessment available, substantial coastal damage).

The four hurricanes meeting these constraints are, from west to east, Ike (9/13/2008), Rita (9/24/2005), Katrina (8/29/2005), and Ivan (9/16/2004). Their paths in the Gulf of Mexico around the time of landfall are shown in Figure 5.

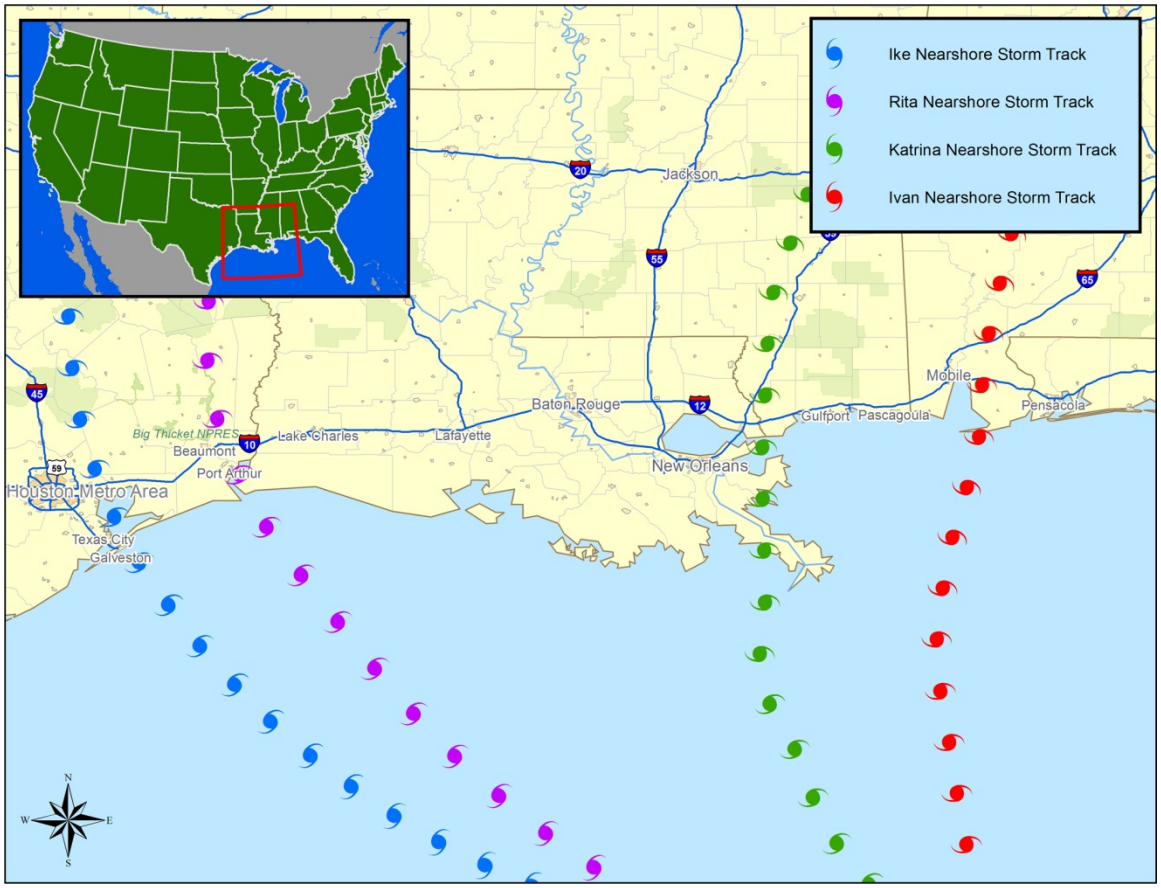

Figure 5. National Hurricane Center best track of Hurricanes Ike, Rita, Katrina and Ivan.

Table 1 summarizes some of the characteristics of the hurricanes studied. The official National Hurricane Center determined Saffir-Simpson category for these storms belies the significant variations among these hurricanes. Hurricane Katrina's category 1 or greater winds covered an area more than ten times larger than Rita and approximately twice the size Ike and Ivan. The maximum gust winds recorded or calculated from damage shows a similar variability with Ike's strongest winds of 49.2 m/s (110 mph) at the low end and Rita and Katrina at the high end with winds of 77.3 m/s (173 mph). Embedded tornado frequency illustrates another facet of the variety among these hurricanes with none

recorded for Ike and 117 recorded for Ivan. Figure 7 shows the percent land cover for all the major National Land Cover Data major categories. Table 1 summarizes this by listing the predominant landscapes for each storm area and the percent of the total area that is a developed class. Ike impacted a large area with the greatest percentage of developed land while Rita impacted a small area that was mostly open water and wetlands (94.4percent) with only 2.8 percent of land falling in a developed class.

One underlying assumption of this research is that wavelet transform analysis can identify the expected addition high frequency content of residential images that have experienced storm damage. Storm damage to residential areas generally causes relatively low frequency content (e.g., a single home, a few trees and small garden sheds) to be transformed into higher frequency content (e.g., roofs are changed from a single roof structure to smaller debris spread throughout the property). Examining other land cover types along with residential properties injects potential errors into the discriminant analysis classification. Large open areas, open water and wide roads can appear to be similar in spatial frequency content as lots that have had all or most of their buildings and vegetation blown away. This same phenomena was the impetus for eliminating image samples with more than 50 percent, by visual inspection, of land covers other than residential area.

Table 1

Hurricane characteristics for Ike, Rita, Katrina and Ivan

	Ike	**Rita**	**Katrina**	**Ivan**
Landfall Date (YYYYMMDD)	20080913	20050924	20050829	20040916
Landfall location	Galveston Island, TX	TX/LA border	MS/LA border	Gulf Shores, AL
Saffir-Simpson Category per NWS	2	3	3	3
Maximum recorded sustained winds at landfall (m/s)	49.2	51.4	56.8	58.1
Maximum gust winds at landfall (m/s)	49.2	77.3	77.3	72.0
Central pressure near landfall (mbars)	935	895	902	910
Radius of hurricane winds at landfall (km)	204	138	167	167
Radius of tropical storm winds at landfall (km)	444	333	370	417
Storm surge height (m)	> 3.0	> 4.3	>6.4	>3.7
Storm surge extent (km)	>214	>97	>161	>105
Embedded tornadoes per NWS	0	21	43	117
Area of category 1 or greater winds (square km)	22,647	2,857	36,143	16,825
Predominant landscape (2006 NLCD) of category 1 or greater winds area	Shrub/scrub and wetlands	Wetlands and open water	Forest, shrub/scrub and wetlands	Forest and shrub/scrub
Land cover percent developed class of category 1 or greater winds area (percent)	20.8	2.8	7.8	10.3

Hurricane Ike

Hurricane Ike made landfall on September 13, 2008 over Galveston, Texas with maximum sustained winds of approximately 49.2 m/s (strong Category 2) and a central pressure of 935 mbar. Hurricane force winds (greater than 32.6 m/s) extended outward approximately 193 km from the center at the

time of landfall. Tropical storm winds (greater than 17.4 m/s) extended outward approximately 443 km from the center at the time of landfall. A 3 meter storm surge accompanying the storm extended approximately 214 km along the coast. The National Weather Service reported no imbedded tornadoes associated with Hurricane Ike. Tens of thousands of homes were severely damaged or destroyed by wind or surge. For example, only 14 of the 3,400 homes in Bridge City, Texas are habitable after the storm (DeBlasio 2008).

Hurricane Rita

Hurricane Rita made landfall on September 24, 2005 near the Texas/Louisiana border with sustained winds of approximately 51.4 m/s (weak Category 3), with reports of winds up to 77.3 m/s. Hurricane force winds (greater than 32.6 m/s) extended outward over 137 km from center at landfall (Knabb, Brown, and Rhome 2006), with tropical storm winds (greater than 17.4 m/s) extending outward over 322 km from the center. The lowest recorded central pressure was 895 mbars. Landfall was accompanied by a 4.3 m storm surge that extended for greater than 97 km along the coast. The National Weather Service reported 21 embedded tornadoes within Rita. The Louisiana Recovery Authority reported 23,636 homes in Louisiana and Texas destroyed from Rita's winds and surge (Kurth and Burckel 2006).

Hurricane Katrina

Hurricane Katrina made landfall on August 29, 2005 near the Mississippi/Louisiana border with officially recorded sustained winds of approximately 56.8 m/s (Category 3), with reports of winds up to 77.3 m/s.

Hurricane force winds extended outward over 161 km from the center at the time of landfall (Knabb, Rhome, and Brown 2005, Updated 2006). Tropical storm winds (greater than 17.4 m/s) extended outward over 370 km from the center. The lowest recorded pressure was 902 mbars. Landfall was accompanied by greater than 6.4 m surge extending over 161 km of coast. The National Weather Service reported forty three embedded tornadoes within Katrina. FEMA reported over 140,000 households damaged in just the three coastal Mississippi counties, affecting over 370,000 people (Richard 2005).

Hurricane Ivan

Hurricane Ivan made its first landfall on September 16, 2004 near Gulf Shores, Alabama with maximum sustained winds of 58.1 m/s (strong Category 3), with reports of winds up to 72.0 m/s. Hurricane force winds (greater than 32.6 m/s) extended outward over 161 km from the center at the time of landfall. Tropical storm force winds (greater than 17.4 m/s) extended outward from the center further than 402 km. The lowest recorded pressure was 910 mbars. Landfall was accompanied by a 3.7 m storm surge along more than 105 km of the coast. The National Weather Service reported 117 embedded tornadoes within Ivan. Florida's Department of Environmental Protection reported major damage to 91 single family dwellings and 149 multi-family dwellings in the October 2004 damage assessment report (Barnett 2004).

Joplin, Missouri Tornado

The May 22, 2011 Joplin, Missouri tornado was the most deadly since the June 8, 1953 Flint, Michigan tornado. The Joplin tornado resulted in more than

150 deaths and more than 1,000 injured. It caused EF-5 damage and contained winds of greater than 89.4 m/s (Proenza 2011a). Its track was approximately 35.6 km long and it was up to 1.6 km in width. The initial touchdown was 0.8 km southwest of JJ Highway and Newton Road in Newton County. Its dissipation was in Newton County at 32nd Street west of Kodiak Road (approximately 7.7 km north northwest of Granby Missouri (Maximuk 2011).

Imagery of the damaged area was secured from NOAA. Georeferenced post storm imagery is available from NOAA National Geodetic Survey's Tornado response site in UTM NAD 83 Zone 15 North projection (Aslaksen 2011a) in JPG with world file format.

Tuscaloosa, Alabama Tornado

The April 27, 2011 Tuscaloosa tornado was a long track, violent tornado event with maximum damage of EF-4 level. This tornado was produced by the supercell thunderstorm that began in Newton County Mississippi at 2:54 pm CDT and dissipated in Macon County North Carolina at 10:18 pm CDT. It initially touched down in northern Greene County, moved northeast through southern Tuscaloosa and western Jefferson Counties, lifting northeast of downtown Birmingham, Alabama. The damage path length was approximately 129.9 km. The EF-4 damage level was caused by an estimated maximum wind speed of 84.9 m/s. The maximum path width of the tornado was 2.4 km when it crossed Interstate 65 (Proenza 2011b). Imagery of the damaged area was secured from NOAA. Georeferenced post storm imagery is available from NOAA National

Geodetic Survey's Tornado response site in UTM NAD 83 Zone 16 North projection (Aslaksen 2011b) in JPG with world file format.

Differences and Similarities

Figure 6 shows the four hurricanes track with the extent of Category 1 or greater winds for each storm. The aerial extent of the Category winds for Hurricane's Ike, Rita, Katrina and Ivan are 22,647 square km, 2,857 square km, 36,143 square km and 16,825 square km, respectively. Hurricane Katrina's severe winds covered 12+ times more ground than Hurricane Rita. Hurricanes Ike and Ivan covered roughly half the extent of Katrina and several times more land area than covered by Hurricane Rita.

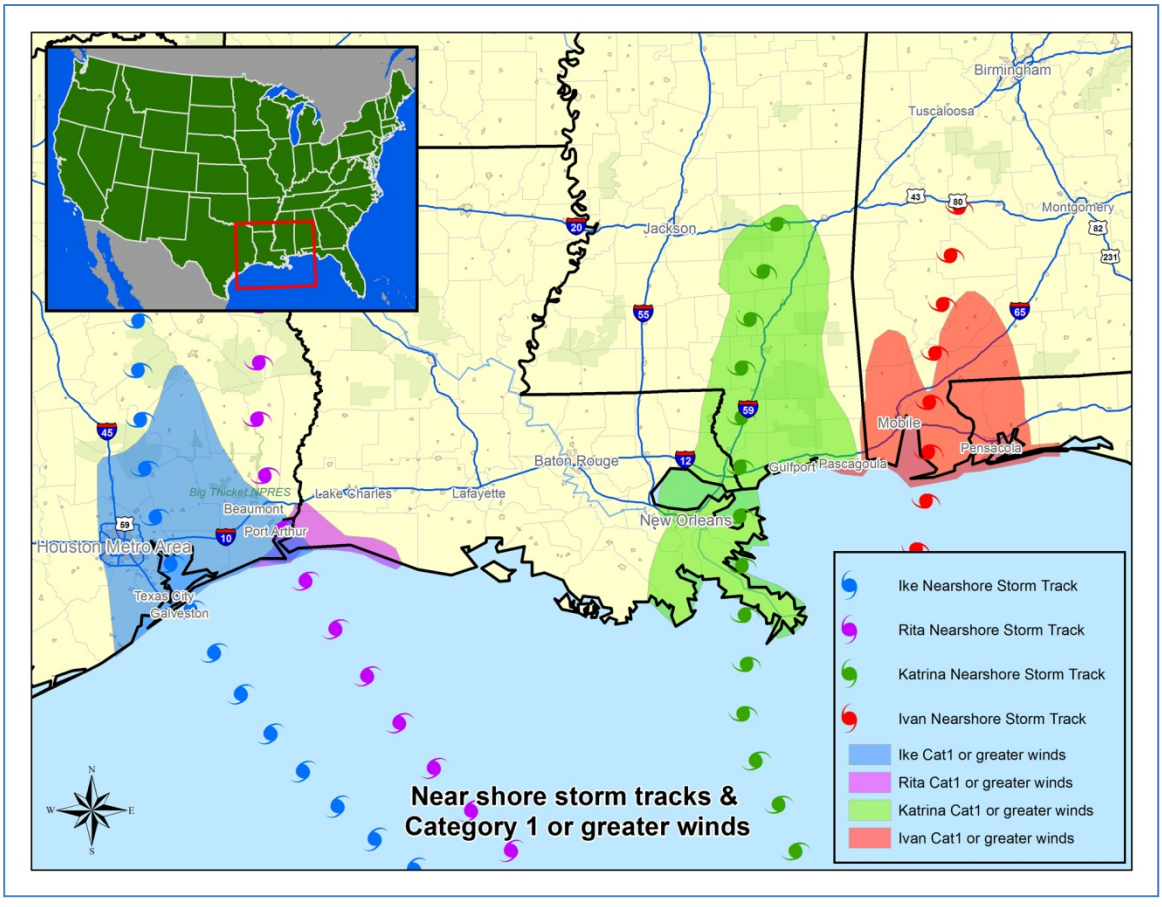

Figure 6. National Hurricane Center best track of Hurricanes Ike, Rita, Katrina, and Ivan and aerial extent Category 1 or greater winds for each.

The hurricanes and hurricane landfall areas in this study are significantly different. Those meeting the necessary data requirements for this research (significant coastal residential damage caused, high resolution imagery, published damage assessment) all made landfall on the Gulf Coast within a three week window in the calendar year between the end of August and late September. All can be grossly estimated to be similar in strength. Rita, Katrina and Ivan all were officially determined to be Saffir-Simpson category 3 hurricanes, with Hurricane Ike ruled a strong category 2. These metrics belie the significant differences between these hurricanes. Hurricane Katrina's category 1 (32.6 m/s) or greater winds covered an area of 36,143 square km, approximately twice as big as covered by either Ike (22,647 square km) or Ivan (16,825 square km), and more than 10 times greater than Hurricane Rita's category 1 winds area (2,857 square km).

The maximum sustained winds recorded by the National Hurricane Center for these hurricanes appear similar (Ike – 49.2 m/s, Rita – 51.4 m/s, Katrina – 56.8 m/s, Ivan – 58.1 m/s). But the winds, including the recorded embedded tornadoes, for these hurricanes are significantly different. Ike's maximum gusts were recorded as 49.2 m/s with no embedded tornadoes recorded by the National Weather Service. Rita and Katrina had reports of gusts of 77.3 m/s, while Ivan had gusts reported as large as 72.0 m/s. Ike had no reported embedded tornadoes. Rita had twenty one embedded tornadoes recorded by the National Weather Service. Katrina had forty three embedded tornadoes recorded by the National Weather Service. The National Weather Service reported 117

embedded tornadoes for Ivan, though these were spread across the eastern Gulf Coast and eastern Atlantic coastal areas.

A further meteorological difference among these hurricanes is the storm surge accompanying landfall. Ike was accompanied by a 3.0 m high storm surge extending for more than 214 km along the coast. Rita's 4.3 m storm surge extended more than 97 km along the coast, similar to Ivan's 3.7 m storm surge which extended more than 105 km along the coast. Katrina's landfall was accompanied by a 6.4 m storm surge that extended more than 161 km along the coast, with reports of greater than an 8.5 m storm surge in some areas.

The nature of hurricanes is varied and complex and the damage impact of hurricane landfalls are further complicated by the variations in the landscape of the landfall areas. Figure 7 shows the percent land cover for each of the hurricane's category 1 or greater winds area. Hurricane Rita's landfall impact area is on the eastern edge of Hurricane Ike's landfall impact area. Despite the proximity of these landfall areas, the land cover impacted by the two storms is vastly different. Rita's 2,857 square km of category 1 or greater winds impacted area is composed of 94.4 percent of open water or wetlands. Hurricane Ike's 22,647 square km of category 1 impacted area is composed of only 33.6 percent open water or wetlands. Hurricane Ivan's 16,825 square km of category 1 or greater winds impacted area has the least open water or wetlands at 24.4 percent. Hurricanes Ike and Katrina fall between these extremes at 33.6 percent and 34.6 percent, respectively. Rita's category 1 or greater impact area contains

the smallest percentage of developed land cover at 2.8 percent, followed by Katrina at 7.8 percent, Ivan at 10.3 percent and Ike at 20.8 percent.

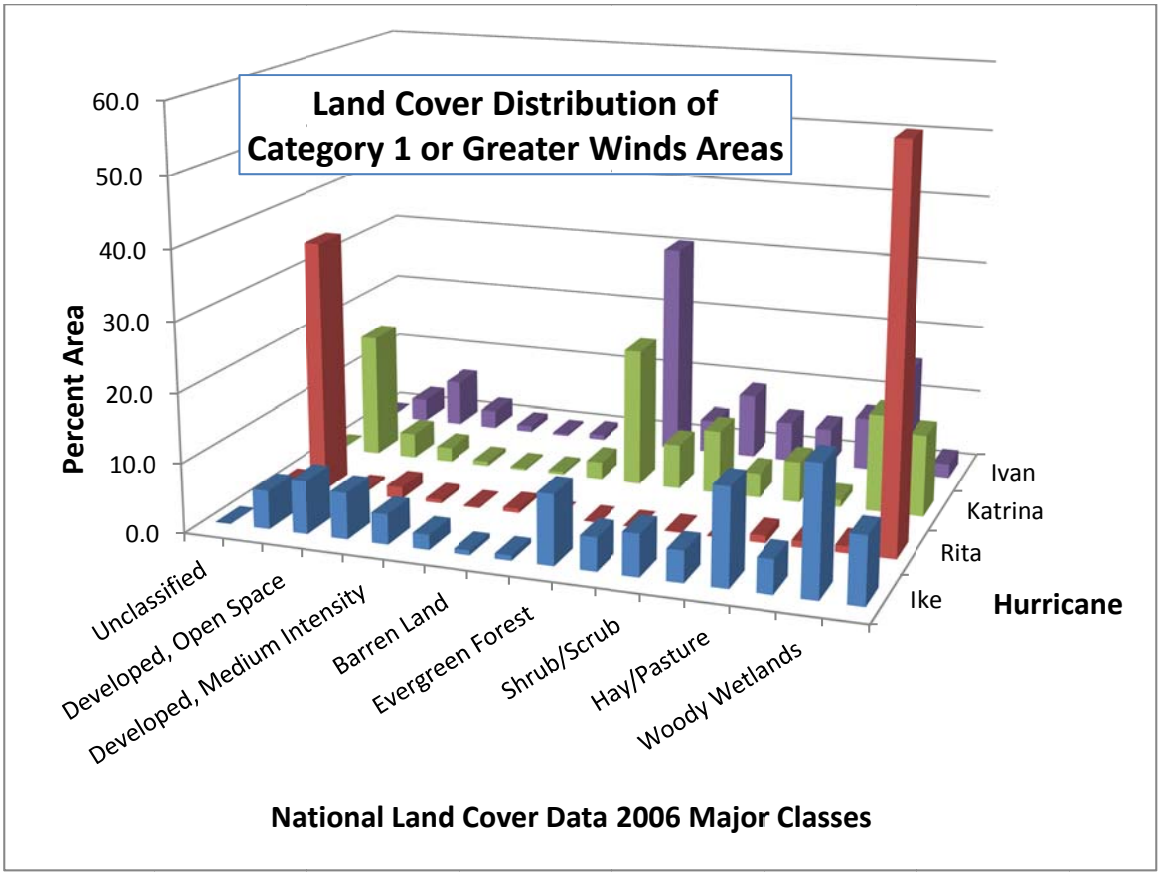

Figure 7. The 2006 National Land Cover Data for each hurricane's category 1 or greater winds areas illustrates some of the differences among the hurricanes. Rita's category 1 or greater winds area, for example, is composed by 94.4percent wetlands or open water.

The discriminant analysis of damage classification of hurricanes revealed unexpected variability, particularly when storm data sets were combined for discriminant analysis. Given damage classification accuracies of 66.7 percent to 88.7 percent of cross validated samples for the hurricanes and combinations of hurricanes, tornadoes were investigated in an attempt to eliminate variability that might be attributable to the variations intrinsic to hurricanes.

The Tuscaloosa and Joplin tornadoes were devastating storms impacting large residential areas. They were classified as EF-4 and EF-5, respectively. The large extent of damage offered the opportunity for collecting fifty or more samples per category, which can be problematic with frequent smaller tornadoes.

Challenges

The wide variability between and within hurricanes and the large areas covered by potentially damaging forces within hurricanes appears to inject variability beyond the variance in samples due to damage condition. Plots of discriminant functions 1 and 2 show two general shapes of the discriminant analysis discriminant function plots. The shape of these plots appear roughly as either a somewhat random, or shotgun blast, shape (e.g., Figure 32, Rita plot of DF 1 and 2 shows category separation with a random appearing, or shotgun blast appearing variability) or as a basketball free-throw line shape (e.g., Figure 34, Katrina plot of DF 1 and 2 shows the damage categories separated but spread vertically in a line like shape (the free throw line), with the no damage category appearing as a separate group from the other categories, where the basket would be positioned). Combinations of hurricane data discriminant analysis plots of DF 1 and 2 show a combination of these two shapes from the individual hurricanes.

This variability within and among hurricane data sets presented the challenge of not being able to separate the variability due to differences in hurricanes from the differences in damage categories. This suggested examining small area, relatively uniform damage events in an effort to explore the utility of

wavelet transform based image processing while minimizing landscape and hurricane variations. Tornado events appear ideal for this limited area, focused damage examination. Tornadoes in the U.S. have a ground footprint on average 45.7 m wide and 1.6 to 3.2 km long (Ramsdell, Rishel, and Buslik 2007). Their ground footprints are significantly smaller than even small hurricanes. The large May 2011 Joplin tornado was approximately 1.6 km wide by 35.4 km long. Even this large tornado, at approximately 57.0 square km in ground footprint size is fifty times smaller than the category 1 or greater wind impacted area of the small hurricane Rita (2,857 square km). Limiting the geographic extent of the study area offers the possibility of minimizing the impact of variations between storms.

Data and Processing

Data

Imagery data for Hurricanes Ike, Rita, Katrina and Ivan and the Joplin and Tuscaloosa tornadoes was acquired from NOAA National Geodetic Survey Emergency Response Imagery archive website (Aslasksen 2010). Imagery for Hurricanes Ike and Katrina, and the Joplin and Tuscaloosa tornadoes was available in georeferenced JPG format with world files. After acquisition it was imported directly into ArcGIS 2010. Imagery for Hurricanes Rita and Ivan was available only in ungeoreferenced JPG format.

Damage assessment layers for hurricanes Ike, Rita, Katrina and Ivan were acquired from FEMA. The damage assessment maps for Ike, Rita and Katrina were available in shapefile format, while Ivan's remote sensing based damage assessment were only available in PDF format. The damage assessment for the

Joplin and Tuscaloosa tornadoes was acquired from NOAA's National Weather Service Weather Forecast Office in KML format.

ESRI provided StreetMap USA background map layers were used for orientation and visualizations within the GIS.

Digital Ortho imagery was acquired from the United States Department of Agriculture's GeoSpatial Data Gateway for each county affected by all storms for use in referencing ungeoreferenced imagery and damage assessment layers.

The National Land Cover Data 2006 layer was acquired for Texas, Louisiana, Mississippi, Alabama, and Florida from the United States Department of Agriculture's GeoSpatial Data Gateway to support comparison and contrast of land cover among the hurricanes.

Tools

Several tools were reviewed for potential use to acquire image samples, calculate wavelet transform coefficients for each image sample, and to perform statistical analysis. ArcView is the market leader in the GIS software space and contains all the necessary GIS tools for image selection and sampling. ArcView was selected as the tool for required GIS manipulation and analysis. ERDAS Imagine was selected as the tool for required image sampling (dicing the post event imagery into subsamples). Ninety wavelet software tools were reviewed as possibilities for performing the necessary wavelet transform analysis. MatLab and the MatLab Wavelet Toolbox were selected as the tools for calculating wavelet transform coefficients of each sample. IBM SPSS was selected as the tool for statistical analysis of the wavelet transform coefficient data.

Georeferencing

Imagery for Ike, Katrina, Ivan, Joplin, and Tuscaloosa were directly ingested into ArcGIS. Imagery for Rita and Ivan were only available as ungeoreferenced image files. Areas of damage were identified from damage assessment maps to identify which images to load into the GIS. These were then georeferenced within ArcGIS using digital orthos as the reference layer. This same process was employed to georeference the Ivan imagery. Hurricane Ivan's FEMA damage assessment was only available in ungeoreferenced PDF format. The Ivan FEMA damage assessment PDF was converted to a JPG file in Adobe Photoshop then loaded into ArcView and georeferenced using the digital orthos and StreetMap USA as reference layers. Georeferenced, shapefile layers were created for the each damage assessment category from the georeferenced FEMA damage assessment image.

Sampling

Myint's research into window sample sizes for complex feature classification accuracy indicates optimal sample size ranges for classification of imagery with complex feature content. He found 63 x 63 meter and 95 x 95 meter window sizes provide the highest accuracy for operational wavelet based algorithm examination of high resolution imagery, though accuracy was found to be variable among classes. A 63 x 63 meter window produced an overall accuracy of 81.84 percent. A 95 x 95 meter window produced an overall accuracy of 78.19 percent accuracy (Myint 2010). Gulf of Mexico coastal property is quite varied in size and shape. Individual property sizes were considered as a

potential factor influencing optimal image sample size. Harrison County Mississippi's property file contains 92,141 individual properties. The average property size for all Harrison County properties is 15,312 square meters with a median of 1,248 square meters and a standard deviation of 120,583 square meters. Property areas and shapes varied so widely along the Gulf of Mexico as to be of little value in guiding selection of sample size.

An image sample size of 78 meters (256 feet) x 78 meters was chosen based on it being approximately the average value of the two highest accuracy sample sizes (63 meter and 95 meter) for residential class reported by Myint (Myint 2010) as well as being, in feet, a factor of 2 supporting 5 levels of wavelet transform deconstruction. Visual examination of imagery for the 4 selected hurricanes indicates that this sample size is generally large enough to contain one or more residential, coastal properties.

In addition to the spatial frequency content of a sample, the number of samples practically available within areas classified by FEMA damage assessment maps was a factor considered in determining sample size. The accuracy of the classification of remotely sensed data is well documented by Congalton and Green (Congalton 1991, Congalton and Green 2009). They suggest collecting fifty samples for each category in an error matrix as a good rule of thumb for imagery sampling. For especially large areas they suggest 75 to 100 samples for each category, with adjustments up suggested for categories with more variability or categories of particular interest.

Hurricane Ike Sampling

Figure 8 shows a layout view of a part of the Ike GIS with the sample areas selected for each damage category.

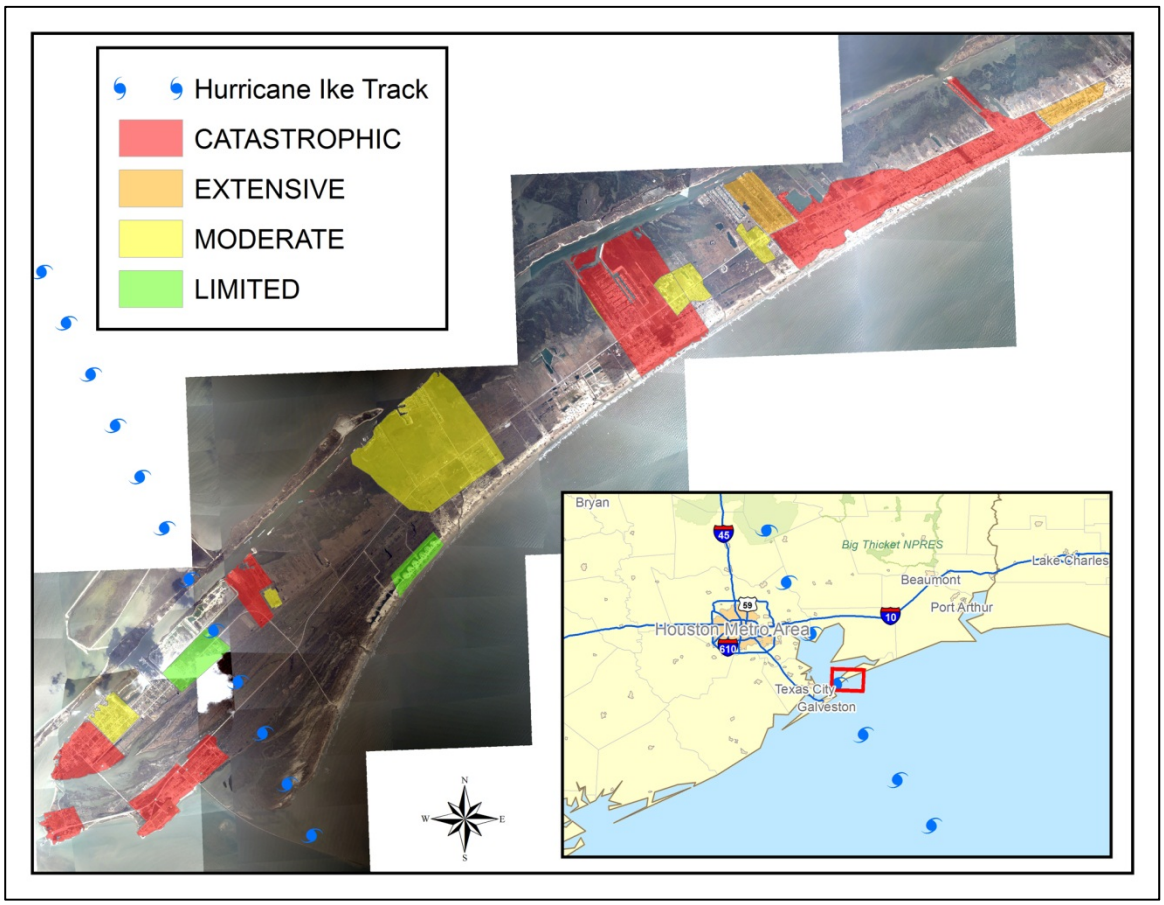

Figure 8. Hurricane Ike sampling areas.

Imagery in each damage assessment category area was clipped from the post landfall imagery and saved by damage category area. The saved damage assessment category imagery was imported into ERDAS Imagine for dicing into 78 x 78 meter (256 x 256 foot) sample image blocks. The sample image blocks were imported back into ArcView. Each sample image block was then visually inspected. Sample image blocks visually containing more than 50percent non-

residential content (water, homogenous ground [e.g., bare grass, pavement, soil, dense forest], etc.) were eliminated from the sample set. Sample image blocks that contain foundations only, such as from Hurricane Katrina, were not eliminated from the sample image block sets. A total of 1,008 samples (274 no damage; 86 limited damage; 94 moderate damage; 105 extensive damage; 449 catastrophic damage) were selected from post landfall hurricane Ike imagery. Figure 9 shows a hurricane Ike catastrophic sample area with non-residential areas eliminated. The purpose of this filtering of non-residential housing areas removes areas that might introduce bias into the damage assessment discriminant analysis. A block diagram representation of the process from data collection through WT damage assessment category prediction performance is shown in Figure 10.

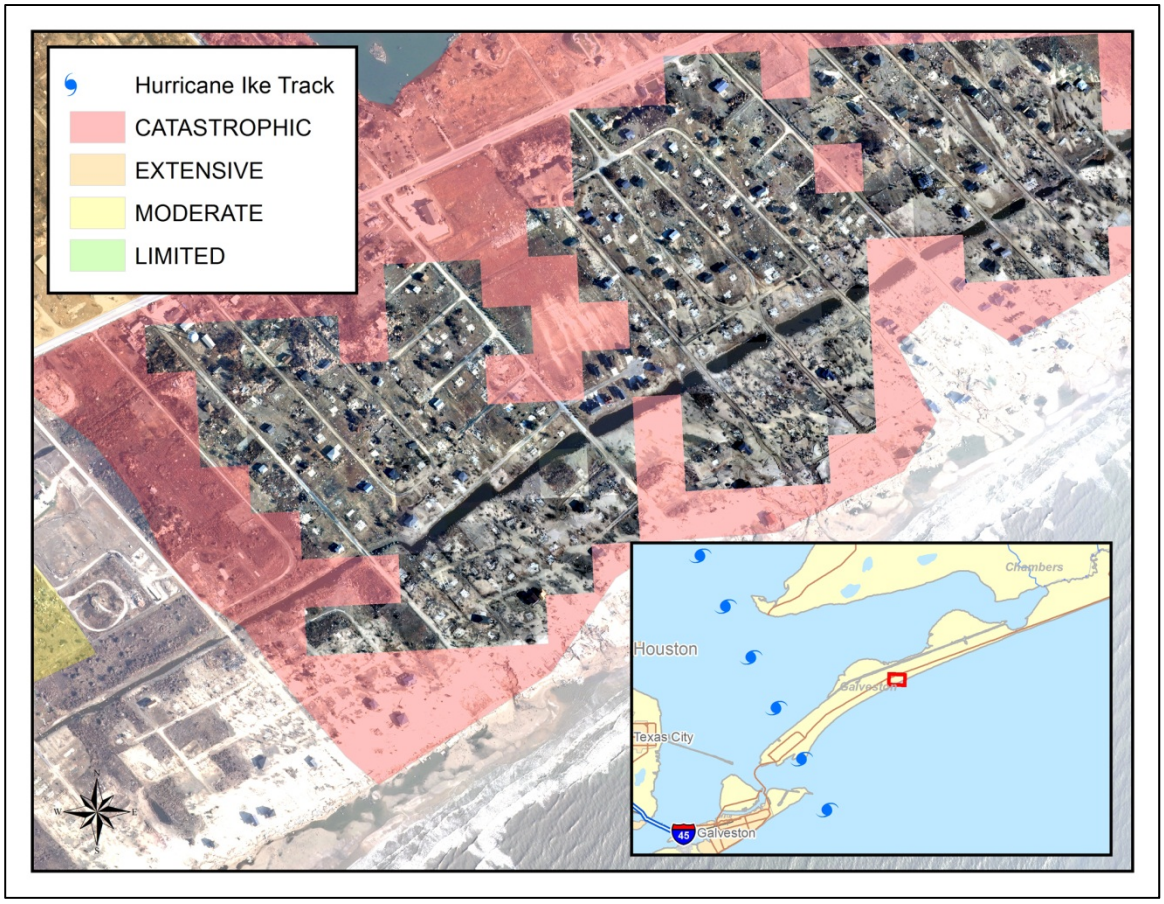

Figure 9. Image sample blocks imported into GIS for filtering out non-residential areas.

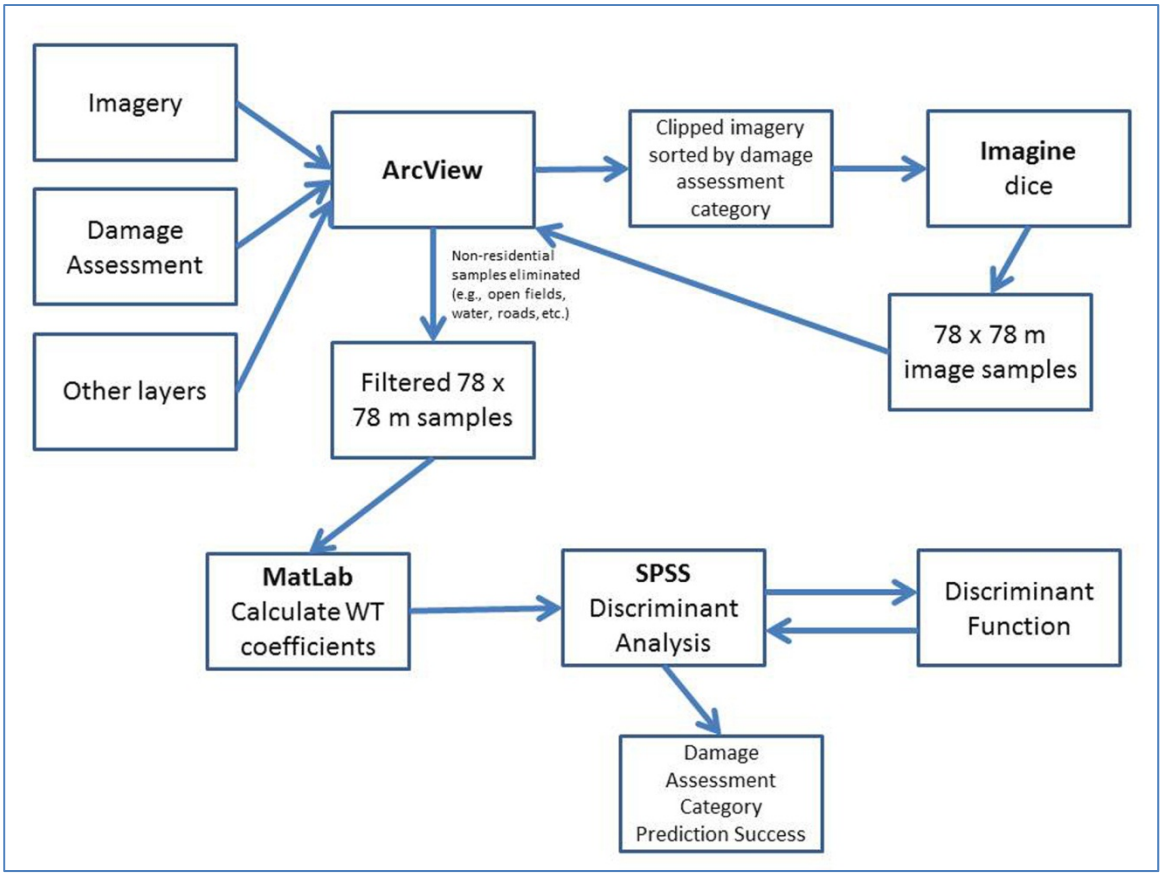

Figure 10. Data processing/analysis block diagram.

Hurricane Katrina Sampling

Hurricane Katrina's post landfall imagery and FEMA damage assessment were available in georeferenced format. This supported direct import of data into ArcGIS. Sampling proceeded as with Hurricane Ike. A total of 1,292 samples (79 no damage; 201 limited damage; 470 moderate damage; 174 extensive damage; 368 catastrophic damage) were selected from post landfall hurricane Katrina imagery for use in discriminant analysis and discriminant function creation. An additional 749 samples (73 no damage; 112 limited damage; 330 moderate damage; 74 extensive damage; 160 catastrophic damage) were collected from Katrina as distant as possible from the original 1,292 samples. These additional

samples were used for evaluating the accuracy of discriminant function models. They were not included in the sample set used to inform the Katrina discriminant function.

Figure 11 shows Hurricane Katrina storm track and FEMA damage assessment in the western Mississippi area. The Hurricane Katrina damage assessment category samples were taken from Hancock and Harrison Counties in Mississippi. Figure 12 shows an example of catastrophic area samples imported back into the GIS and filtered for residential area only.

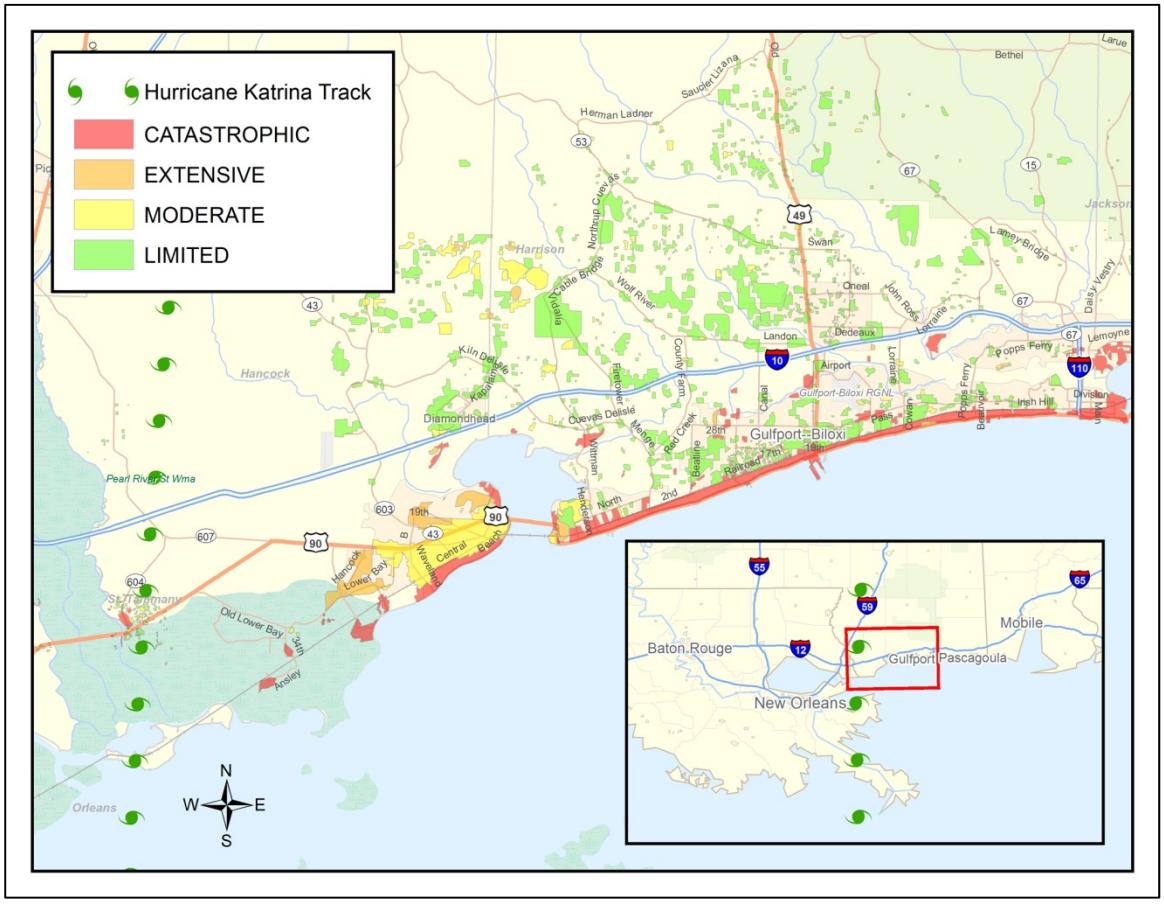

Figure 11. Hurricane Katrina sampling areas.

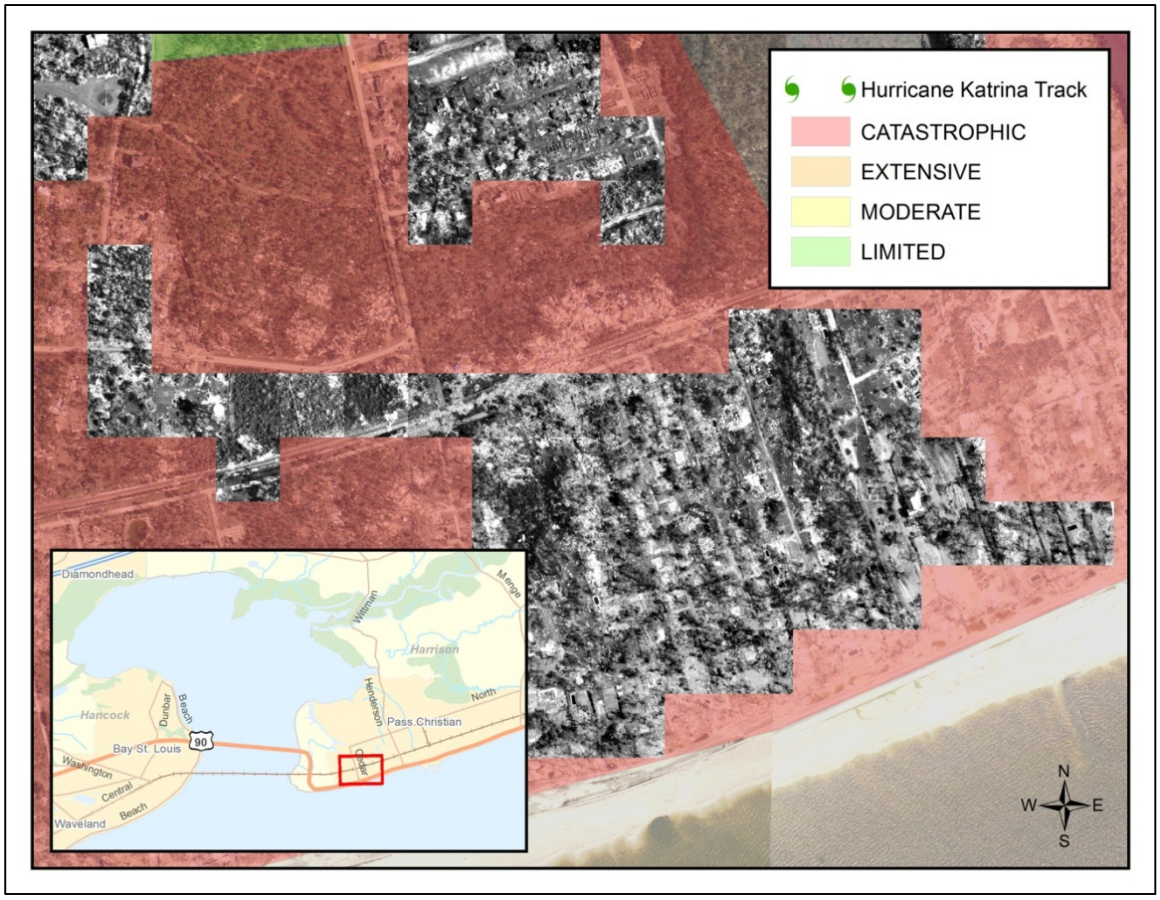

Figure 12. Example of image sample blocks imported into GIS for residential area filtering.

Hurricane Rita Sampling

The FEMA damage assessment maps for Hurricane Rita were available in georeferenced format. These were imported directly into ArcGIS. The Hurricane Rita post landfall imagery was available from NOAA's Emergency Response Imagery archive (Aslaksen 2010) only in non-georeferenced JPG format. These images were imported into ArcGIS and georeferenced. The Rita imagery was then sampled as with Hurricane Ike. A total of 1,298 samples (285 no damage; 240 limited damage; 190 moderate damage; 177 extensive damage; 406

catastrophic damage) were selected from post landfall hurricane Rita imagery for use in discriminant analysis and discriminant function creation.

Figure 13 shows the track of Hurricane Rita and the distribution of FEMA damage assessment areas. Figure 14 shows the largest catastrophic damage area associated with Hurricane Rita.

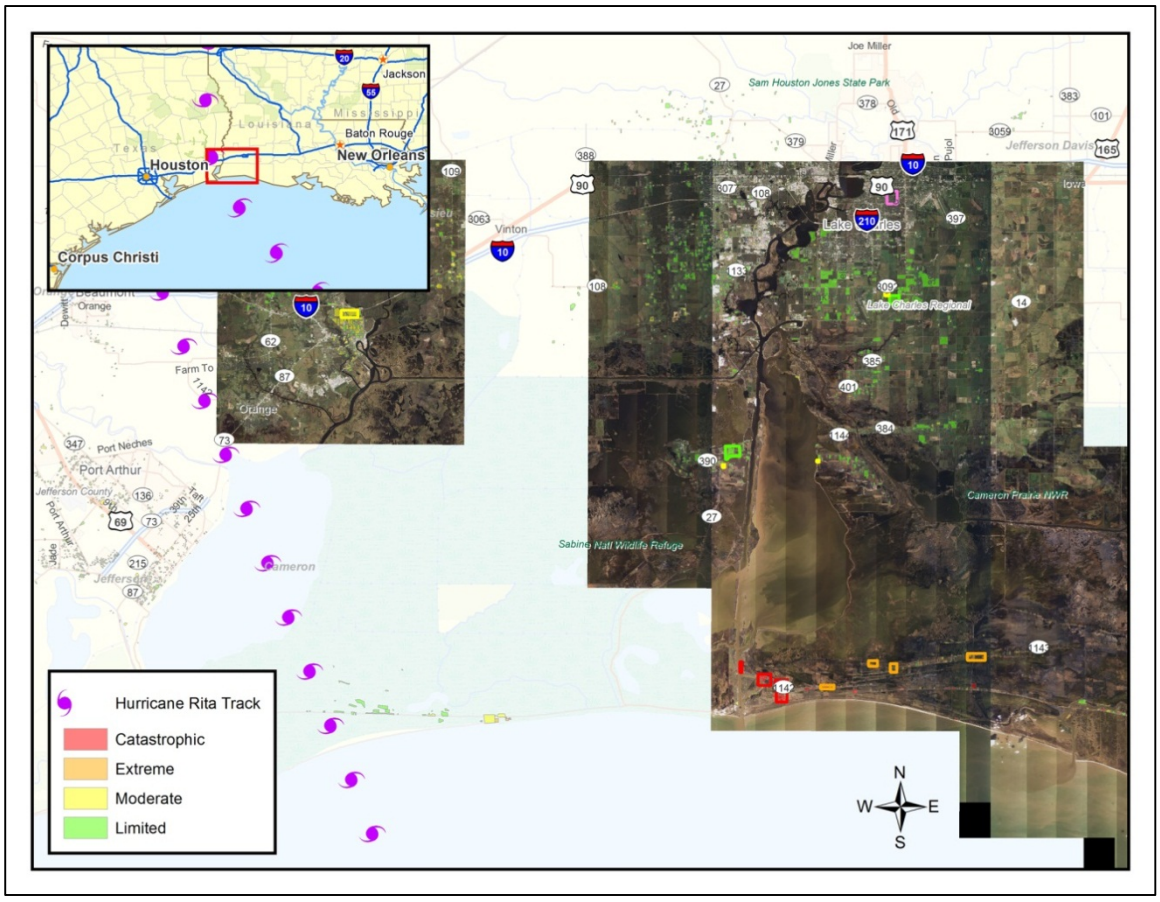

Figure 13. Hurricane Rita imagery sampling area.

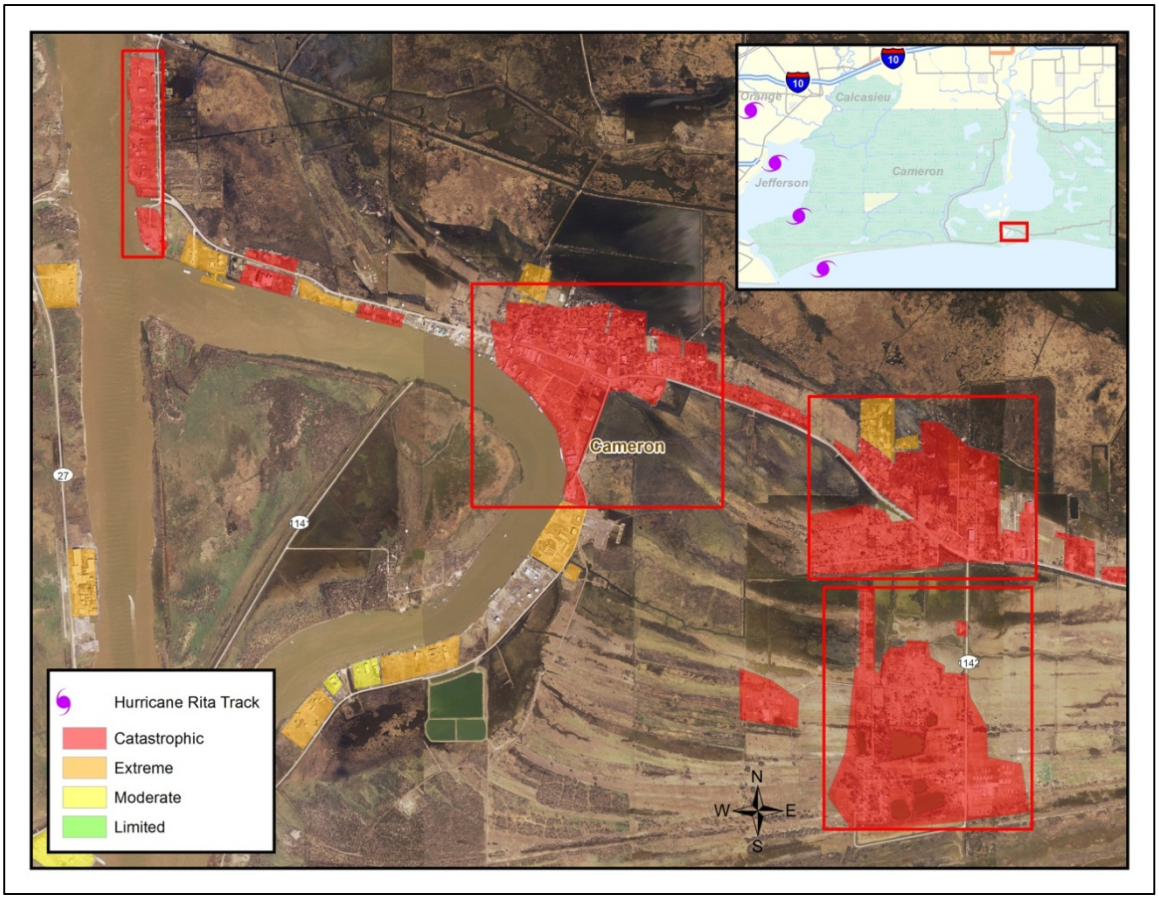

Figure 14. Hurricane Rita catastrophic damage sampling area.

Hurricane Ivan Sampling

The FEMA damage assessment maps for Hurricane Ivan were available only in non-georeferenced, PDF format. These PDFs were imported into ArcGIS as the source for creating georeferenced damage assessment shapes. The Hurricane Ivan post landfall imagery was available from NOAA's Emergency Response Imagery archive (Aslaksen 2010) only in non-georeferenced JPG format. These images were imported into ArcView and georeferenced and sampled as with Ike. A total of 716 samples (73 no damage; 150 limited damage; 401 moderate damage; 83 extensive damage;

9 catastrophic damage) were selected from post landfall hurricane Rita imagery for use in discriminant analysis and discriminant function creation.

Figure 15 shows the track of Hurricane Ivan and the distribution of FEMA damage assessment areas. Figure 16 shows post landfall imagery sampled, diced, and imported back into ArcView.

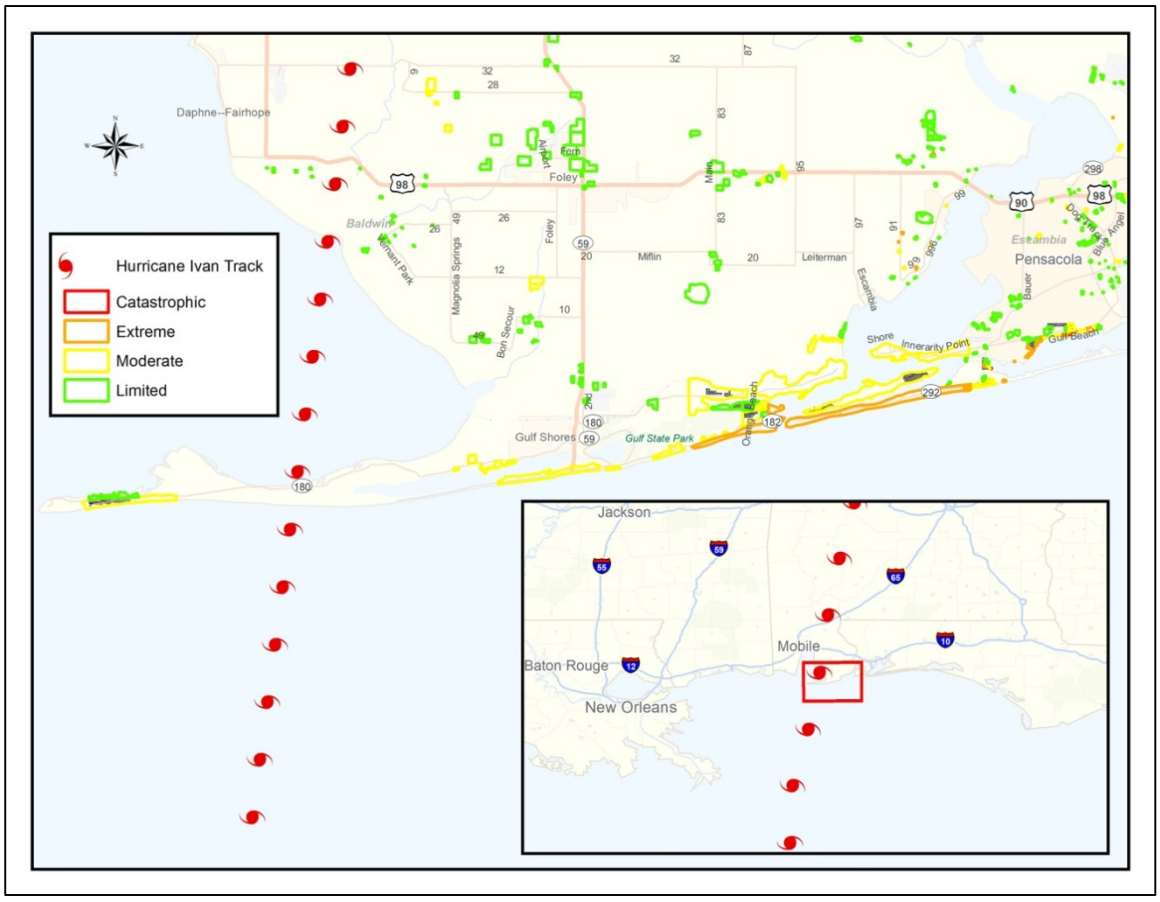

Figure 15. Hurricane Ivan sampling area.

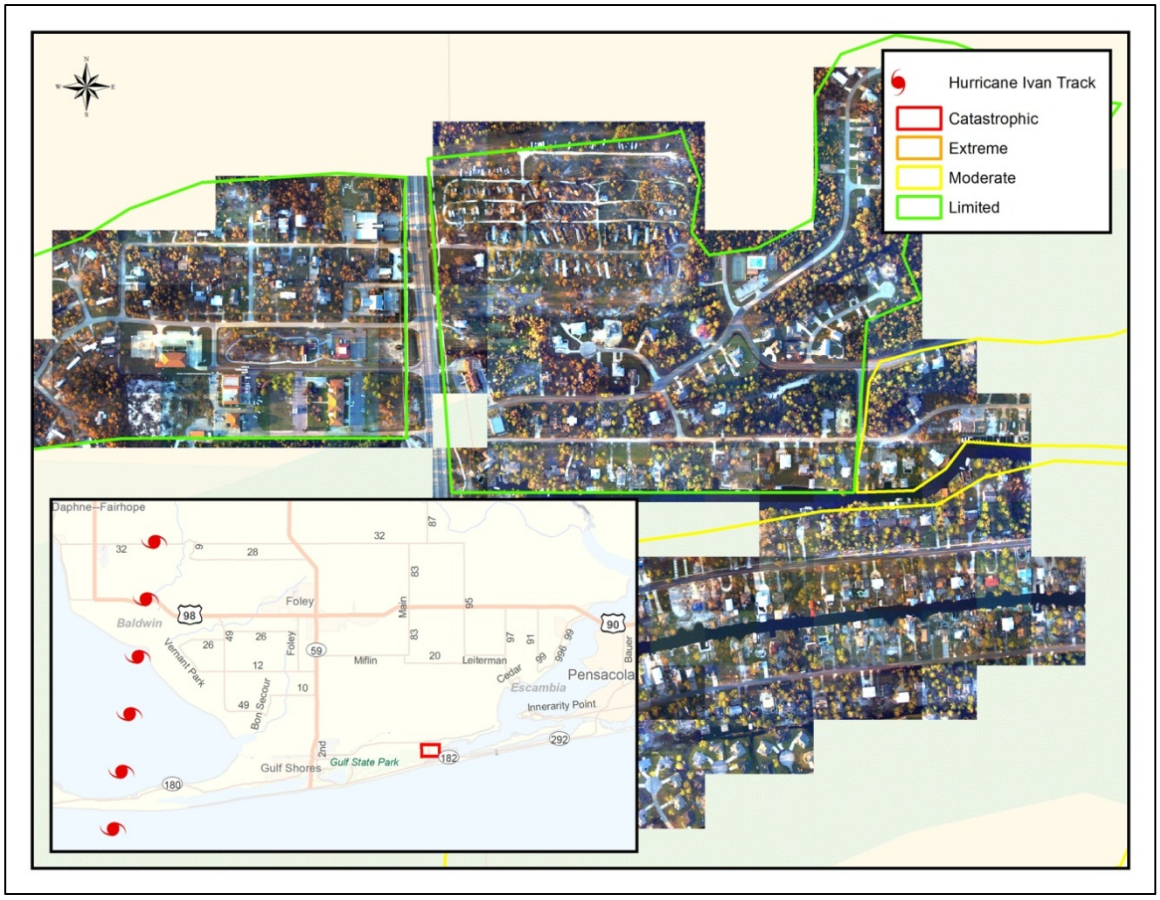

Figure 16. Hurricane Ivan sampling area.

Joplin Tornado Sampling

The damage assessment maps for the Joplin tornado were available in georeferenced format from the National Weather Service. These were imported directly into ArcGIS. The imagery was available from NOAA's Emergency Response Imagery archive (Aslaksen 2011a) in georeferenced JPG format. The imagery was then sampled as with Hurricane Ike. Two sets of samples were collected from the imagery. One set was used to inform a damage discriminant function. One set was used to assess the accuracy of the damage discriminant function. A total of 282 samples (130 no damage; 173 catastrophic damage) were selected from the imagery.

Figure 17 shows the samples selected from the Joplin imagery. Samples used to inform a damage model are outlined in purple. Samples used to assess the accuracy of the damage model are outlined in blue.

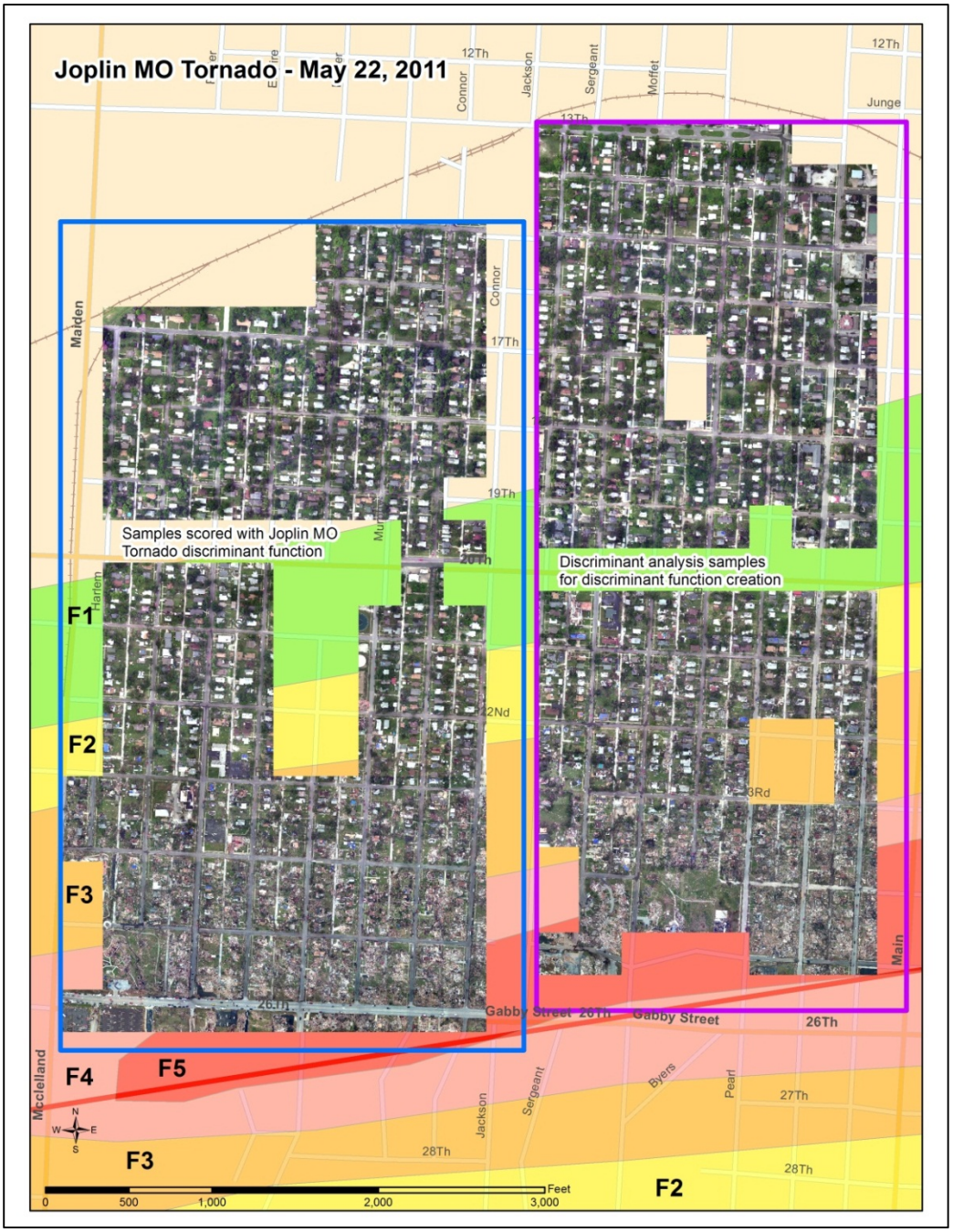

Figure 17. Two image sample groups were collected from the post Joplin tornado imagery. The group on the right, outlined in purple, was used to inform a discriminant function of tornado damage. The group on the left, outlined in blue, was used to test the accuracy of the tornado damage discriminant function.

Tuscaloosa Tornado Sampling

Damage assessment maps for the Tuscaloosa tornado were available in non-georeferenced format from The University of Alabama's Center for Advanced Public Safety. The imagery was imported directly into ArcGIS. The damage assessment was georeferenced as with hurricane Ivan. The imagery was then sampled as with Hurricane Ike. A total of 3,493 samples (1,713 no damage; 1,780 catastrophic damage) were selected from the imagery.

Figure 18 shows the sample selection area from the Tuscaloosa imagery.

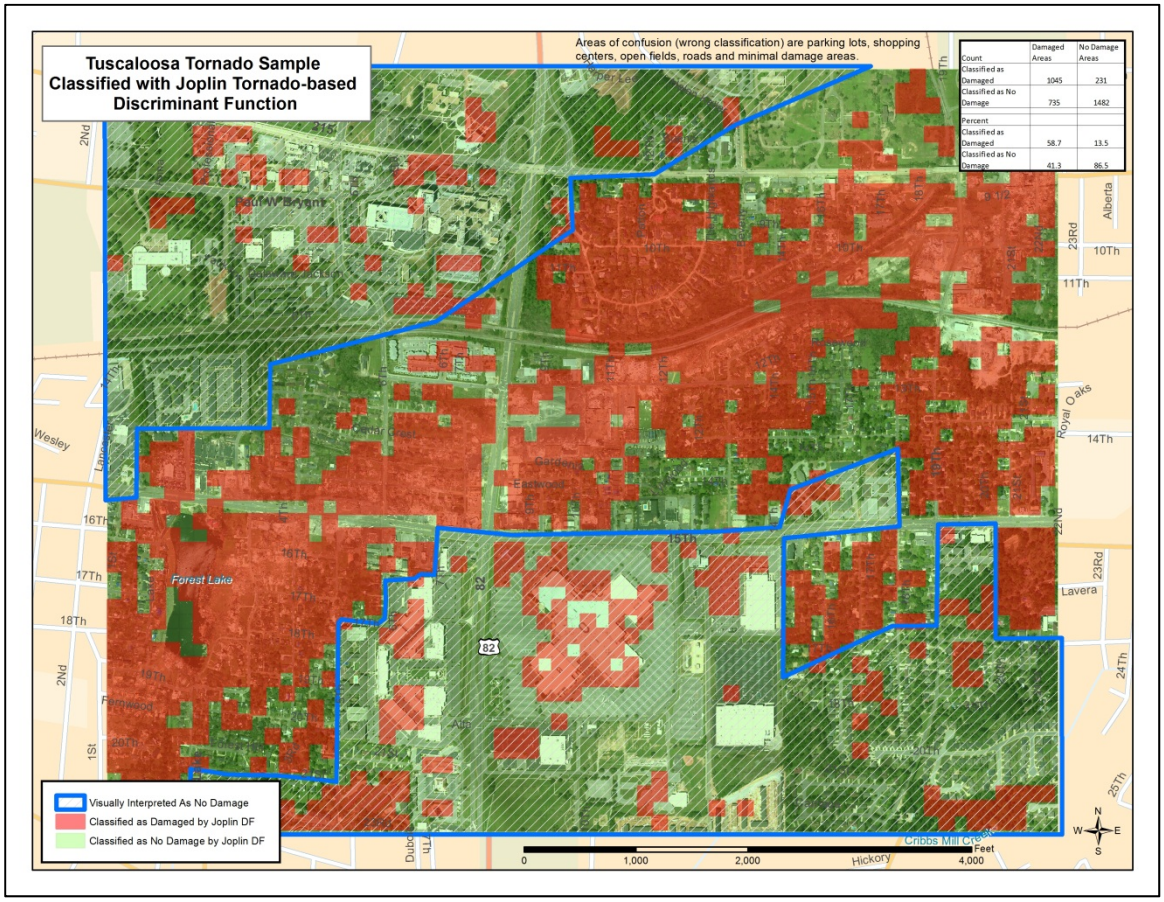

Figure 18. A large image sample set (3,493 image samples) was collected from high resolution, post Tuscaloosa tornado imagery. The Joplin-based tornado damage discriminant function was applied to these samples to test this function's damage assessment accuracy.

Wavelet Transforms

Wavelet transform analysis is the extraction of signal or image information at different positions and at different scales (Watson 1999). Continuous wavelet transformation can be thought of as the convolution of the wavelet function with the signal function. When the wavelet function and the signal function are similar, the transform result is a high value. When the wavelet transform function and the signal function are dissimilar, the result is a low value. Another way to think of wavelet transform is as a high pass filter and low pass filter in the horizontal, vertical and diagonal directions (Rao and Bopardikar 1998).

A test target with varying sized horizontal, vertical, diagonal and random image features was created to illustrate image wavelet transform analysis. Figure 19 shows the test target image.

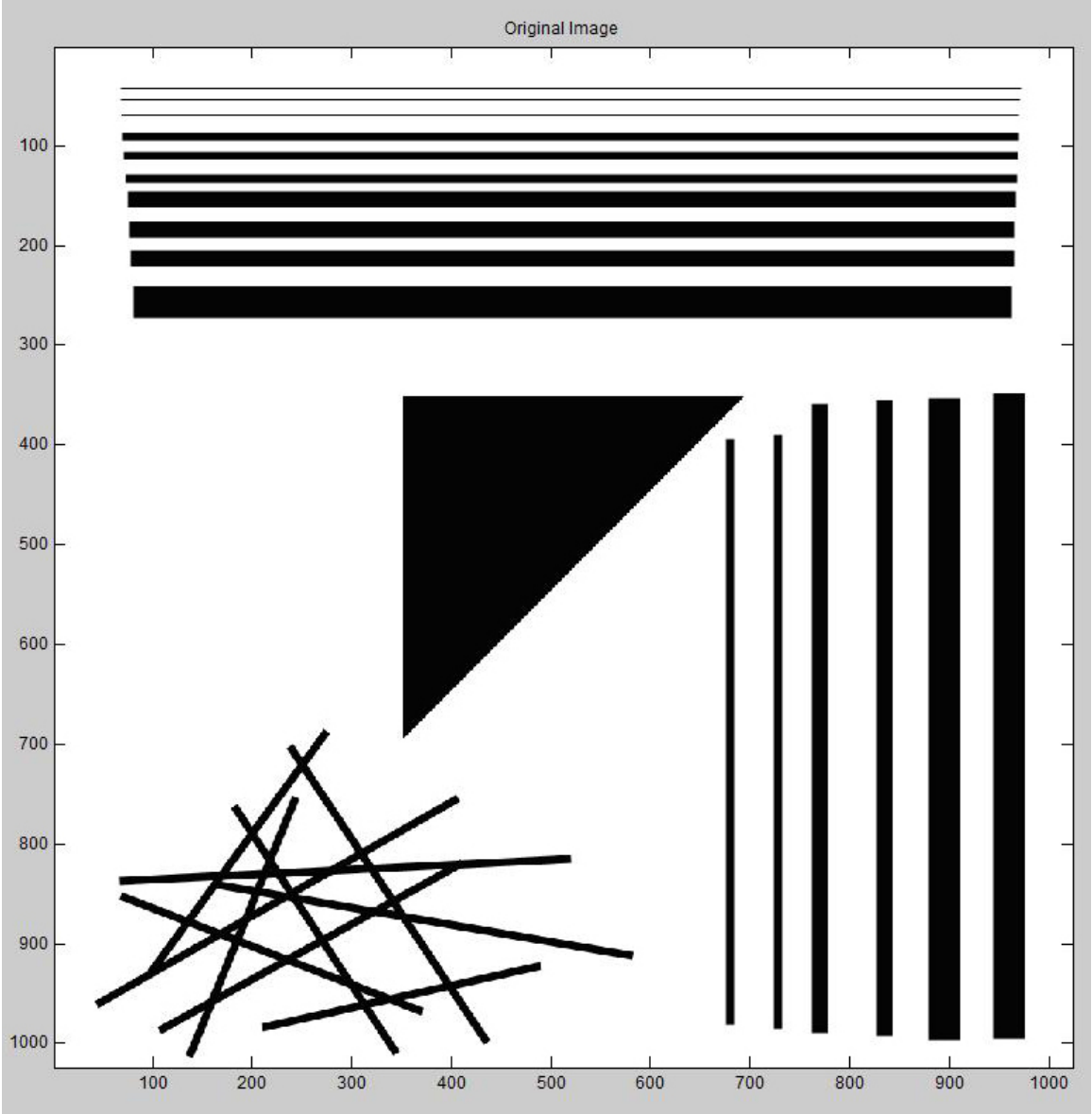

Figure 19. Test target image with horizontal, vertical, diagonal and random features for illustrating wavelet transform operations. Axis values are pixel number.

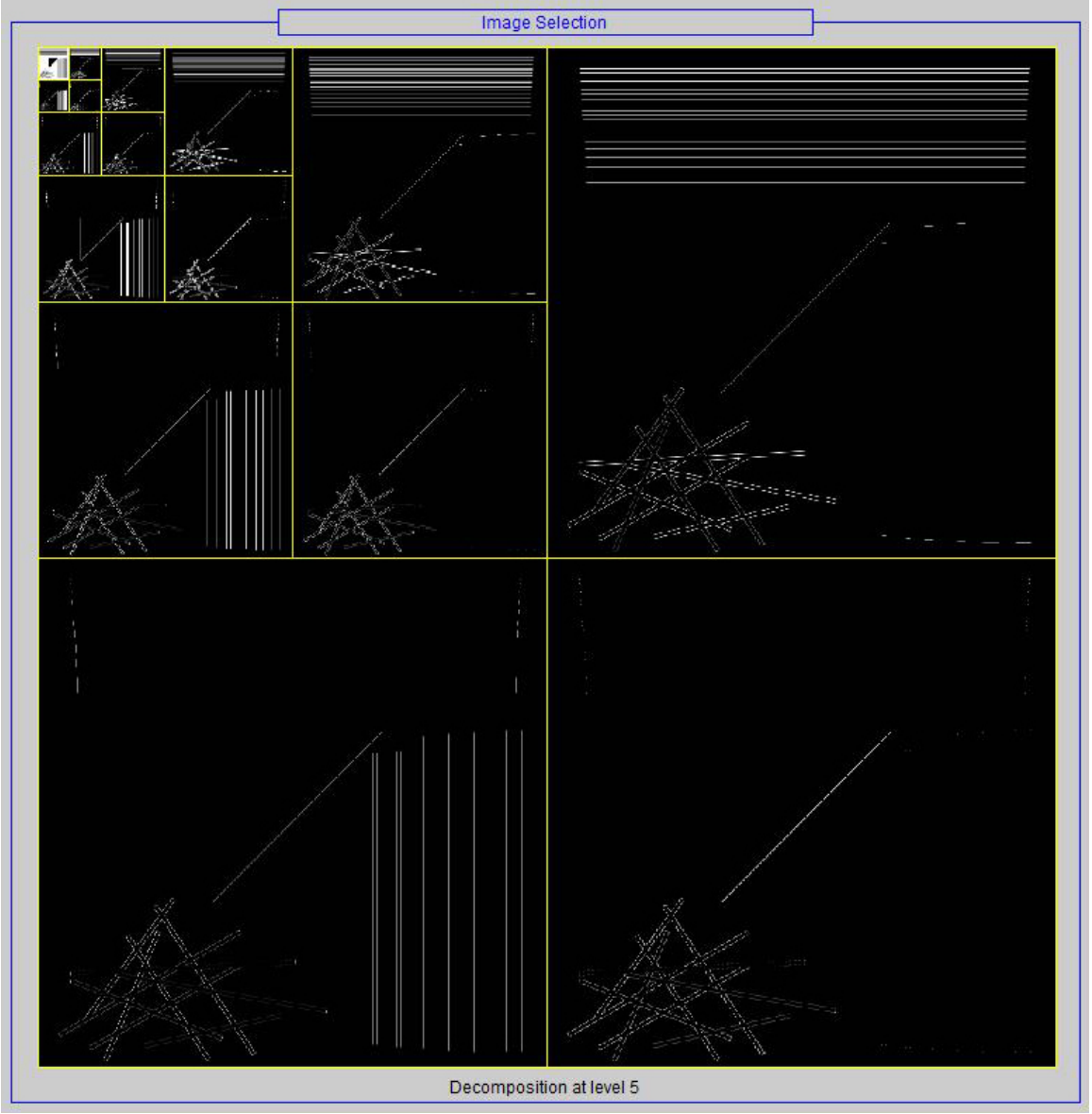

Figure 20. Five level Haar wavelet transform decomposition of the test target image.

Figure 21. First level diagonal detail coefficient image of the Haar wavelet transform of the test target image. Notice the presence of diagonal features only in this diagonal detail and the almost complete lack of any horizontal or vertical features. The Haar wavelet is particularly adept at identifying edges as exhibited by the presence of the triangle's diagonal edge and the edges of the random orientation bars. Its ability to pick up fast changing features is illustrated by it sensing the corners of the horizontal and vertical bars.

The Haar wavelet mother function, shown at upper left in Figure 22, functions as an edge detector (Watson 1999). When this function is convolved with a signal the result is an average of zero for constant signals. It returns a high

value when a discontinuity, or edge, is encountered. Figure 20 shows a five-level Haar wavelet transform decomposition of the test target. Figure 21 shows the first level diagonal Haar detail transform image of the test target.

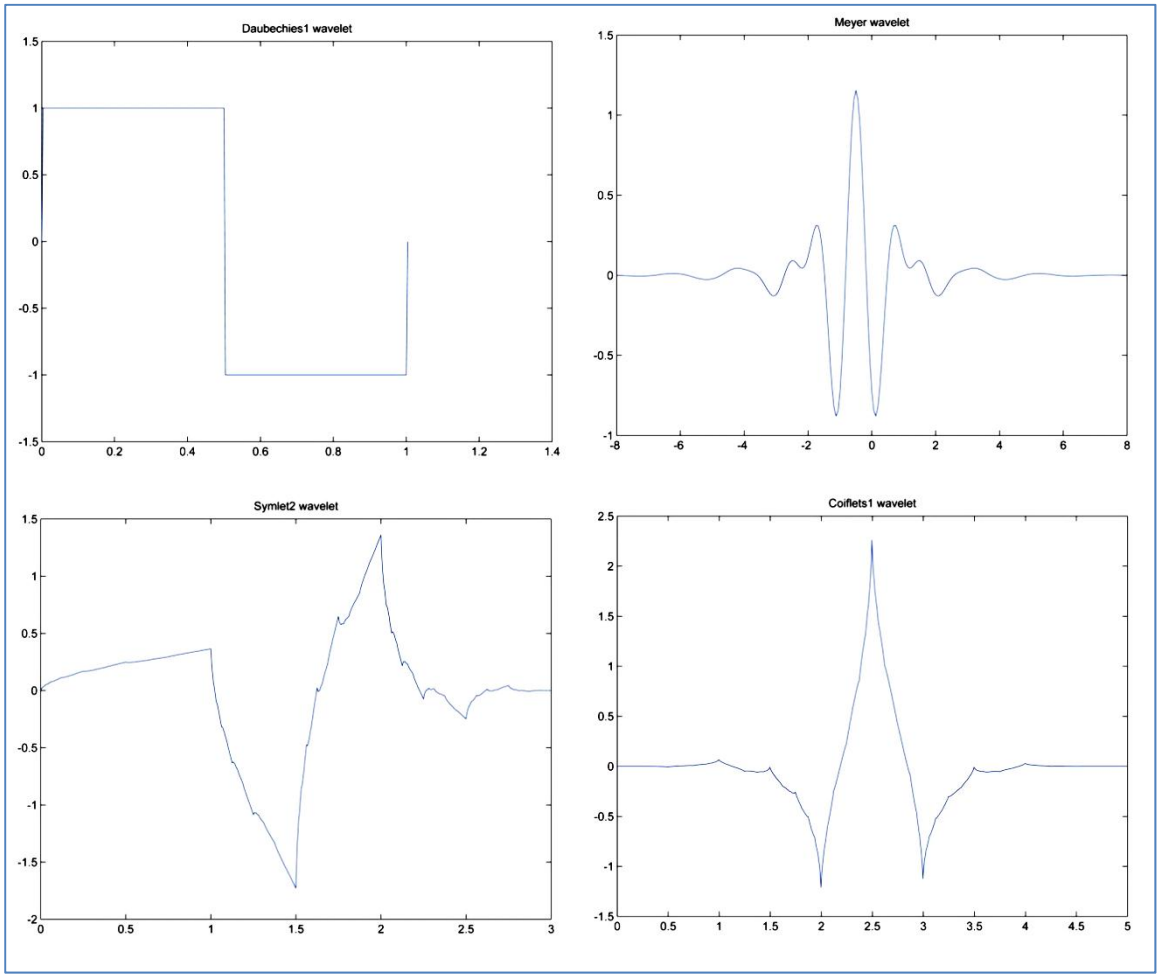

Figure 22. Wavelet mother functions investigated.

The Meyer function is a relatively symmetrical, fast changing function. It senses or is similar to fast changing signals in the scene (for example, boards, tree branches and other debris would be picked up by the Meyer function). Stripes in a parking lot would also be picked up by the Meyer function in the direction perpendicular to the stripes. Figure 22 shows a Meyer function in the upper right corner. Figure 23 shows a five level Meyer wavelet transform

decomposition of the test target image. Figure 24 shows the first level Meyer diagonal detail transform image of the test target.

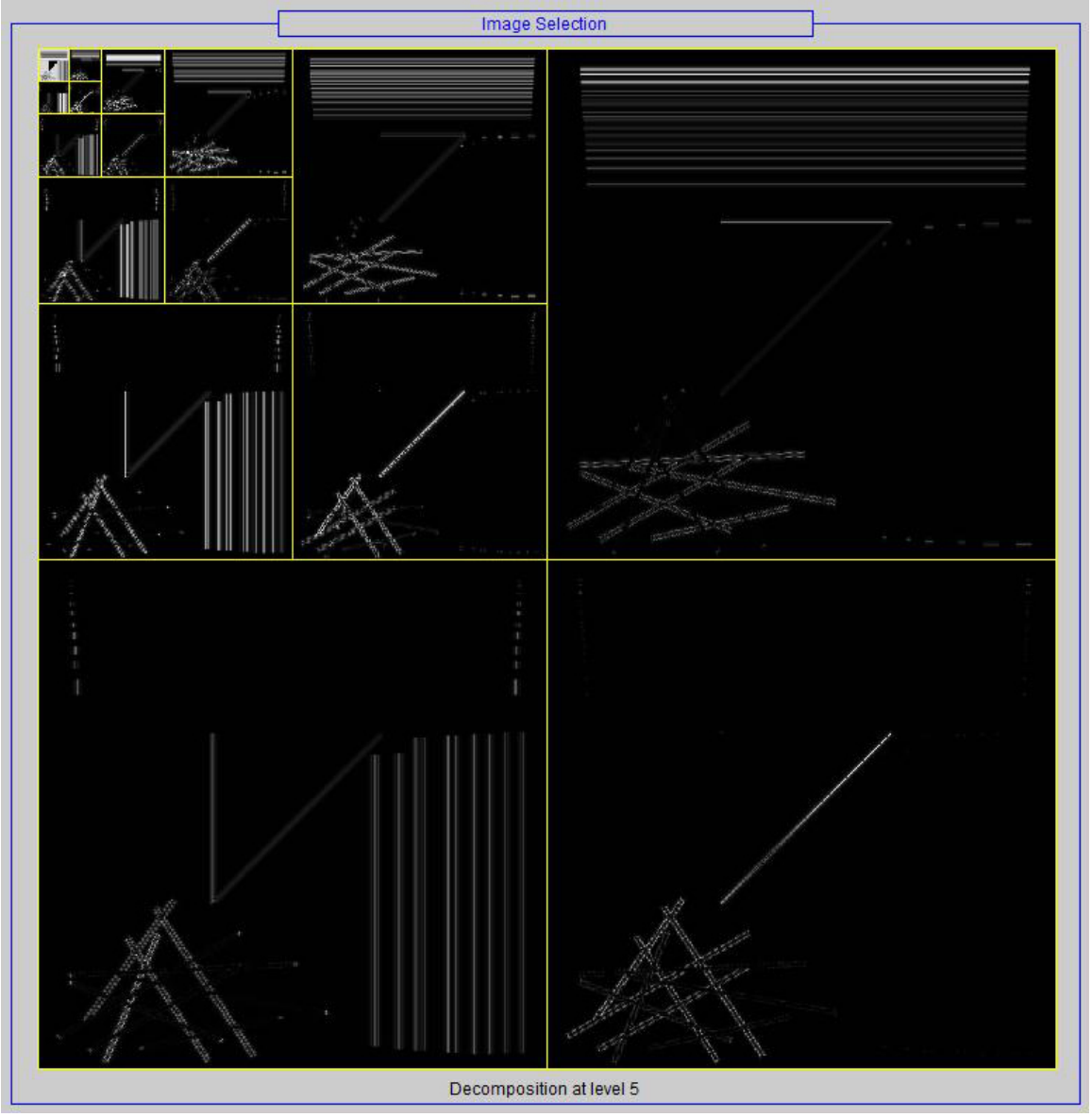

Figure 23. Five level Meyer wavelet transform decomposition of the test target image.

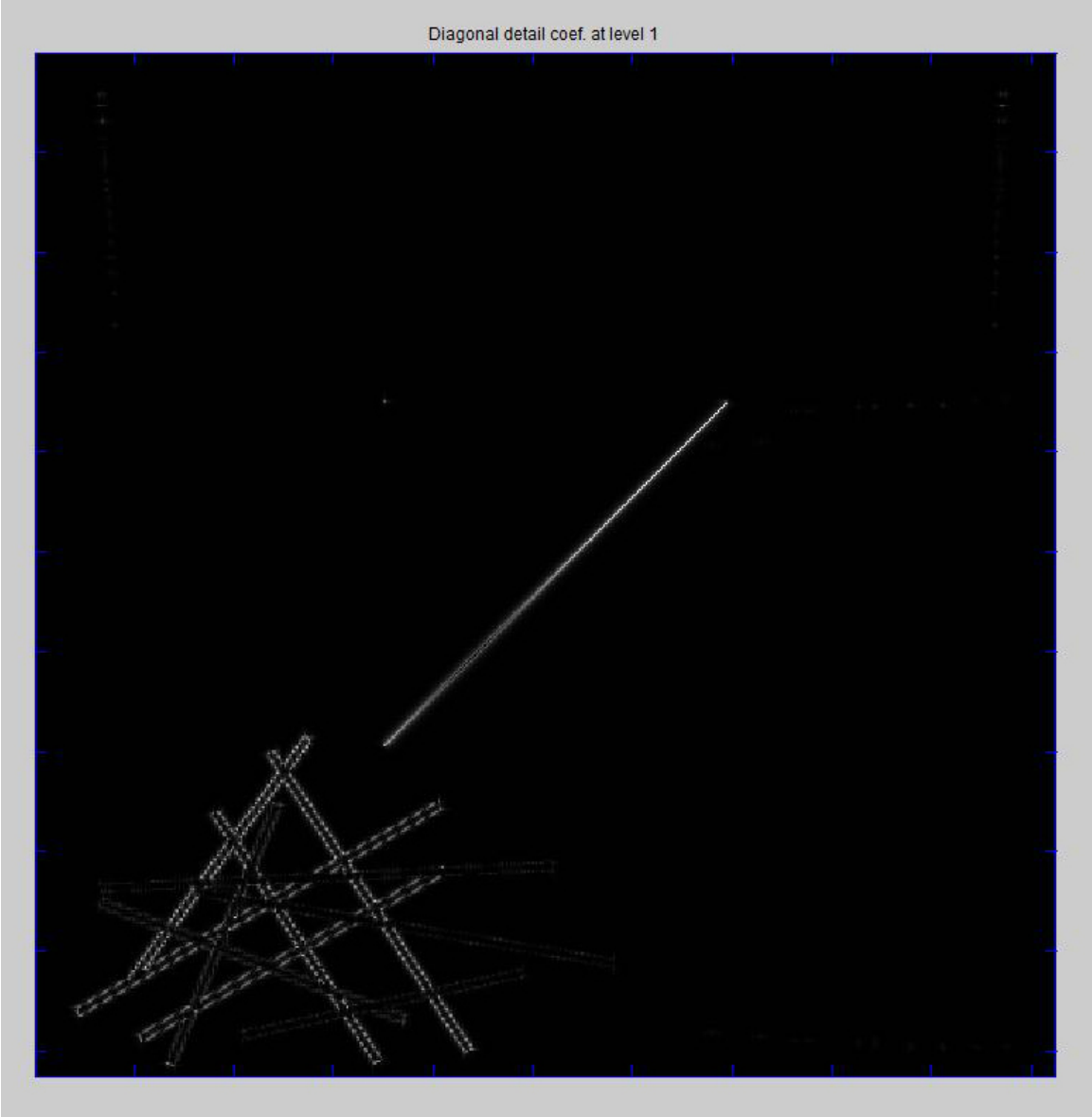

Figure 24. First level diagonal detail coefficient image of the Meyer wavelet transform of the test target image. Notice the presence of diagonal features only in this diagonal detail and the lack of any horizontal or vertical features, similar to the Haar. The Meyer wavelet identifies fast changing edges and small features similar to Haar, though the Meyer is less sensitive to small, very fast changing edges as illustrated by it not picking up corners of the vertical and horizontal bars as well as the Haar transform.

The Coiflets wavelet function, shown in the lower right of Figure 22, is similar to the Meyer wavelet function in that it is symmetrical. It has fewer zero with sharper peaks and a slightly broader base between the two negative peaks.

Generally, it will detect similar image features as the Meyer function, though it will sense simpler fast changing features. For example, a single board against a soil background would yield a high value with the Coiflets wavelet. In comparison, the Meyer wavelet function would yield a high value with three parallel boards against a soil background. Figures 25 and 26 show the five-level Coiflets decomposition image of the test target and the first level diagonal detail Coiflets wavelet transform image.

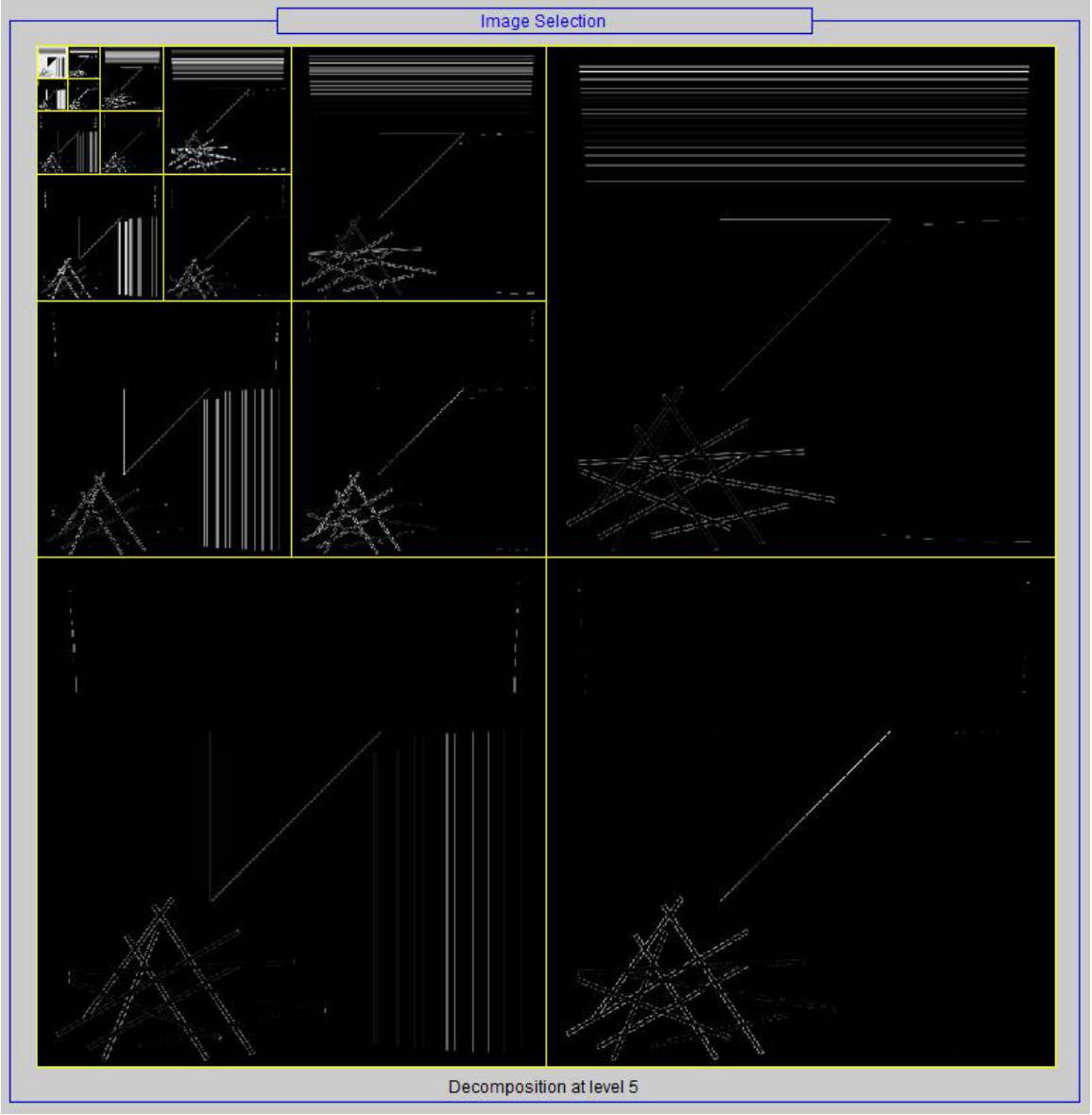

Figure 25. Five level Coiflets wavelet transform decomposition of the test target image.

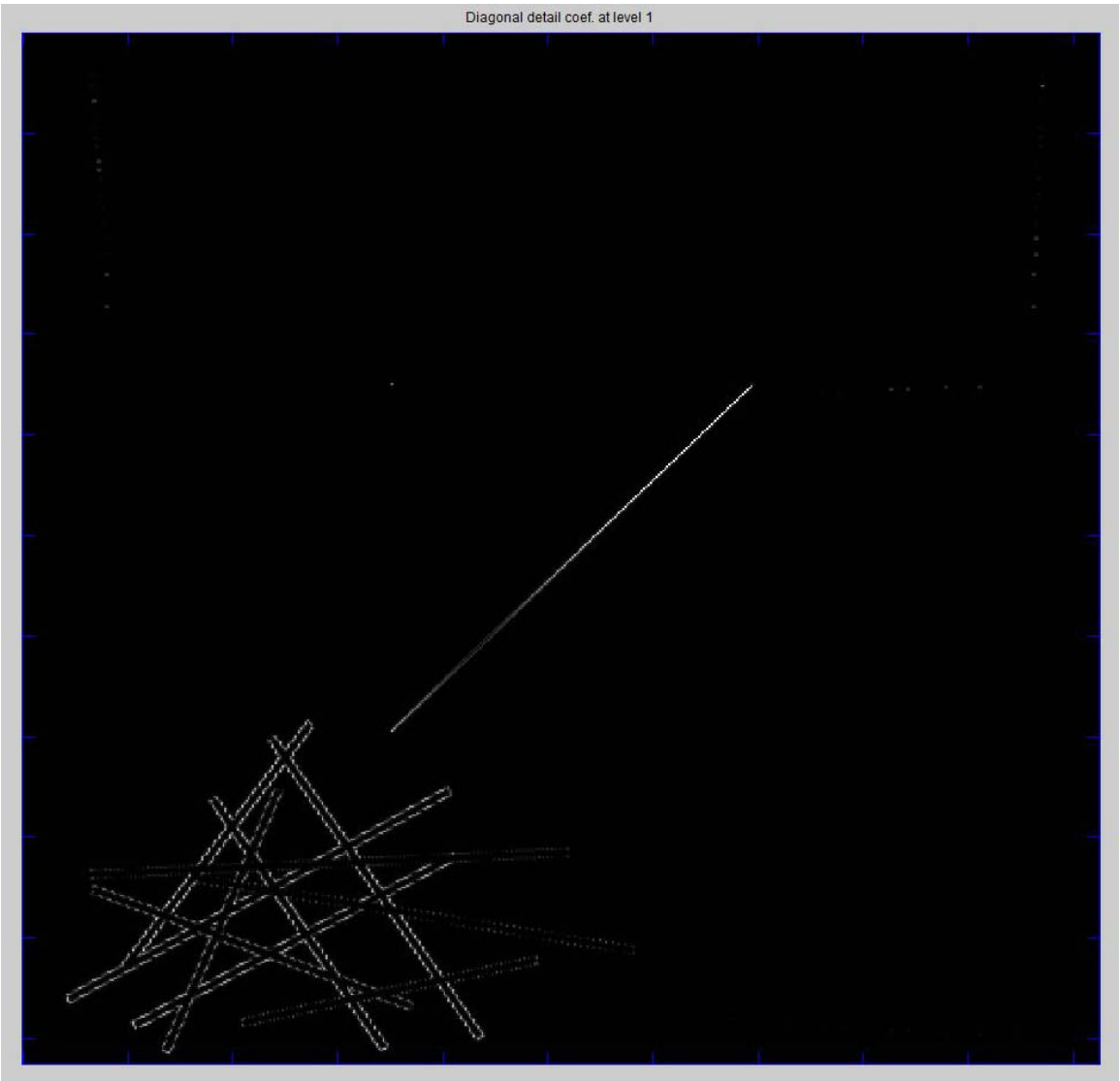

Figure 26. First level diagonal detail coefficient image of the Coiflets wavelet transform of the test target image.

The Symlets wavelet function, shown in the lower left of Figure 22, is also a fast changing function, but unlike the Meyer, Coiflets or Haar wavelet functions it is not symmetrical. It is sensitive to signals that are non-symmetrical (e.g., it might pick up piles of debris where there is a smooth edge with a non-uniform, relatively wide signal shape, such as 3-tab shingles). Figures 27 and 28 show the five level Symlets decomposition image of the test target and the first level diagonal detail Symlets wavelet transform image.

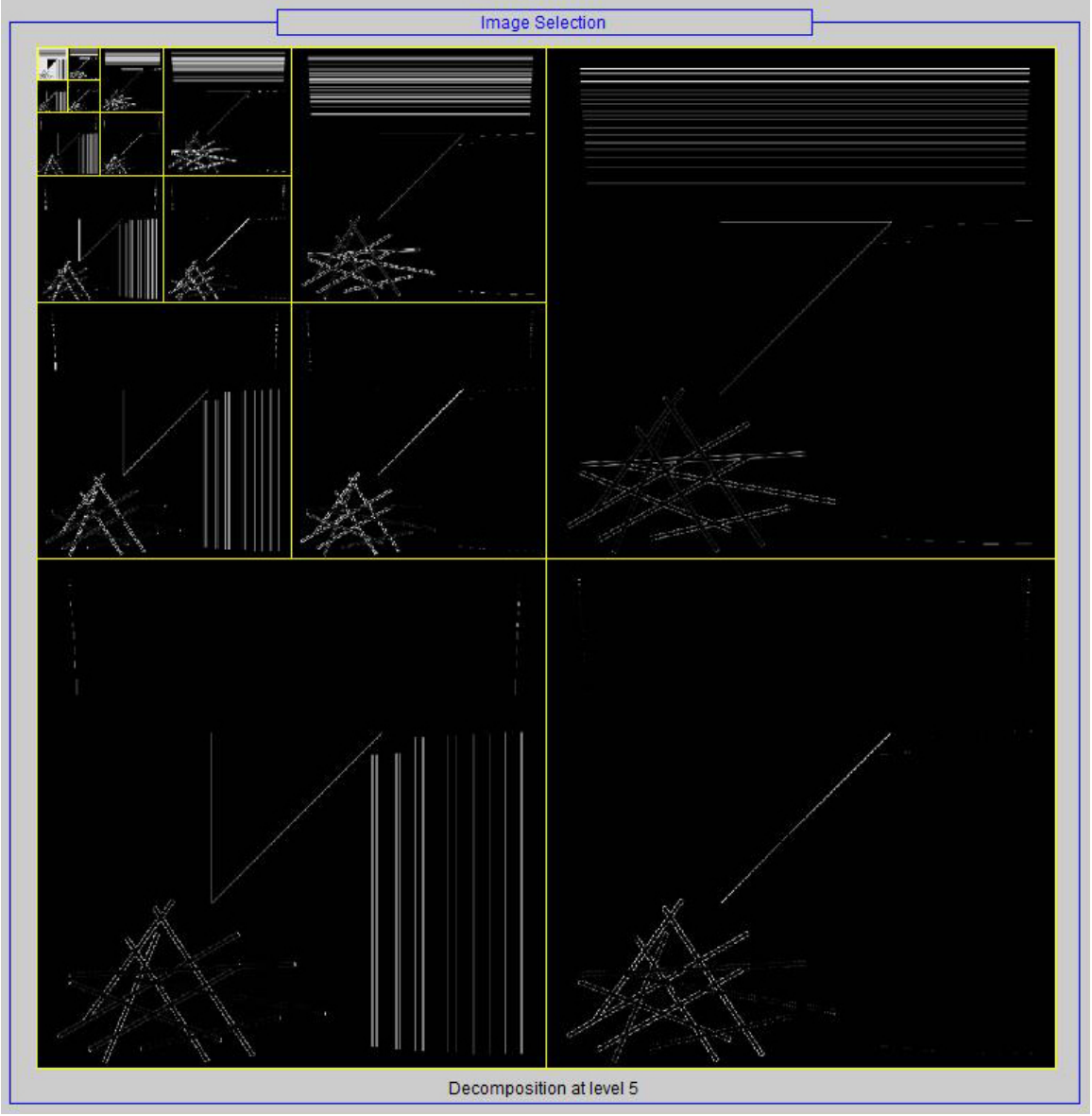

Figure 27. Five level Symlets wavelet transform decomposition of the test target image.

Figure 28. First level diagonal detail coefficient image of the Coiflets wavelet transform of the test target image.

Urban classification performance is increased when Haar wavelet coefficients are used in combination with the traditional spatial LOG, SHAN, and ENG indices (Myint and Mesev 2012). Wavelet analysis provides insight into trends, discontinuities, and self-similarity beyond the capability of other approaches such as Fourier analysis or windowed Fourier analysis (Misiti et al. 2011). Storm winds and surge cause changes on the landscape that are higher

frequency than the undamaged landscape (e.g., buildings are decomposed from a single structure to many component parts). Wavelet mother functions were chosen for analysis that has strong edge and high frequency components to maximize the potential for identifying the high frequency spatial signature of post storm landscapes. Myint found good success using the Haar wavelet mother function on urban imagery (Myint 2001). The upper left quadrant of figure 22 shows the Haar mother function (also known as the Daubechies1 mother function). Other wavelet mother functions investigated in this research include the Meyer (Figure 22 upper right), the Symlet2 (Figure 22 lower left) and the Coiflets1 (Figure 22 lower right).

Each 78 x 78 meter (256 x 256 foot) image sample for each storm was wavelet transformed using MatLab and Wavelet Toolbox software. In addition to five-level wavelet transformations with each mother wavelet of each image sample, the signal mean, signal standard deviation and ENG index was calculated for each image sample and each transformed image sample. Haar wavelet transformation combined with ENG index was found by Myint to provide the highest classification accuracy for urban areas when compared with Haar wavelet transform compared with the LOG and SHAN index (Myint and Mesev 2012).

ENG, energy or the angular second momentum is equal to the absolute value of the sum of the rows and columns of the coefficients in a sample image, divided by the product of the number of rows and columns, where c(I, j) is a

wavelet coefficient of a sub-image, or sample, with M rows and N columns at I, j at one level.

$$ENG = \left(\frac{1}{M * N}\right) \sum_{i=1}^{M} \sum_{j=1}^{N} |c(i,j)|$$

ENG can be thought of as a measure of how well the wavelet transform matches the signals in the sample image. When the wavelet function and the image match, the wavelet transform value will be high at that position in the image. ENG provides a measure of how well the wavelet function at that scale matches the image overall.

Five level Meyer, Symlets, and Coiflets wavelet transforms were also performed on each image sample in addition to five-level Haar wavelet transforms. The image and transformed image calculations yielded 242 independent variables as input for the discriminant analysis. A complete list and description of all 242 independent variables appears in Appendix B. The independent variables include sample image signal mean, sample image signal standard deviation, and wavelet transform coefficients image-based coefficients for Haar, Meyer, Symlets and Coiflets mother wavelet functions. Each wavelet transform mother and level results in the following coefficients: approximation mean, approximation standard deviation, approximation ENG index, horizontal mean, horizontal standard deviation, horizontal ENG index, vertical mean, vertical standard deviation, vertical ENG index, diagonal mean, diagonal standard deviation, and diagonal ENG index.

CHAPTER IV

RESULTS AND DISCUSSION

Statistical Analysis

Discriminant analysis is valuable for investigating differences between groups or categories and is used to identify which independent variables contribute most to explaining the variability between groups. Discriminant analysis optimizes equations to minimize the variability within groups while maximizing the variability between groups (Burns and Burns 2008). The first question asked in this research is if wavelet processed overhead imagery can identify post storm damage categories. FEMA's remote sensing damage assessment maps were used as damage category references for the hurricane storms. The National Weather Service's damage assessment was used as the damage category reference for the Joplin tornado. The University of Alabama's Center for Advanced Public Safety created a ground survey-based damage assessment for the Tuscaloosa tornado, which was used as the category reference it. These category reference maps informed the identification of the damage condition of post storm sample images. The independent variables resulting from the wavelet transformation of each image sample were inputs into discriminant analyses along with the damage condition identified from the damage category reference maps.

The independent variables for each storm, and combinations of storms, were analyzed using discriminant analysis in SPSS statistical analysis software. Hurricane samples were combined and discriminant analyses performed to

assess the accuracy of damage category prediction with samples from individual hurricane and combinations of hurricane image sample data sets. Discriminant analysis was performed on the following hurricane data sets: Ike, Rita, Katrina, Ivan, Ike and Rita, Ike and Katrina, Ike and Ivan, Rita and Katrina, Rita and Ivan, Katrina and Ivan, Ike and Rita and Katrina, Ike and Rita and Ivan, Ike and Katrina and Ivan, Rita and Katrina and Ivan, and Ike and Rita and Katrina and Ivan. Table 2 shows the hurricane data set combinations analyzed with discriminant analysis. The table is sorted in descending order of accuracy performance, with the top row (Ike sample data) showing the highest percent of original cases correctly classified by the discriminant analysis. The last row (Rita sample data) shows the lowest accuracy performance. The green filled cells indicate what storm samples were included in the analysis that is summarized in the columns to the right for that row. For example, the third row has the cells in the Ike and Katrina columns colored green, indicating that the discriminant analysis results to the right in that row are for the instance where image samples from Ike and Katrina informed the discriminant analysis. Table 2 columns list the percent of variability explained by discriminant functions 1 and 2, the percent of the input samples correctly classified and the percent of cross-validated cases that were correctly classified.

Table 2

Hurricane data sets analyzed with discriminant analysis, percent variation in samples explained by discriminant functions 1 and 2, percent of cases correctly classified, and percent of cross-validated cases correctly classified.

Ike (2008)	Rita (2005)	Katrina (2005)	Ivan (2004)	percent variation explained by DF 1 and 2	percent original cases correctly classified	percent cross-validated cases correctly classified
X				99.2	89.5	88.7
		X		98.8	84.7	82.3
X		X		97.7	76.6	76.2
X		X	X	92.7	71.7	70.8
			X	89.6	76.4	75.2
		X	X	86.3	75.3	73.9
X	X	X	X	82.6	67.6	66.7
X	X	X		82.4	73.7	72.5
X	X			80.5	77.2	75.7
			X	78.0	72.5	71.4
X	X		X	75.3	69.4	68.2
	X	X	X	74.5	69.1	67.4
	X	X		73.6	77.8	75.7
	X		X	70.4	69.6	67.5
	X			69.9	86.0	84.7

The statistical analyses for all combinations are based on independent variables extracted from post storm imagery using wavelet transformation of the image samples. Each image sample is wavelet transformed to five levels with each of the four wavelet functions examined (Coiflets, Haar, Meyer, Symlets). Appendix B lists all the independent variables. The Haar and Symlets wavelet

functions are edge detectors. The Haar function senses or is similar to sharp edges and will identify increased edges in a sample scene due to storm damage. The Symlets function is similar to the Haar in that it will return a low result for constant image areas and a higher result for areas in the image with edges. The difference between Haar and Symlets in this application is that the Symlets function senses or is more similar to relatively fast changing edges. Where the Haar function is a single edge the Symlets function begins with a fast reduction from zero followed by a fast increase with a final fast reduction back to zero. The Meyer and Coiflets functions will sense or are similar to fast changing scene content with two closely spaced edges such as lumber or tree branch debris. The literature does not yet contain a reference library of the spatial content of storm damaged areas. Without apriori knowledge of the spatial nature of storm damaged areas a suite of wavelet functions at five levels are used as independent variable to investigate the general capability of this approach. A valuable future research area is to identify average or characteristic damage images for spatial characterization.

Hurricane Ike

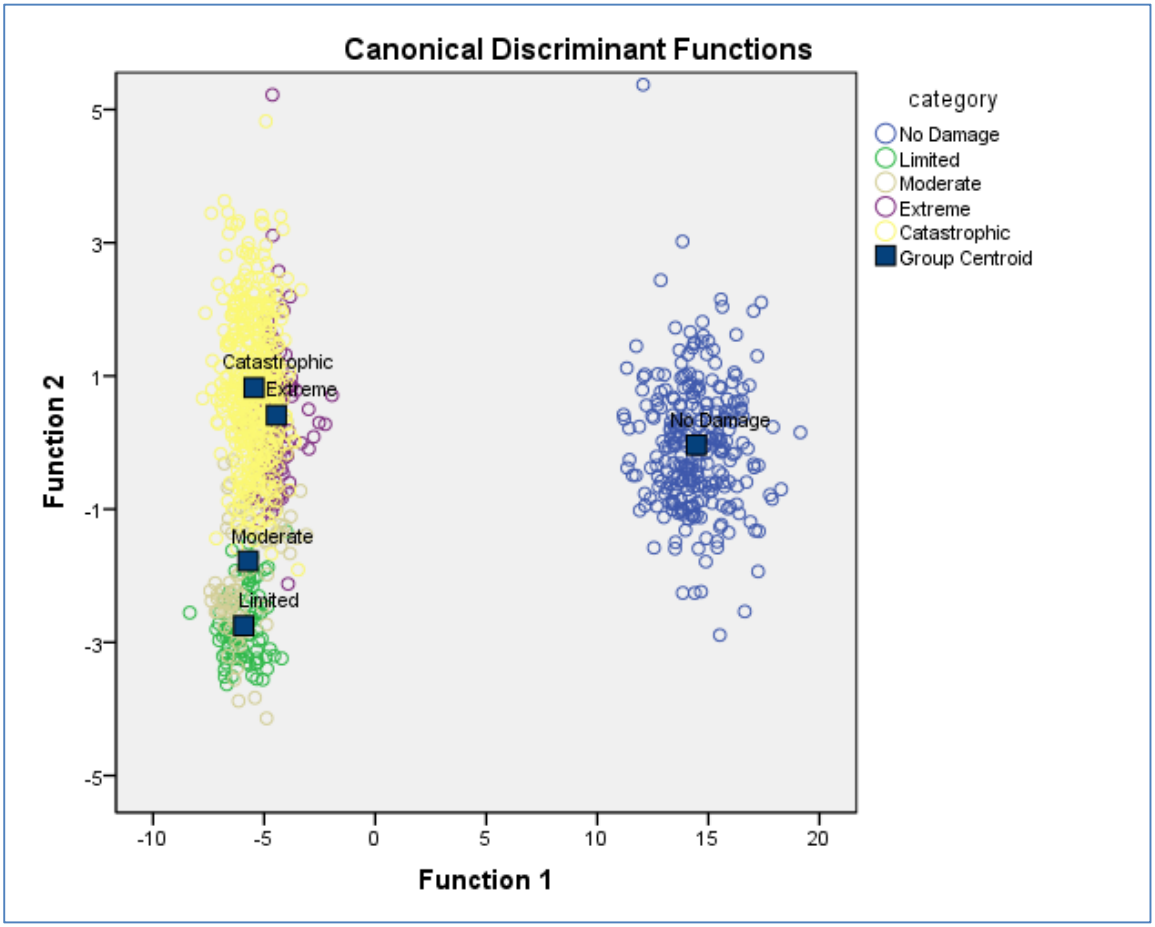

Figure 29. Hurricane Ike sample groups plotted against canonical discriminant functions 1 and 2. Discriminant functions 1 and 2 account for 99.2percent of the total variance in the Hurricane Ike image sample data set.

This discriminant analysis (see Figure 29 for discriminant function plot showing significant canonical discriminant at 95 percent confidence level) answers question 1 (can wavelet processed post storm overhead imagery identify areas of residential damage) affirmatively if the null hypothesis is rejected at the 95 percent confidence level. The null hypothesis is that wavelet transform classification does not discriminate among FEMA damage assessment categories (no discernible damage, limited damage, moderate damage,

extensive damage, catastrophic damage). Wilk's Lambda tests differences of means and shows which variables' contributions are significant. The value of Lambda ranges between 0 and 1. Lambda values close to 0 indicates group means differ. Lambda values close to 1 indicates group means are the same. The Wilk's Lambda results for Hurricane Ike samples in Table 3 indicate that the group means are different for discriminant functions 1 and 2 at the 95percent confidence level (significance less than 0.05). The other rows in the Wilk's Lambda table show the contribution and significance of the twenty seven independent variables contributing to discriminant functions 1 and 2 for the Hurricane Ike discriminant analysis. Therefore, the null hypothesis associated with question 1 is rejected. Significance levels for all statistical tests are reported at the 0.05 level.

Based on post hurricane Ike imagery, the answer to research question 1 is yes, wavelet transform processed post storm imagery identifies areas of residential damage. Analysis of the other storms examined reveal that for all storms, wavelet transform processed imagery identifies areas of residential damage, albeit with classification accuracies as low as 66.7percent and as high as 88.7percent (percent of cross-validated cases correctly classified).

Ike's DF1 and DF2 plot (Figure 29) shows a distinct, free throw type, shape with the no damage samples clearly separated from all categories of damage samples. This separation is accomplished primarily by DF1, which explains 97.7 percent of the variability. DF2 only explains 1.6 percent of the variability. This suggests that the no damage samples are more different from all

the damage classes than all the variation between the damage samples. The vagueness of the damage definitions and the variability in visual interpretation of damaged areas may account for this large difference. The centroid of the no damage samples is 20 units from the centroids of all the damage classes centroids while the centroids of the damage classes are separated only by 4 units. The top 20 percent (6 of 27) of the discriminant coefficients for DF1 and DF2 (by absolute value) show two coefficients in common among DF1 and DF2, level 1 Meyer vertical ENG and level 1Haar horizontal ENG. DF1 contained all 4 wavelet functions considered at level 1 and the ENG coefficient for 5 of these 6 coefficients. In contrast, DF2 coefficients are composed of Haar, Coiflet and Meyer coefficients. These appeared at levels 2, 2, 4, 1, 1, and 1, from largest to smallest. The largest factor discriminating damage from no damage areas in DF1 is the Meyer level 1 diagonal ENG coefficient with a value approximately twice larger than the other top 6 DF1 factors.

Table 3

Wilk's Lambda results for Hurricane Ike discriminant analysis samples.

						Exact F				Approximate F			
Stp	**#Var**	**Lmbd**	**df1**	**df2**	**df3**	**Stat**	**df1**	**df2**	**Sig.**	**Stat**	**df1**	**df2**	**Sig.**
1	1	.061	1	4	1003	3848	4	1003	.000				
2	2	.031	2	4	1003	1169	8	2004	.000				
3	3	.021	3	4	1003					726.920	12	2648.689	.000
4	4	.017	4	4	1003					536.432	16	3055.688	.000
5	5	.013	5	4	1003					453.254	20	3314.258	.000
6	6	.009	6	4	1003					406.289	24	3482.816	.000
7	7	.009	7	4	1003					352.617	28	3596.157	.000
8	8	.007	8	4	1003					319.360	32	3674.662	.000
9	9	.007	9	4	1003					293.308	36	3730.463	.000
10	10	.006	10	4	1003					270.750	40	3770.987	.000
11	9	.006	9	4	1003					302.985	36	3730.463	.000
12	10	.005	10	4	1003					278.260	40	3770.987	.000
13	11	.005	11	4	1003					254.774	44	3800.924	.000
14	12	.005	12	4	1003					236.377	48	3823.326	.000
15	13	.005	13	4	1003					219.904	52	3840.237	.000
16	14	.005	14	4	1003					205.759	56	3853.061	.000
17	15	.004	15	4	1003					193.544	60	3862.786	.000

Table 3 (continued).

						Exact F				Approximate F			
Stp	**#Var**	**Lmbd**	**df1**	**df2**	**df3**	**Stat**	**df1**	**df2**	**Sig.**	**Stat**	**df1**	**df2**	**Sig.**
18	16	.004	16	4	1003					182.741	64	3870.122	.000
19	17	.004	17	4	1003					173.090	68	3875.586	.000
20	18	.004	18	4	1003					164.385	72	3879.567	.000
21	19	.004	19	4	1003					156.589	76	3882.357	.000
22	20	.004	20	4	1003					150.009	80	3884.179	.000
23	21	.004	21	4	1003					143.952	84	3885.208	.000
24	22	.004	22	4	1003					138.229	88	3885.581	.000
25	23	.004	23	4	1003					132.966	92	3885.407	.000
26	24	.004	24	4	1003					128.171	96	3884.773	.000
27	25	.003	25	4	1003					123.504	100	3883.749	.000
28	26	.003	26	4	1003					119.188	104	3882.393	.000
29	27	.003	27	4	1003					115.225	108	3880.753	.000

Tests of equality of group means, high F and low Wilk's Lambda, indicate significant difference between groups. Classification accuracy for Ike is 89.5 percent of original grouped cases correctly classified and 88.7 percent of cross-validated grouped cases correctly classified (shown in Table 4). Near perfect classification for no damage (100 percent) and catastrophic damage (92.4 percent) categories suggests accurate predictive ability for these categories.

Sixty-five to 78 percent correct classifications for limited, moderate and extreme categories might be attributed to the poor definition of the categories in that they are not clear nor are they clearly mutually exclusive. The poor category definitions, with respect to application from remotely sensed imagery, are a contributor to confusion among damage categories. Wilk's Lambda results for the other cases analyzed answer question 1 in the same way with similar significance, though with different sets of independent variables and differing levels of accuracy.

Ike's discriminant analysis yielded a discriminant function with 27 coefficients. Level 1 coefficients include ENG or standard deviation of diagonal, horizontal and vertical detail for all four wavelet functions. This suggests that the image sample contents at level one are a mixture of edges and fast changing signals indicative of storm damage and debris. Level 2 coefficients include ENG and standard deviation of diagonal, horizontal and vertical detail for Haar, Meyer and Symlets functions. At this level there continue to be a mixture of fast changing image contents for damaged areas. Levels 3 through 5 contain fewer coefficients, with six at level 3 and three coefficients at level 4 and 5. Level 3 continues to be composed of Haar, Meyer and Symlets coefficients. Level 4 contains only one Coiflets coefficient and two Symlets coefficients. Level 5 contains two Haar coefficients and one Symlets coefficient.

Ike's DF 1 and 2 plot shows separation between no damage and the other damage categories. This indicates that the image samples of no damage are significantly different in their spatial frequency content from all the damage

categories. The samples in the damage categories show a general tight linear layout with near catastrophic and extreme group means separated from the closely spaced limited and moderate group means. The lack of implementable category definitions and the potential variability in the visual interpretation of the damage categories may account for the tight grouping of the damage categories clearly separated from the no damage category.

Figure 30 shows an ideal classification accuracy bar chart. This chart represents 100 percent accurate classification of all samples in all categories. The canonical discriminant function plots and classification results for the remaining hurricane storms are shown in Figures 32 through 37, Tables 5 through 7 below, and Appendix C. The classification results of hurricane combinations appear in Appendix C.

Table 4

Classification results of the discriminant analysis performed on the 1,008 Hurricane Ike image samples.

			Predicted Group Membership					
		category	**No Dmg**	**Limited**	**Moderat**	**Extreme**	**Cat**	**Total**
Original	Count	No Dmg	274	0	0	0	0	274
		Limited	0	67	18	0	1	86
		Moderate	0	0	70	0	24	94
		Extreme	0	0	4	71	30	105
		Cat	0	1	11	17	420	449
	percent	No Dmg	100.0	.0	.0	.0	.0	100.0
		Limited	.0	77.9	20.9	.0	1.2	100.0
		Moderate	.0	.0	74.5	.0	25.5	100.0
		Extreme	.0	.0	3.8	67.6	28.6	100.0
		Cat	.0	.2	2.4	3.8	93.5	100.0
Cross-validated[a]	Count	No Dmg	274	0	0	0	0	274
		Limited	0	67	18	1	0	86
		Moderate	0	0	69	0	25	94
		Extreme	0	0	5	69	31	105
		Cat	0	1	17	16	415	449
	percent	No Dmg	100.0	.0	.0	.0	.0	100.0
		Limited	.0	77.9	20.9	1.2	.0	100.0
		Moderate	.0	.0	73.4	.0	26.6	100.0
		Extreme	.0	.0	4.8	65.7	29.5	100.0
		Cat	.0	.2	3.8	3.6	92.4	100.0

a. Cross validation is done only for those cases in the analysis. In cross validation, each case is classified by the functions derived from all cases other than that case.

b. 89.5 percent of original grouped cases correctly classified.

c. 88.7 percent of cross-validated grouped cases correctly classified.

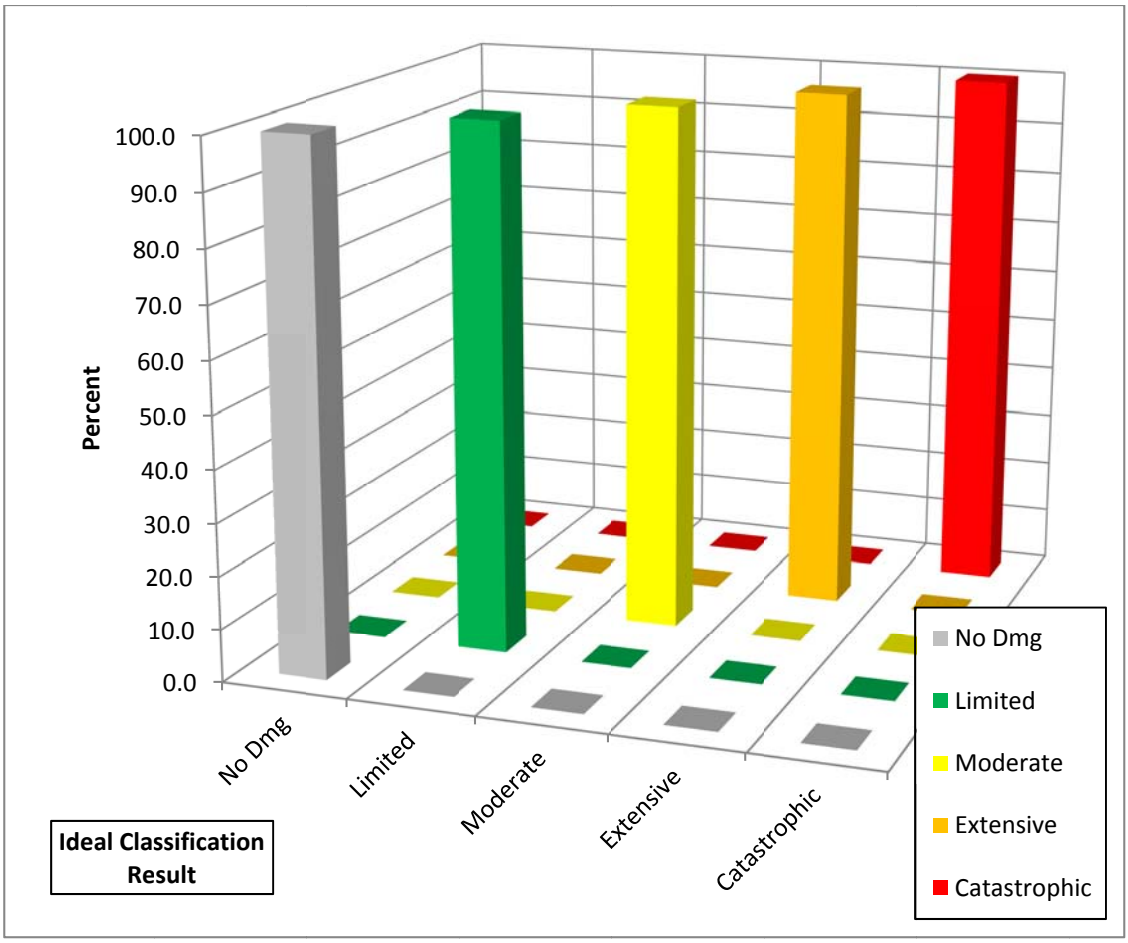

Figure 30. Ideal classification accuracy bar chart. The ideal case of percent of correctly classified samples is plotted below. If all the samples from each case are correctly classified the chart will show 100percent bars along the diagonal. Variations from this configuration show the distribution of how samples from each category are classified by the discriminant analysis.

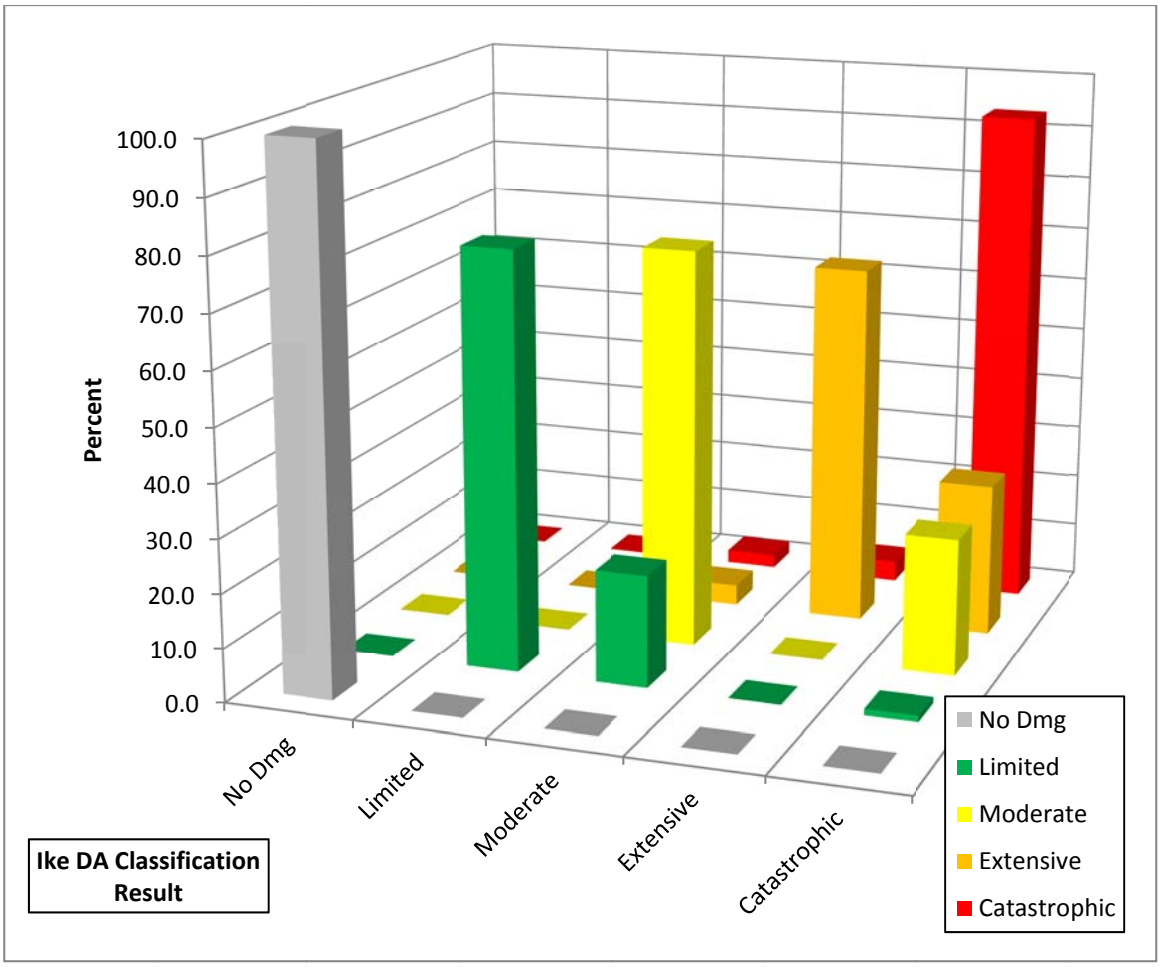

Figure 31. Classification accuracy bar chart for hurricane Ike classification results. The discriminant analysis of hurricane Ike samples shows good discrimination between the damage groups and, high accuracy of classification. Errors appear in the classification of some of the damage samples in adjacent or higher level damage categories.

The classification accuracy bar chart for the hurricane Ike discriminant analysis shows (Figure 31) accurate discrimination between groups. All the no damage categories are classified correctly and most (93.5 percent) of the catastrophic damage samples are correctly classified. Errors appear in the classification of limited, moderate and extensive damage category samples. Approximately 22 percent of the limited damage category samples are classified

by the discriminant analysis in the moderate damage category. Approximately 26 percent of the moderate damage category samples are classified by the discriminant analysis in the catastrophic damage category. Approximately 42 percent of the extensive damage category samples are classified as either catastrophic or moderate damage. A few of the catastrophic damage category samples are classified by the discriminant analysis as extensive, moderate or limited damage. Overall the shape of the classification accuracy bar chart shows that the damage categories are accurately discriminated. The misclassifications in the damage categories might be explained by the difficulty of correctly classifying damaged areas near the boundaries of damage categories. For example, an area of damage near the boundary between extensive and catastrophic damage could be classified by visual interpretation to either category. The definition of extensive damage is “some solid structures are destroyed; most sustain exterior and interior damage (e.g., roofs missing, interior walls exposed), most mobile home and light structures are destroyed.” (Gabe 2005) The definition of catastrophic damage is “most solid and all light or mobile structures destroyed.” (Gabe 2005) If the area covered by a sample contains only solid structures it is difficult to determine the difference between some solid structures destroyed and most solid structures destroyed. Similar potential overlap exists between all the damage categories used by FEMA except for the no damage category. The overlap in sample points among the limited, moderate, extensive and catastrophic categories in the canonical discriminant functions 1 and 2 plot (Figure 29) suggests that the discriminant analysis accurately

separates no damage from the damage categories, however it also shows overlap among the damage categories that might be attributed to category definition vagueness. This is also suggested by the nearness of the group centroids of the limited and moderate damage categories and the extreme and catastrophic categories. These pairs of adjacent damage category sample points are separated from each other and from the no damage category, further supporting the idea that the category definitions, or their implementation, are less than unambiguous.

Hurricane Rita

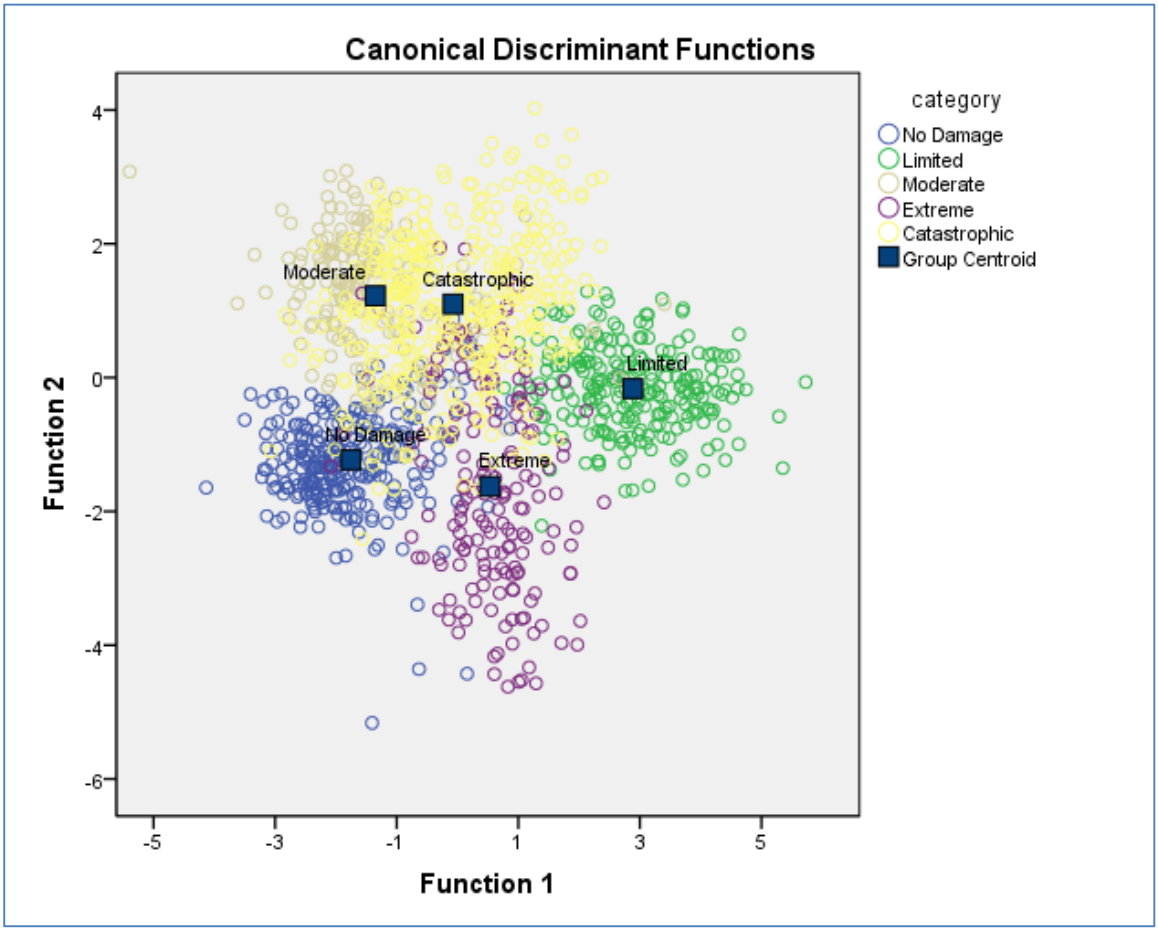

Figure 32. Hurricane Rita sample groups plotted against canonical discriminant functions 1 and 2. Discriminant functions 1 and 2 account for 69.9 percent of the total variance in the Hurricane Rita image sample data set.

Figure 32 and Table 5 show the discriminant function 1 and 2 plot and the classification accuracy results. Figure 33 shows the Rita classification bar chart. Separation of group means between all categories indicates accurate category differentiation. Overlap between category samples remains and includes noticeable overlap among the no damage and the catastrophic and extreme categories. Rita's discriminant analysis resulted in 44 coefficients in the discriminant function. Of the 20 possible combinations of 5 levels and 4 wavelet

functions, five were without a coefficient, Level 1 contains 19 coefficients spread among Coiflets, Haar, Meyer and Symlets wavelet functions. The number of coefficients in the remaining levels drops precipitously with only nine, five, two, and eight coefficients in levels 2 through 5. The large number of coefficients in level one indicates significant complexity at higher spatial resolution in the Rita data. The reduced number of coefficients at higher levels indicates reduced complexity at lower spatial frequencies. Rita's significant quantity of open water, wetland and undeveloped areas, which are intrinsically low spatial frequency land cover areas, explains the relatively few higher level coefficients.

The shape of the DF 1 and 2 plot in the form of separated categories with random appearing variance suggests that the differences between no damage and damage categories are not unique. Unlike Ike and Katrina, which display a grouping among the damage categories and a separation of the no damage category from all the damage categories, Rita's distribution of group centroids shows a similar separation among all the categories. This may be due to Rita's landscape being relatively uniform (94.4 percent open water or wetlands). A comparison of the top 20 percent of Rita coefficients (9 of 44) reveals three coefficients in common between DF1 and DF2 (level 1 Haar diagonal ENG, level 1 Symlet horizontal ENG, and level 1 Symlet diagonal ENG). DF1 explains 46.2 percent of the variability while DF2 explains 23.7 percent of the variability. The range of distribution of the class centroids is approximately the same for DF1 and DF2 (10 units in either direction). In contrast to Ike and Katrina, this random

appearing spread of samples within each class and among the classes suggests that the differences between classes are similar.

Table 5

Classification results of the discriminant analysis performed on the 1,298 Hurricane Rita image samples.

			Predicted Group Membership					
		category	**No Dmg**	**Limited**	**Moderat**	**Extreme**	**Cat**	**Total**
Original	Count	No Dmg	255	1	2	7	20	285
		Limited	0	223	0	1	16	240
		Moderate	7	5	158	0	20	190
		Extreme	6	1	0	130	40	177
		Cat	25	5	16	10	350	406
	percent	No Dmg	89.5	.4	.7	2.5	7.0	100.0
		Limited	.0	92.9	.0	.4	6.7	100.0
		Moderate	3.7	2.6	83.2	.0	10.5	100.0
		Extreme	3.4	.6	.0	73.4	22.6	100.0
		Catastrophic	6.2	1.2	3.9	2.5	86.2	100.0
Cross-validated[a]	Count	No Dmg	253	1	2	9	20	285
		Limited	0	222	0	1	17	240
		Moderate	9	6	153	1	21	190
		Extreme	6	4	0	126	41	177
		Cat	26	6	18	11	345	406
	percent	No Dmg	88.8	.4	.7	3.2	7.0	100.0
		Limited	.0	92.5	.0	.4	7.1	100.0
		Moderate	4.7	3.2	80.5	.5	11.1	100.0
		Extreme	3.4	2.3	.0	71.2	23.2	100.0
		Cat	6.4	1.5	4.4	2.7	85.0	100.0

a. Cross validation is done only for those cases in the analysis. In cross validation, each case is classified by the functions derived from all cases other than that case.

b. 86.0 percent of original grouped cases correctly classified.

c. 84.7 percent of cross-validated grouped cases correctly classified.

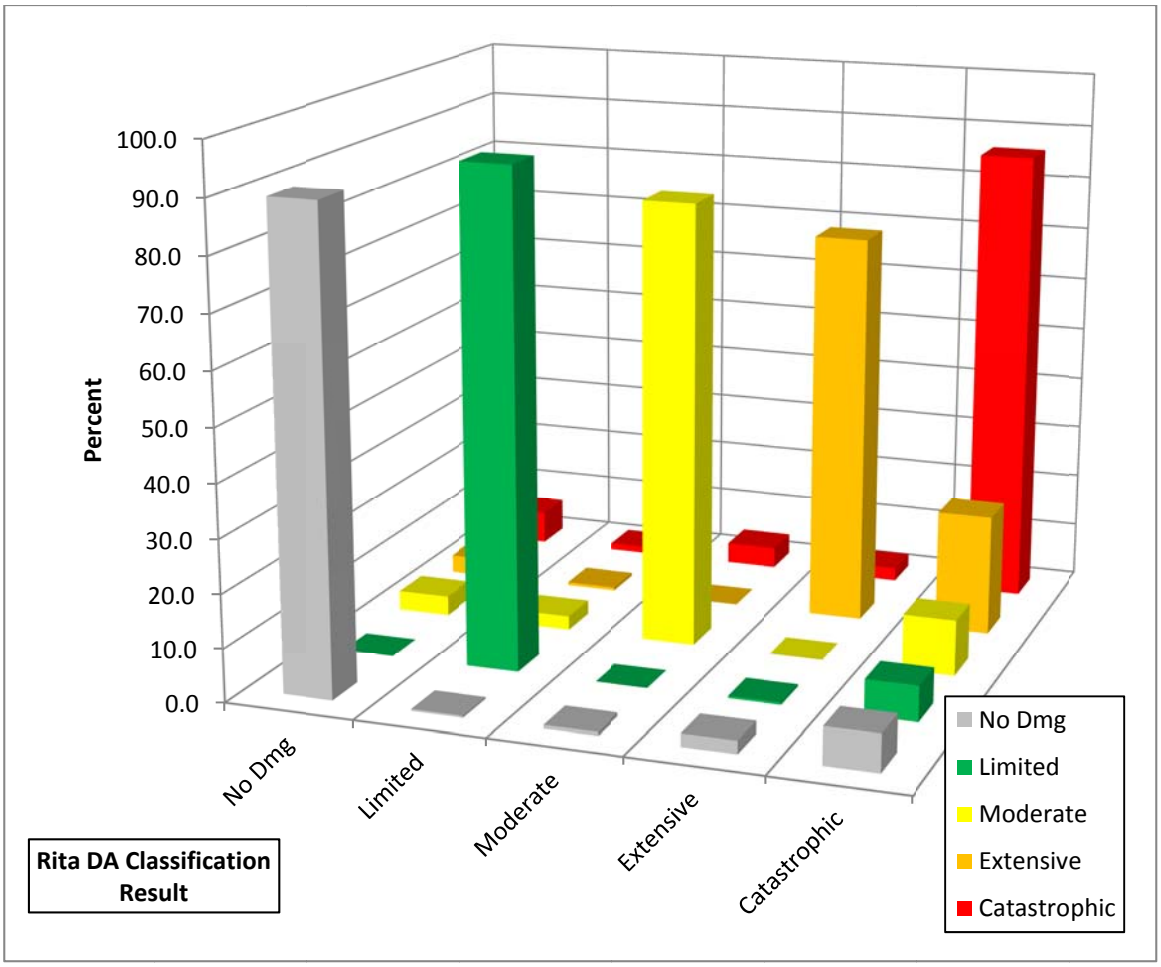

Figure 33. Classification accuracy bar chart for hurricane Rita classification results. The discriminant analysis of hurricane Rita samples shows good discrimination between the damage groups and relatively high accuracy of classification. Errors appear in the classification of some of the samples from all the groups being classified as catastrophic damage.

The discriminant analysis of the hurricane Rita samples shows separation of damage groups between all the groups (see Figure 32 for the discriminant functions 1 and 2 plot) and accurate classification of samples. A few of the samples from all the groups are incorrectly classified as catastrophic damage. The land cover for the area experiencing Rita's category 1 or greater winds is predominantly open water and wetlands (94.4 percent). The most extreme

hurricane damage near the coast can render the landscape similar to open water or wetland, which may account for the misclassification of some samples from all the groups into the catastrophic category.

Hurricane Katrina

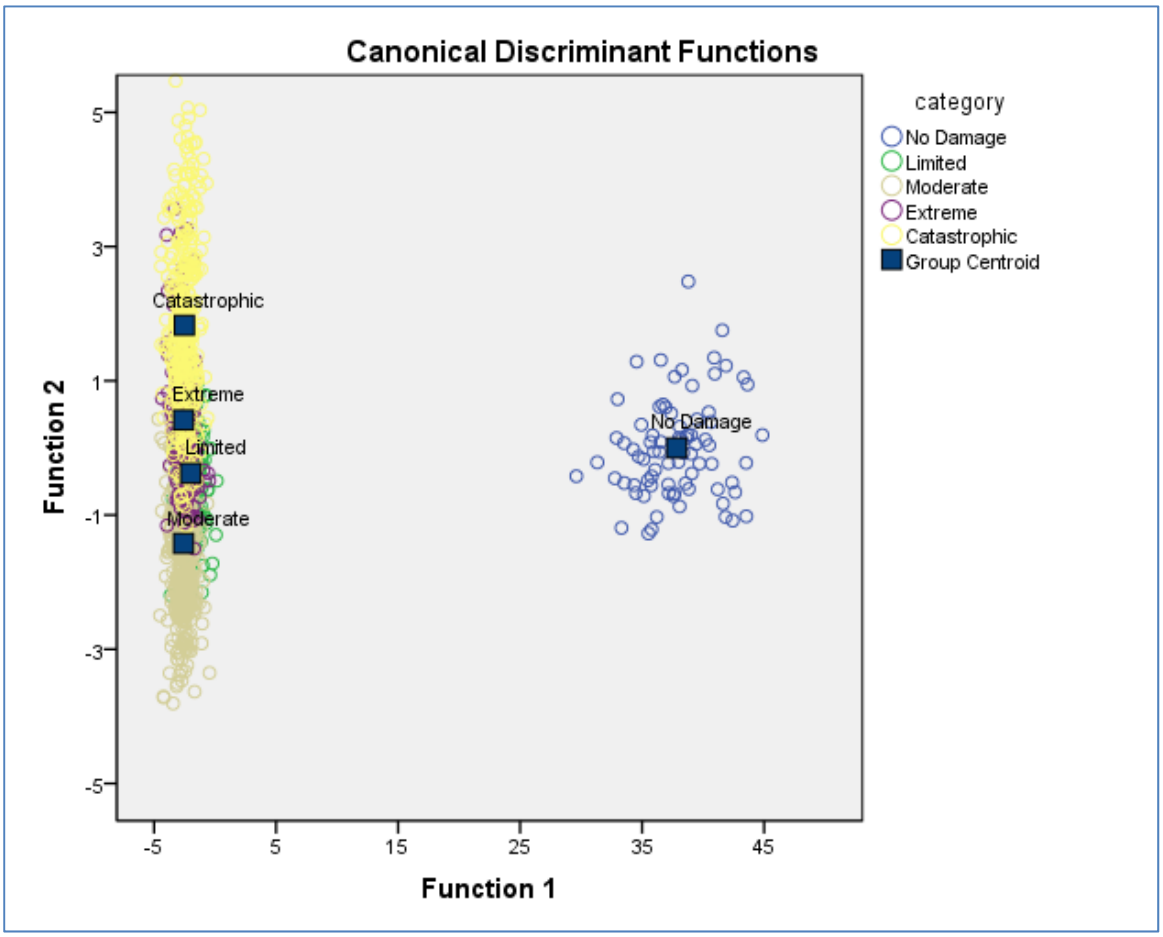

Figure 34. Hurricane Katrina sample groups plotted against canonical discriminant functions 1 and 2. Discriminant functions 1 and 2 account for 98.8percent of the total variance in the Hurricane Katrina image sample data set.

Separation of group means indicates accurate category discrimination. Katrina's discriminant analysis resulted in forty five coefficients in the discriminant function. Of the twenty possible combinations of 5 levels and 4 wavelet functions, only four were without a coefficient, Haar and Meyer level 4 and Haar and

Symlets level 5. The wavelet functions sense or are similar to image features as in and described under Hurricane Ike above. The large number of level 1 (18) and level 2 (14) coefficients suggests that Katrina's damage is heavily weighted with higher frequency (faster changing) spatial features. This large amount of debris on damaged property (e.g., large debris piles along the coast in the catastrophic damage areas) agrees with the notion that a large number of level 1 and 2 coefficients indicated large quantities of debris resulting from this storms impact. The separation between the no damage and the damage categories in Katrina is similar to Ike. However, Ike's discriminant function contained only 27 coefficients compared with the 45 Katrina coefficients. The similar discriminant function 1 and 2 plots of Katrina and Ike might suggest the damage from these storms is similar. However Katrina's almost twice as many coefficients suggests more complexity in the spatial content of the remotely sensed imagery from this storm.

Katrina's DF1/DF2 plot (figure 34) shows a distribution within classes and among the classes is similar to Ike's distribution. The no damage class is widely separated from the other classes. The damage classes appear to be vertically aligned with statistically significant separation among the damage class centroids. The damage classes are separated much less than they all are from the no damage class (10 units versus 50 units). As with Ike, Katrina's top 20 percent of coefficients (9 of 45) DF1 and DF2 show only level one coefficients for DF1 with a mix of levels for DF2, suggesting high resolution features clearly

discriminate between damage and no damage while damage categories require levels 1 and 2 transformations to separate the damage classes.

Table 6

Classification results of the discriminant analysis performed on the 1,292 Hurricane Katrina image samples.

			Predicted Group Membership					
		category	**No Dmg**	**Limited**	**Moderat**	**Extreme**	**Catastrophi**	**Total**
Original	Count	No Dmg	79	0	0	0	0	79
		Limited	0	172	12	10	7	201
		Moderate	0	26	420	15	9	470
		Extreme	0	16	14	126	18	174
		Catastrophi	0	19	17	35	297	368
	percent	No Dmg	100.0	.0	.0	.0	.0	100.0
		Limited	.0	85.6	6.0	5.0	3.5	100.0
		Moderate	.0	5.5	89.4	3.2	1.9	100.0
		Extreme	.0	9.2	8.0	72.4	10.3	100.0
		Catastrophi	.0	5.2	4.6	9.5	80.7	100.0
Cross-validated[a]	Count	No Dmg	79	0	0	0	0	79
		Limited	0	166	15	12	8	201
		Moderate	0	28	411	20	11	470
		Extreme	0	21	18	115	20	174
		Catastrophi	0	20	20	36	292	368
	percent	No Dmg	100.0	.0	.0	.0	.0	100.0
		Limited	.0	82.6	7.5	6.0	4.0	100.0
		Moderate	.0	6.0	87.4	4.3	2.3	100.0
		Extreme	.0	12.1	10.3	66.1	11.5	100.0
		Catastrophi	.0	5.4	5.4	9.8	79.3	100.0

a. Cross validation is done only for those cases in the analysis. In cross validation, each case is classified by the functions derived from all cases other than that case.

b. 84.7 percent of original grouped cases correctly classified.

c. 82.3 percent of cross-validated grouped cases correctly classified.

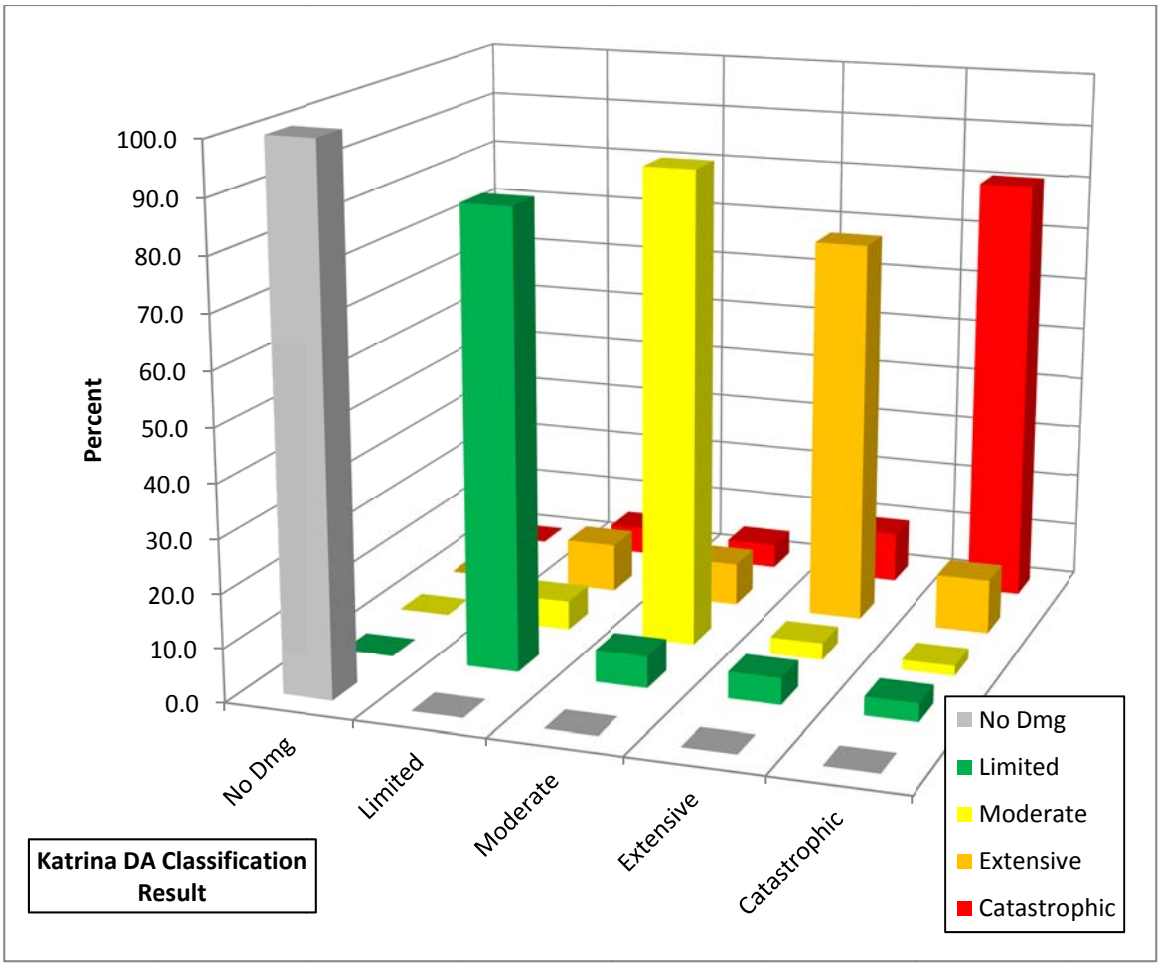

Figure 35. Classification accuracy bar chart for hurricane Katrina classification results. The discriminant analysis of hurricane Rita samples shows good discrimination between the damage groups and relatively high accuracy of classification.

Hurricane Ivan

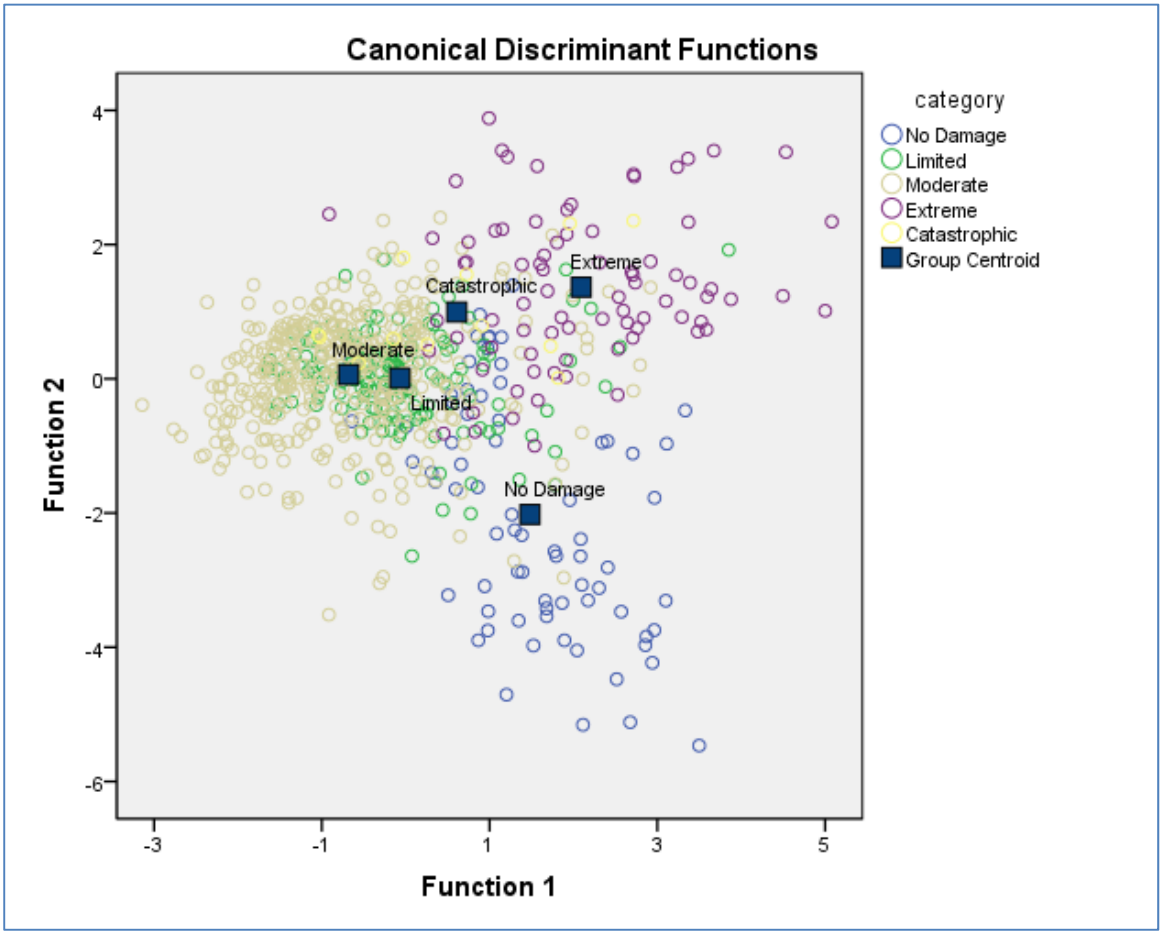

Figure 36. Hurricane Ivan sample groups plotted against canonical discriminant functions 1 and 2. Discriminant functions 1 and 2 account for 78.0 percent of the total variance in the Hurricane Ivan image sample data set.

Separation of group means between all categories indicates accurate category differentiation. Overlap between damage categories is similar to that seen with Rita, though Ivan's discriminant functions 1 and 2 plot shows a shape between Ike's well defined separation of the damage categories and the no damage category and Rita's random appearing distribution of samples around separated group means. Ivan's discriminant analysis resulted in eighteen coefficients in the discriminant function. Only 9 of the 20 possible combinations of

5 levels and 4 wavelet functions contained coefficients. As with the other three hurricanes, level 1 has the most coefficients which are spread among all four wavelet types. Levels 2 through 5 contain three, one, three and three coefficients respectively. Level 2 contains only Meyer coefficients (ENG and standard deviations). Level 3 contains a single coefficient for Haar (ENG). Level 4 contains 3 Haar coefficients (ENG and approximation mean). Level 5's three coefficients include ENG and standard deviation of the Coiflets function and ENG of the approximation for Haar.

The majority of coefficients fall in either Level 1 or in the Haar function category. Level 1 coefficients indicate high spatial frequency content. Haar indicates sharp edge image content. Ivan's DF1 DF2 plot shape is relatively shotgun shaped, similar to Rita's. An examination of the largest 20 percent (4 of 18) of Ivan's coefficients shows no pattern in the differences between DF1 and DF2 coefficients. DF1 explains 47.0 percent of the variability. DF2 explains 30.9 percent of the variability. The level 1 vertical Haar ENG coefficient appears in both DF1 and DF2 as does the level 1 vertical Symlet ENG coefficient. As with Rita and Joplin, high spatial frequency coefficients (level 1) dominate DF1 and DF2, with the top 20 percent of coefficients in both being composed of ENG coefficients.

Table 7

Classification results of the discriminant analysis performed on the 716 Hurricane Ivan image samples.

			Predicted Group Membership					
		category	**No Dmg**	**Limited**	**Moderat**	**Extreme**	**Catastrophi**	**Total**
Original	Count	No Dmg	44	7	19	2	1	73
		Limited	3	99	41	6	1	150
		Moderate	10	62	315	13	1	401
		Extreme	1	6	14	59	0	80
		Catastrophi	0	0	6	4	2	12
	percent	No Dmg	60.3	9.6	26.0	2.7	1.4	100.0
		Limited	2.0	66.0	27.3	4.0	.7	100.0
		Moderate	2.5	15.5	78.6	3.2	.2	100.0
		Extreme	1.3	7.5	17.5	73.8	.0	100.0
		Catastrophi	.0	.0	50.0	33.3	16.7	100.0
Cross-validated[a]	Count	No Dmg	44	7	19	2	1	73
		Limited	4	96	43	6	1	150
		Moderate	10	64	311	15	1	401
		Extreme	1	6	14	59	0	80
		Catastrophi	0	0	7	4	1	12
	percent	No Dmg	60.3	9.6	26.0	2.7	1.4	100.0
		Limited	2.7	64.0	28.7	4.0	.7	100.0
		Moderate	2.5	16.0	77.6	3.7	.2	100.0
		Extreme	1.3	7.5	17.5	73.8	.0	100.0
		Catastrophi	.0	.0	58.3	33.3	8.3	100.0

a. Cross validation is done only for those cases in the analysis. In cross validation, each case is classified by the functions derived from all cases other than that case.

b. 72.5 percent of original grouped cases correctly classified.

c. 71.4 percent of cross-validated grouped cases correctly classified.

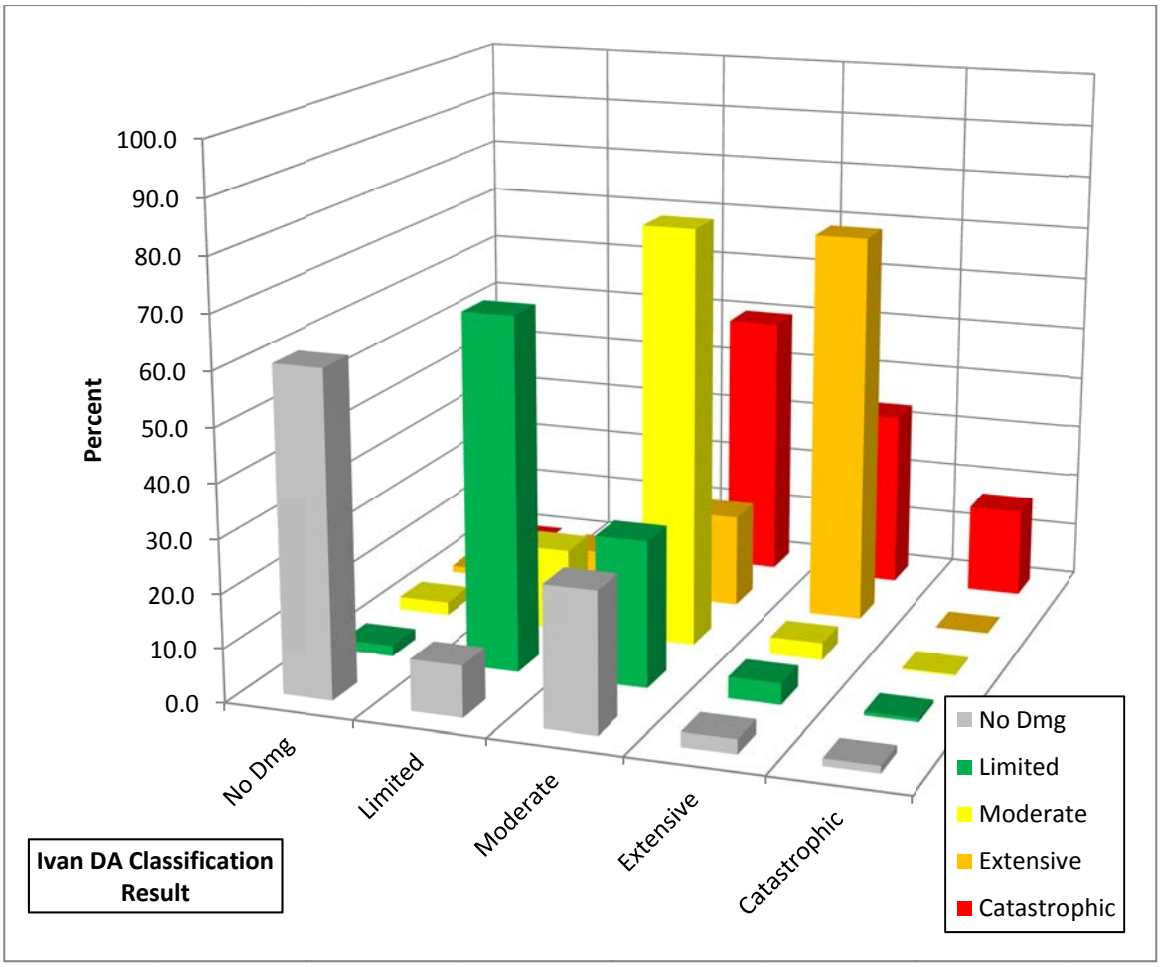

Figure 37. Classification accuracy bar chart for hurricane Ivan classification results. The discriminant analysis of hurricane Ivan samples shows statistically significant group discrimination, though accuracy of group classifications are relatively poor.

Hurricane Combination Discriminant Analysis Performance

The discriminant functions resulting from the discriminant analysis of the 15 combinations of the 4 sets of hurricane image samples (Ike, Rita, Katrina, and Ivan) are composed of between 18 (for Hurricane Ivan) to 59 (for Hurricanes Rita and Katrina) independent variables. Table 19, a replication of Table 2 with an added column, shows the hurricane image sample combinations, the percent variation explained by discriminant functions 1 and 2, the percent of original

cases correctly classified, the percent of cross-validated cases correctly classified and the number of independent variables in discriminant function 1 for that combination. 152 of the 242 unique independent variables are used in one or more of the discriminant functions.

The discriminant function 1 and 2 plots for all the combinations appear in Appendix C, as are the classification accuracies. The combined hurricane data sets result in group separations and overlaps of groups that are combinations of the results found for the individual storms. For example, the Ike-Katrina combination yields the third highest percent of variability explained by discriminant functions 1 and 2, below the first and second highest accuracy held by Ike and Katrina.

Table 8

Number of independent variables in discriminant functions for each of the hurricane data set combinations analyzed with discriminant analysis. Nineteen of the 242 independent variables appear in 8 or more of the 15 hurricane image sample combination discriminant functions. Table 8 below shows the frequency distribution for the most frequently occurring independent variables.

Ike (2008)	Rita (2005)	Katrina (2005)	Ivan (2004)	percent variation explained by DF 1 and 2	percent original cases correctly classified	percent cross-validated cases correctly classified	# ind. variables in DF 1
X				99.2	89.5	88.7	27
		X		98.8	84.7	82.3	45
X		X		97.7	76.6	76.2	19
X		X	X	92.7	71.7	70.8	29
X			X	89.6	76.4	75.2	30
		X	X	86.3	75.3	73.9	33
X	X	X	X	82.6	67.6	66.7	36
X	X	X		82.4	73.7	72.5	57
X	X			80.5	77.2	75.7	52
			X	78.0	72.5	71.4	18
X	X		X	75.3	69.4	68.2	44
	X	X	X	74.5	69.1	67.4	41
	X	X		73.6	77.8	75.7	59
	X		X	70.4	69.6	67.5	31
	X			69.9	86.0	84.7	44

Table 8 above shows the classification accuracy of each storm model and each storm combination model. Rita samples were evaluated with the discriminant functions derived from Ike, Ike and Katrina, and Ike, Katrina and

Ivan discriminant functions. Table 9 shows how Hurricane Rita image samples' classification improves as more hurricane sample data sets are added to the discriminant analysis. Hurricane Rita's damaged area is troublesome to classify in 94.4 percent is either open water or wetlands. Much of the damaged area near the coast is camp like with more debris-looking features in the image samples than the other hurricanes. Using the discriminant function from Hurricane Ike discriminant analysis to classify Hurricane Rita image samples performs poorly. Almost all the Rita image samples classify as Extensive or Catastrophic using the Hurricane Ike discriminant function. Hurricane Rita image samples classified using the discriminant function from the Hurricanes Ike and Katrina discriminant analysis shows some increase in classification accuracy, though many samples continue to be misclassified. With the addition of Ivan to the Katrina and Ike image samples for the discriminant analysis, the resulting discriminant function begins to perform with more accuracy on Hurricane Rita image samples. Using the discriminant function from the Hurricanes Ike, Katrina and Ivan discriminant analysis results in almost 60 percent or greater of the image samples in each damage category being classified in the correct category. The Ike, Katrina and Ivan-based discriminant functions 1 and 2 explain 92.7 percent of the variation in the samples, correctly classify 71.7 percent of the original cases and 70.8 percent of the cross-validated cases are correctly classified with this discriminant function.

Table 9

Hurricane Rita image samples classification performance when scored using Ike, Ike and Katrina, and Ike, Katrina and Ivan discriminant functions improves as more hurricanes are added to the discriminant function.

		Rita classified with Ike Discriminant Function 'Classified as' categories					
	Count / percent	**No Damage**	**Limited**	**Moderate**	**Extreme**	**Catastrophic**	**Total**
Original	No damage	0 / 0	1 / 0.4	1 / 0.4	251 / 88.1	32 / 11.2	285
categories	Limited damage		0 / 0	23 / 9.6	178 / 74.2	39 / 16.3	240
	Moderate damage	3 / 1.6	1 / 0.5	0 / 0	153 / 80.5	33 / 17.4	190
	Extensive damage			6 / 3.4	137 / 77.4	34 / 19.2	177
	Cat damage	14 / 3.4		1 / 0.2	305 / 75.1	86 / 21.0	406

Rita classified with Ike and Katrina discriminant function

'Classified as' categories

	Count / percent	No Damage	Limited	Moderate	Extreme	Catastrophic	Total
Original	No damage	6 / 2.1	24 / 8.4	167 / 58.6	2 / 0.7	85 / 29.8	285
categories	Limited damage		128 / 53.3	11 / 4.6	27 / 11.3	74 / 30.8	240
	Moderate damage	4 / 2.1	8 / 4.2	154 / 81.1		24 / 12.6	190
	Extensive damage	3 / 1.7	71 / 40.1	27 / 15.3	25 / 14.1	51 / 28.8	177
	Cat damage	21 / 5.2	36 / 8.9	116 / 28.6	13 / 3.2	220 / 54.2	406

Rita classified with Ike, Katrina and Ivan discriminant function

'Classified as' categories

	Count / percent	No Damage	Limited	Moderate	Extreme	Catastrophic	Total
Original	No damage	177 / 62.1	2 / 0.7	25 / 8.8	1 / 0.4	80 / 28.1	285
categories	Limited damage	5 / 2.1	151 / 62.9		5 / 2.1	79 / 32.9	240
	Moderate damage	41 / 21.6	7 / 3.7	113 / 59.5	5 / 2.6	24 / 12.6	190
	Extensive damage	14 / 7.9	5 / 2.8	2 / 1.1	105 / 59.3	51 / 28.8	177
	Cat damage	20 / 4.9	10 / 2.5	10 / 2.5	13 / 3.2	353 / 86.9	406

The poor classification performance of the Ike, Ike-Katrina, and Ike-Katrina-Ivan discriminant functions to correctly classify Rita samples raises the question of why these models perform poorly to classify Rita damage. Several factors play a role in the variability within and between hurricane data sets. The geographic extent of hurricane damage can be massive, extending hundreds of miles across the Gulf Coast and covering thousands of square miles. Rita's hurricane force winds extended over 170 miles in width with tropical storm form winds extending over 400 miles along the coast. Hurricane Ike's hurricane force winds exceeded 250 miles in width with tropical storm winds extending greater than 400 miles along the coast. Hurricanes also vary in the number of embedded tornadoes. Hurricane Ike had no reported embedded tornadoes while hurricane Ivan had 117 embedded tornadoes recorded by the National Weather Service. Rita contained twenty one embedded tornadoes and Katrina contained forty three. As indicated by Table 1, the hurricanes examined in this research vary significantly in their extent, severity and characteristics. Their impact size is another significant variable. Ike's category 1 or greater winds covered an area of 8,744 square miles. Rita's category 1 or greater winds covered an area of only 1,103 square miles. Katrina's category 1 or greater winds covered a massive area of 13,955 square miles. Ivan's category 1 or greater winds covered an area of 6,596 square miles. These factors suggest that each storm is significantly different from the others, which may account for the poor classification accuracy of one storm's discriminant function applied to another storm.

A further difference that may account for the discriminant function performance variability is the landscape of the area damage. An analysis of the land cover within the area defined by category 1 or stronger winds for each hurricane reveals surprising differences. Figure 7 shows the percentage distribution of land cover for each hurricane's category 1 or stronger winds. This shows, for example, that Rita's damage area is composed predominantly of open water and wetlands. Hurricane Ike's damage area land cover is relatively spread out over all the categories, with the majority of land cover falling in the developed classes (20.8 percent), forest classes (15.6 percent), and scrub/shrub/pasture classes (29.2 percent). Hurricanes Katrina and Ivan are the most similar in percentage land cover. Both are predominated by developed, forest and scrub/shrub/pasture classes.

Based on Saffir-Simpson category, these storms appear to be similar. A closer look at the characteristics of each hurricane and the area impacted by them reveals that they are unique and in some respects very different. These factors could account for the poorer classification results from discriminant analysis for combinations of hurricane data sets.

Appendix A lists the entire hurricane and hurricane combination cases which were examined with discriminant analysis along with which of the 242 independent variables were included in each discriminant function for each case. Figure 60 shows an abbreviated histogram of the independent variables for all the hurricane storm cases examined along with the eighteen most commonly occurring coefficients.

The first question of this research inquired about the ability of wavelet processed, post storm imagery to identify areas of residential damage. The discriminant analysis of all fifteen hurricane combinations revealed that the answer to this question is yes with varying accuracies depending upon the storm combination. Classification accuracies ranged from 67.5 percent (Rita and Ivan combined) to 88.7 percent (Ike) using percent of cross validated cases as a metric. Using percent variation explained by discriminant functions 1 and 2 as the metric, the highest accuracy achieved with hurricanes remained Ike. The lowest accuracy using this metric changed to Rita, with 99.2 percent and 69.9 percent of the variation explained.

Question 2 of this research asks what wavelet transform mother functions and decomposition levels identify damage in remotely sensed imagery. Wavelet mother functions investigated include Coiflets, Haar, Meyer and Symlets. Decomposition levels investigated included levels 1 through 5.

One hundred fifty two of the 242 independent variables appear in one or more discriminant functions resulting from the discriminant analysis of 15 hurricane combinations. All four wavelet function forms appear in every hurricane discriminant function. While several of the wavelet coefficients appear in many of the discriminant functions, none of them appear in all the discriminant functions. Eighteen of the 242 independent variables appear in more than half the fifteen discriminant functions, as shown in Figure 38. The Haar, level 1, diagonal ENG coefficient appears in all but the Hurricane Ike and Hurricane Ivan image sample discriminant function. Some form of Haar wavelet coefficient appears in every

hurricane or hurricane combination, appearing as between 15 and 39 percent of the discriminant function coefficients.

Haar wavelet transformation is particularly well suited to identifying abrupt changes at all scales. Haar wavelets are useful for detecting abrupt change such as is found in hurricane damaged coastal, residential areas. Symlets, Coiflets, and Meyer wavelet transforms also appear in all the discriminant functions for individual and grouped hurricane image samples. These wavelet forms are symmetrical and relatively fast changing, which identify fast changing, relatively symmetrical landform changes typical of coastal hurricane damage. The second question asks what wavelet mother functions and levels identify damage in remotely sensed imagery. Taking all the hurricane combinations together, all four wavelet functions and all five decomposition levels identify damage in remotely sensed imagery.

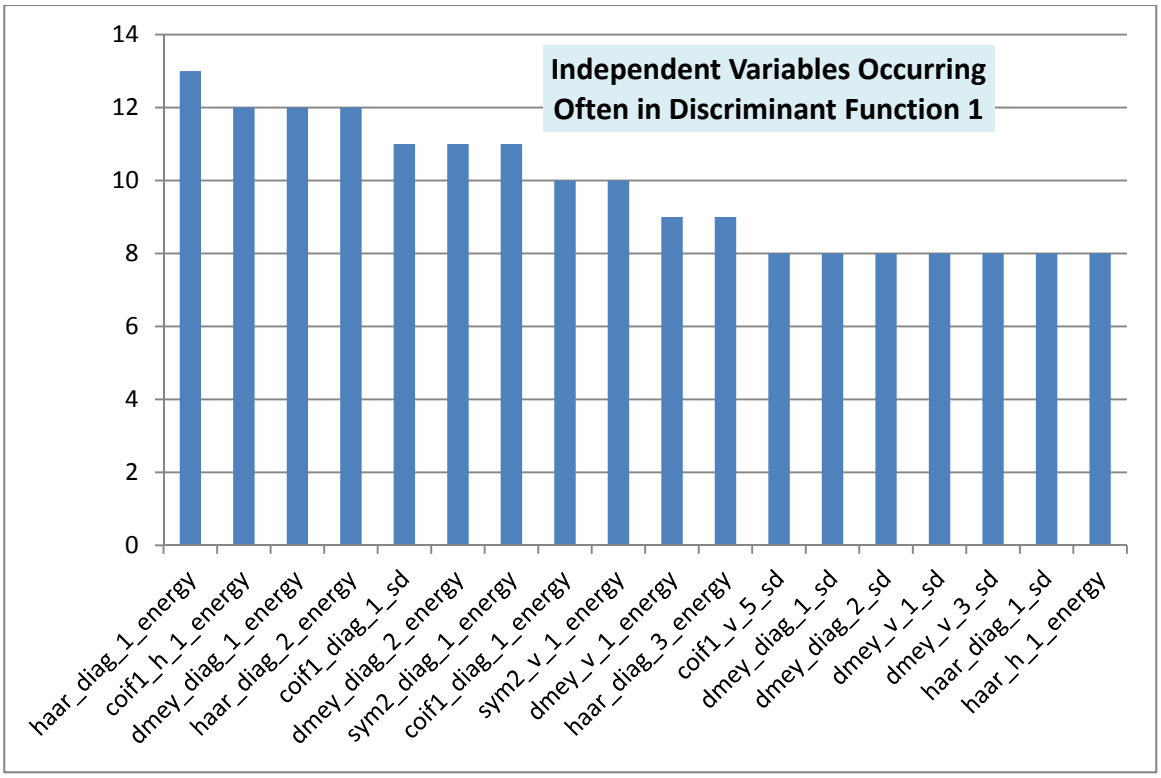

Figure 38. Histogram of independent variable occurring most frequently in eight or more discriminant functions of individual and groups of hurricane image sample data sets.

The third question examined in this research inquires about the performance of a discriminant function created with image data from one hurricane to accurately classifying damage from other hurricanes.

Table 10 shows the results of classifying Rita, Katrina and Ivan samples using the hurricane Ike discriminant function. The hurricane Ike discriminant function inaccurately predicts hurricanes Rita, Katrina and Ivan damage categories. Table 9 shows the increase in damage category performance when classifying Rita samples when hurricane Ike samples are combined with hurricane Katrina, with hurricane Ivan and with hurricanes Katrina and Ivan. Based on the four hurricanes in this research, it is anticipated that the combined

hurricane Ike, Katrina and Ivan discriminant function will perform with 50 percent or greater classification accuracy predicting damage categories for hurricanes making landfall in the Gulf of Mexico from Texas to the Florida panhandle.

Table 10

Hurricane's Rita, Katrina and Ivan image samples classified using Ike-only based discriminant function. Generally poor damage classification results for all three hurricanes despite good self-classification results.

		Rita classified with Ike Discriminant Function 'Classified as' categories					
	Count / percent	**No Damage**	**Limited**	**Moderate**	**Extensive**	**Catastrophic**	**Total**
Original	No damage	0 / 0	1 / 0.4	1 / 0.4	251 / 88.1	32 / 11.2	285
categories	Limited damage		0 / 0	23 / 9.6	178 / 74.2	39 / 16.3	240
	Moderate damage	3 / 1.6	1 / 0.5	0 / 0	153 / 80.5	33 / 17.4	190
	Extensive damage			6 / 3.4	137 / 77.4	34 / 19.2	177
	Cat damage	14 / 3.4		1 / 0.2	305 / 75.1	86 / 21.0	406

		Katrina classified with Ike discriminant function 'Classified as' categories					
	Count / percent	No Damage	Limited	Moderate	Extensive	Catastrophic	Total
Original	No damage			3 / 3.8	60 / 75.9	16 / 20.3	79
categories	Limited damage			50 / 24.9	111 / 55.2	40 / 19.9	201
	Moderate damage		25 / 5.3	85 / 18.1	294 / 62.6	66 / 14.0	470
	Extensive damage			15 / 8.6	137 / 78.7	22 / 12.6	174
	Cat damage	18 / 4.9	1 / 0.3	16 / 4.3	231 / 62.8	102 / 27.7	368

		Ivan classified with Ike discriminant function 'Classified as' categories					
	Count / percent	No Damage	Limited	Moderate	Extensive	Catastrophic	Total
Original	No damage	73 / 100					73
categories	Limited damage	150 / 100					150
	Moderate damage	383 / 95.5	9 / 2.2		4 / 1.0	5 / 1.2	401
	Extensive damage	83 / 100					83
	Cat damage	9 / 100					9

The answer to the question about how well a hurricane based discriminant function performs on a hurricane not used to inform the discriminant function is dependent upon how closely the impacted land cover and hurricane characteristics match those used to inform a discriminant function for classification. Based on an Ike informed discriminant function it can be concluded that the analysis does not recommend a single storm informed discriminant function for classifying other storm damage. Based on the increasingly accurate classification of Rita data by combining Ike, Katrina and Ivan to inform the discriminant function, it can be concluded that an Ike-Katrina-Ivan based discriminant function is likely to classify damage with better than 50 percent accuracy.

Tornado Storm Damage Classification

The large extent, wide separation and variation in land cover likely explain some of the variability in hurricane discriminant analysis found in this research. Discriminant analysis of the four individual hurricanes revealed damage classification accuracies ranging from 71.4 percent for Ivan to 88.7 percent for Ike. The same analysis of all combinations of these storms reveals reduced classification accuracies ranging from 66.7 percent for all four to 76.2 percent for Ike and Rita combined. Tornadoes provide an opportunity to test the wavelet transform methodology on damaged areas with reduced variation due to extent and land cover changes.

Two sample groups were collected from the Joplin tornado, one was used to inform a discriminant analysis (Figure 39 shows discriminant functions 1 and 2

plot) resulting in a discriminant function. The other was used to assess the classification accuracy performance of the Joplin discriminant function with nearby samples that were not used in the discriminant function creation.

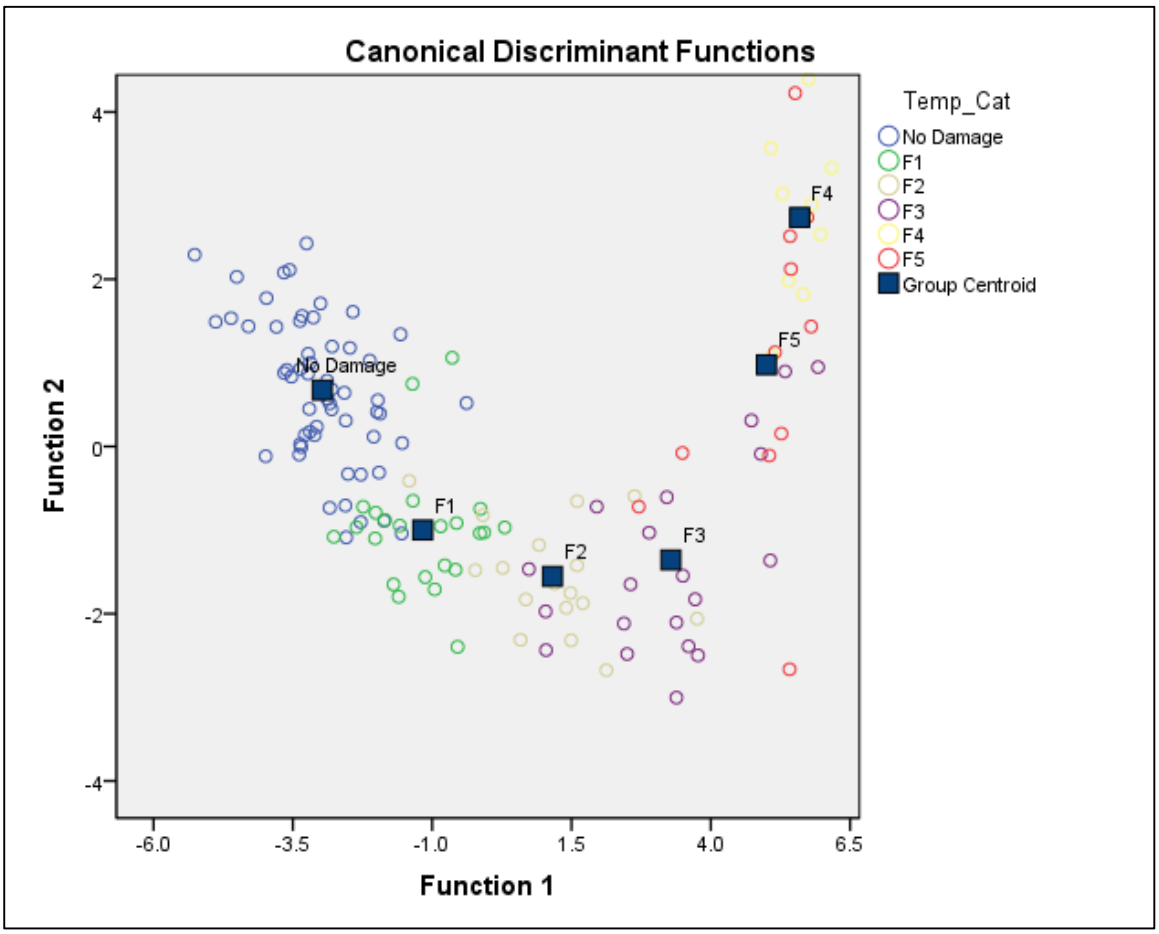

Figure 39. Joplin tornado canonical discriminant functions 1 and 2. Discriminant functions 1 and 2 account for 98.6percent of the total variance in the Joplin tornado data set.

Approximately 81.2 percent of the original cases were correctly classified using no damage, F1, F2, F3, F4 and F5 as groups. Approximately 76.8 percent of the cross-validated cases were correctly classified with these groups. The discriminant analysis yielded a discriminant function with six coefficients (compared to the smallest hurricane discriminant model (Ike and Katrina) which

is composed of 19 coefficients). The Joplin discriminant function's coefficients are first level Meyer diagonal ENG, first level Meyer diagonal standard deviation, second level Meyer diagonal ENG, second level Meyer diagonal standard deviation, second level Symlets diagonal standard deviation, and third level Haar approximation standard deviation. Unlike the variety of coefficients in the simplest hurricane discriminate model, the tornado model uses four coefficients from the Meyer wavelet function and one each from the Haar and Symlets wavelet functions. These coefficients suggest that the tornado damage wrought by this F5 tornado results in remotely sensed imagery composed largely of relatively uniform, high frequency content. In other words, the Joplin discriminant function coincides what can be seen on the ground after one of these storms – low frequency content (e.g., homes and trees) are transformed into piles of debris. Table 11 shows the classification results for the Joplin tornado, with over 90 percent of the undamaged areas correctly classified.

Table 11

Joplin tornado image samples classified with 6 categories (no damage, F1, F2, F3, F4 and F5).

			Predicted Group Membership						
		Category	**No Damage**	**F1**	**F2**	**F3**	**F4**	**F5**	**Total**
Original	Count	No Damag	54	3	0	0	0	0	57
		F1	2	20	1	0	0	0	23
		F2	0	3	12	2	0	0	17
		F3	0	0	4	12	1	3	20
		F4	0	0	0	0	8	2	10
		F5	0	0	0	3	2	6	11
	percent	No Damag	94.7	5.3	.0	.0	.0	.0	100.0
		F1	8.7	87.0	4.3	.0	.0	.0	100.0
		F2	.0	17.6	70.6	11.8	.0	.0	100.0
		F3	.0	.0	20.0	60.0	5.0	15.0	100.0
		F4	.0	.0	.0	.0	80.0	20.0	100.0
		F5	.0	.0	.0	27.3	18.2	54.5	100.0
Cross-validated[a]	Count	No Damag	52	4	1	0	0	0	57
		F1	3	19	1	0	0	0	23
		F2	0	3	12	2	0	0	17
		F3	0	0	5	11	1	3	20
		F4	0	0	0	0	7	3	10
		F5	0	0	1	2	3	5	11
	percent	No Damag	91.2	7.0	1.8	.0	.0	.0	100.0
		F1	13.0	82.6	4.3	.0	.0	.0	100.0
		F2	.0	17.6	70.6	11.8	.0	.0	100.0
		F3	.0	.0	25.0	55.0	5.0	15.0	100.0
		F4	.0	.0	.0	.0	70.0	30.0	100.0
		F5	.0	.0	9.1	18.2	27.3	45.5	100.0

a. Cross validation is done only for those cases in the analysis. In cross validation, each case is classified by the functions derived from all cases other than that case.

b. 81.2 percent of original grouped cases correctly classified.

c. 76.8 percent of cross-validated grouped cases correctly classified.

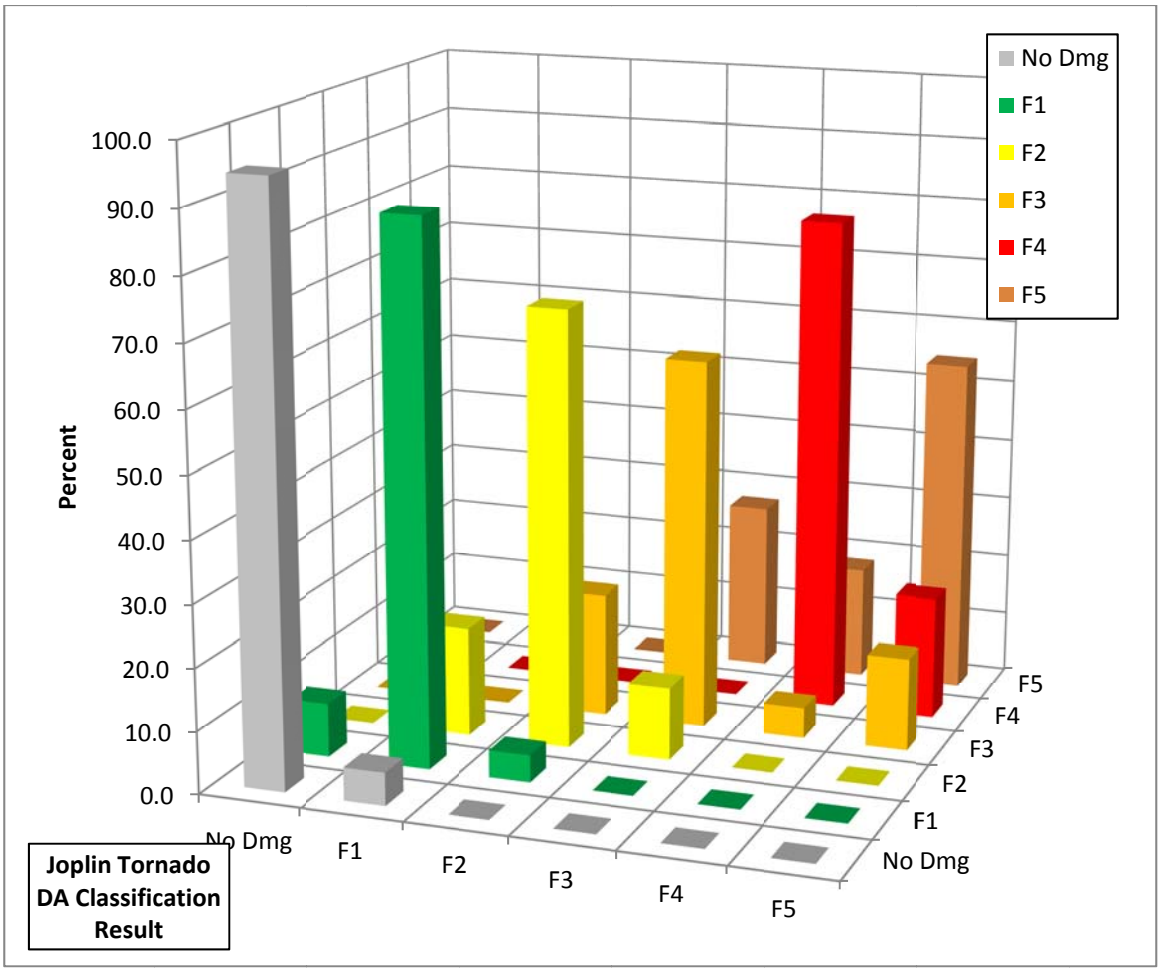

Figure 40. Classification accuracy bar chart for Joplin tornado using 6 classes. The discriminant analysis shows statistically significant group discrimination and group classification accuracy of 81.2 percent of the original grouped cases correctly classified and 76.8 percent of cross-validated grouped cases correctly classified. Discriminant functions 1 and 2 account for 98.6 percent of the total variance in the Joplin image samples.

The Joplin tornado classification accuracy bar chart (Figure 40) shows the classification accuracy for each category and illustrates that the variability in the damage categories (F1 through F5) is into adjacent classes and very few (5.3 percent) no damage samples are incorrectly categorized into the adjacent F1 category.

Figure 17 shows that the Joplin damaged area was sampled twice. The first sample informed the 6 coefficient discriminant function described above. The second sample is adjacent to the original sample. None of these comparison area samples were used in the previous discriminant analysis. This sample was classified using the Joplin discriminant function. The resultant 6 category classification is 50.7 percent accurate when considering all categories (no damage, F1, F2, F3, F4, and F5). Figure 41 shows the classification accuracy bar chart for the Joplin comparison area classified using the Joplin discriminant function. Despite the impression given by an overall 50.7 percent classification accuracy, it can be seen from the classification accuracy bar chart that most of the no damage areas are correctly classified (86.5 percent). This chart also illustrates that the damage category errors are into adjacent categories. Misclassification of samples into categories adjacent to their true damage level is operationally less significant than samples classified into non-adjacent categories.

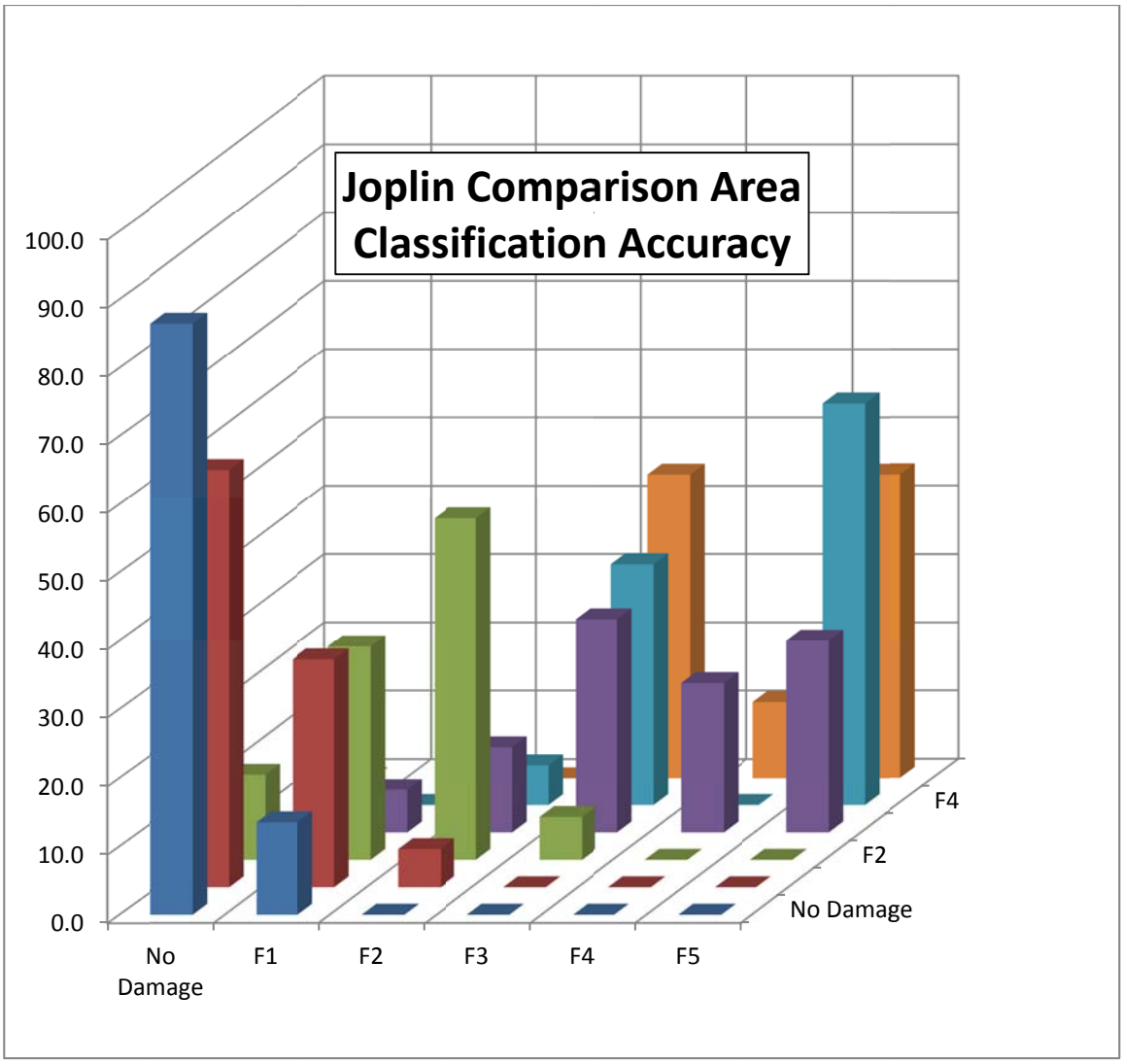

Figure 41. Classification accuracy bar chart of the Joplin comparison area classified used the Joplin discriminant function showing an overall classification accuracy of 50.7 percent.

CHAPTER V

CONCLUSIONS AND RECOMMENDATIONS

Conclusions

U.S. Hurricanes and tornadoes cause significant financial and human damage, on the order of billions of dollars and hundreds of lives per year (Pielke et al. 2008). One immediate response need to these disasters is an assessment of the damage as accurately and quickly as possible (Clarke et al. 2007). A speedy and accurate damage assessment can be used by first responders to rally and guide response, assess recovery and for long-term monitoring.

Current methodologies employed by NWS, FEMA, and others who produce post disaster damage assessment depend predominantly on visual interpretation of remotely sensed imagery or ground surveys. In many cases ground surveys cannot be performed quickly enough for early first response. A damage assessment approach that speeds an accurate assessment into the hands of users would be welcomed by all.

In addition to the direct financial and life loses caused by these storms, there are often legal disputes arising directly or indirectly from these disasters. Lawsuits brought because of the impacts of hurricane Katrina, for example, continue to the present, seven years after landfall (e.g., Mitchell v. Murphy). The damage condition and extent caused by Katrina is often in dispute or is an important fact in post-storm legal matters. Katrina spawned hundreds of large cases and thousands of smaller cases, many which needed clear, defendable damage assessment and attribution. Some of the Katrina related legal matters

include the fate, transport and cleanup of an oil spill from a coastal refinery, the cause of the destruction of the Louisiana Superdome roof, the likely cause of damage to Mississippi coastal residents' homes and businesses, substantial business loss to a national medical diagnostic company and more. A common characteristic of many post Katrina cases is how much damage was wrought by the storm at specific locations. In some instances, cases only reach the stage where experts who can address the geographic questions occur years after an event. This can mean that the only contemporaneous objective evidence of damage is remotely sensed imagery. Damage assessment approaches addressing the court's guidelines for acceptance of scientific evidence speeds, or least does not hinder, the possibility of trial or a settlement.

Myint (2001) has established a body of wavelet transform image processing beginning with his dissertation on urban classification and continuing as recently as this year (2012) with a look at spatial indices and wavelet classification. Curran's (2001) observation that the spatial domain has been historically neglected when it comes to extracting information from remotely sensed images using the spatial domain encouraged interest in extracting storm damage classification from this regime. The two major factors hindering the wide use of spatial domain information within remotely sensed imagery identified by Curran (the difficulty of extracting this information using computational methods and the ease of extracting this information by trained visual interpretation) have recently succumbed to nullifying forces. Computational capability on the desktop is advanced enough to allow almost limitless computational capability. This

research, for example, examined 8,838 image subsamples of 65,536 pixels each. Each of these samples were wavelet transformed with several wavelet functions to five decomposition levels on a desktop processing platform, yielding 242 independent variables for each image sample. The capability to extract spatial content from remotely sensed imagery is possible like never before. Visual interpretation of remotely sensed imagery depends upon skilled technicians and is limited by the available qualified workforce. Hurricane events can cover many thousands of square miles (e.g., Katrina's Category 1 or greater winds covered a land area of 13,955 square miles). Visual interpretation of large quantities of imagery can require significant time to complete. Automated algorithmic damage classification approaches can reduce the damage classification time such that the limiting factor in delivering a damage assessment is the time required to collect the imagery.

This research examined three facets of extracting post storm damage from remotely sensed imagery using wavelet transform-based approaches. First, the ability of wavelet transform methods to identify post storm damage was examined. Second, wavelet functions and decomposition levels were examined. Third, discriminant functions were examined with regard to their classification accuracy when applied to storms not informing the discriminant function.

Discriminant analysis of imagery collected immediately after hurricanes Ike, Rita, Katrina, and Ivan revealed classification accuracy near 90 percent for individual hurricane-based models (e.g., Ike – 89.5 percent of 1,008 original cases correctly classified). Combinations of hurricane storm imagery examined

yielded classification accuracy as high as 67 percent correctly classified or better. Table 12 shows the classification accuracy of all the hurricane cases investigated, sorted from highest to lowest in percent of cross-validated cases correctly classified. The individual cases of Ike, Rita and Katrina performed best, correctly classifying over 80 percent of cross-validated cases. Even the worst performers correctly classified more than 66 percent of the cross-validated cases.

Table 12

Classification accuracy of hurricane data set combinations sorted highest to lowest by the percent of cross-validated cases correctly classified.

Ike (2008)	Rita (2005)	Katrina (2005)	Ivan (2004)	percent variation explained by DF 1 and 2	percent original cases correctly classified	percent cross-validated cases correctly classified
X				99.2	89.5	88.7
	X			69.9	86	84.7
		X		98.8	84.7	82.3
X		X		97.7	76.6	76.2
X	X			80.5	77.2	75.7
	X	X		73.6	77.8	75.7
X			X	89.6	76.4	75.2
		X	X	86.3	75.3	73.9
X	X	X		82.4	73.7	72.5
			X	78	72.5	71.4
X		X	X	92.7	71.7	70.8
X	X		X	75.3	69.4	68.2
	X		X	70.4	69.6	67.5
	X	X	X	74.5	69.1	67.4
X	X	X	X	82.6	67.6	66.7

The wide variation of classification accuracy among these cases naturally raises the question of what accounts for this variability? At first glance these storms appear to be similar. Three of them are Saffir-Simpson Category 3 storms with the fourth a strong Category 2 storm. All four made landfall along the coast of the Gulf of Mexico. Three of them occurred within twelve months. If these storms are similar and they made landfall in similar areas, they would be expected to cause similar damage and be classifiable in a similarly accurate manner. The surface similarities belie the vast differences between these storms and the damage they wrought.

The wavelet transform-based classification methodology extracts spatial content from the imagery. All the combinations examined had opportunity to use all 242 independent variables extracted from the imagery. The first hint of significant variability among and within the hurricanes was the quantity of independent variables included in the discriminant functions by the discriminant analysis. Appendix A lists all fifteen hurricane case combinations investigated and shows which of the 242 independent variables are included in each model. Figure 38 shows a histogram of the eighteen most frequently appearing independent variables. These most frequently occurring coefficients include all 4 wavelet functions studied. Table 8 lists each hurricane case investigated along with classification accuracy metrics and the number of independent variables included by the discriminant analysis for each case. The simplest discriminant function was for the Ike-Katrina case, which included 19 independent variables.

The most complex discriminant function was for the Rita-Katrina case, which included fifty nine independent variables.

This complexity combined with the low classification accuracy of even the best model on data not used to inform the discriminant function led to an investigation for why these models are so complex and classify damage with low accuracy. In other words, the search was on for an answer to why these hurricane models performed with such low classification accuracy. For example, the best hurricane classification model is the Ike-Katrina-Ivan model, which correctly classified 70.8 percent of the cross-validated cases using 29 of the 242 independent variables. It correctly classified approximately 60 percent of the no damage, limited damage, moderate damage and extreme damage cases and 87 percent of the catastrophic damage cases from the Rita samples.

An answer to the source of the variability in damage classification of the hurricane models is in the variation among the hurricanes and the variability of the land impacted by the hurricanes. Table 1 is a summary of some of the hurricane characteristics that were found to vary between hurricanes. The size of the impacted area for each hurricane was more than an order of magnitude between the smallest and largest. Katrina's Category 1 or greater winds impacted a land area of 36,143 square km. Rita's Category 1 or greater winds impacted 2,857 square km. Ivan contained a reported 117 embedded tornadoes. Ike had no reported embedded tornadoes. Ivan was accompanied by a 3.7 m high 105 km wide storm surge. Katrina was accompanied by a storm surge more than 6.4 m high over more than 161 km of coast. As widely varying as some of

these hurricane characteristics are, the biggest variation appeared in the differences of impacted land cover among the hurricanes. Figure 7 shows the percent land cover distribution over the category 1 or greater winds affected area for the four hurricanes. Rita's 2,857 square km of category 1 or greater winds is composed of more than 94percent open water or wetlands. Hurricane Ike's 22,647 square km of impacted area is composed of only 33.6percent open water or wetlands. The percent develop land cover for each hurricane's category 1 or greater wind affected area was 2.8 percent, 7.8 percent, 10.3 percent, and 20.8percent for Rita, Katrina, Ivan, and Ike respectively. While these open areas were not classified with the discriminant functions, their presence or absence can have a significant influence on the effects of storm winds and water.

Hurricanes generally cover large areas, which naturally introduces variability that can change the spatial nature of the hurricane damage. As the impact area grows, changes in housing type, housing distribution, lot size, house size, land cover, landscape, proximity to open space, open water, the shore and varying height buildings, previous damage, and building codes are more likely. If the extent, dwell time and land cover of affected areas of hurricanes are the factors inducing the poor classification due to changes over the affected areas, then studying a small area should result in higher classification accuracy. Tornadoes are a small area extent, high wind speed type storm that might eliminate the variability seen across and among hurricanes.

A discriminant analysis on a small, densely developed residential areas hit by the 2011 Joplin tornado yielded a discriminant function with six wavelet

transform-based coefficients (four Meyer, one Haar, one Symlet). This discriminant function (using 6 classes of damage – no damage, F1, F2, F3, F4, and F5) correctly classified 81.2 percent of the original cases, with 76.8 percent of the cross-validated cases correctly classified. When these 6 classes are collapsed to two categories (damage and no damage), the overall classification accuracy increased to 96.4percent of all the samples correctly classified. This is due to the elimination of errors due to misclassification into adjacent damage categories (e.g., F2 damage classified as F3 damage). When this discriminant function is applied to another sample of Joplin data that did not inform the discriminant analysis, the percent of correctly classified cases fell to 86.5 percent of the no damage samples correctly classified and 85.9 percent of the damage samples correctly classified.

First responders need information about the extent of damage and severity of damage. An operational application of wavelet transform based damage classification could be applied using two categories, damage and no damage. When collapsed to two categories, the classification accuracy of the no damage category is unchanged, ranging from 60.3 percent to 100 percent accuracy (for the 15 combinations considered). The classification accuracies of the damage categories increase from a range of 16.7 percent to 96.3 percent to a range of 93.7 percent to 100 percent. The apparent increase in damage category accuracy is because most of the classification errors in the damage categories are due to misclassification into adjacent categories.

The accuracy of the tornado discriminant analysis increased to 96.4 percent if the categories are reduced from five (no damage and F1 through F5) to two (damage and no damage). Figure 42 shows the classification accuracy chart for the two category Joplin tornado discriminant analysis. Figure 43 shows the classification accuracy chart for the comparison Joplin tornado image samples classified into two categories.

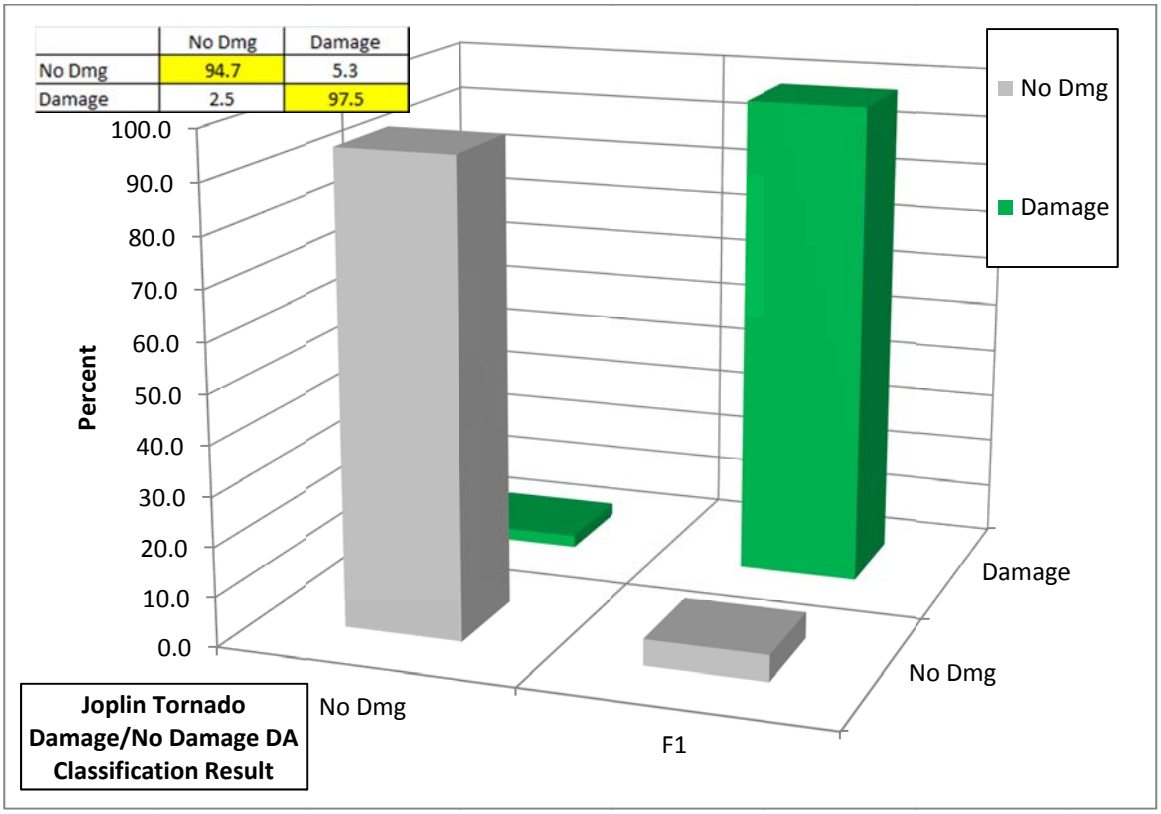

Figure 42. Classification accuracy bar chart of Joplin tornado using 2 classes (damage and no damage). Collapsing the F-level groups to a single damage category results in an overall classification accuracy of 96.4 percent. This is due to eliminating the errors due to F1 through F5 damage being classified in the wrong F category. Figure 62 shows that the F category classification errors occur in adjacent F categories. The F1 damage category is the only F category with samples misclassified into the no damage category.

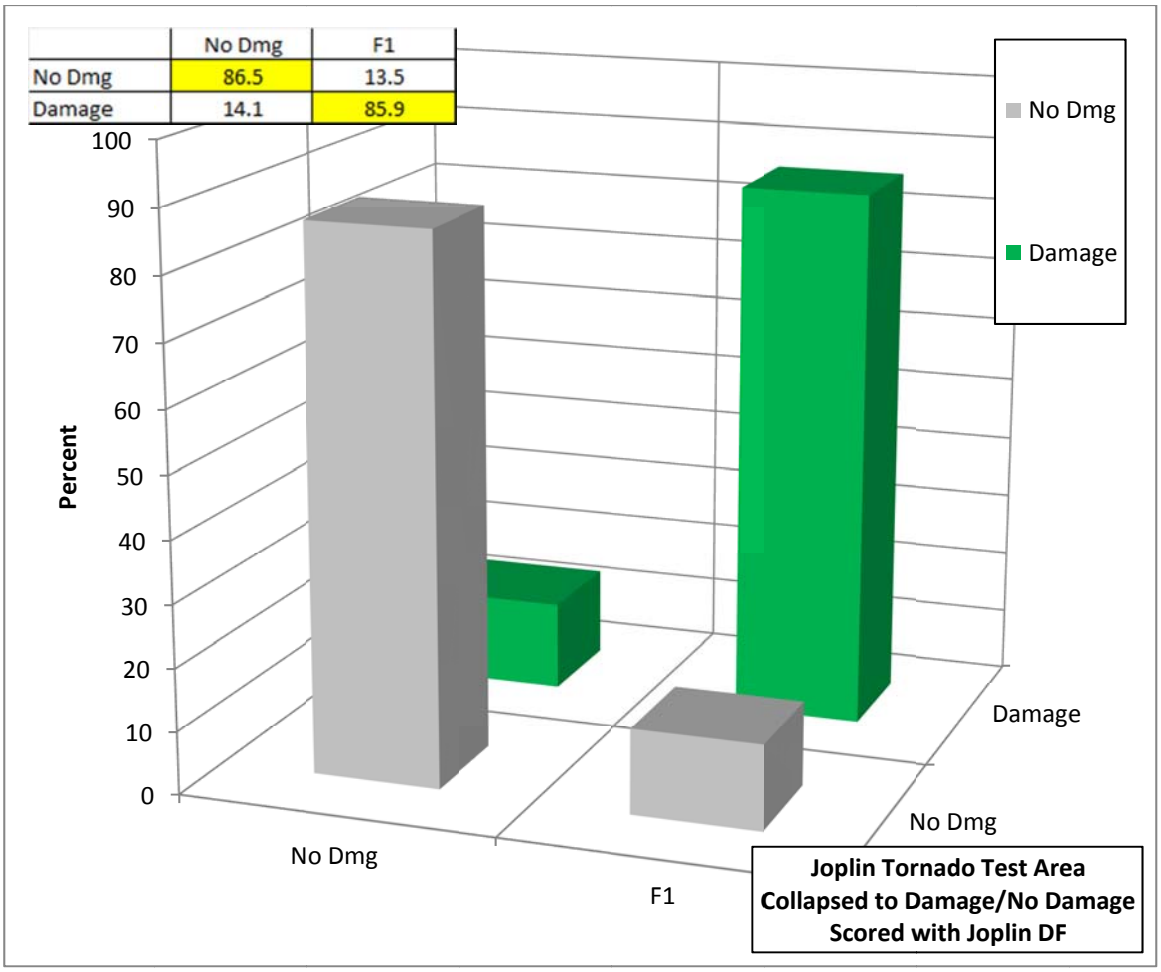

Figure 43. Classification accuracy bar chart for the Joplin test area samples. These samples were not used to inform the Joplin tornado discriminant function. Approximately 86 percent of all these samples were correctly classified. The accuracy of the classification of the no damage area samples was 86.5 percent. The accuracy of the classification of the damage area samples was 85.9 percent.

The performance of the 6 coefficient Joplin tornado discriminant function hints at the potential for accurately classifying tornado damage from tornadoes not used to inform the discriminant function. This guided the collection and analysis of image samples from the Tuscaloosa tornado. Beginning with a data set 67 samples wide by 54 samples long (3,618 samples), non-residential areas (parking lots, open areas, open water, roads, and commercial building areas)

were eliminated leaving 3,493 samples for damage classification analysis. These remaining Tuscaloosa residential area samples were classified with the Joplin tornado 6 coefficient discriminant function. Figure 44 shows the classification accuracy bar chart of this classification.

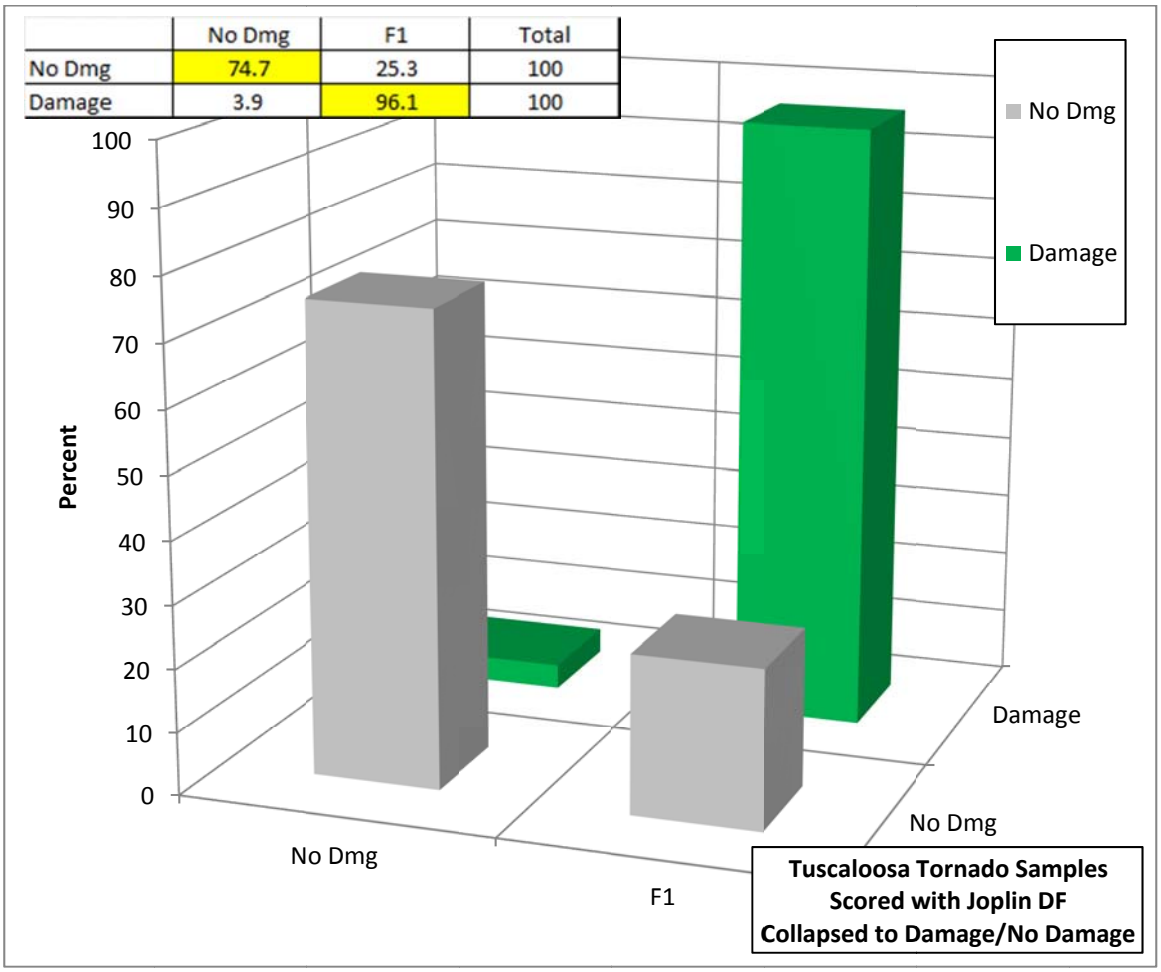

Figure 44. Classification accuracy bar chart of the Tuscaloosa tornado samples. 85.2percent of all the samples were correctly classified. 74.7 percent of the no damage areas were correctly classified. 96.1 percent of the damaged areas were correctly classified. Correct classification of these samples was determined by visually determining damage for each sample.

The ability of the Joplin tornado discriminate function to accurately classify damage from the Tuscaloosa tornado can be attributed to two factors. First,

tornadoes damage much smaller areas than hurricanes. This limits the variation in land cover that can introduce variability in the classification results. For example, the samples used to create the Joplin discriminant function and the samples from the Joplin tornado not used to inform the discriminant function were all high density residential land cover areas. Second, strong tornadoes such as the Joplin and Tuscaloosa events typically cause either catastrophic damage or no damage. This damage is almost exclusively caused by high winds and flying debris within the tornado over a few seconds to a few minutes. This very small geographic extent, high intensity, short time period event intrinsically has less variation compared to hurricane events. The relative uniformity of damage factors over small areas likely accounts for the few wavelet transform coefficients required to accurately classify tornado damage.

Another tornado was sampled to further test the robustness of the 6 coefficient, Joplin damage classification discriminant function. Approximately 3,500 image samples from one area of the 2011 Tuscaloosa tornado were collected and scored with the Joplin tornado informed discriminant function. The result was 74.7 percent of the no damage image samples were correctly classified and 96.1 percent of the damage image samples were correctly classified. In summary, the 6-coefficient Joplin tornado discriminant function correctly classified 85.2 percent of the Tuscaloosa image samples.

Can wavelet processed post storm overhead imagery identify areas of residential damage? Yes, with demonstrated 85 percent classification accuracy for similar storms impacting similar land cover areas. The variations in hurricanes

and land cover of the areas impacted by large storms limits the damage classification accuracy of a discriminant function not informed by samples within that storm.

What wavelet mother functions and levels identify damage in remotely sensed imagery? It depends on the storm, the resultant damage and the land cover of the impacted area. Discriminant analysis of four hurricanes and combinations of these resulted in damage classification discriminant functions composed of coefficients of all four wavelet functions examined at all 5 decomposition levels. Discriminant analysis of tornado damage resulted in a relatively simple discriminant function composed of 6 coefficients.

The sensitivity of wavelet transform-based classification accuracy depends upon the variability of the storms being classified and the variability of the land cover affected by the storms. Uniform storms impacting constant land cover types can be accurately classified with relatively simple discriminant functions. Complex storms impacting widely varying land cover areas require much more complex discriminant function models. In the cases studied herein, the widely varying hurricanes required 10s of wavelet transform-based coefficients to achieve classification accuracies greater than 60 percent. Classification accuracies of 85 percent were achieved with two different tornado storms over relatively similar land covered areas.

How accurately does a wavelet transform-based discriminant function classify damage in imagery not used to inform that discriminant function? If the land cover and storm variations are minimal, as with tornadoes hitting similar

land cover areas, a wavelet transform-based discriminant function can classify damage in imagery not used to inform the discriminant function with approximately 85 percent classification accuracy.

Spectral Limitations

Radiometric image corrections were not performed on the imagery for this research. The focus on imagery typically collected for immediate storm response limited the spectral characteristics to what is available in the existing emergency response imagery (typically true color RGB imagery collected from aerial platforms as soon as the weather allows for aircraft flights at relatively low altitudes). Given that wavelet transformation relies on matching wavelet functions to similar features in the scene, enhancing or optimizing contrast could have an impact on damage classification accuracy.

One of the simplest and longest used contrast enhancement techniques is dark pixel subtraction. This approach assumes that the lowest value, or darkest, pixel values in each band should be zero and any value above zero is a result of atmospheric additive errors (Pouncey, Swanson, and Hart 1999). Dark pixel subtraction is accomplished by subtracting the pixel value of the lowest, or darkest, pixel in the scene from all pixels in the scene. Future research could apply the dark pixel subtraction method to image samples prior to wavelet transform and classification to investigate the potential classification performance effect.

Linear and nonlinear contrast stretches also improve the contrast of remotely sensed imagery. A linear contrast stretch applies a linear function to

improve the contrast of remotely sensed imagery. While this approach can improve mid-tone contrast, it can simultaneously reduce image contrast in the bright and dark areas. A piece wise linear contrast stretch addresses this limitation by the application of several linear functions to optimize contrast throughout the image signal range (typically in the dark, mid-tone and bright areas of an image). A nonlinear contrast stretch can be applied to smoothly and preferentially increase or decrease contrast over a range. Nonlinear stretches are used to gradually increase or decrease contrast over a range (e.g., significantly increasing contrast in dark areas, moderately increasing contrast in midrange areas and decreasing contrast in highlight areas (Al-amri, Kalyankar and Khamitkar 2010).

Myint et al. (2004) analyzed band combinations (ATLAS visible, NIR and thermal), with wavelet transform levels (levels 1 and 2) and level differences (level 1 minus level 2). Using six urban texture feature samples, they found the highest classification accuracy when combining all three bands and subtracting wavelet transform level 2 from level 1. This approach yielded overall accuracies exceeding the standard acceptable accuracy of 85 percent (Townshend 1981). In all cases the subtraction of wavelet transform level 2 from level 1 resulted in increased accuracy. The increased performance of these methods was not investigated in this research and could improve damage classification. To investigate these methods using imagery collected immediately after storms a pre-storm plan would need to be in place to fly a sensor with NIR and thermal imagery capability (which is not available in the current event response imagery).

Recommendations

One of the issues noticed during the execution of this research is the vague nature of published damage descriptions used by FEMA on post hurricane damaged areas. While these descriptions have been used for more than a decade, damage that falls at or near the boundary between two damage categories can easily be classified in the wrong category or classified randomly to one or the other adjacent categories. This introduces unwanted variability that can be minimized by the use of categories that are mutually exclusive and in terms that can be applied to remotely sensed imagery. Adopting better defined, mutually exclusive category descriptions could increase the classification accuracy achieved by either visual interpretation or algorithmic approaches.

The density and distribution of residential structures was not considered in this research. Future work could include an analysis with residential density and surrounding land cover as factors. The overall nature of residential areas and the surrounding areas (e.g., density, elevation, wind tunnels, etc.) influence wind fields which could be expected to impact the resultant damage. For example, an analysis considering these factors might explain the variation between coastal hurricane Rita areas of low density surrounded by wetlands and open water versus other hurricane impacted areas with much denser residential structures surrounded by taller structures and forest-type vegetation.

While this research focused on coastal residential areas, an investigation including land cover as an independent variable could reveal damage dependence on specific land cover classes. In combination with analysis of

density and surrounding land cover, land cover is expected to influence the spatial nature of damage. Adding these additional factors to the damage classification analysis could explain some of the variability found.

A characteristic not revealed by this research is the nature or distribution of damage caused by hurricanes and tornadoes with respect to the specific spatial nature of damage. Future studies should consider a systematic examination of well characterized damage to investigate what, if any, specific wavelet function best reveals specific types of damage. For example, a series of wavelet functions can be examined for their ability to identify missing roof shingles from asphalt, 3-tab residential roofs. Another feature to investigate for specific wavelet function is residential tree branch debris. Several other features common to hurricane and wind damage could be investigated individually against a range of wavelet functions and decomposition levels.

Four wavelet functions were investigated herein. Additional wavelet functions should be investigated. Those included in this research are the Haar, Meyer, Symlets2 and Coiflets1 wavelet function. Additional functions meriting investigation include Daubechies2, Daubechies10, Daubechies20, Symlets6, Symlets7, Coiflets4, Biorthogonal2.6 and Biorthogonal3.7.

This research examined imagery collected by NOAA, FEMA and the U.S. Army Corps of Engineers in response to hurricanes and tornadoes. A valuable addition to the body of wavelet transform-based damage classification is a library of damage imagery for typical and representative damage. This could build on the test target image created for this research by creating idealized images of

types of damage. These could include surge created debris piles typical of hurricane storm surge, slab properties, minor roof and vegetation damage, and major roof damage, among others.

This research focused on hurricanes and tornadoes which cause damage by high wind loads on human structures and other land cover. Earthquake damage is a common disaster around the world that has not been examined with wavelet transform-based classification methods. Examining the classification accuracy of wavelet transform-based methods of remotely sensed imagery of earthquake damaged areas could be valuable for the theoretical knowledge base, and if successful could provide significant benefit to first responders of these disasters.

The high (93.7 percent-100 percent) accuracy of classification of damaged areas when considering only two categories (damage and no-damage) could be valuable for operational first response applications. An accurate estimate of the extent of areas damaged by tornadoes or hurricanes could be produced shortly after collection of imagery. Applying the wavelet transform methods examined in this research might best be tested in an operational setting using a two category approach.

Finally, it might be possible to sample hurricane damaged areas by land cover and then apply a wavelet transform-based model informed by only that land cover damage type. If this approach proves fruitful it may be possible to develop a series of wavelet transform discriminant functions specific to each land cover type within a storm damaged area.

APPENDIX A

DISCRIMINANT FUNCTION COEFFICIENTS

Discriminant function coefficients for all fifteen hurricane models and the Joplin tornado model. 153 of the 242 wavelet coefficient independent variables appear in at least one of the hurricane discriminant function models. Only six coefficients appear in the Joplin damage discriminant function (five Meyer and one Haar wavelet coefficient).

Variables	Ike	Katrina	Ike and Katrina	Ike, Katrina and Ivan	Ike and Ivan	Katrina and Ivan	Ike, Rita, Katrina and Ivan	Ike, Rita and Katrina	Ike and Rita	Ivan	Ike, Rita and Ivan	Rita, Katrina and Ivan	Rita and Katrina	Rita and Ivan	Rita	Joplin Tornado DF	frequency in models
coif1_h_1_energy		X		X	X	X	X	X	X	X	X	X	X	X	X		13
dmey_diag_1_energy	X		X	X	X	X	X	X	X	X	X		X		X	X	13
haar_diag_1_energy		X	X	X	X	X	X	X	X		X	X	X	X	X		13
haar_diag_2_energy		X	X	X	X	X	X	X	X	X	X	X	X		X		13
coif1_diag_1_sd	X	X				X		X	X	X	X	X	X	X	X		11
dmey_diag_2_energy	X	X	X	X	X	X	X	X		X	X		X			X	11
sym2_diag_1_energy		X	X	X			X	X	X		X	X	X	X	X		11
coif1_diag_1_energy	X	X					X	X	X		X	X	X	X	X		10
dmey_diag_1_sd		X		X			X	X	X			X	X	X	X	X	10
dmey_diag_2_sd					X			X	X	X	X	X	X	X		X	9
dmey_v_1_energy	X	X	X			X		X	X			X	X		X		9
sym2_v_1_energy		X	X			X		X	X	X			X	X	X		9
coif1_v_5_sd		X					X	X	X		X	X	X	X			8
dmey_v_1_sd	X	X			X			X	X			X	X		X		8
haar_diag_1_sd		X				X		X	X			X	X	X	X		8
haar_diag_3_energy		X		X	X		X	X			X		X	X			8

DISCRIMINANT FUNCTION COEFFICIENTS (continued).

Variables	Ike	Katrina	Ike and Katrina	Ike, Katrina and Ivan	Ike and Ivan	Katrina and Ivan	Ike, Rita, Katrina and Ivan	Ike, Rita and Katrina	Ike and Rita	Ivan	Ike, Rita and Ivan	Rita, Katrina and Ivan	Rita and Katrina	Rita and Ivan	Rita	Joplin Tornado DF	frequency in models
haar_h_1_energy	X	X	X		X		X		X		X			X			8
sym2_diag_2_sd						X	X	X			X	X	X	X		X	8
coif1_diag_2_energy		X		X				X	X			X	X		X		7
coif1_v_5_energy		X					X	X	X			X	X		X		7
dmey_h_1_sd			X			X	X		X		X		X		X		7
dmey_h_2_energy		X				X	X	X			X	X	X				7
dmey_v_2_energy	X					X		X	X			X	X		X		7
dmey_v_3_sd		X			X	X		X	X			X	X				7
sym2_diag_1_sd					X			X	X		X	X	X	X			7
sym2_h_1_energy	X	X	X					X	X				X		X		7
sym2_v_1_sd		X	X						X		X	X	X		X		7
coif1_a_3_energy		X	X	X					X		X				X		6
dmey_diag_3_energy							X				X	X	X	X	X		6
dmey_h_1_energy	X	X	X		X			X		X							6
dmey_v_2_sd							X	X	X	X	X		X				6
haar_h_5_sd	X		X				X		X		X		X				6
haar_v_1_energy		X				X	X	X		X			X				6
sym2_diag_4_sd			X	X		X	X	X	X								6
coif1_a_4_energy	X	X			X							X		X			5
coif1_diag_3_sd			X				X		X		X		X				5
coif1_h_1_sd		X						X	X				X		X		5

DISCRIMINANT FUNCTION COEFFICIENTS (continued).

Variables	Ike	Katrina	Ike and Katrina	Ike, Katrina and Ivan	Ike and Ivan	Katrina and Ivan	Ike, Rita, Katrina and Ivan	Ike, Rita and Katrina	Ike and Rita	Ivan	Ike, Rita and Ivan	Rita, Katrina and Ivan	Rita and Katrina	Rita and Ivan	Rita	Joplin Tornado DF	frequency in models
dmey_h_2_sd	X							X	X				X	X			5
dmey_v_5_energy								X	X		X	X	X				5
haar_a_5_sd	X							X			X		X		X		5
haar_diag_2_sd	X		X		X						X				X		5
haar_h_2_sd		X						X	X		X			X			5
sym2_diag_2_energy				X	X			X			X		X				5
sym2_diag_3_energy			X				X	X	X						X		5
sym2_diag_5_sd				X	X		X	X	X								5
sym2_h_5_energy						X	X	X				X	X				5
coif1_a_5_sd		X						X				X			X		4
coif1_h_3_sd						X	X							X	X		4
coif1_v_1_sd				X							X		X		X		4
coif1_v_3_sd							X		X		X				X		4
dmey_a_1_energy											X	X	X		X		4
dmey_a_2_mean						X	X						X		X		4
haar_a_5_energy				X		X	X			X							4
haar_h_3_sd	X								X		X	X					4
sym2_a_4_energy					X						X	X		X			4
sym2_h_2_sd	X	X	X			X											4
sym2_v_2_energy		X		X	X								X				4
coif1_diag_2_sd		X							X						X		3

DISCRIMINANT FUNCTION COEFFICIENTS (continued).

Variables	Ike	Katrina	Ike and Katrina	Ike, Katrina and Ivan	Ike and Ivan	Katrina and Ivan	Ike, Rita, Katrina and Ivan	Ike, Rita and Katrina	Ike and Rita	Ivan	Ike, Rita and Ivan	Rita, Katrina and Ivan	Rita and Katrina	Rita and Ivan	Rita	Joplin Tornado DF	frequency in models
coif1_diag_3_energy								X				X	X				3
coif1_diag_4_sd					X	X					X						3
coif1_h_2_energy		X			X										X		3
coif1_h_2_sd						X							X		X		3
coif1_h_4_energy					X			X			X						3
coif1_h_4_mean							X	X					X				3
coif1_h_5_energy									X	X					X		3
coif1_h_5_sd									X	X					X		3
coif1_v_1_energy						X	X			X							3
coif1_v_2_energy													X	X	X		3
dmey_diag_3_sd	X			X							X						3
dmey_h_3_sd				X				X	X								3
dmey_v_1_mean		X						X				X					3
haar_diag_3_sd					X	X		X									3
haar_diag_4_energy						X		X		X							3
haar_diag_4_sd				X	X	X											3
haar_h_2_energy		X							X				X				3
haar_h_4_energy				X	X					X							3
haar_v_2_energy	X	X						X									3
haar_v_2_sd	X	X						X									3
haar_v_5_energy						X						X	X				3

DISCRIMINANT FUNCTION COEFFICIENTS (continued).

Variables	Ike	Katrina	Ike and Katrina	Ike, Katrina and Ivan	Ike and Ivan	Katrina and Ivan	Ike, Rita, Katrina and Ivan	Ike, Rita and Katrina	Ike and Rita	Ivan	Ike, Rita and Ivan	Rita, Katrina and Ivan	Rita and Katrina	Rita and Ivan	Rita	Joplin Tornado DF	frequency in models
sym2_a_2_sd								X			X		X				3
sym2_diag_3_sd				X					X		X						3
sym2_diag_4_energy		X						X	X				X				3
sym2_h_1_sd									X				X		X		3
sym2_h_3_sd	X											X	X				3
sym2_h_5_sd									X					X	X		3
sym2_v_4_energy	X	X						X									3
coif1_a_5_energy												X		X			2
coif1_diag_4_energy		X									X						2
coif1_diag_5_energy												X		X			2
coif1_diag_5_sd									X						X		2
coif1_h_3_energy		X				X											2
dmey_a_1_mean								X			X						2
dmey_a_1_sd									X				X				2
dmey_a_2_energy							X							X			2
dmey_a_5_sd												X		X			2
dmey_diag_4_sd							X	X									2
haar_a_3_sd													X			X	2
haar_a_4_mean										X					X		2
haar_a_5_mean												X		X			2
haar_diag_5_energy						X		X							X		2

DISCRIMINANT FUNCTION COEFFICIENTS (continued).

Variables	Ike	Katrina	Ike and Katrina	Ike, Katrina and Ivan	Ike and Ivan	Katrina and Ivan	Ike, Rita, Katrina and Ivan	Ike, Rita and Katrina	Ike and Rita	Ivan	Ike, Rita and Ivan	Rita, Katrina and Ivan	Rita and Katrina	Rita and Ivan	Rita	Joplin Tornado DF	frequency in models
haar_h_3_energy	X												X				2
haar_h_4_sd				X	X												2
haar_h_5_energy						X	X										2
haar_v_1_sd		X									X						2
haar_v_3_energy						X				X							2
haar_v_3_sd				X		X											2
haar_v_4_energy													X		X		2
haar_v_4_sd							X		X								2
sym2_a_2_mean				X					X								2
sym2_a_4_mean											X			X			2
sym2_a_5_sd							X		X								2
sym2_h_2_energy		X				X											2
sym2_v_2_sd					X	X											2
coif1_a_1_energy						X											1
coif1_a_2_energy							X										1
coif1_a_2_sd														X			1
coif1_a_3_mean				X													1
coif1_a_3_sd								X									1
coif1_a_4_mean					X												1
coif1_a_4_sd											X						1
coif1_a_5_mean					X												1

DISCRIMINANT FUNCTION COEFFICIENTS (continued).

Variables	Ike	Katrina	Ike and Katrina	Ike, Katrina and Ivan	Ike and Ivan	Katrina and Ivan	Ike, Rita, Katrina and Ivan	Ike, Rita and Katrina	Ike and Rita	Ivan	Ike, Rita and Ivan	Rita, Katrina and Ivan	Rita and Katrina	Rita and Ivan	Rita	Joplin Tornado DF	frequency in models
coif1_h_4_sd					X												1
coif1_h_5_mean						X											1
coif1_v_1_mean				X													1
coif1_v_2_sd		X															1
coif1_v_4_energy													X				1
coif1_v_4_sd												X					1
dmey_a_2_sd												X					1
dmey_a_5_mean											X						1
dmey_diag_4_energy												X					1
dmey_diag_5_sd		X															1
dmey_v_3_energy												X					1
dmey_v_4_energy						X											1
dmey_v_4_sd															X		1
haar_a_4_sd													X				1
haar_diag_5_sd									X								1
haar_h_1_sd									X								1
haar_h_5_mean				X													1
haar_v_5_sd								X									1
signal_mean												X					1
signal_sd													X				1
sym2_a_1_energy															X		1

DISCRIMINANT FUNCTION COEFFICIENTS (continued).

Variables	Ike	Katrina	Ike and Katrina	Ike, Katrina and Ivan	Ike and Ivan	Katrina and Ivan	Ike, Rita, Katrina and Ivan	Ike, Rita and Katrina	Ike and Rita	Ivan	Ike, Rita and Ivan	Rita, Katrina and Ivan	Rita and Katrina	Rita and Ivan	Rita	Joplin Tornado DF	frequency in models
sym2_a_3_energy	X																1
sym2_a_3_sd								X									1
sym2_a_4_sd														X			1
sym2_a_5_mean					X												1
sym2_diag_5_energy		X									X		X				1
sym2_h_1_mean				X				X									1
sym2_h_3_energy	X																1
sym2_h_5_mean														X			1
sym2_v_3_sd				X													1
sym2_v_4_sd	X																1
sym2_v_5_energy	X																1

APPENDIX B

242 INDEPENDENT VARIABLES

List of 242 independent variables used in all discriminant analyses. As few as eighteen and as many as fifty seven appear in hurricane and hurricane combination discriminant functions. Only six appear in the Joplin tornado discriminant function.

Variable Name	**Description**
hurr_name	Text hurricane name such (e.g., Ike, Katrina, etc.)
hurricane	Numeric representation of hurricane name (e.g., 1 for hurricane Ike samples)
category	Numeric value representing the damage category (e.g., 1 for No Damage)
signal_mean	Mean value of the image sample pixels
signal_sd	Standard deviation of the values of image sample pixels
haar_a_1_mean	Mean value of the first level Haar wavelet transform approximation coefficients
haar_a_1_energy	Energy, ENG, or angular second moment, of the first level Haar wavelet transform approximation $$ENG = (\frac{1}{M * N}) \sum_{i=1}^{M} \sum_{j=1}^{N} \mid c(i,j) \mid$$ Where c(i,j) is a wavelet coefficient of a subimage with M rows and N columns at i, j at one level
haar_a_1_sd	Standard deviation of the first level Haar wavelet transform approximation coefficients
haar_h_1_mean	Mean value of the first level horizontal Haar wavelet transform coefficients

242 INDEPENDENT VARIABLES (continued).

Variable Name	Description
haar_h_1_energy	ENG value of the first level horizontal Haar wavelet transform coefficients
haar_h_1_sd	Standard deviation of the first level horizontal Haar wavelet coefficients
haar_v_1_mean	Mean value of the first level vertical Haar wavelet coefficients
haar_v_1_energy	ENG value of the first level vertical Haar wavelet coefficients
haar_v_1_sd	Standard deviation of the first level vertical Haar wavelet coefficients
haar_diag_1_mean	Mean value of the first level diagonal Haar wavelet transform coefficients
haar_diag_1_energy	ENG of the first level diagonal Haar wavelet transform coefficients
haar_diag_1_sd	Standard deviation of the first level diagonal Haar wavelet transform coefficients
dmey_a_1_mean	Mean value of the first level discrete Meyer wavelet transform approximation coefficients
dmey_a_1_energy	ENG of the first level discrete Meyer wavelet transform approximation coefficients
dmey_a_1_sd	Standard deviation of the first level discrete Meyer wavelet transform approximation coefficients
dmey_h_1_mean	Mean of the first level discrete Meyer horizontal wavelet transform coefficients

242 INDEPENDENT VARIABLES (continued).

Variable Name	Description
dmey_h_1_energy	ENG of the first level discrete Meyer horizontal wavelet transform coefficients
dmey_h_1_sd	Standard deviation of the first level discrete Meyer horizontal wavelet transform coefficients
dmey_v_1_mean	Mean of the first level discrete Meyer vertical wavelet transform coefficients
dmey_v_1_energy	ENG of the first level discrete Meyer vertical wavelet transform coefficients
dmey_v_1_sd	Standard deviation of the first level discrete Meyer vertical wavelet transform coefficients
dmey_diag_1_mean	Mean of the first level discrete Meyer diagonal wavelet transform coefficients
dmey_diag_1_energy	ENG of the first level discrete Meyer diagonal wavelet transform coefficients
dmey_diag_1_sd	Standard deviation of the first level discrete Meyer diagonal wavelet transform coefficients
coif1_a_1_mean	Mean of the first level Coiflet wavelet transform approximation
coif1_a_1_energy	ENG of the first level Coiflet wavelet transform approximation coefficients
coif1_a_1_sd	Standard deviation of the first level Coiflet wavelet transform approximation coefficients
coif1_h_1_mean	Mean of the first level horizontal Coiflet wavelet transform coefficients

242 INDEPENDENT VARIABLES (continued).

Variable Name	Description
coif1_h_1_energy	ENG of the first level horizontal Coiflet wavelet transform coefficients
coif1_h_1_sd	Standard deviation of the first level horizontal Coiflet wavelet transform coefficients
coif1_v_1_mean	Mean of the first level vertical Coiflet wavelet transform coefficients
coif1_v_1_energy	ENG of the first level vertical Coiflet wavelet transform coefficients
coif1_v_1_sd	Standard deviation of the first level vertical Coiflet wavelet transform coefficients
coif1_diag_1_mean	Mean of the first level diagonal Coiflet wavelet transform coefficients
coif1_diag_1_energy	ENG of the first level diagonal Coiflet wavelet transform coefficients
coif1_diag_1_sd	Standard deviation of the first level diagonal Coiflet wavelet transform coefficients
sym2_a_1_mean	Mean of the first level Symlet wavelet approximation coefficients
sym2_a_1_energy	ENG of the first level Symlet wavelet approximation coefficients
sym2_a_1_sd	Standard deviation of the first level Symlet wavelet transform approximation coefficients
sym2_h_1_mean	Mean of the first level horizontal Symlet wavelet transform coefficients

242 INDEPENDENT VARIABLES (continued).

Variable Name	Description
sym2_h_1_energy	ENG of the first level horizontal Symlet wavelet transform coefficients
sym2_h_1_sd	Standard deviation of the first level horizontal Symlet wavelet transform coefficients
sym2_v_1_mean	Mean of the first level vertical Symlet wavelet transform coefficients
sym2_v_1_energy	ENG of the first level vertical Symlet wavelet transform coefficients
sym2_v_1_sd	Standard deviation of the first level vertical Symlet wavelet transform coefficients
sym2_diag_1_mean	Mean of the first level diagonal Symlet wavelet transform coefficients
sym2_diag_1_energy	ENG of the first level diagonal Symlet wavelet transform coefficients
sym2_diag_1_sd	Standard deviation of the first level diagonal Symlet wavelet transform coefficients
haar_a_2_mean	Mean of the second level Haar wavelet transform approximation coefficients
haar_a_2_energy	ENG of the second level Haar wavelet transform approximation coefficients
haar_a_2_sd	Standard deviation of the second level Haar wavelet transform coefficients
haar_h_2_mean	Mean of the second level horizontal Haar wavelet transform coefficients

242 INDEPENDENT VARIABLES (continued).

Variable Name	Description
haar_h_2_energy	ENG of the second level horizontal Haar wavelet transform coefficients
haar_h_2_sd	Standard deviation of the second level horizontal Haar wavelet coefficients
haar_v_2_mean	Mean value of the second level vertical Haar wavelet coefficients
haar_v_2_energy	ENG value of the second level vertical Haar wavelet coefficients
haar_v_2_sd	Standard deviation of the second level vertical Haar wavelet coefficients
haar_diag_2_mean	Mean value of the second level diagonal Haar wavelet transform coefficients
haar_diag_2_energy	ENG of the second level diagonal Haar wavelet transform coefficients
haar_diag_2_sd	Standard deviation of the second level diagonal Haar wavelet transform coefficients
dmey_a_2_mean	Mean value of the second level discrete Meyer wavelet transform approximation coefficients
dmey_a_2_energy	ENG of the second level discrete Meyer wavelet transform approximation coefficients
dmey_a_2_sd	Standard deviation of the second level discrete Meyer wavelet transform approximation coefficients
dmey_h_2_mean	Mean of the second level discrete Meyer horizontal wavelet transform coefficients

242 INDEPENDENT VARIABLES (continued).

Variable Name	Description
dmey_h_2_energy	ENG of the second level discrete Meyer horizontal wavelet transform coefficients
dmey_h_2_sd	Standard deviation of the second level discrete Meyer horizontal wavelet transform coefficients
dmey_v_2_mean	Mean of the second level discrete Meyer vertical wavelet transform coefficients
dmey_v_2_energy	ENG of the second level discrete Meyer vertical wavelet transform coefficients
dmey_v_2_sd	Standard deviation of the second level discrete Meyer vertical wavelet transform coefficients
dmey_diag_2_mean	Mean of the second level discrete Meyer diagonal wavelet transform coefficients
dmey_diag_2_energy	ENG of the second level discrete Meyer diagonal wavelet transform coefficients
dmey_diag_2_sd	Standard deviation of the second level discrete Meyer diagonal wavelet transform coefficients
coif1_a_2_mean	Mean of the second level Coiflet wavelet transform approximation
coif1_a_2_energy	ENG of the second level Coiflet wavelet transform approximation coefficients
coif1_a_2_sd	Standard deviation of the second level Coiflet wavelet transform approximation coefficients
coif1_h_2_mean	Mean of the second level horizontal Coiflet wavelet transform coefficients

242 INDEPENDENT VARIABLES (continued).

Variable Name	Description
coif1_h_2_energy	ENG of the second level horizontal Coiflet wavelet transform coefficients
coif1_h_2_sd	Standard deviation of the second level horizontal Coiflet wavelet transform coefficients
coif1_v_2_mean	Mean of the second level vertical Coiflet wavelet transform coefficients
coif1_v_2_energy	ENG of the second level vertical Coiflet wavelet transform coefficients
coif1_v_2_sd	Standard deviation of the second level vertical Coiflet wavelet transform coefficients
coif1_diag_2_mean	Mean of the second level diagonal Coiflet wavelet transform coefficients
coif1_diag_2_energy	ENG of the second level diagonal Coiflet wavelet transform coefficients
coif1_diag_2_sd	Standard deviation of the second level diagonal Coiflet wavelet transform coefficients
sym2_a_2_mean	Mean of the second level Symlet wavelet approximation coefficients
sym2_a_2_energy	ENG of the second level Symlet wavelet approximation coefficients
sym2_a_2_sd	Standard deviation of the second level Symlet wavelet transform approximation coefficients
sym2_h_2_mean	Mean of the second level horizontal Symlet wavelet transform coefficients

242 INDEPENDENT VARIABLES (continued).

Variable Name	Description
sym2_h_2_energy	ENG of the second level horizontal Symlet wavelet transform coefficients
sym2_h_2_sd	Standard deviation of the second level horizontal Symlet wavelet transform coefficients
sym2_v_2_mean	Mean of the second level vertical Symlet wavelet transform coefficients
sym2_v_2_energy	ENG of the second level vertical Symlet wavelet transform coefficients
sym2_v_2_sd	Standard deviation of the second level vertical Symlet wavelet transform coefficients
sym2_diag_2_mean	Mean of the second level diagonal Symlet wavelet transform coefficients
sym2_diag_2_energy	ENG of the second level diagonal Symlet wavelet transform coefficients
sym2_diag_2_sd	Standard deviation of the second level diagonal Symlet wavelet transform coefficients
haar_a_3_mean	Mean of the third level Haar wavelet transform approximation coefficients
haar_a_3_energy	ENG of the third level Haar wavelet transform approximation coefficients
haar_a_3_sd	Standard deviation of the third level Haar wavelet transform coefficients
haar_h_3_mean	Mean of the third level horizontal Haar wavelet transform coefficients

242 INDEPENDENT VARIABLES (continued).

Variable Name	Description
haar_h_3_energy	ENG of the third level horizontal Haar wavelet transform coefficients
haar_h_3_sd	Standard deviation of the third level horizontal Haar wavelet coefficients
haar_v_3_mean	Mean value of the third level vertical Haar wavelet coefficients
haar_v_3_energy	ENG value of the third level vertical Haar wavelet coefficients
haar_v_3_sd	Standard deviation of the third level vertical Haar wavelet coefficients
haar_diag_3_mean	Mean value of the third level diagonal Haar wavelet transform coefficients
haar_diag_3_energy	ENG of the third level diagonal Haar wavelet transform coefficients
haar_diag_3_sd	Standard deviation of the third level diagonal Haar wavelet transform coefficients
dmey_a_3_mean	Mean value of the third level discrete Meyer wavelet transform approximation coefficients
dmey_a_3_energy	ENG of the third level discrete Meyer wavelet transform approximation coefficients
dmey_a_3_sd	Standard deviation of the third level discrete Meyer wavelet transform approximation coefficients
dmey_h_3_mean	Mean of the third level discrete Meyer horizontal wavelet transform coefficients

242 INDEPENDENT VARIABLES (continued).

Variable Name	Description
dmey_h_3_energy	ENG of the third level discrete Meyer horizontal wavelet transform coefficients
dmey_h_3_sd	Standard deviation of the third level discrete Meyer horizontal wavelet transform coefficients
dmey_v_3_mean	Mean of the third level discrete Meyer vertical wavelet transform coefficients
dmey_v_3_energy	ENG of the third level discrete Meyer vertical wavelet transform coefficients
dmey_v_3_sd	Standard deviation of the third level discrete Meyer vertical wavelet transform coefficients
dmey_diag_3_mean	Mean of the third level discrete Meyer diagonal wavelet transform coefficients
dmey_diag_3_energy	ENG of the third level discrete Meyer diagonal wavelet transform coefficients
dmey_diag_3_sd	Standard deviation of the third level discrete Meyer diagonal wavelet transform coefficients
coif1_a_3_mean	Mean of the third level Coiflet wavelet transform approximation
coif1_a_3_energy	ENG of the third level Coiflet wavelet transform approximation coefficients
coif1_a_3_sd	Standard deviation of the third level Coiflet wavelet transform approximation coefficients
coif1_h_3_mean	Mean of the third level horizontal Coiflet wavelet transform coefficients

242 INDEPENDENT VARIABLES (continued).

Variable Name	Description
coif1_h_3_energy	ENG of the third level horizontal Coiflet wavelet transform coefficients
coif1_h_3_sd	Standard deviation of the third level horizontal Coiflet wavelet transform coefficients
coif1_v_3_mean	Mean of the third level vertical Coiflet wavelet transform coefficients
coif1_v_3_energy	ENG of the third level vertical Coiflet wavelet transform coefficients
coif1_v_3_sd	Standard deviation of the third level vertical Coiflet wavelet transform coefficients
coif1_diag_3_mean	Mean of the third level diagonal Coiflet wavelet transform coefficients
coif1_diag_3_energy	ENG of the third level diagonal Coiflet wavelet transform coefficients
coif1_diag_3_sd	Standard deviation of the third level diagonal Coiflet wavelet transform coefficients
sym2_a_3_mean	Mean of the third level Symlet wavelet approximation coefficients
sym2_a_3_energy	ENG of the third level Symlet wavelet approximation coefficients
sym2_a_3_sd	Standard deviation of the third level Symlet wavelet transform approximation coefficients
sym2_h_3_mean	Mean of the third level horizontal Symlet wavelet transform coefficients

242 INDEPENDENT VARIABLES (continued).

Variable Name	Description
sym2_h_3_energy	ENG of the third level horizontal Symlet wavelet transform coefficients
sym2_h_3_sd	Standard deviation of the third level horizontal Symlet wavelet transform coefficients
sym2_v_3_mean	Mean of the third level vertical Symlet wavelet transform coefficients
sym2_v_3_energy	ENG of the third level vertical Symlet wavelet transform coefficients
sym2_v_3_sd	Standard deviation of the third level vertical Symlet wavelet transform coefficients
sym2_diag_3_mean	Mean of the third level diagonal Symlet wavelet transform coefficients
sym2_diag_3_energy	ENG of the third level diagonal Symlet wavelet transform coefficients
sym2_diag_3_sd	Standard deviation of the third level diagonal Symlet wavelet transform coefficients
haar_a_4_mean	Mean of the fourth level Haar wavelet transform approximation coefficients
haar_a_4_energy	ENG of the fourth level Haar wavelet transform approximation coefficients
haar_a_4_sd	Standard deviation of the fourth level Haar wavelet transform coefficients
haar_h_4_mean	Mean of the fourth level horizontal Haar wavelet transform coefficients

242 INDEPENDENT VARIABLES (continued).

Variable Name	Description
haar_h_4_energy	ENG of the fourth level horizontal Haar wavelet transform coefficients
haar_h_4_sd	Standard deviation of the fourth level horizontal Haar wavelet coefficients
haar_v_4_mean	Mean value of the fourth level vertical Haar wavelet coefficients
haar_v_4_energy	ENG value of the fourth level vertical Haar wavelet coefficients
haar_v_4_sd	Standard deviation of the fourth level vertical Haar wavelet coefficients
haar_diag_4_mean	Mean value of the fourth level diagonal Haar wavelet transform coefficients
haar_diag_4_energy	ENG of the fourth level diagonal Haar wavelet transform coefficients
haar_diag_4_sd	Standard deviation of the fourth level diagonal Haar wavelet transform coefficients
dmey_a_4_mean	Mean value of the fourth level discrete Meyer wavelet transform approximation coefficients
dmey_a_4_energy	ENG of the fourth level discrete Meyer wavelet transform approximation coefficients
dmey_a_4_sd	Standard deviation of the fourth level discrete Meyer wavelet transform approximation coefficients
dmey_h_4_mean	Mean of the fourth level discrete Meyer horizontal wavelet transform coefficients

242 INDEPENDENT VARIABLES (continued).

Variable Name	Description
dmey_h_4_energy	ENG of the fourth level discrete Meyer horizontal wavelet transform coefficients
dmey_h_4_sd	Standard deviation of the fourth level discrete Meyer horizontal wavelet transform coefficients
dmey_v_4_mean	Mean of the fourth level discrete Meyer vertical wavelet transform coefficients
dmey_v_4_energy	ENG of the fourth level discrete Meyer vertical wavelet transform coefficients
dmey_v_4_sd	Standard deviation of the fourth level discrete Meyer vertical wavelet transform coefficients
dmey_diag_4_mean	Mean of the fourth level discrete Meyer diagonal wavelet transform coefficients
dmey_diag_4_energy	ENG of the fourth level discrete Meyer diagonal wavelet transform coefficients
dmey_diag_4_sd	Standard deviation of the fourth level discrete Meyer diagonal wavelet transform coefficients
coif1_a_4_mean	Mean of the fourth level Coiflet wavelet transform approximation
coif1_a_4_energy	ENG of the fourth level Coiflet wavelet transform approximation coefficients
coif1_a_4_sd	Standard deviation of the fourth level Coiflet wavelet transform approximation coefficients
coif1_h_4_mean	Mean of the fourth level horizontal Coiflet wavelet transform coefficients

242 INDEPENDENT VARIABLES (continued).

Variable Name	Description
coif1_h_4_energy	ENG of the fourth level horizontal Coiflet wavelet transform coefficients
coif1_h_4_sd	Standard deviation of the fourth level horizontal Coiflet wavelet transform coefficients
coif1_v_4_mean	Mean of the fourth level vertical Coiflet wavelet transform coefficients
coif1_v_4_energy	ENG of the fourth level vertical Coiflet wavelet transform coefficients
coif1_v_4_sd	Standard deviation of the fourth level vertical Coiflet wavelet transform coefficients
coif1_diag_4_mean	Mean of the fourth level diagonal Coiflet wavelet transform coefficients
coif1_diag_4_energy	ENG of the fourth level diagonal Coiflet wavelet transform coefficients
coif1_diag_4_sd	Standard deviation of the fourth level diagonal Coiflet wavelet transform coefficients
sym2_a_4_mean	Mean of the fourth level Symlet wavelet approximation coefficients
sym2_a_4_energy	ENG of the fourth level Symlet wavelet approximation coefficients
sym2_a_4_sd	Standard deviation of the fourth level Symlet wavelet transform approximation coefficients
sym2_h_4_mean	Mean of the fourth level horizontal Symlet wavelet transform coefficients

242 INDEPENDENT VARIABLES (continued).

Variable Name	Description
sym2_h_4_energy	ENG of the fourth level horizontal Symlet wavelet transform coefficients
sym2_h_4_sd	Standard deviation of the fourth level horizontal Symlet wavelet transform coefficients
sym2_v_4_mean	Mean of the fourth level vertical Symlet wavelet transform coefficients
sym2_v_4_energy	ENG of the fourth level vertical Symlet wavelet transform coefficients
sym2_v_4_sd	Standard deviation of the fourth level vertical Symlet wavelet transform coefficients
sym2_diag_4_mean	Mean of the fourth level diagonal Symlet wavelet transform coefficients
sym2_diag_4_energy	ENG of the fourth level diagonal Symlet wavelet transform coefficients
sym2_diag_4_sd	Standard deviation of the fourth level diagonal Symlet wavelet transform coefficients
haar_a_5_mean	Mean of the fifth level Haar wavelet transform approximation coefficients
haar_a_5_energy	ENG of the fifth level Haar wavelet transform approximation coefficients
haar_a_5_sd	Standard deviation of the fifth level Haar wavelet transform coefficients
haar_h_5_mean	Mean of the fifth level horizontal Haar wavelet transform coefficients

242 INDEPENDENT VARIABLES (continued).

Variable Name	Description
haar_h_5_energy	ENG of the fifth level horizontal Haar wavelet transform coefficients
haar_h_5_sd	Standard deviation of the fifth level horizontal Haar wavelet coefficients
haar_v_5_mean	Mean value of the fifth level vertical Haar wavelet coefficients
haar_v_5_energy	ENG value of the fifth level vertical Haar wavelet coefficients
haar_v_5_sd	Standard deviation of the fifth level vertical Haar wavelet coefficients
haar_diag_5_mean	Mean value of the fifth level diagonal Haar wavelet transform coefficients
haar_diag_5_energy	ENG of the fifth level diagonal Haar wavelet transform coefficients
haar_diag_5_sd	Standard deviation of the fifth level diagonal Haar wavelet transform coefficients
dmey_a_5_mean	Mean value of the fifth level discrete Meyer wavelet transform approximation coefficients
dmey_a_5_energy	ENG of the fifth level discrete Meyer wavelet transform approximation coefficients
dmey_a_5_sd	Standard deviation of the fifth level discrete Meyer wavelet transform approximation coefficients
dmey_h_5_mean	Mean of the fifth level discrete Meyer horizontal wavelet transform coefficients

242 INDEPENDENT VARIABLES (continued).

Variable Name	Description
dmey_h_5_energy	ENG of the fifth level discrete Meyer horizontal wavelet transform coefficients
dmey_h_5_sd	Standard deviation of the fifth level discrete Meyer horizontal wavelet transform coefficients
dmey_v_5_mean	Mean of the fifth level discrete Meyer vertical wavelet transform coefficients
dmey_v_5_energy	ENG of the fifth level discrete Meyer vertical wavelet transform coefficients
dmey_v_5_sd	Standard deviation of the fifth level discrete Meyer vertical wavelet transform coefficients
dmey_diag_5_mean	Mean of the fifth level discrete Meyer diagonal wavelet transform coefficients
dmey_diag_5_energy	ENG of the fifth level discrete Meyer diagonal wavelet transform coefficients
dmey_diag_5_sd	Standard deviation of the fifth level discrete Meyer diagonal wavelet transform coefficients
coif1_a_5_mean	Mean of the fifth level Coiflet wavelet transform approximation
coif1_a_5_energy	ENG of the fifth level Coiflet wavelet transform approximation coefficients
coif1_a_5_sd	Standard deviation of the fifth level Coiflet wavelet transform approximation coefficients
coif1_h_5_mean	Mean of the fifth level horizontal Coiflet wavelet transform coefficients

242 INDEPENDENT VARIABLES (continued).

Variable Name	Description
coif1_h_5_energy	ENG of the fifth level horizontal Coiflet wavelet transform coefficients
coif1_h_5_sd	Standard deviation of the fifth level horizontal Coiflet wavelet transform coefficients
coif1_v_5_mean	Mean of the fifth level vertical Coiflet wavelet transform coefficients
coif1_v_5_energy	ENG of the fifth level vertical Coiflet wavelet transform coefficients
coif1_v_5_sd	Standard deviation of the fifth level vertical Coiflet wavelet transform coefficients
coif1_diag_5_mean	Mean of the fifth level diagonal Coiflet wavelet transform coefficients
coif1_diag_5_energy	ENG of the fifth level diagonal Coiflet wavelet transform coefficients
coif1_diag_5_sd	Standard deviation of the fifth level diagonal Coiflet wavelet transform coefficients
sym2_a_5_mean	Mean of the fifth level Symlet wavelet approximation coefficients
sym2_a_5_energy	ENG of the fifth level Symlet wavelet approximation coefficients
sym2_a_5_sd	Standard deviation of the fifth level Symlet wavelet transform approximation coefficients
sym2_h_5_mean	Mean of the fifth level horizontal Symlet wavelet transform coefficients

242 INDEPENDENT VARIABLES (continued).

Variable Name	Description
sym2_h_5_energy	ENG of the fifth level horizontal Symlet wavelet transform coefficients
sym2_h_5_sd	Standard deviation of the fifth level horizontal Symlet wavelet transform coefficients
sym2_v_5_mean	Mean of the fifth level vertical Symlet wavelet transform coefficients
sym2_v_5_energy	ENG of the fifth level vertical Symlet wavelet transform coefficients
sym2_v_5_sd	Standard deviation of the fifth level vertical Symlet wavelet transform coefficients
sym2_diag_5_mean	Mean of the fifth level diagonal Symlet wavelet transform coefficients
sym2_diag_5_energy	ENG of the fifth level diagonal Symlet wavelet transform coefficients
sym2_diag_5_sd	Standard deviation of the fifth level diagonal Symlet wavelet transform coefficients

APPENDIX C

DISCRIMINANT ANALYSIS AND CLASSIFICATION PERFORMANCE CHARTS

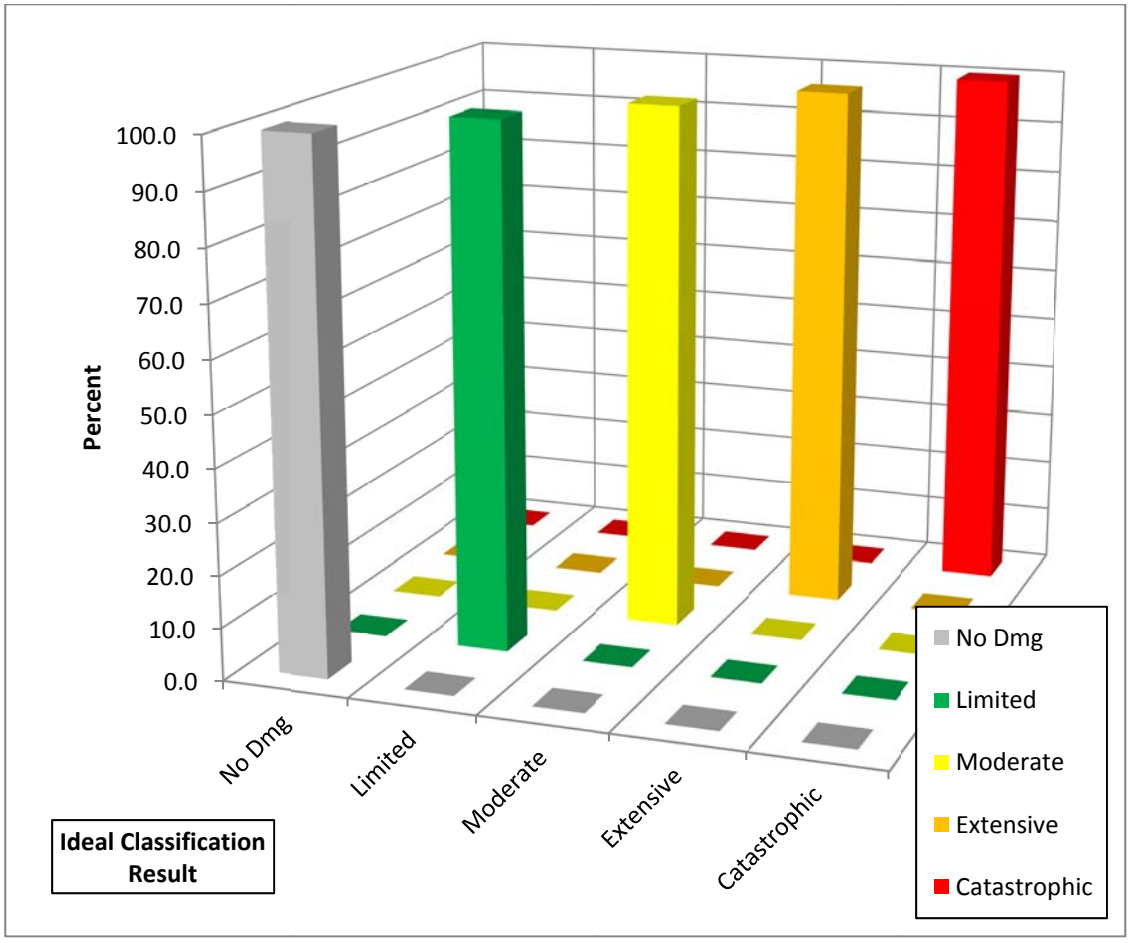

Ideal discriminant analysis classification accuracy bar chart.

Ideal discriminant analysis classification accuracy table.

Ideal Classification Result – 100 percent correct classification

Count	No Dmg	Limited	Moderate	Extensive	Catastrophic	Total
No Dmg	73	0	0	0	0	73
Limited	0	112	0	0	0	112
Moderate	0	0	330	0	0	330
Extensive	0	0	0	74	0	74
Catastrophic	0	0	0	0	160	160

Percent	No Dmg	Limited	Moderate	Extensive	Catastrophic	Total
No Dmg	100.0	0.0	0.0	0.0	0.0	100
Limited	0.0	100.0	0.0	0.0	0.0	100
Moderate	0.0	0.0	100.0	0.0	0.0	100
Extensive	0.0	0.0	0.0	100.0	0.0	100
Catastrophic	0.0	0.0	0.0	0.0	100.0	100

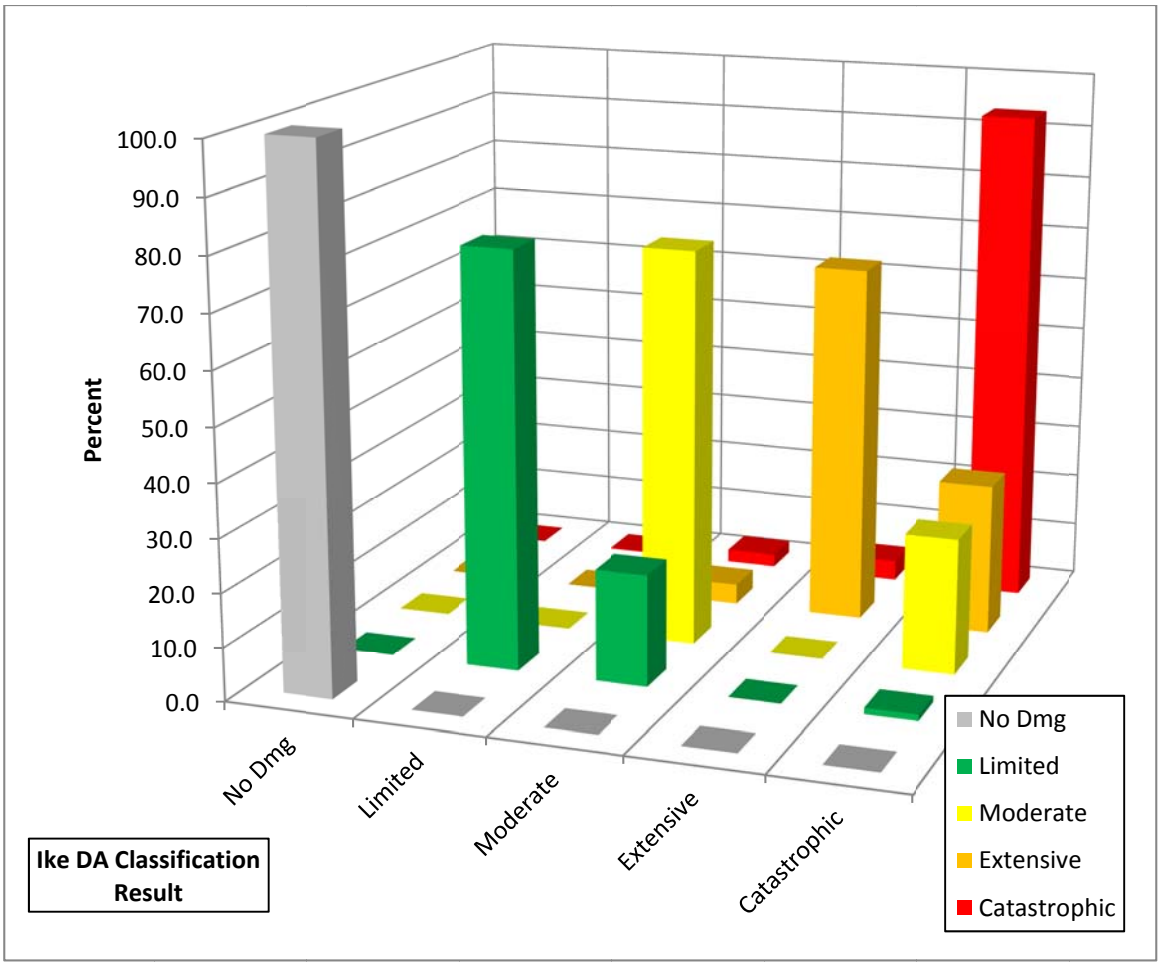

Ike discriminant analysis classification accuracy bar chart.

Ike discriminant analysis classification accuracy table.

Ike DA Classification Result - 89.5 percent correct classification

Count	No Dmg	Limited	Moderate	Extensive	Catastrophic	Total
No Dmg	274	0	0	0	0	274
Limited	0	67	18	0	1	86
Moderate	0	0	70	0	24	94
Extensive	0	0	4	71	30	105
Catastrophic	0	1	11	17	420	449

Percent	No Dmg	Limited	Moderate	Extensive	Catastrophic	Total
No Dmg	100.0	0.0	0.0	0.0	0.0	100
Limited	0.0	77.9	20.9	0.0	1.2	100
Moderate	0.0	0.0	74.5	0.0	25.5	100
Extensive	0.0	0.0	3.8	67.6	28.6	100
Catastrophic	0.0	0.2	2.4	3.8	93.5	100

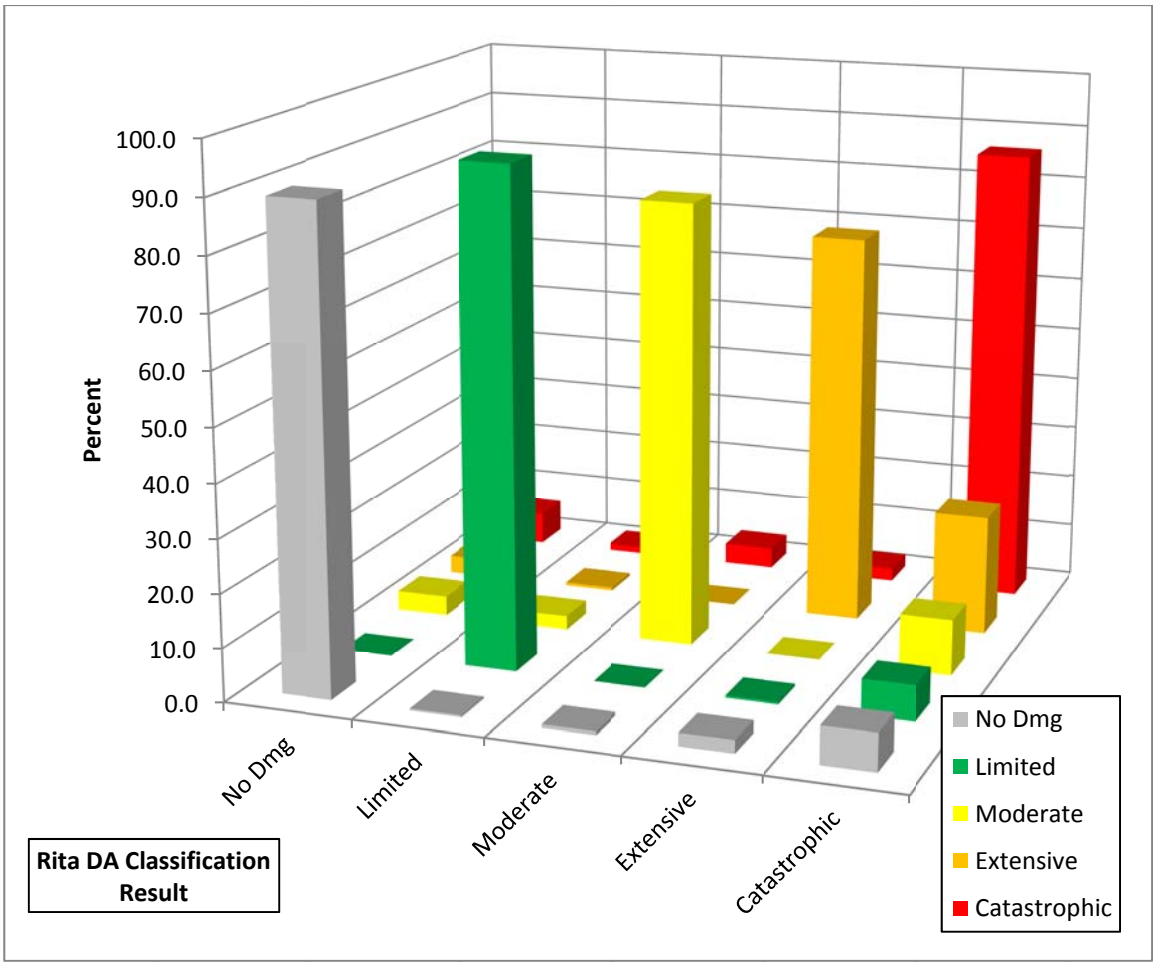

Rita discriminant analysis classification accuracy bar chart.

Rita discriminant analysis classification accuracy table.

Rita DA Classification Result - 86.0 percent correct classification

Count	No Dmg	Limited	Moderate	Extensive	Catastrophic	Total
No Dmg	255	1	2	7	20	285
Limited	0	223	0	1	16	240
Moderate	7	5	158	0	20	190
Extensive	6	1	0	130	40	177
Catastrophic	25	5	16	10	350	406

Percent	No Dmg	Limited	Moderate	Extensive	Catastrophic	Total
No Dmg	89.5	0.4	0.7	2.5	7.0	100
Limited	0.0	92.9	0.0	0.4	6.7	100
Moderate	3.7	2.6	83.2	0.0	10.5	100
Extensive	3.4	0.6	0.0	73.4	22.6	100
Catastrophic	6.2	1.2	3.9	2.5	86.2	100

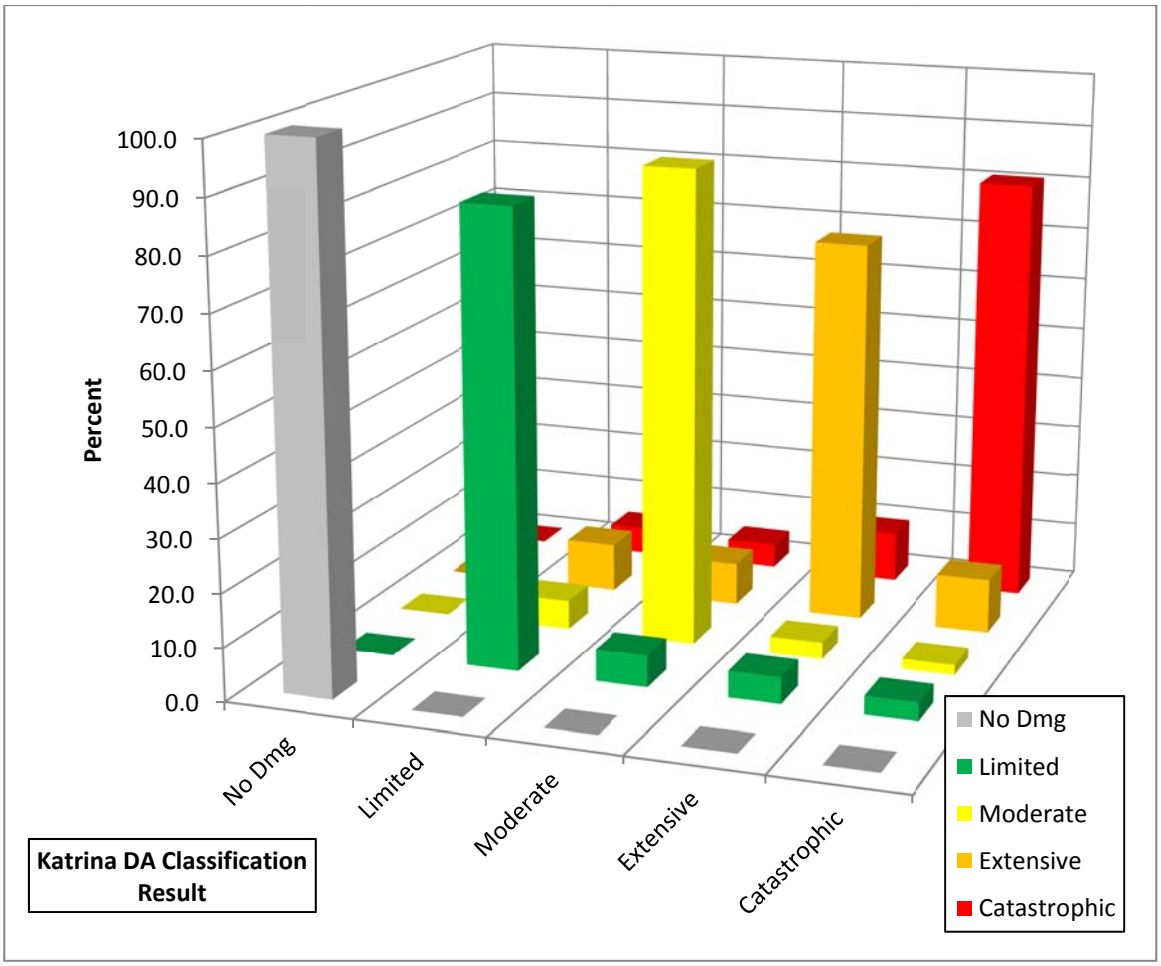

Katrina discriminant analysis classification accuracy bar chart.

Katrina discriminant analysis classification accuracy table.

Katrina DA Classification Result - 84.7 percent correct classification

Count	No Dmg	Limited	Moderate	Extensive	Catastrophic	Total
No Dmg	79	0	0	0	0	79
Limited	0	172	12	10	7	201
Moderate	0	26	420	15	9	470
Extensive	0	16	14	126	18	174
Catastrophic	0	19	17	35	297	368

Percent	No Dmg	Limited	Moderate	Extensive	Catastrophic	Total
No Dmg	100.0	0.0	0.0	0.0	0.0	100
Limited	0.0	85.6	6.0	5.0	3.5	100
Moderate	0.0	5.5	89.4	3.2	1.9	100
Extensive	0.0	9.2	8.0	72.4	10.3	100
Catastrophic	0.0	5.2	4.6	9.5	80.7	100

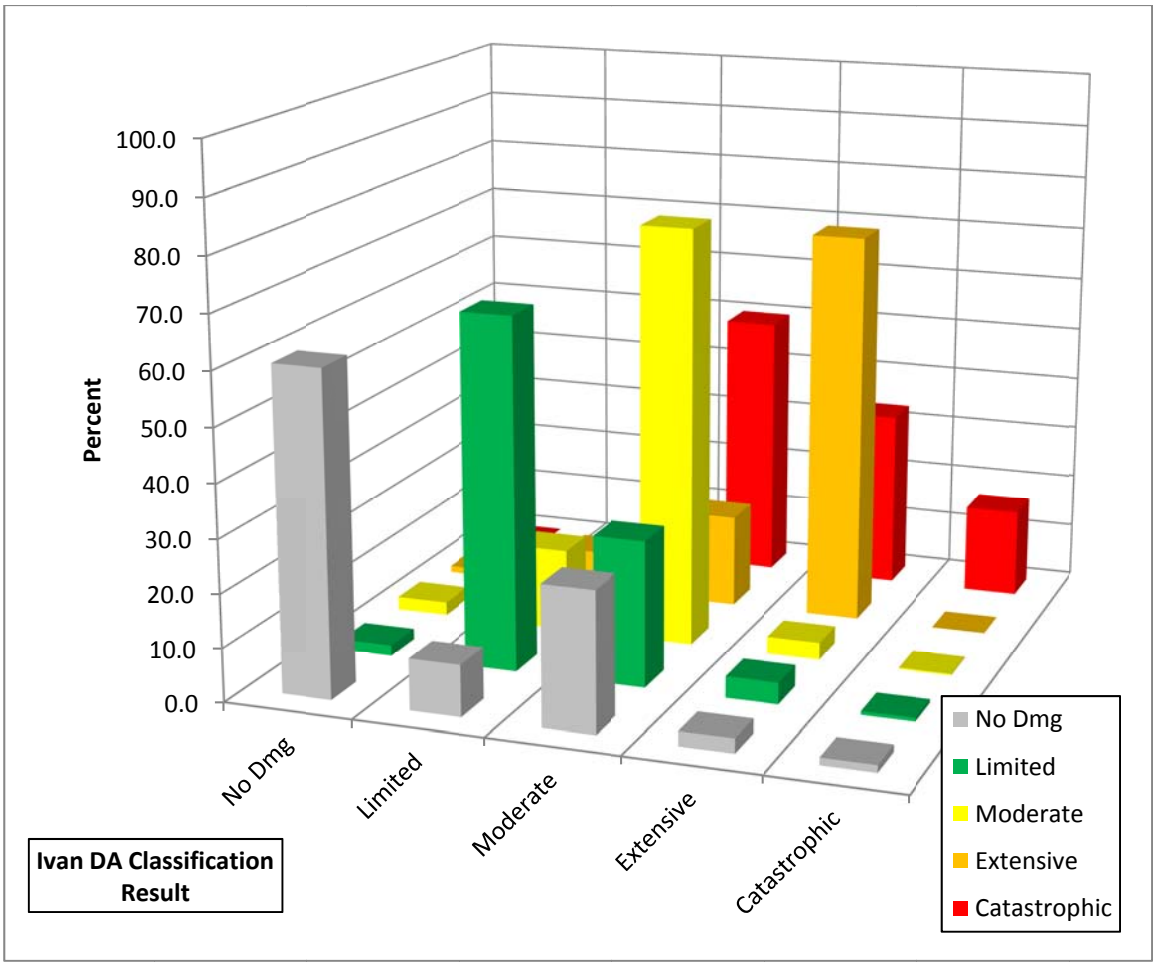

Ivan discriminant analysis classification accuracy bar chart.

Ivan discriminant analysis classification accuracy table.

Ivan DA Classification Result - 72.5 percent correct classification

Count	**No Dmg**	**Limited**	**Moderate**	**Extensive**	**Catastrophic**	**Total**
No Dmg	44	7	19	2	1	73
Limited	3	99	41	6	1	150
Moderate	10	62	315	13	1	401
Extensive	1	6	14	59	0	80
Catastrophic	0	0	6	4	2	12

Percent	No Dmg	Limited	Moderate	Extensive	Catastrophic	Total
No Dmg	60.3	9.6	26.0	2.7	1.4	100
Limited	2.0	66.0	27.3	4.0	0.7	100
Moderate	2.5	15.5	78.6	3.2	0.2	100
Extensive	1.3	7.5	17.5	73.8	0.0	100
Catastrophic	0.0	0.0	50.0	33.3	16.7	100

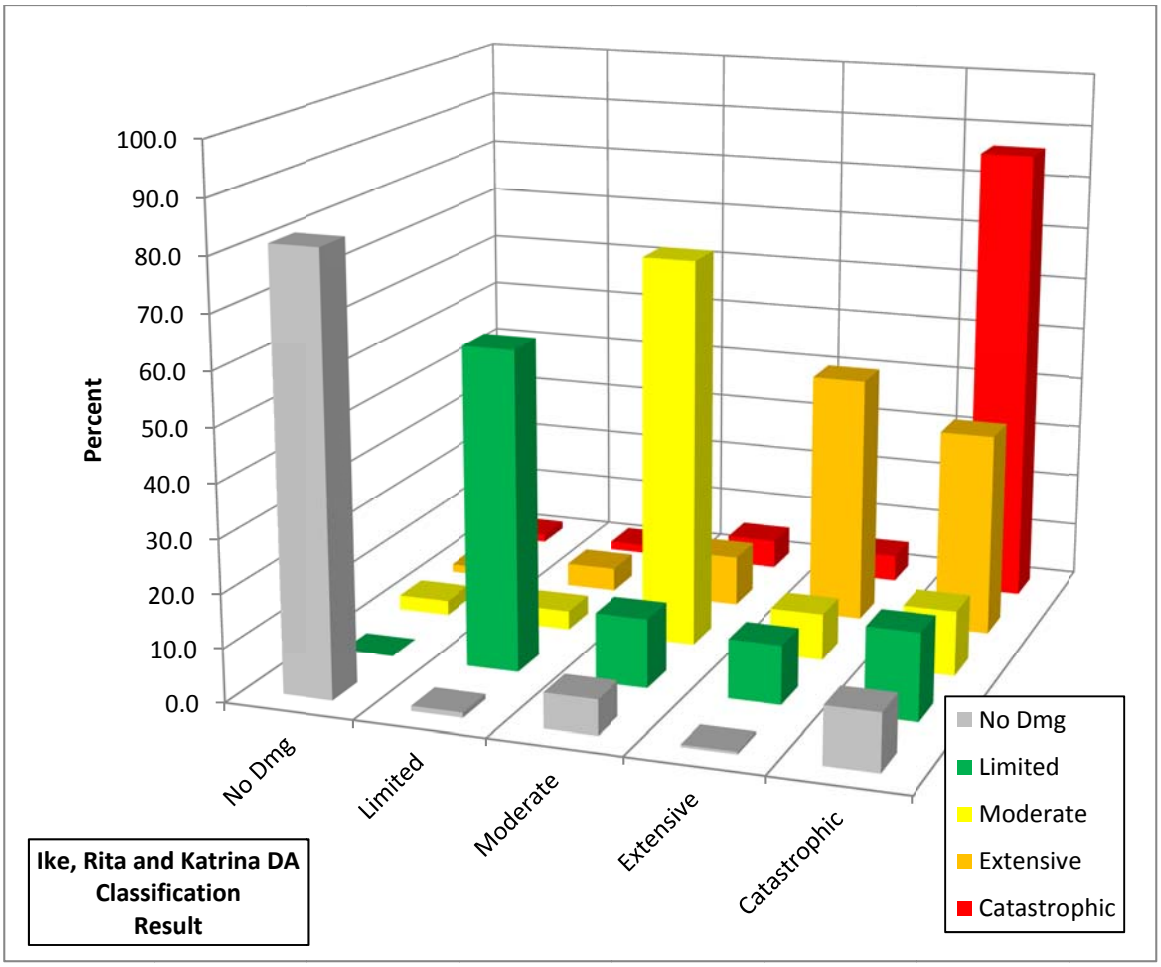

Ike, Rita and Katrina discriminant analysis classification accuracy bar chart.

Ike, Rita and Katrina discriminant analysis classification accuracy table.

Ike, Rita and Katrina DA Classification Result - 73.7 percent correct classification

Count	**No Dmg**	**Limited**	**Moderate**	**Extensive**	**Catastrophic**	**Total**
No Dmg	519	6	42	3	68	638
Limited	0	315	68	58	86	527
Moderate	21	27	548	66	92	754
Extensive	7	20	43	212	174	456
Catastrophic	18	20	66	61	1058	1223

Percent	No Dmg	Limited	Moderate	Extensive	Catastrophic	Total
No Dmg	81.3	0.9	6.6	0.5	10.7	100
Limited	0.0	59.8	12.9	11.0	16.3	100
Moderate	2.8	3.6	72.7	8.8	12.2	100
Extensive	1.5	4.4	9.4	46.5	38.2	100
Catastrophic	1.5	1.6	5.4	5.0	86.5	100

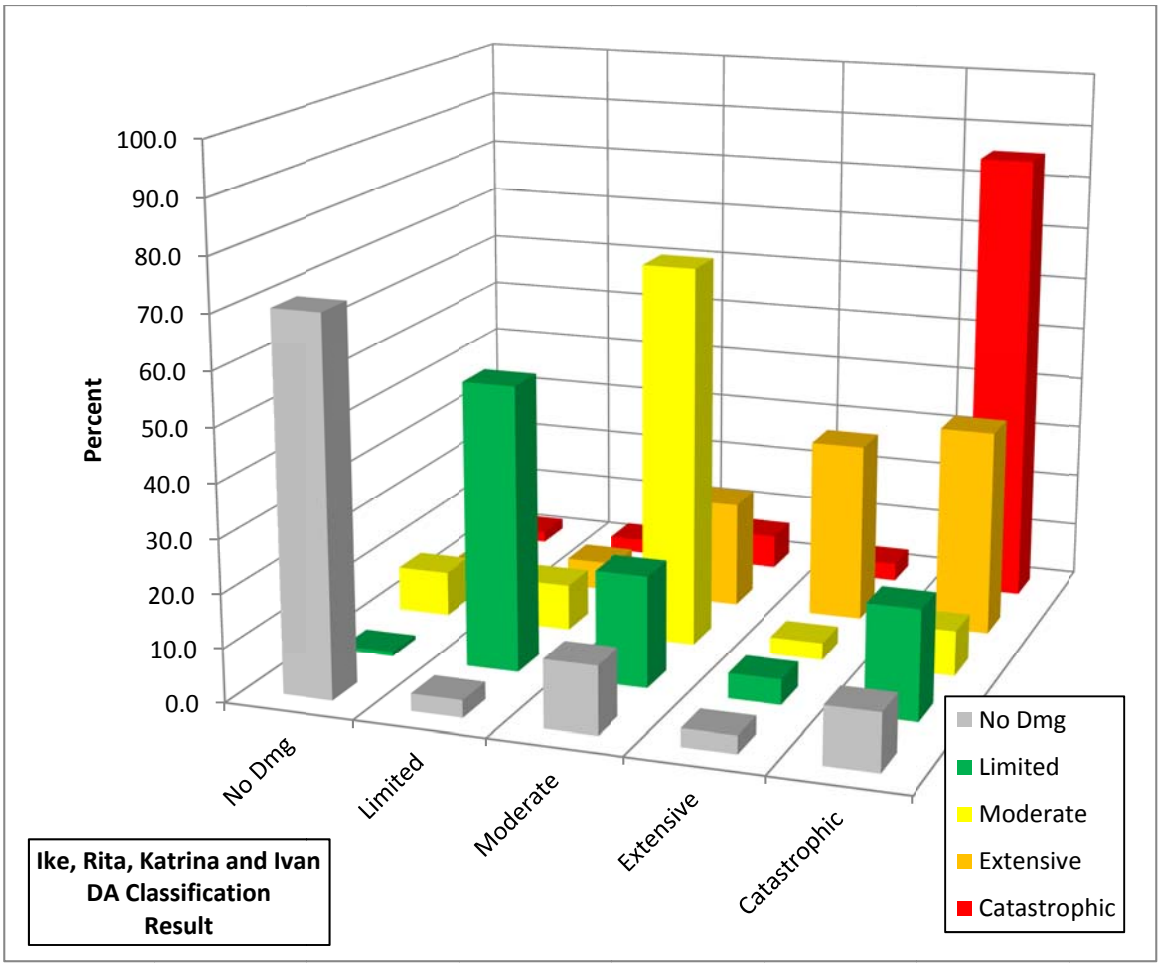

Ike, Rita, Katrina and Ivan discriminant analysis classification accuracy bar chart.

Ike, Rita, Katrina and Ivan discriminant analysis classification accuracy table.

Ike, Rita, Katrina and Ivan DA Classification Result - 67.6 percent correct classification

Count	No Dmg	Limited	Moderate	Extensive	Catastrophic	Total
No Dmg	498	23	90	24	76	711
Limited	5	360	141	32	139	677
Moderate	97	100	823	37	98	1155
Extensive	11	29	107	181	208	536
Catastrophic	25	33	79	42	1056	1235

Percent	No Dmg	Limited	Moderate	Extensive	Catastrophic	Total
No Dmg	70.0	3.2	12.7	3.4	10.7	100
Limited	0.7	53.2	20.8	4.7	20.5	100
Moderate	8.4	8.7	71.3	3.2	8.5	100
Extensive	2.1	5.4	20.0	33.8	38.8	100
Catastrophic	2.0	2.7	6.4	3.4	85.5	100

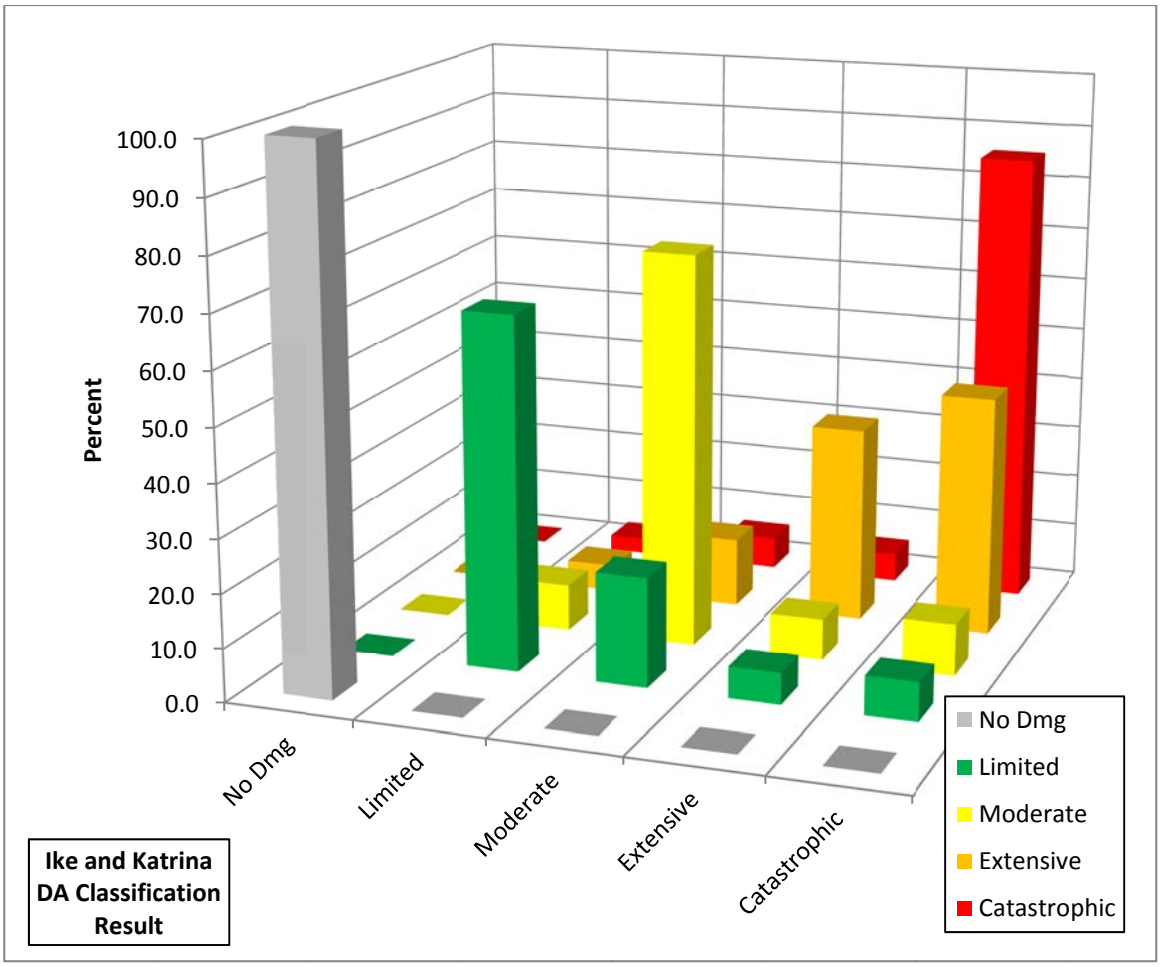

Ike and Katrina discriminant analysis classification accuracy bar chart.

Ike and Katrina discriminant analysis classification accuracy table.

Ike and Katrina DA Classification Result - 76.6 percent correct classification

Count	**No Dmg**	**Limited**	**Moderate**	**Extensive**	**Catastrophic**	**Total**
No Dmg	353	0	0	0	0	353
Limited	0	190	59	17	21	287
Moderate	0	49	416	44	55	564
Extensive	0	14	36	103	126	279
Catastrophic	0	24	49	44	700	817

Percent	No Dmg	Limited	Moderate	Extensive	Catastrophic	Total
No Dmg	100.0	0.0	0.0	0.0	0.0	100
Limited	0.0	66.2	20.6	5.9	7.3	100
Moderate	0.0	8.7	73.8	7.8	9.8	100
Extensive	0.0	5.0	12.9	36.9	45.2	100
Catastrophic	0.0	2.9	6.0	5.4	85.7	100

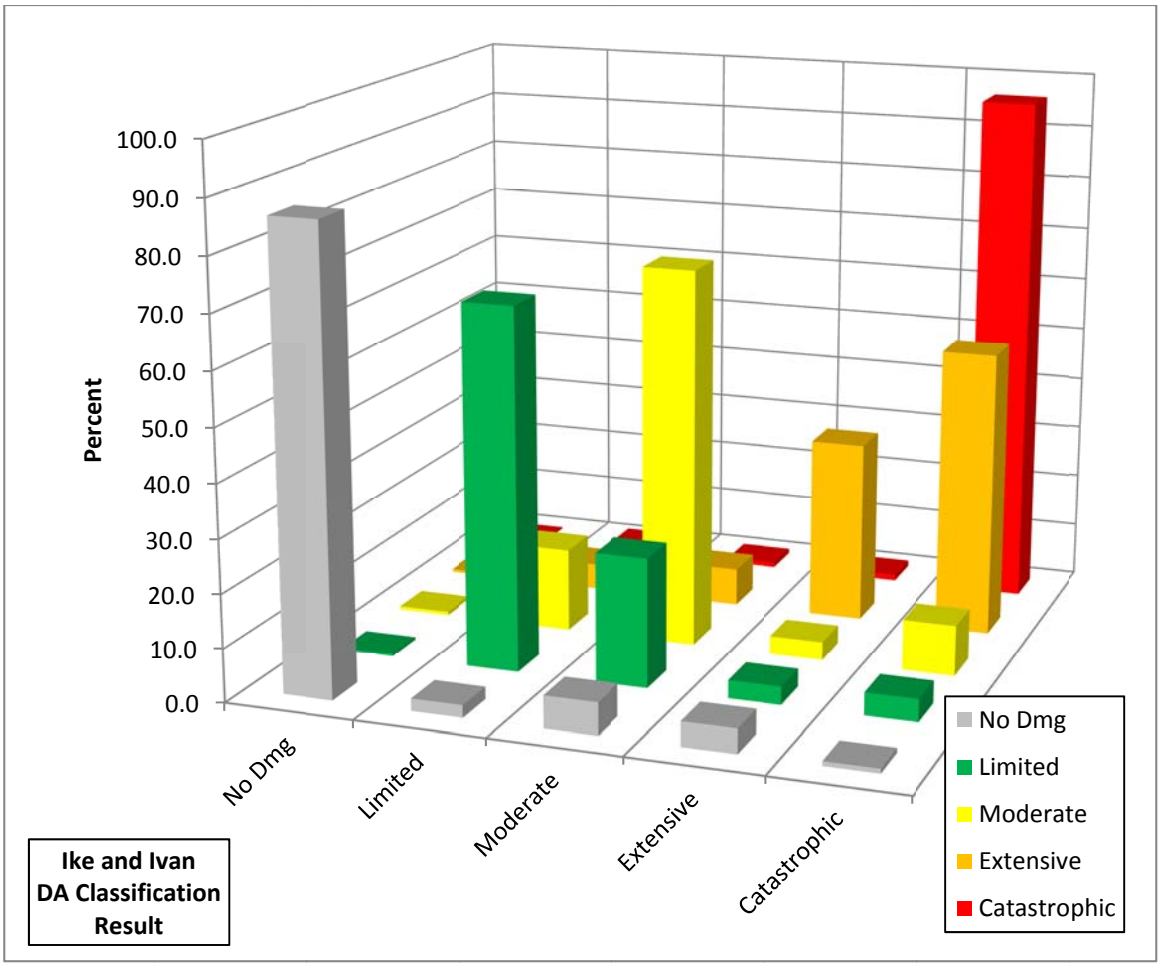

Ike and Ivan discriminant analysis classification accuracy bar chart.

Ike and Ivan discriminant analysis classification accuracy table.

Ike and Ivan DA Classification Result - 76.4 percent correct classification

Count	**No Dmg**	**Limited**	**Moderate**	**Extensive**	**Catastrophic**	**Total**
No Dmg	299	8	21	16	3	347
Limited	1	160	57	8	10	236
Moderate	3	77	351	17	47	495
Extensive	1	9	13	63	99	185
Catastrophic	1	7	4	5	444	461

Percent	No Dmg	Limited	Moderate	Extensive	Catastrophic	Total
No Dmg	86.2	2.3	6.1	4.6	0.9	100
Limited	0.4	67.8	24.2	3.4	4.2	100
Moderate	0.6	15.6	70.9	3.4	9.5	100
Extensive	0.5	4.9	7.0	34.1	53.5	100
Catastrophic	0.2	1.5	0.9	1.1	96.3	100

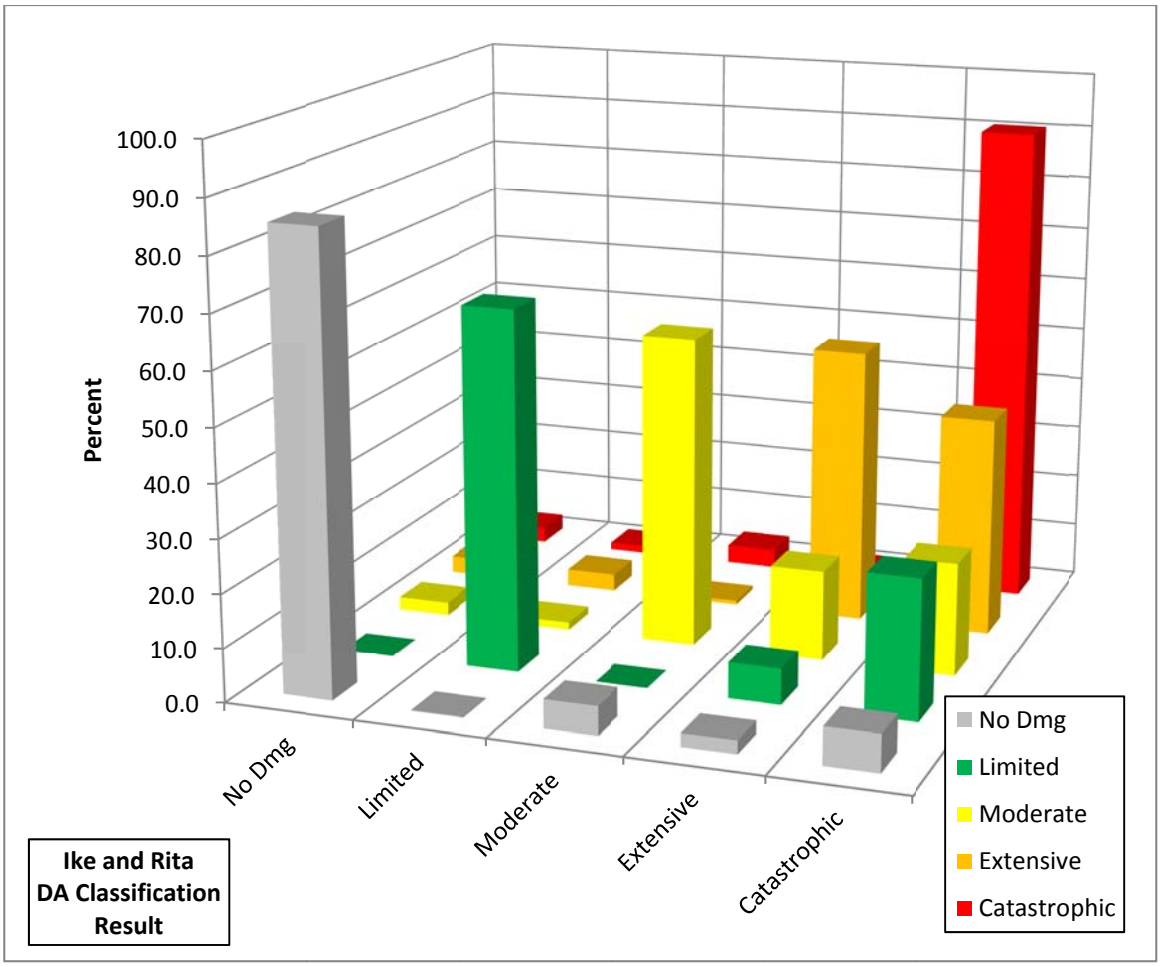

Ike and Rita discriminant analysis classification accuracy bar chart.

Ike and Rita discriminant analysis classification accuracy table.

Ike and Rita DA Classification Result - 77.2 percent correct classification

Count	**No Dmg**	**Limited**	**Moderate**	**Extensive**	**Catastrophic**	**Total**
No Dmg	475	1	30	14	39	559
Limited	0	219	0	22	85	326
Moderate	7	4	165	48	60	284
Extensive	9	9	2	146	116	282
Catastrophic	25	12	30	13	775	855

Percent	No Dmg	Limited	Moderate	Extensive	Catastrophic	Total
No Dmg	85.0	0.2	5.4	2.5	7.0	100
Limited	0.0	67.2	0.0	6.7	26.1	100
Moderate	2.5	1.4	58.1	16.9	21.1	100
Extensive	3.2	3.2	0.7	51.8	41.1	100
Catastrophic	2.9	1.4	3.5	1.5	90.6	100

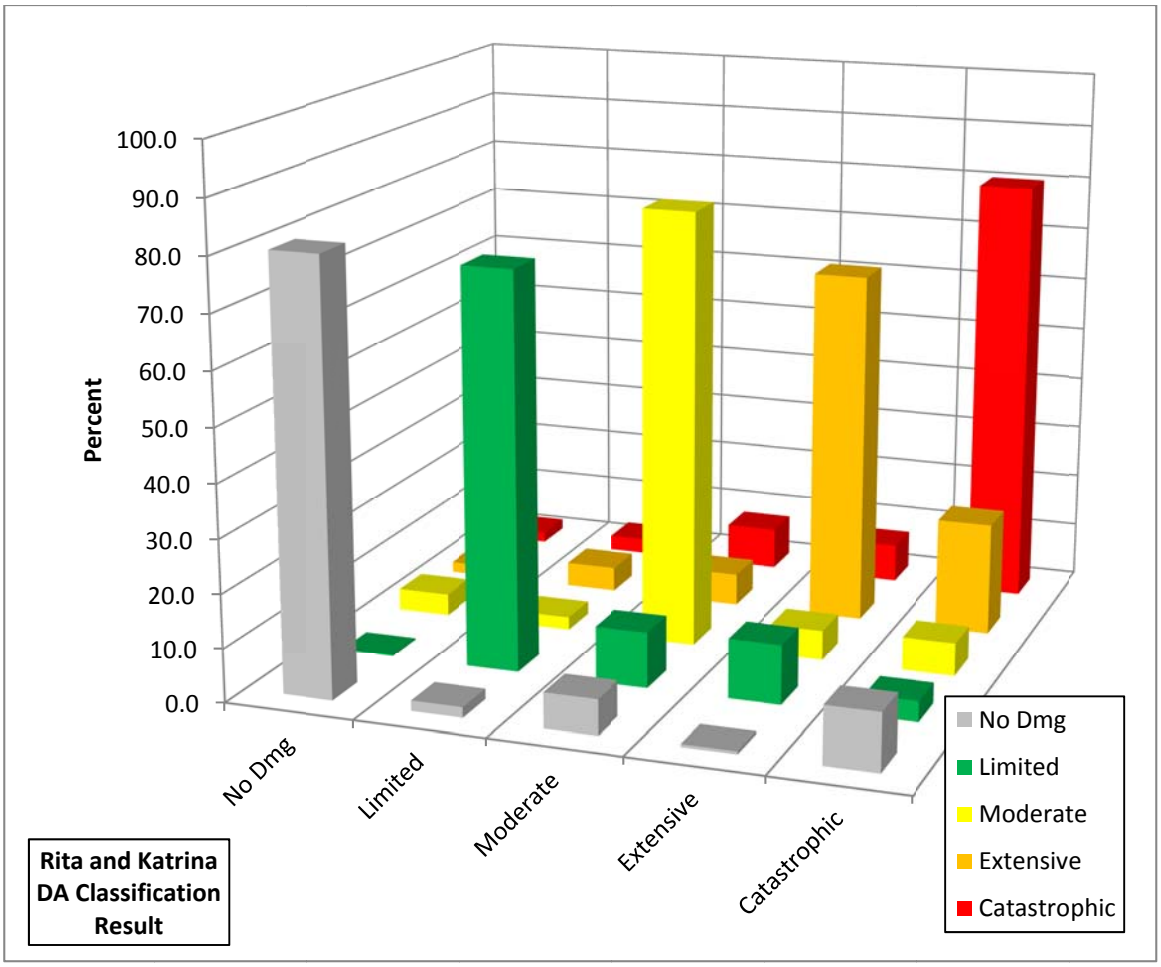

Rita and Katrina discriminant analysis classification accuracy bar chart.

Rita and Katrina discriminant analysis classification accuracy table.

Rita and Katrina DA Classification Result - 77.8 percent correct classification

Count	**No Dmg**	**Limited**	**Moderate**	**Extensive**	**Catastrophic**	**Total**
No Dmg	292	7	24	2	39	364
Limited	1	328	46	49	17	441
Moderate	27	16	539	37	41	660
Extensive	7	16	21	233	74	351
Catastrophic	15	22	60	55	622	774

Percent	No Dmg	Limited	Moderate	Extensive	Catastrophic	Total
No Dmg	80.2	1.9	6.6	0.5	10.7	100
Limited	0.2	74.4	10.4	11.1	3.9	100
Moderate	4.1	2.4	81.7	5.6	6.2	100
Extensive	2.0	4.6	6.0	66.4	21.1	100
Catastrophic	1.9	2.8	7.8	7.1	80.4	100

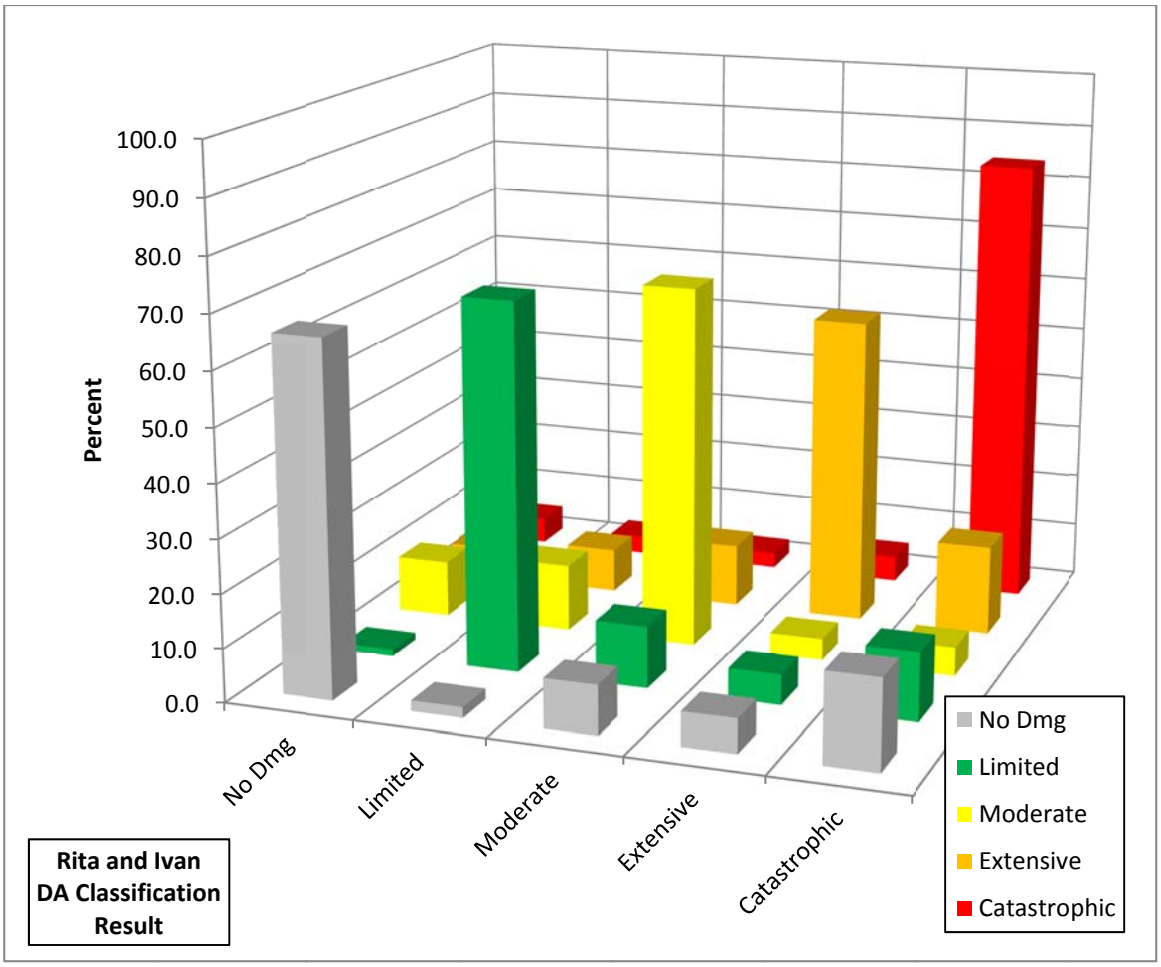

Rita and Ivan discriminant analysis classification accuracy bar chart.

Rita and Ivan discriminant analysis classification accuracy table.

Rita and Ivan DA Classification Result - 69.6 percent correct classification

Count	**No Dmg**	**Limited**	**Moderate**	**Extensive**	**Catastrophic**	**Total**
No Dmg	235	7	33	23	60	358
Limited	5	268	45	22	50	390
Moderate	62	74	399	24	32	591
Extensive	15	21	30	148	43	257
Catastrophic	20	14	12	20	352	418

Percent	No Dmg	Limited	Moderate	Extensive	Catastrophic	Total
No Dmg	65.6	2.0	9.2	6.4	16.8	100
Limited	1.3	68.7	11.5	5.6	12.8	100
Moderate	10.5	12.5	67.5	4.1	5.4	100
Extensive	5.8	8.2	11.7	57.6	16.7	100
Catastrophic	4.8	3.3	2.9	4.8	84.2	100

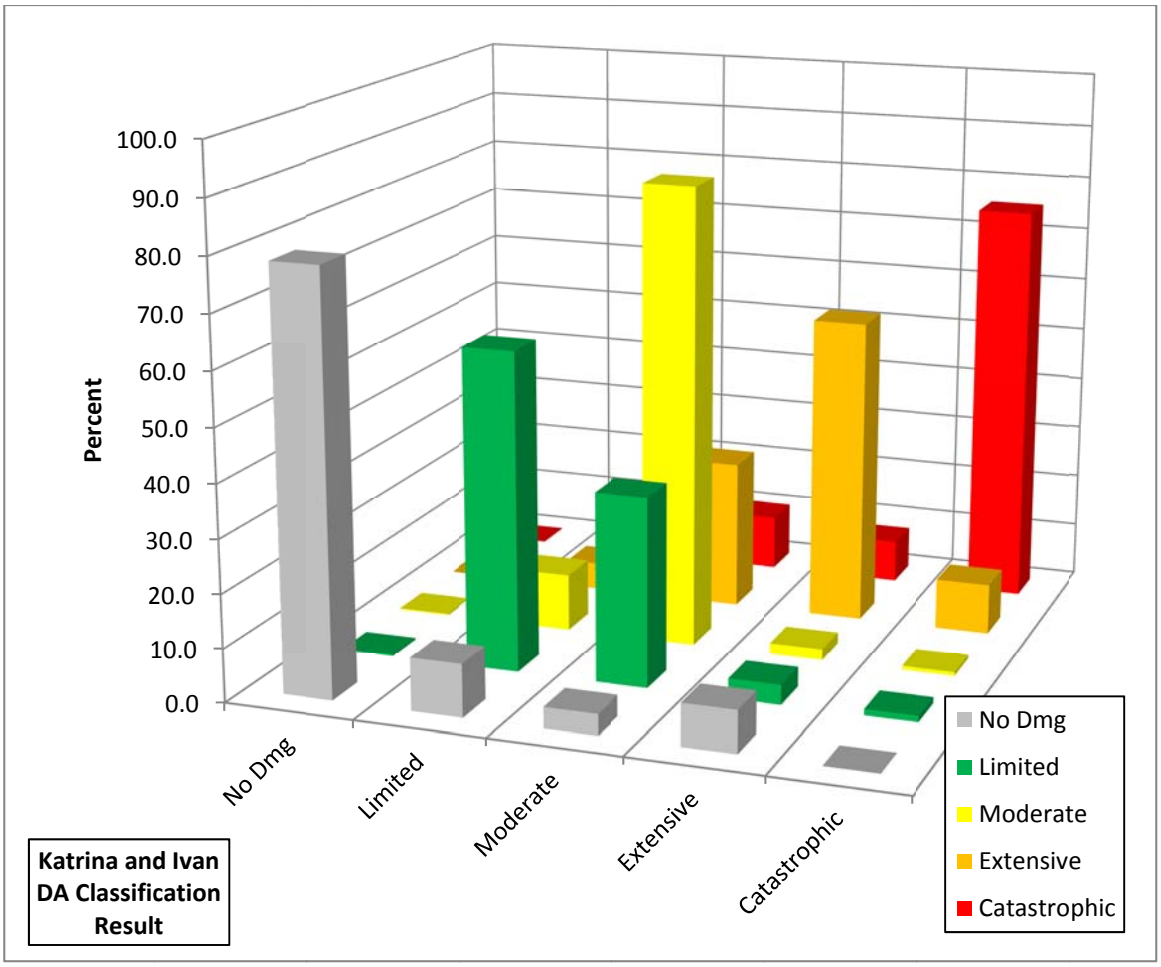

Katrina and Ivan discriminant analysis classification accuracy bar chart.

Katrina and Ivan discriminant analysis classification accuracy table.

Katrina and Ivan DA Classification Result - 75.3 percent correct classification

Count	**No Dmg**	**Limited**	**Moderate**	**Extensive**	**Catastrophic**	**Total**
No Dmg	119	15	6	12	0	152
Limited	1	209	124	13	4	351
Moderate	2	93	752	18	6	871
Extensive	0	13	71	146	24	254
Catastrophic	0	24	39	30	287	380

Percent	No Dmg	Limited	Moderate	Extensive	Catastrophic	Total
No Dmg	78.3	9.9	3.9	7.9	0.0	100
Limited	0.3	59.5	35.3	3.7	1.1	100
Moderate	0.2	10.7	86.3	2.1	0.7	100
Extensive	0.0	5.1	28.0	57.5	9.4	100
Catastrophic	0.0	6.3	10.3	7.9	75.5	100

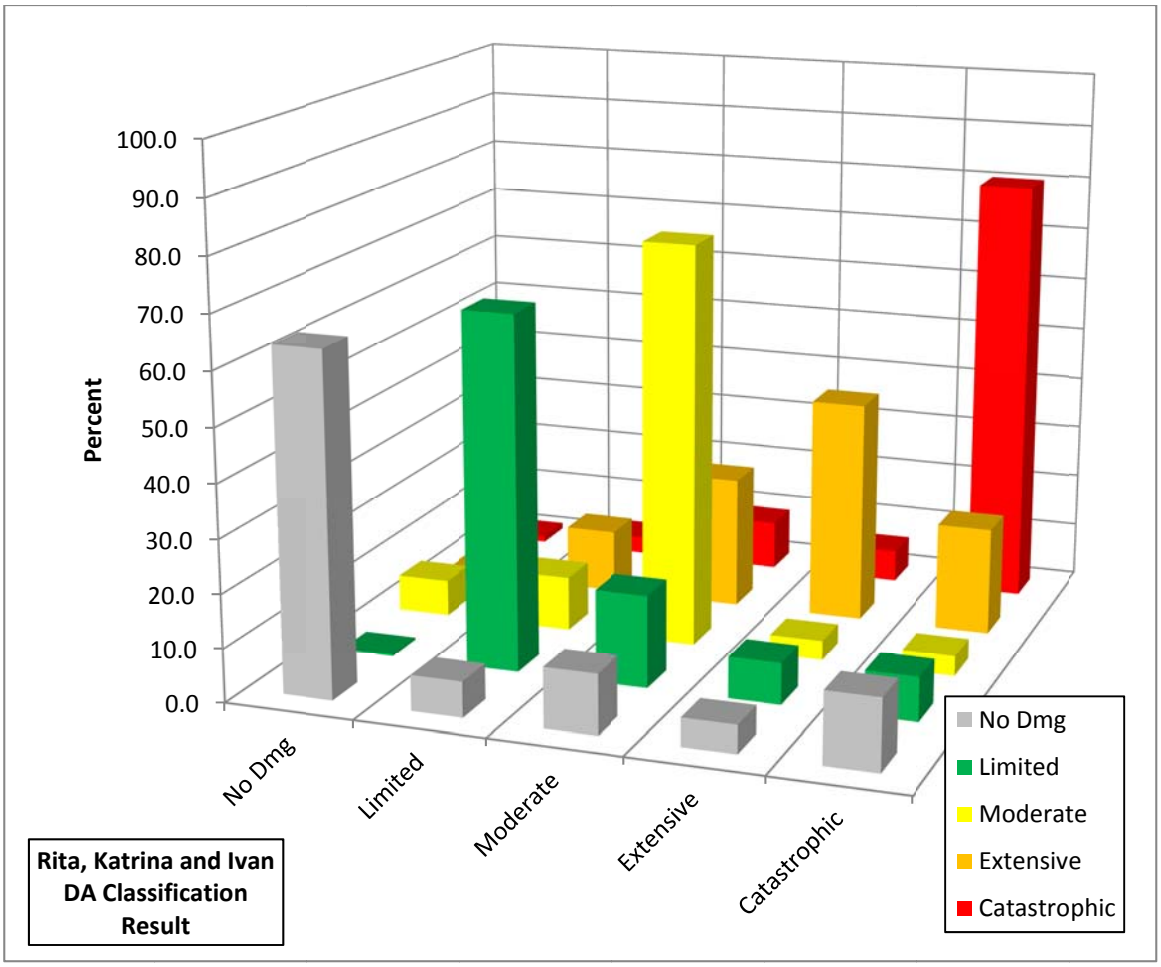

Rita, Katrina and Ivan discriminant analysis classification accuracy bar chart.

Rita, Katrina and Ivan discriminant analysis classification accuracy table.

Rita, Katrina and Ivan DA Classification Result - 69.1 percent correct classification

Count	**No Dmg**	**Limited**	**Moderate**	**Extensive**	**Catastrophic**	**Total**
No Dmg	278	29	49	23	58	437
Limited	2	392	102	46	49	591
Moderate	72	108	802	39	40	1061
Extensive	6	51	107	180	87	431
Catastrophic	9	26	72	47	632	786

Percent	No Dmg	Limited	Moderate	Extensive	Catastrophic	Total
No Dmg	63.6	6.6	11.2	5.3	13.3	100
Limited	0.3	66.3	17.3	7.8	8.3	100
Moderate	6.8	10.2	75.6	3.7	3.8	100
Extensive	1.4	11.8	24.8	41.8	20.2	100
Catastrophic	1.1	3.3	9.2	6.0	80.4	100

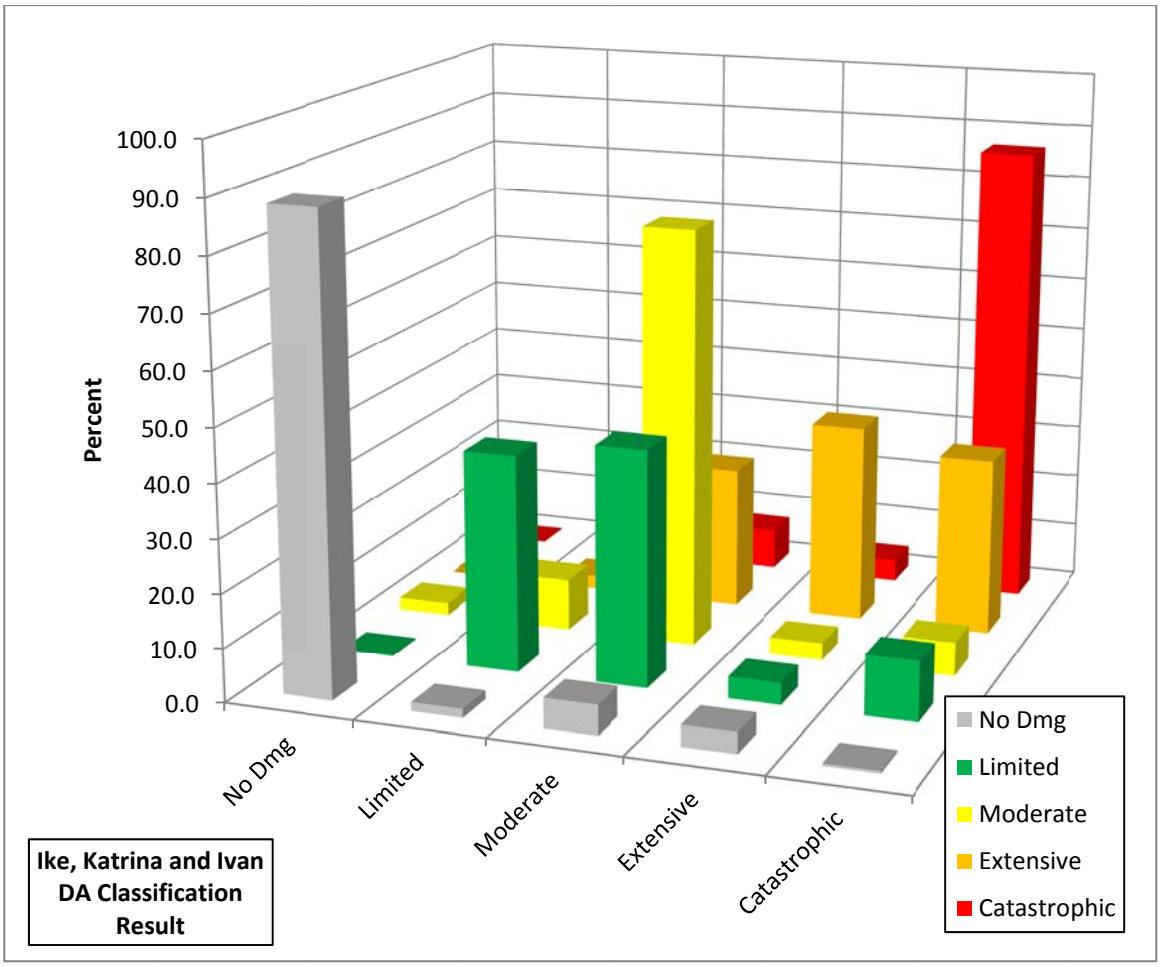

Ike, Katrina and Ivan discriminant analysis classification accuracy bar chart.

Ike, Katrina and Ivan discriminant analysis classification accuracy table.

Ike, Katrina and Ivan DA Classification Result - 71.7 percent correct classification

Count	**No Dmg**	**Limited**	**Moderate**	**Extensive**	**Catastrophic**	**Total**
No Dmg	376	7	24	17	2	426
Limited	1	177	192	18	49	437
Moderate	23	94	756	31	61	965
Extensive	0	9	96	134	120	359
Catastrophic	0	13	63	34	719	829

Percent	No Dmg	Limited	Moderate	Extensive	Catastrophic	Total
No Dmg	88.3	1.6	5.6	4.0	0.5	100
Limited	0.2	40.5	43.9	4.1	11.2	100
Moderate	2.4	9.7	78.3	3.2	6.3	100
Extensive	0.0	2.5	26.7	37.3	33.4	100
Catastrophic	0.0	1.6	7.6	4.1	86.7	100

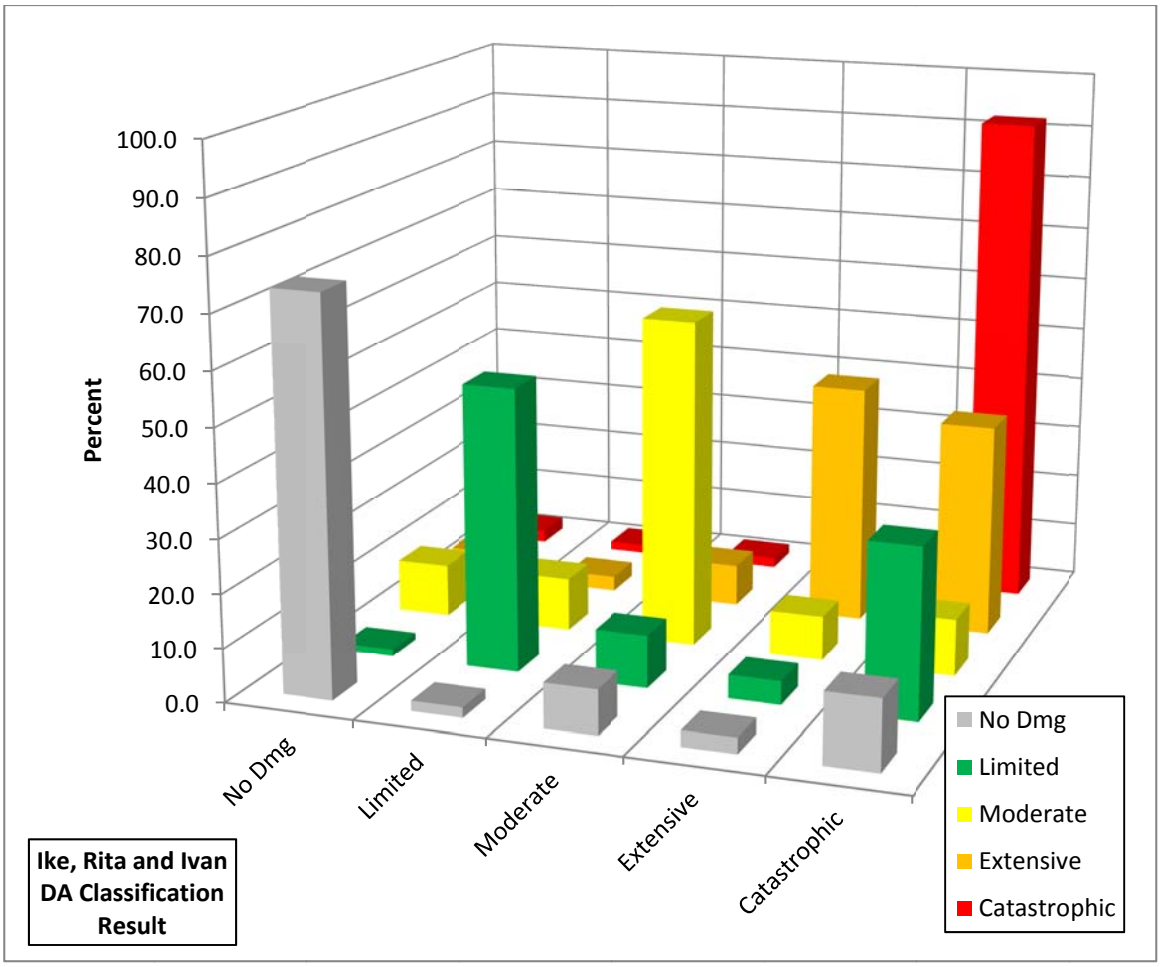

Ike, Rita and Ivan discriminant analysis classification accuracy bar chart.

Ike, Rita and Ivan discriminant analysis classification accuracy table.

Ike, Rita and Ivan DA Classification Result - 69.4 percent correct classification

Count	**No Dmg**	**Limited**	**Moderate**	**Extensive**	**Catastrophic**	**Total**
No Dmg	465	12	53	19	83	632
Limited	6	251	47	21	151	476
Moderate	67	68	420	57	73	685
Extensive	18	10	28	162	144	362
Catastrophic	20	14	16	17	800	867

Percent	No Dmg	Limited	Moderate	Extensive	Catastrophic	Total
No Dmg	73.6	1.9	8.4	3.0	13.1	100
Limited	1.3	52.7	9.9	4.4	31.7	100
Moderate	9.8	9.9	61.3	8.3	10.7	100
Extensive	5.0	2.8	7.7	44.8	39.8	100
Catastrophic	2.3	1.6	1.8	2.0	92.3	100

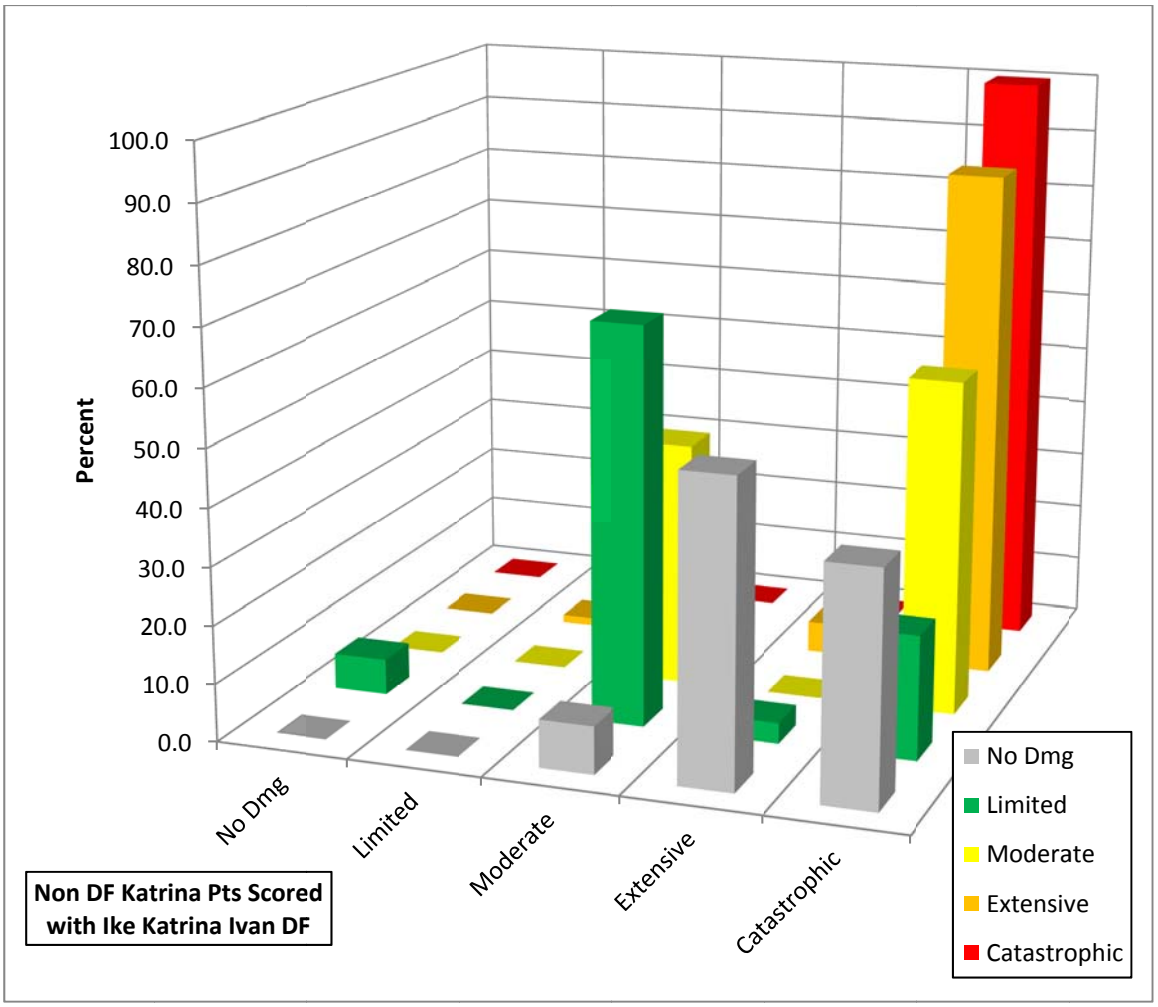

Classification accuracy bar chart of nonDF Katrina samples scored with Ike-Katrina-Ivan discriminant function.

Classification accuracy table of NonDF Katrina samples scored with Ike-Katrina-Ivan discriminant function.

NonDF Katrina Points Scored with Ike-Katrina-Ivan – 41 percent correct classification

Count	**No Dmg**	**Limited**	**Moderate**	**Extensive**	**Catastrophic**	**Total**
No Dmg	0	0	6	38	29	73
Limited	7	0	77	4	24	112
Moderate	0	0	140	0	190	330
Extensive	0	1	4	4	65	74
Catastrophic	0	0	0	0	160	160

Percent	No Dmg	Limited	Moderate	Extensive	Catastrophic	Total
No Dmg	0.0	0.0	8.2	52.1	39.7	100
Limited	6.3	0.0	68.8	3.6	21.4	100
Moderate	0.0	0.0	42.4	0.0	57.6	100
Extensive	0.0	1.4	5.4	5.4	87.8	100
Catastrophic	0.0	0.0	0.0	0.0	100.0	100

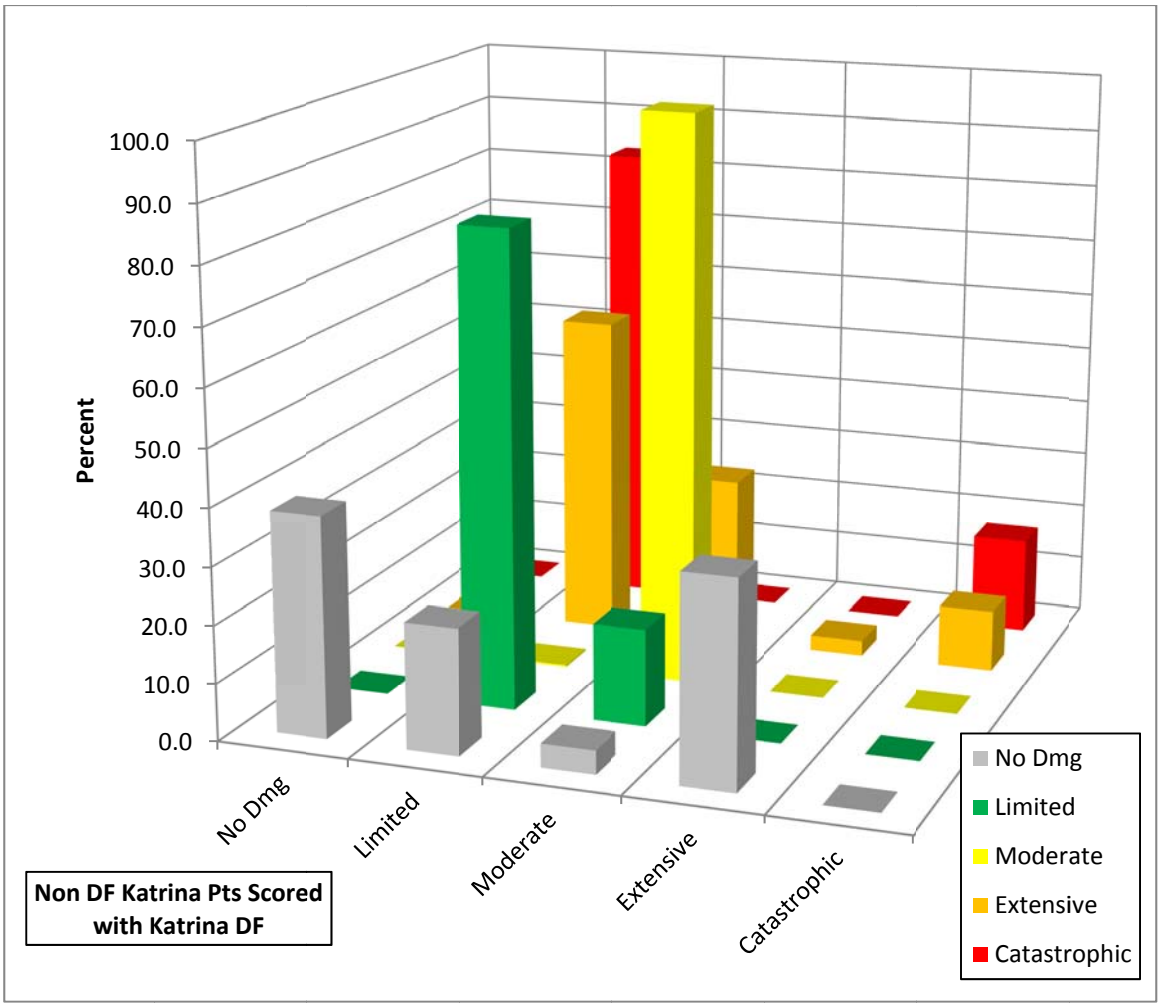

Classification accuracy bar chart of NonDF Katrina samples scored with Katrina discriminant function.

Classification accuracy table of NonDF Katrina samples scored with Katrina discriminant function.

NonDF Katrina Points Scored with Katrina DF – 64 percent correct classification

Count	No Dmg	Limited	Moderate	Extensive	Catastrophic	Total
No Dmg	28	16	3	26	0	73
Limited	0	93	19	0	0	112
Moderate	0	1	329	0	0	330
Extensive	0	42	22	2	8	74
Catastrophic	0	133	0	0	27	160

Percent	No Dmg	Limited	Moderate	Extensive	Catastrophic	Total
No Dmg	38.4	21.9	4.1	35.6	0.0	100
Limited	0.0	83.0	17.0	0.0	0.0	100
Moderate	0.0	0.3	99.7	0.0	0.0	100
Extensive	0.0	56.8	29.7	2.7	10.8	100
Catastrophic	0.0	83.1	0.0	0.0	16.9	100

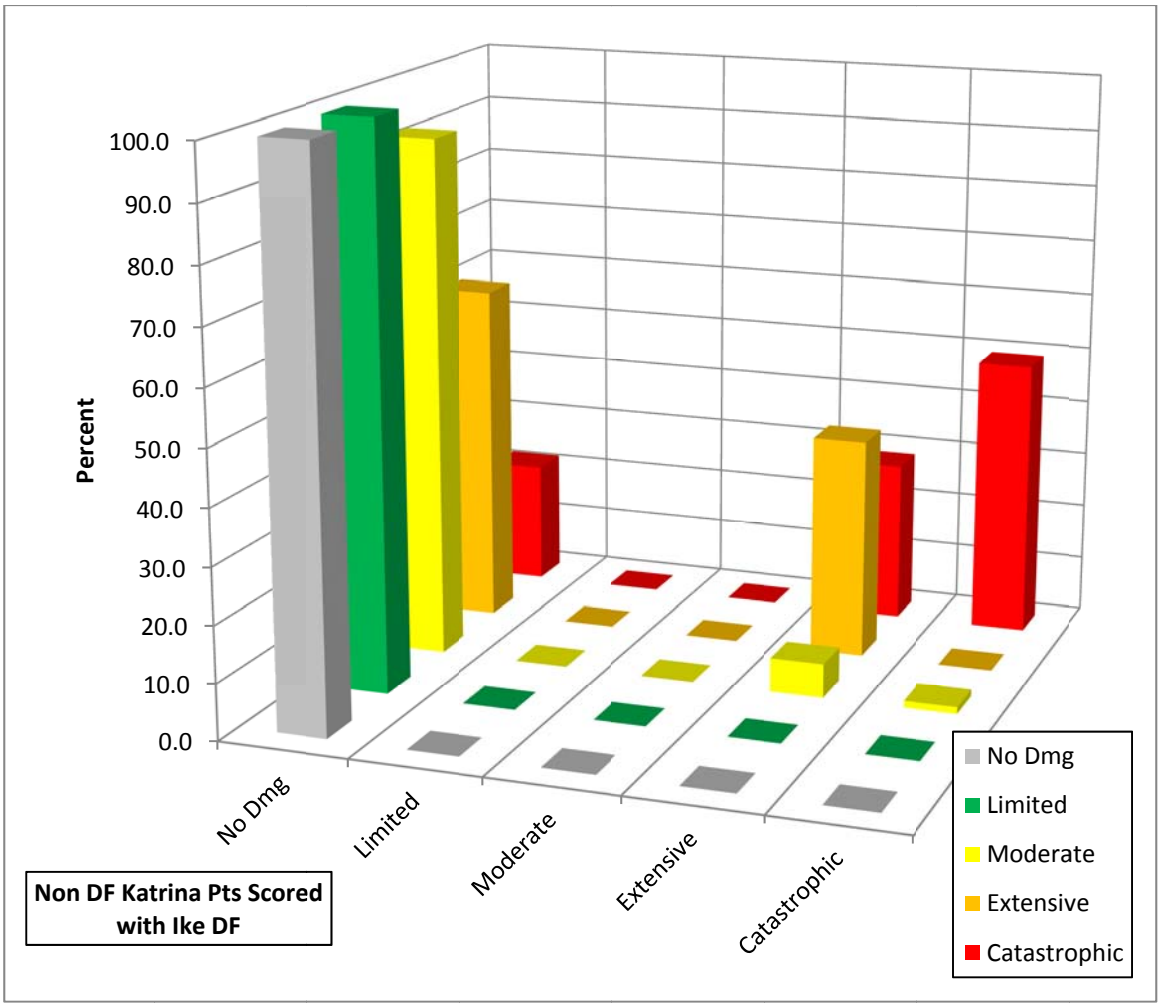

Classification accuracy bar chart of NonDF Katrina samples scored with Ike discriminant function.

Classification accuracy table of NonDF Katrina samples scored with Ike discriminant function.

NonDF Katrina Points Scored with Ike DF – 24 percent correct classification

Count	**No Dmg**	**Limited**	**Moderate**	**Extensive**	**Catastrophic**	**Total**
No Dmg	73	0	0	0	0	73
Limited	112	0	0	0	0	112
Moderate	306	0	0	20	4	330
Extensive	45	0	0	29	0	74
Catastrophic	35	0	0	46	79	160

Percent	No Dmg	Limited	Moderate	Extensive	Catastrophic	Total
No Dmg	100.0	0.0	0.0	0.0	0.0	100
Limited	100.0	0.0	0.0	0.0	0.0	100
Moderate	92.7	0.0	0.0	6.1	1.2	100
Extensive	60.8	0.0	0.0	39.2	0.0	100
Catastrophic	21.9	0.0	0.0	28.8	49.4	100

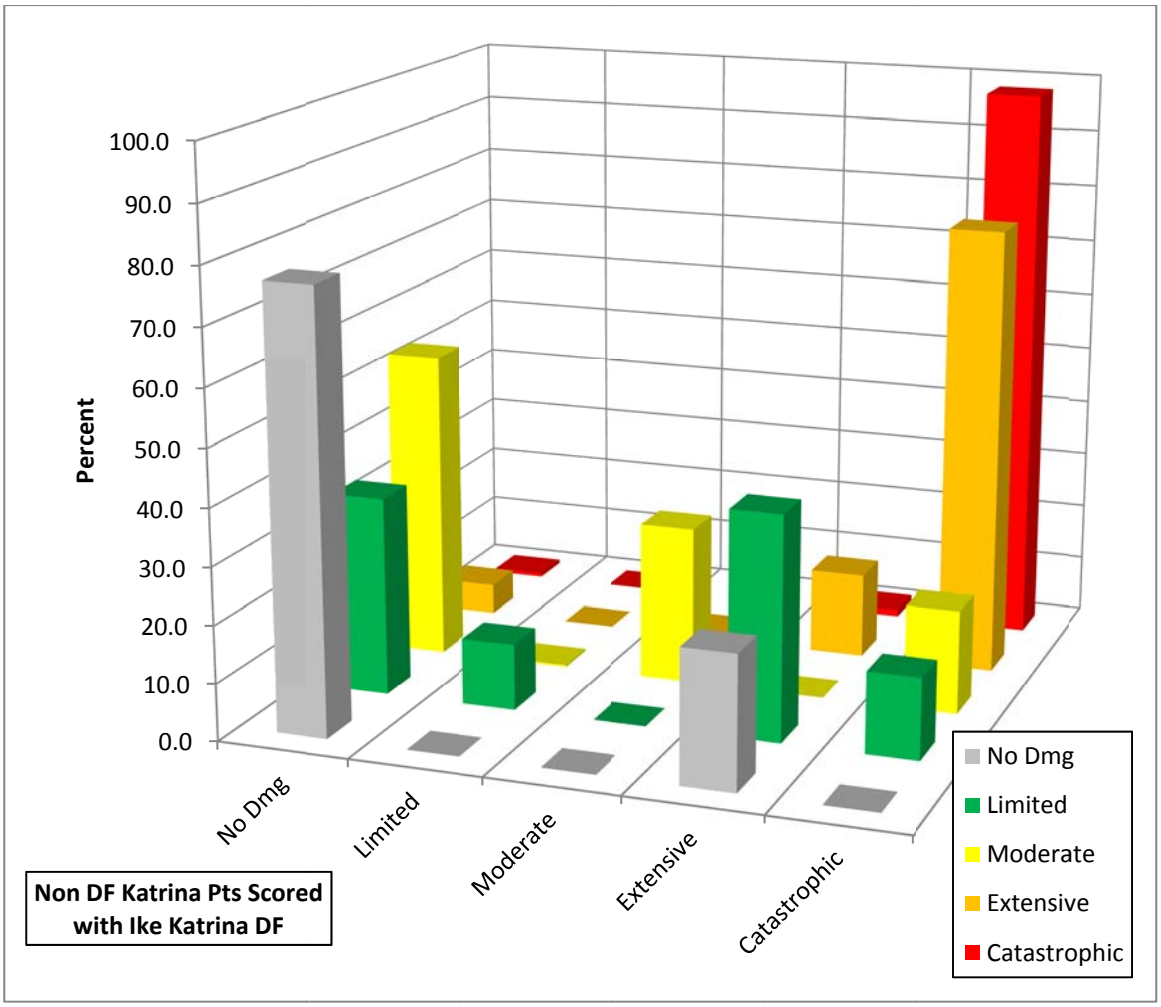

Classification accuracy bar chart of NonDF Katrina samples scored with Ike-Katrina discriminant function.

Classification accuracy table of NonDF Katrina samples scored with Ike-Katrina discriminant function.

NonDF Katrina Points Scored with Ike Katrina DF – 44 percent correct classification

Count	**No Dmg**	**Limited**	**Moderate**	**Extensive**	**Catastrophic**	**Total**
No Dmg	56	0	0	17	0	73
Limited	39	13	0	44	16	112
Moderate	178	1	91	0	60	330
Extensive	4	0	1	11	58	74
Catastrophic	1	0	0	2	157	160

Percent	No Dmg	Limited	Moderate	Extensive	Catastrophic	Total
No Dmg	76.7	0.0	0.0	23.3	0.0	100
Limited	34.8	11.6	0.0	39.3	14.3	100
Moderate	53.9	0.3	27.6	0.0	18.2	100
Extensive	5.4	0.0	1.4	14.9	78.4	100
Catastrophic	0.6	0.0	0.0	1.3	98.1	100

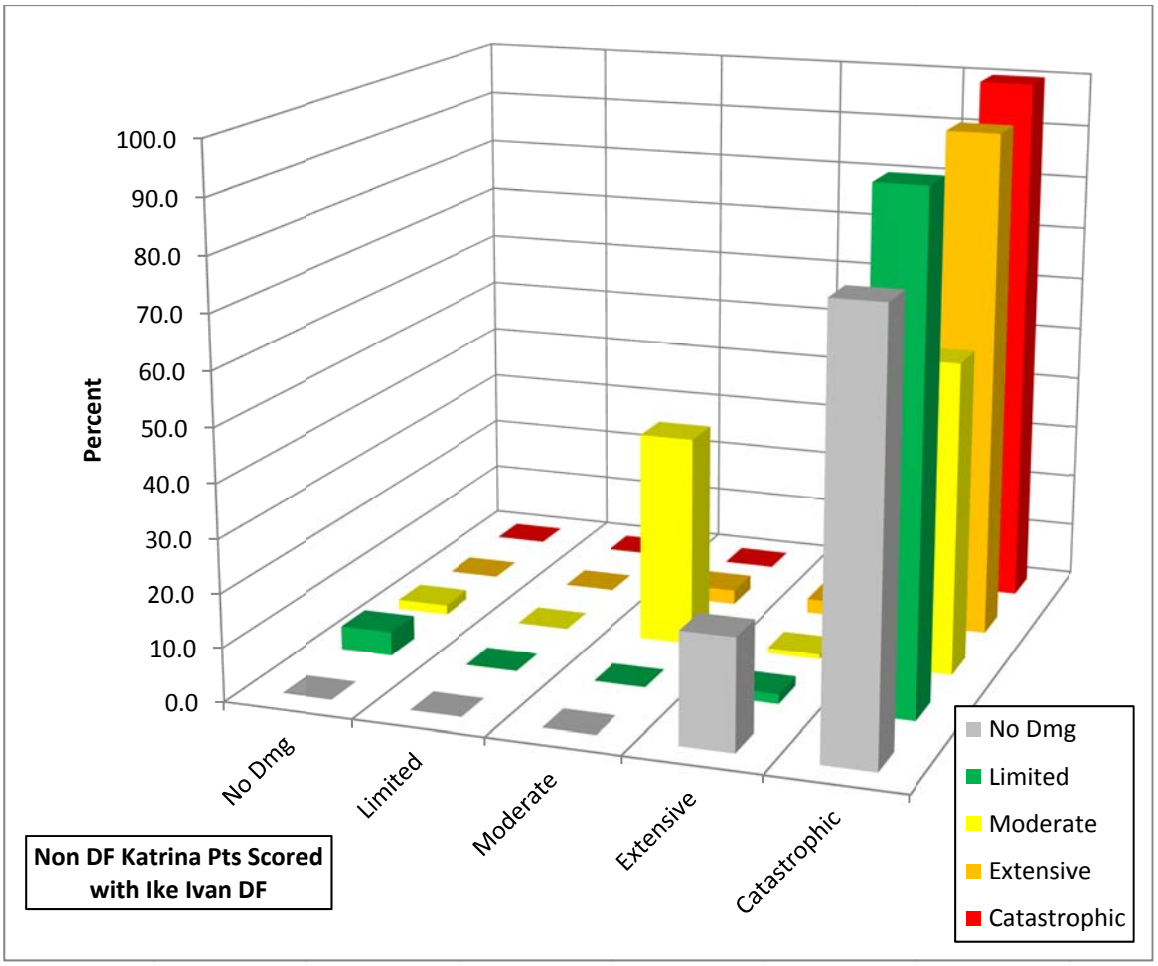

Classification accuracy bar chart of NonDF Katrina samples scored with Ike-Ivan discriminant function.

Classification accuracy table of NonDF Katrina samples scored with Ike-Ivan discriminant function.

NonDF Katrina Points Scored with Ike Ivan DF – 39 percent correct classification

Count	**No Dmg**	**Limited**	**Moderate**	**Extensive**	**Catastrophic**	**Total**
No Dmg	0	0	0	15	58	73
Limited	5	0	0	2	105	112
Moderate	6	0	130	3	191	330
Extensive	0	0	2	2	70	74
Catastrophic	0	0	0	0	160	160

Percent	No Dmg	Limited	Moderate	Extensive	Catastrophic	Total
No Dmg	0.0	0.0	0.0	20.5	79.5	100
Limited	4.5	0.0	0.0	1.8	93.8	100
Moderate	1.8	0.0	39.4	0.9	57.9	100
Extensive	0.0	0.0	2.7	2.7	94.6	100
Catastrophic	0.0	0.0	0.0	0.0	100.0	100

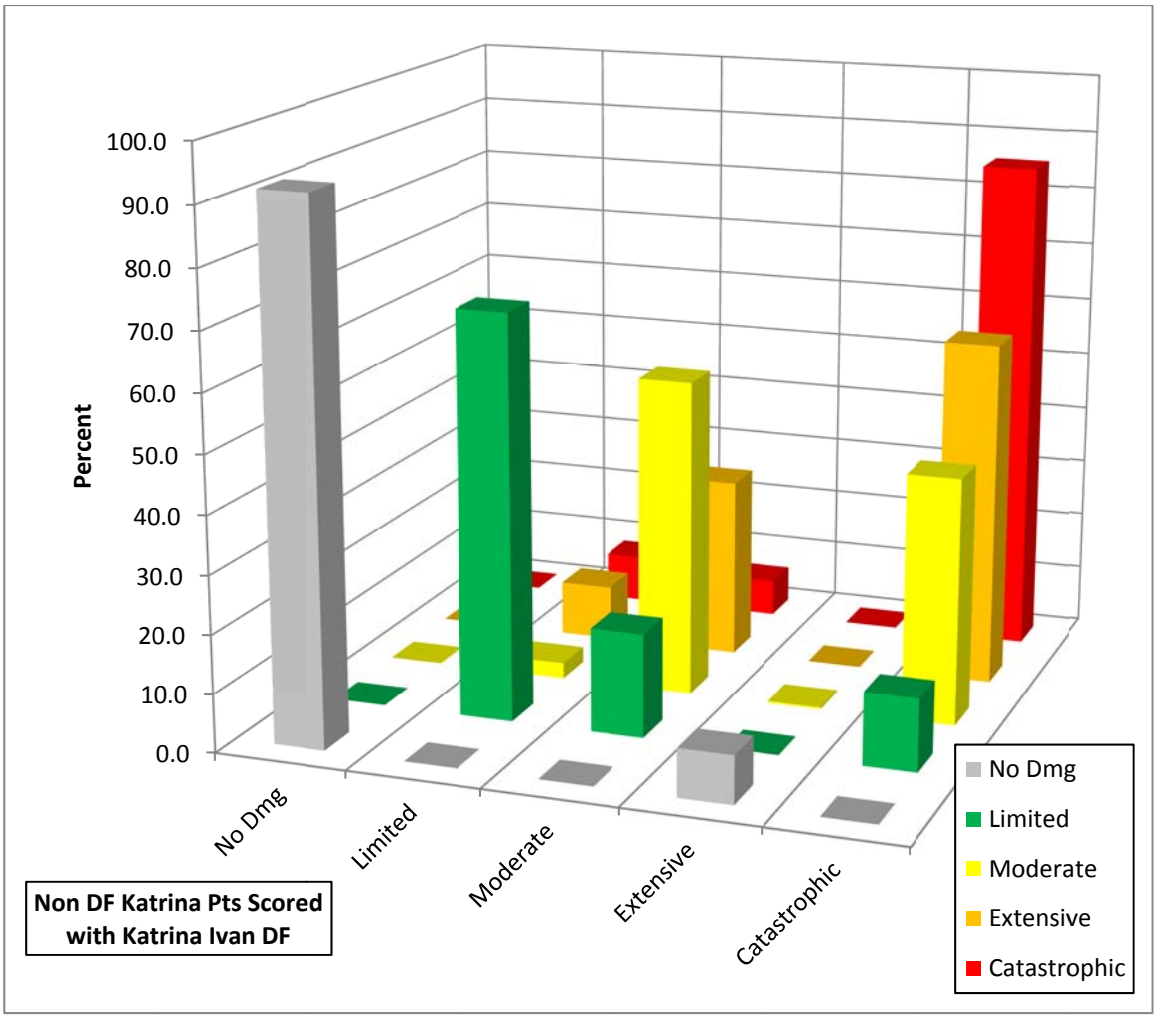

Classification accuracy bar chart of NonDF Katrina samples scored with Katrina-Ivan discriminant function.

Classification accuracy table of NonDF Katrina samples scored with Katrina-Ivan discriminant function.

NonDF Katrina Points Scored with Katrina Ivan DF – 62 percent correct classification

Count	**No Dmg**	**Limited**	**Moderate**	**Extensive**	**Catastrophic**	**Total**
No Dmg	67	0	0	6	0	73
Limited	0	78	20	0	14	112
Moderate	0	9	180	1	140	330
Extensive	0	7	23	0	44	74
Catastrophic	0	13	10	0	137	160

Percent	No Dmg	Limited	Moderate	Extensive	Catastrophic	Total
No Dmg	91.8	0.0	0.0	8.2	0.0	100
Limited	0.0	69.6	17.9	0.0	12.5	100
Moderate	0.0	2.7	54.5	0.3	42.4	100
Extensive	0.0	9.5	31.1	0.0	59.5	100
Catastrophic	0.0	8.1	6.3	0.0	85.6	100

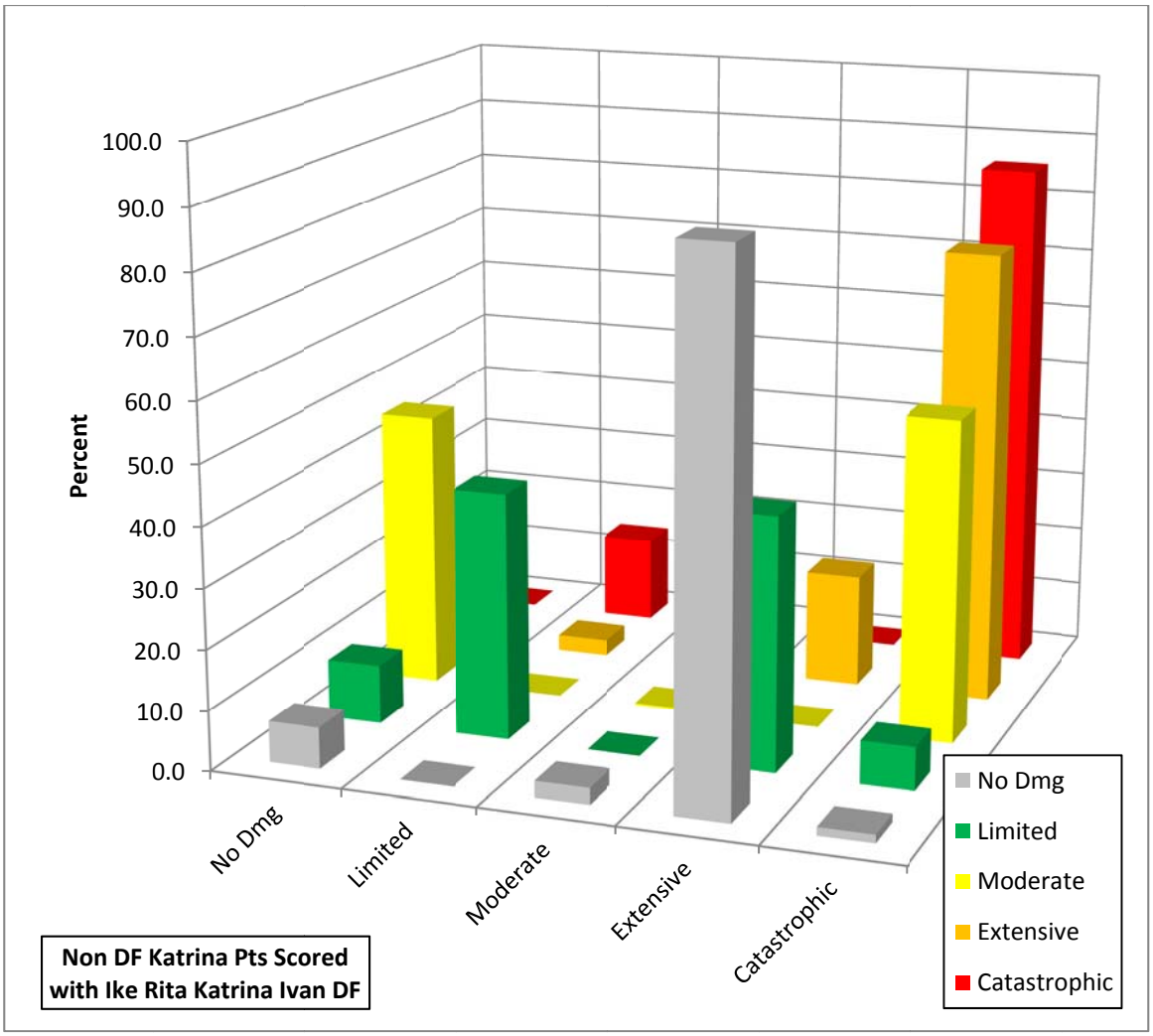

Classification accuracy bar chart of NonDF Katrina samples scored with Ike-Rita-Katrina-Ivan discriminant function.

Classification accuracy table of NonDF Katrina samples scored with Ike-Rita-Katrina-Ivan discriminant function.

NonDF Katrina Points Scored with Ike Rita Katrina Ivan DF – 27 percent correct classification

Count	**No Dmg**	**Limited**	**Moderate**	**Extensive**	**Catastrophic**	**Total**
No Dmg	5	0	2	65	1	73
Limited	11	46	0	47	8	112
Moderate	152	0	1	0	177	330
Extensive	2	2	0	14	56	74
Catastrophic	0	23	0	0	137	160

Percent	No Dmg	Limited	Moderate	Extensive	Catastrophic	Total
No Dmg	6.8	0.0	2.7	89.0	1.4	100
Limited	9.8	41.1	0.0	42.0	7.1	100
Moderate	46.1	0.0	0.3	0.0	53.6	100
Extensive	2.7	2.7	0.0	18.9	75.7	100
Catastrophic	0.0	14.4	0.0	0.0	85.6	100

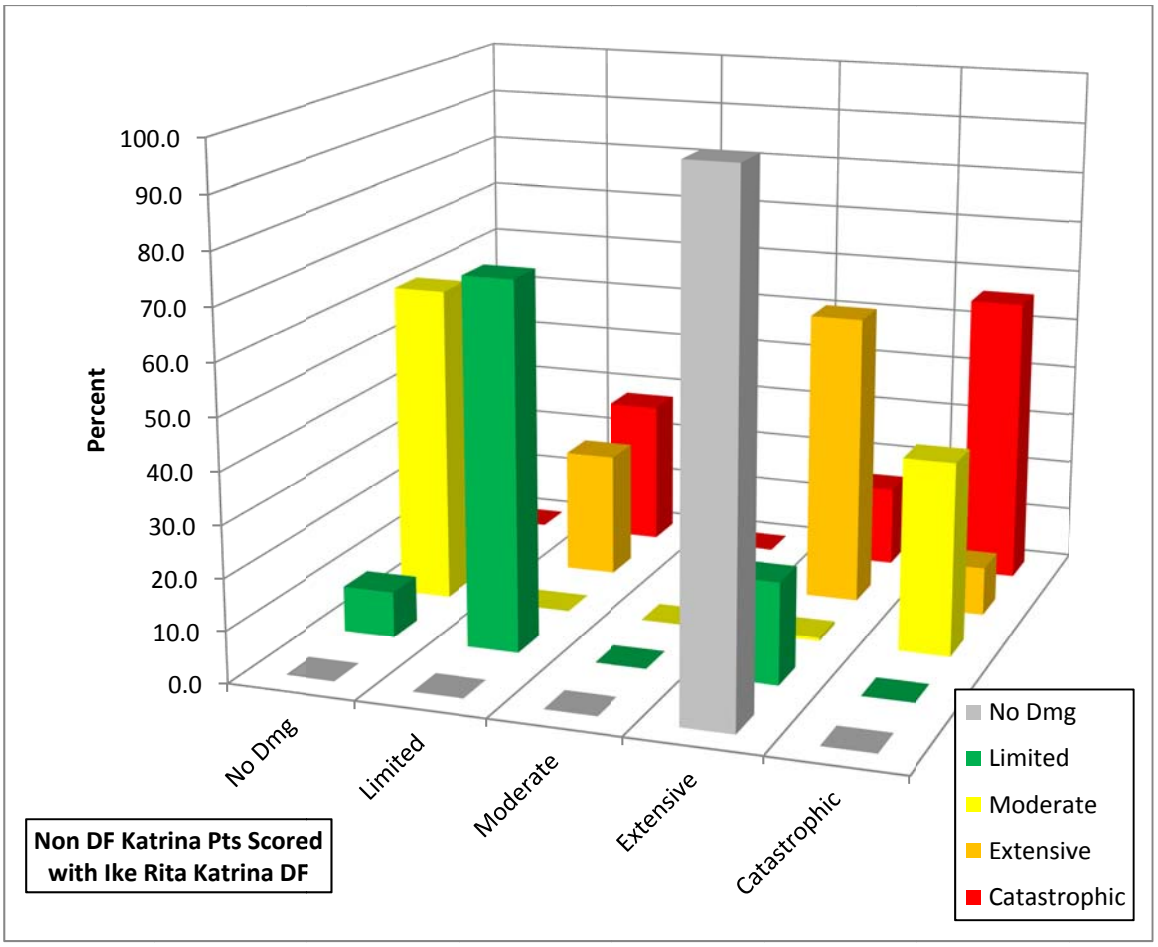

Classification accuracy bar chart of NonDF Katrina samples scored with Ike-Rita-Katrina discriminant function.

Classification accuracy table of NonDF Katrina samples scored with Ike-Rita-Katrina discriminant function.

NonDF Katrina Points Scored with Ike Rita Katrina DF – 28 percent correct classification

Count	**No Dmg**	**Limited**	**Moderate**	**Extensive**	**Catastrophic**	**Total**
No Dmg	0	0	0	73	0	73
Limited	10	80	0	22	0	112
Moderate	204	0	0	2	124	330
Extensive	7	18	0	42	7	74
Catastrophic	0	45	0	25	90	160

Percent	No Dmg	Limited	Moderate	Extensive	Catastrophic	Total
No Dmg	0.0	0.0	0.0	100.0	0.0	100
Limited	8.9	71.4	0.0	19.6	0.0	100
Moderate	61.8	0.0	0.0	0.6	37.6	100
Extensive	9.5	24.3	0.0	56.8	9.5	100
Catastrophic	0.0	28.1	0.0	15.6	56.3	100

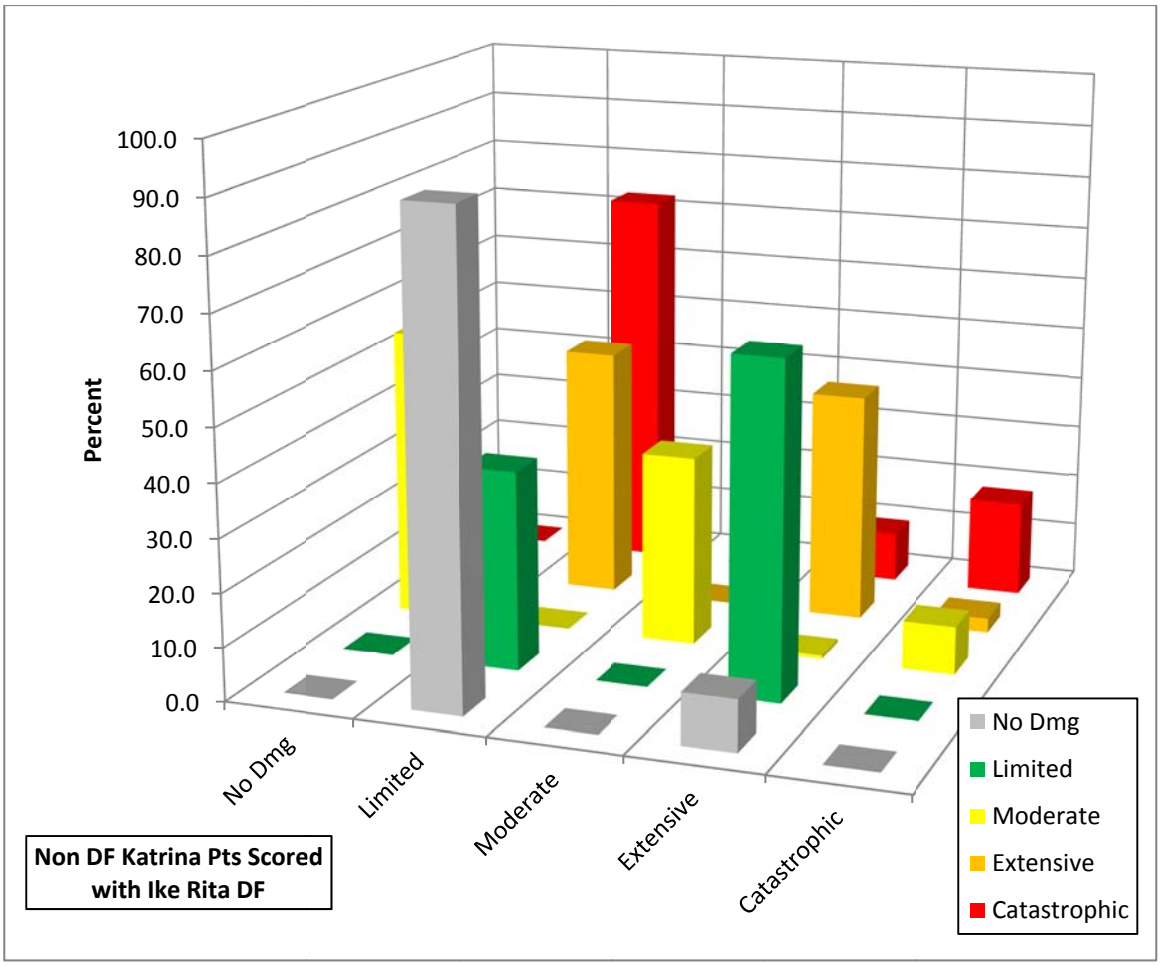

Classification accuracy bar chart of NonDF Katrina samples scored with Ike-Rita discriminant function.

Classification accuracy table of NonDF Katrina samples scored with Ike-Rita discriminant function.

NonDF Katrina Points Scored with Ike Rita DF – 30 percent correct classification

Count	No Dmg	Limited	Moderate	Extensive	Catastrophic	Total
No Dmg	0	66	0	7	0	73
Limited	0	42	0	70	0	112
Moderate	180	0	118	2	30	330
Extensive	5	35	0	32	2	74
Catastrophic	0	116	0	15	29	160

Percent	No Dmg	Limited	Moderate	Extensive	Catastrophic	Total
No Dmg	0.0	90.4	0.0	9.6	0.0	100
Limited	0.0	37.5	0.0	62.5	0.0	100
Moderate	54.5	0.0	35.8	0.6	9.1	100
Extensive	6.8	47.3	0.0	43.2	2.7	100
Catastrophic	0.0	72.5	0.0	9.4	18.1	100

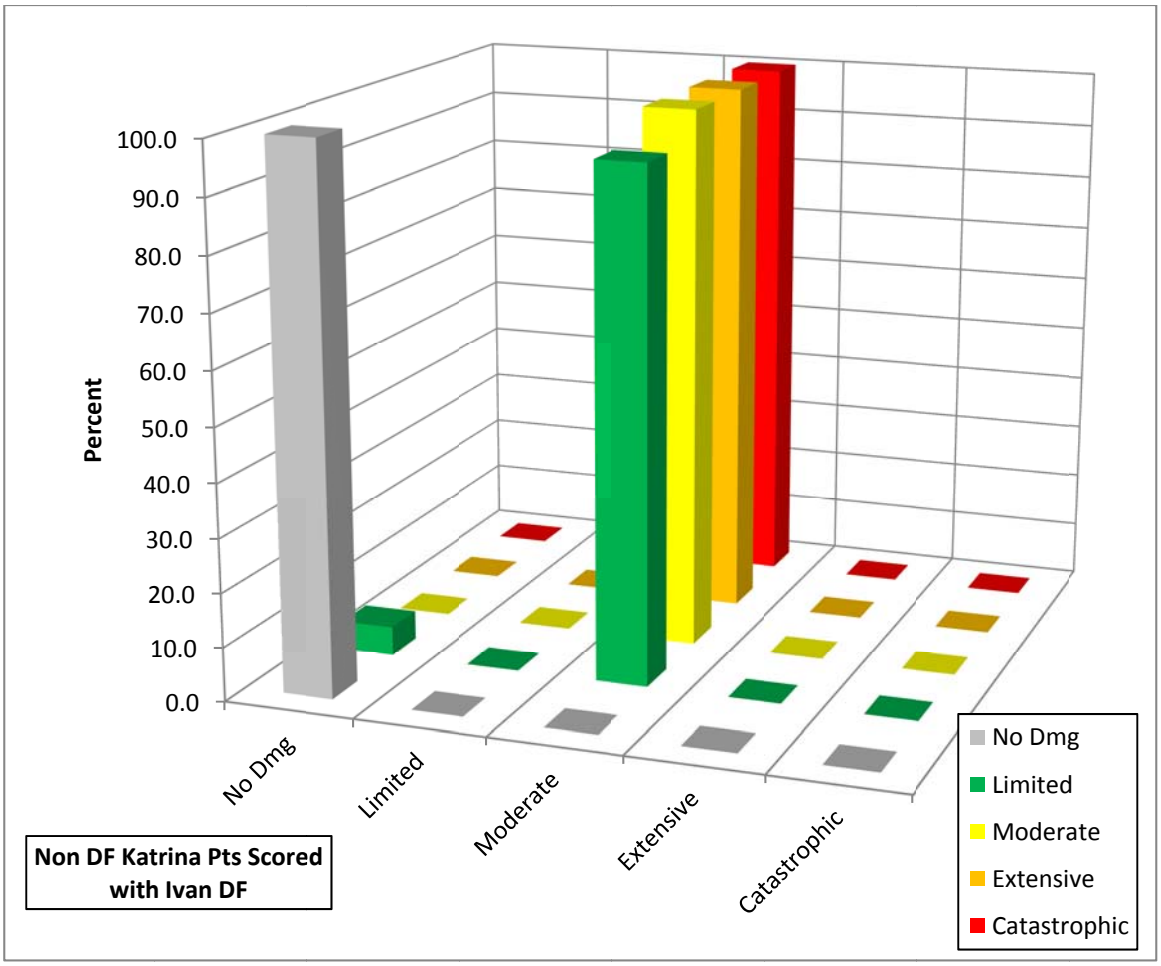

Classification accuracy bar chart of NonDF Katrina samples scored with Ivan discriminant function.

Classification accuracy table of NonDF Katrina samples scored with Ivan discriminant function.

NonDF Katrina Points Scored with Ivan DF – 54 percent correct classification

Count	**No Dmg**	**Limited**	**Moderate**	**Extensive**	**Catastrophic**	**Total**
No Dmg	73	0	0	0	0	73
Limited	6	0	106	0	0	112
Moderate	0	0	330	0	0	330
Extensive	0	0	74	0	0	74
Catastrophic	0	0	160	0	0	160

Percent	No Dmg	Limited	Moderate	Extensive	Catastrophic	Total
No Dmg	100.0	0.0	0.0	0.0	0.0	100
Limited	5.4	0.0	94.6	0.0	0.0	100
Moderate	0.0	0.0	100.0	0.0	0.0	100
Extensive	0.0	0.0	100.0	0.0	0.0	100
Catastrophic	0.0	0.0	100.0	0.0	0.0	100

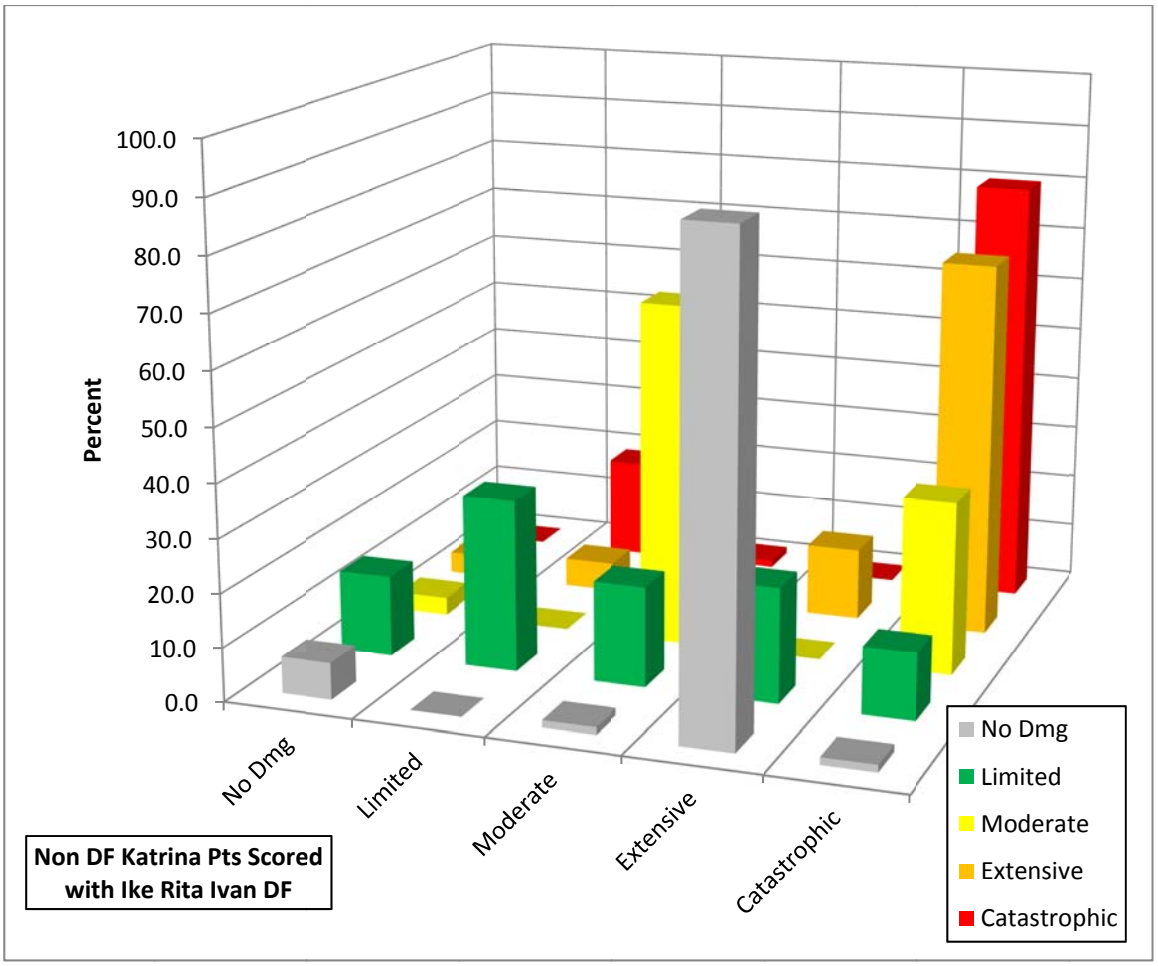

Classification accuracy bar chart of NonDF Katrina samples scored with Ike-Rita-Ivan discriminant function.

Classification accuracy table of NonDF Katrina samples scored with Ike-Rita-Ivan discriminant function.

NonDF Katrina Points Scored with Ike Rita Ivan DF – 52 percent correct classification

Count	**No Dmg**	**Limited**	**Moderate**	**Extensive**	**Catastrophic**	**Total**
No Dmg	5	0	1	66	1	73
Limited	17	36	21	24	14	112
Moderate	11	0	212	0	107	330
Extensive	3	4	5	10	52	74
Catastrophic	0	30	2	0	128	160

Percent	No Dmg	Limited	Moderate	Extensive	Catastrophic	Total
No Dmg	6.8	0.0	1.4	90.4	1.4	100
Limited	15.2	32.1	18.8	21.4	12.5	100
Moderate	3.3	0.0	64.2	0.0	32.4	100
Extensive	4.1	5.4	6.8	13.5	70.3	100
Catastrophic	0.0	18.8	1.3	0.0	80.0	100

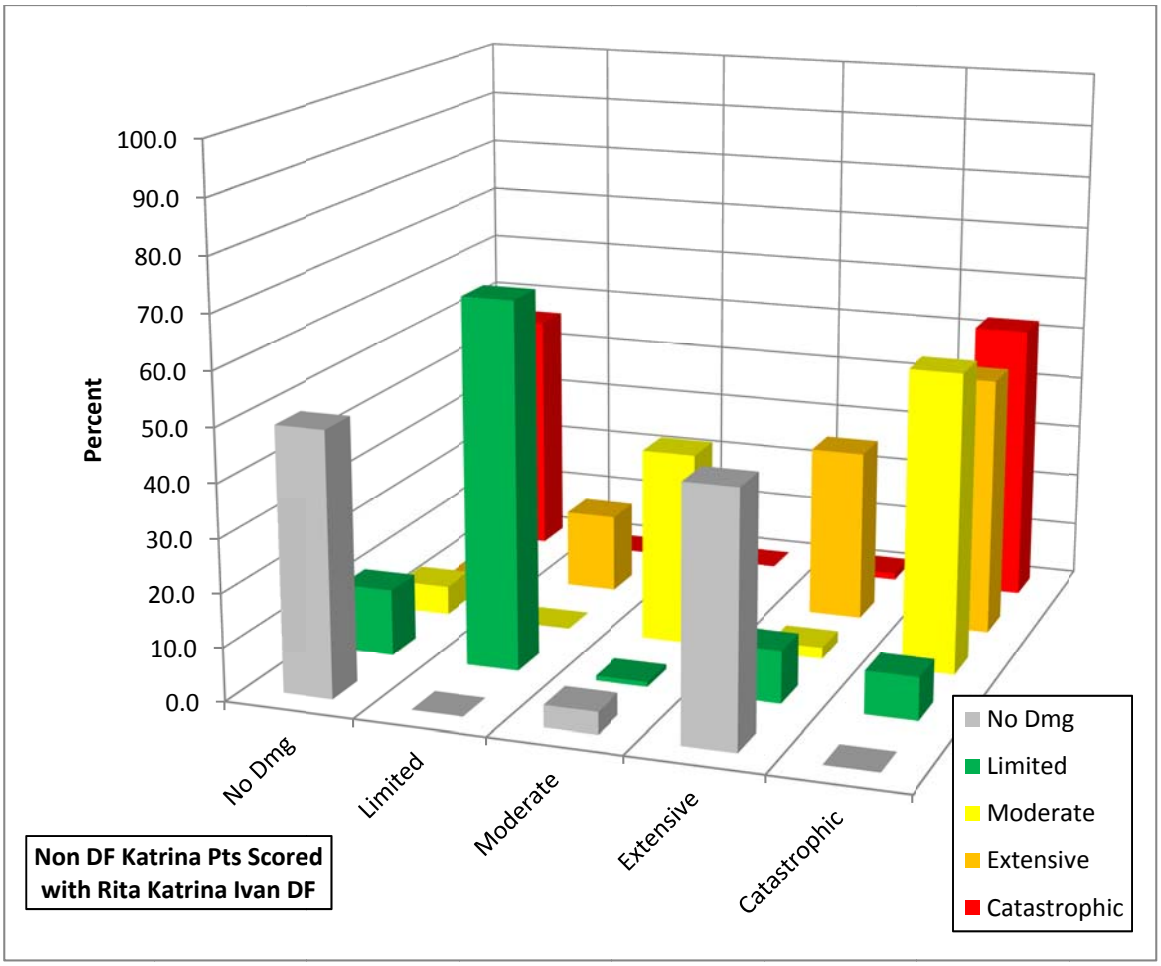

Classification accuracy bar chart of NonDF Katrina samples scored with Rita-Katrina-Ivan discriminant function.

Classification accuracy table of NonDF Katrina samples scored with Rita-Katrina-Ivan discriminant function.

NonDF Katrina Points Scored with Rita Katrina Ivan DF – 46 percent correct classification

Count	**No Dmg**	**Limited**	**Moderate**	**Extensive**	**Catastrophic**	**Total**
No Dmg	36	0	3	34	0	73
Limited	14	77	1	11	9	112
Moderate	18	0	120	7	185	330
Extensive	0	11	3	24	36	74
Catastrophic	74	0	0	2	84	160

Percent	No Dmg	Limited	Moderate	Extensive	Catastrophic	Total
No Dmg	49.3	0.0	4.1	46.6	0.0	100
Limited	12.5	68.8	0.9	9.8	8.0	100
Moderate	5.5	0.0	36.4	2.1	56.1	100
Extensive	0.0	14.9	4.1	32.4	48.6	100
Catastrophic	46.3	0.0	0.0	1.3	52.5	100

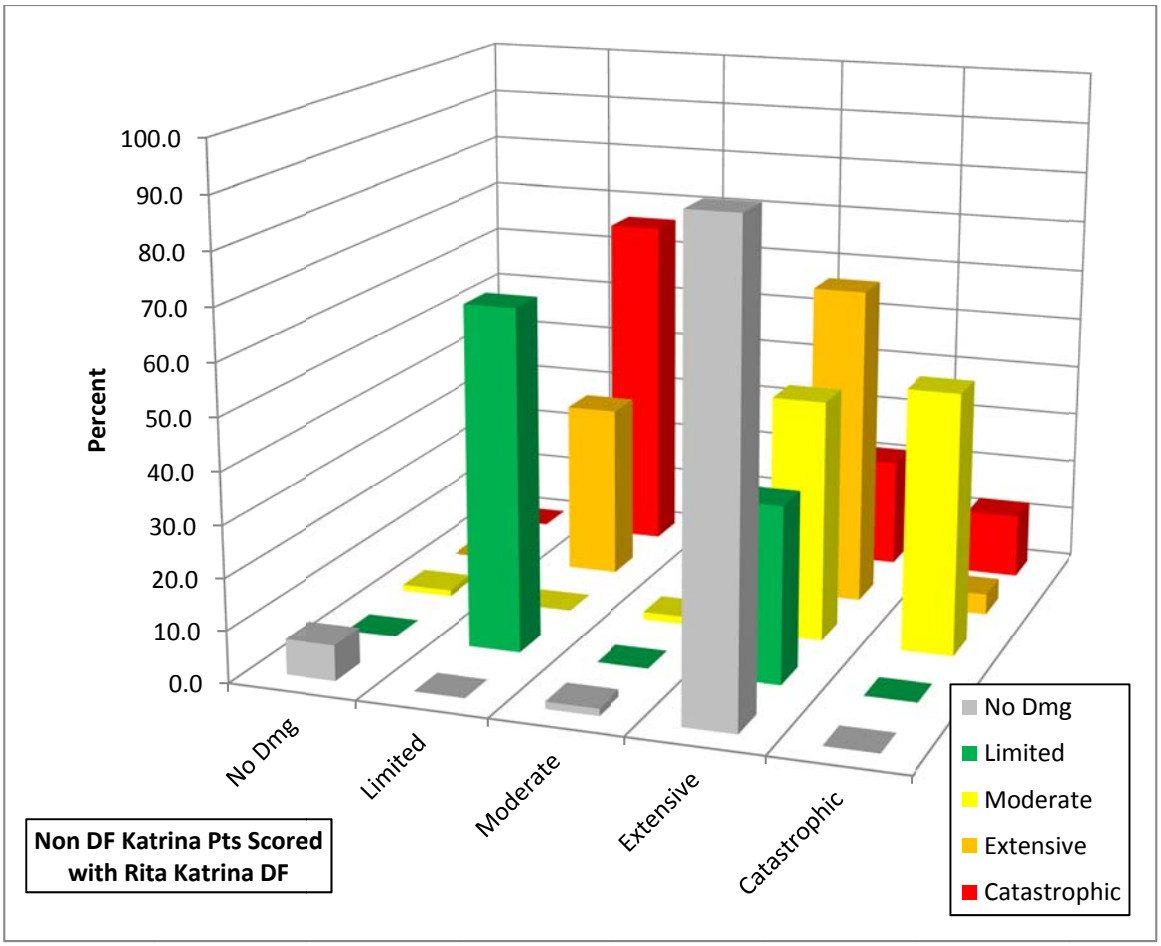

Classification accuracy bar chart of NonDF Katrina samples scored with Rita-Katrina discriminant function.

Classification accuracy table of NonDF Katrina samples scored with Rite-Katrina discriminant function.

NonDF Katrina Points Scored with Rita Katrina DF – 20 percent correct classification

Count	**No Dmg**	**Limited**	**Moderate**	**Extensive**	**Catastrophic**	**Total**
No Dmg	5	0	1	67	0	73
Limited	0	74	0	38	0	112
Moderate	4	0	5	154	167	330
Extensive	0	25	0	46	3	74
Catastrophic	0	106	0	34	20	160

Percent	No Dmg	Limited	Moderate	Extensive	Catastrophic	Total
No Dmg	6.8	0.0	1.4	91.8	0.0	100
Limited	0.0	66.1	0.0	33.9	0.0	100
Moderate	1.2	0.0	1.5	46.7	50.6	100
Extensive	0.0	33.8	0.0	62.2	4.1	100
Catastrophic	0.0	66.3	0.0	21.3	12.5	100

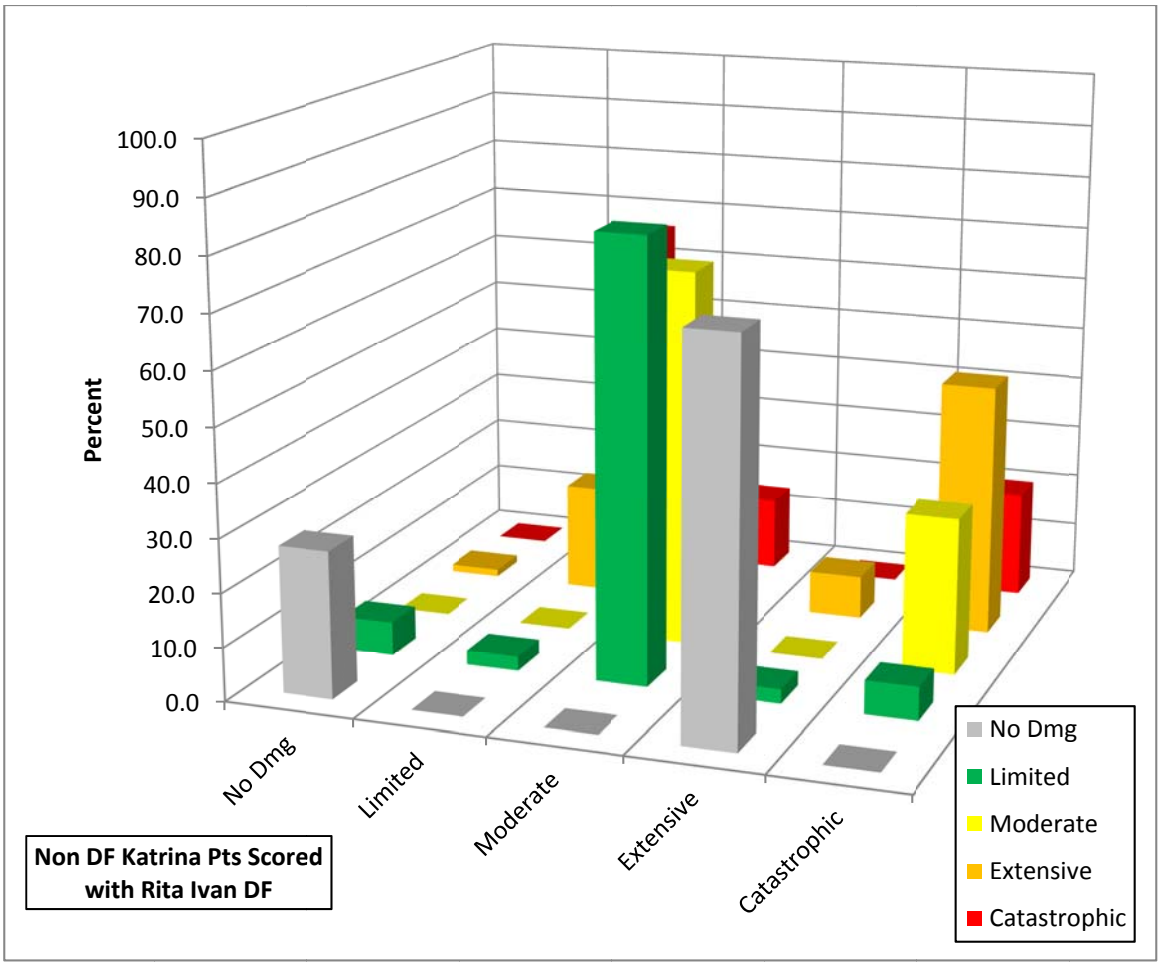

Classification accuracy bar chart of NonDF Katrina samples scored with Rita-Ivan discriminant function.

Classification accuracy table of NonDF Katrina samples scored with Rita-Ivan discriminant function.

NonDF Katrina Points Scored with Rita Ivan DF – 39 percent correct classification

Count	**No Dmg**	**Limited**	**Moderate**	**Extensive**	**Catastrophic**	**Total**
No Dmg	20	0	0	53	0	73
Limited	7	3	92	3	7	112
Moderate	0	0	233	0	97	330
Extensive	1	15	17	6	35	74
Catastrophic	0	106	22	0	32	160

Percent	No Dmg	Limited	Moderate	Extensive	Catastrophic	Total
No Dmg	27.4	0.0	0.0	72.6	0.0	100
Limited	6.3	2.7	82.1	2.7	6.3	100
Moderate	0.0	0.0	70.6	0.0	29.4	100
Extensive	1.4	20.3	23.0	8.1	47.3	100
Catastrophic	0.0	66.3	13.8	0.0	20.0	100

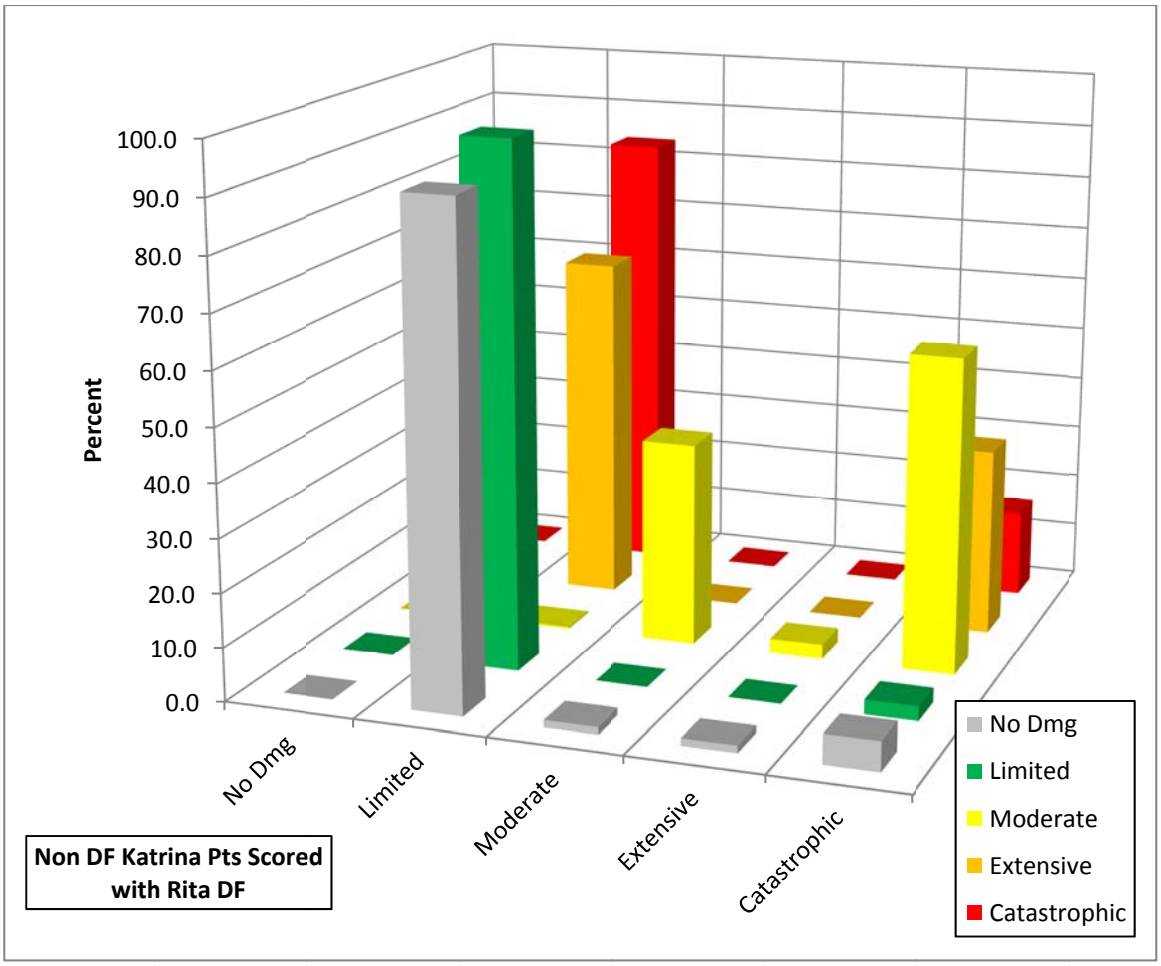

Classification accuracy bar chart of NonDF Katrina samples scored with Rita discriminant function.

Classification accuracy table of NonDF Katrina samples scored with Rita discriminant function.

NonDF Katrina Points Scored with Rita DF - 35 percent correct classification

Count	No Dmg	Limited	Moderate	Extensive	Catastrophic	Total
No Dmg	0	67	1	1	4	73
Limited	0	109	0	0	3	112
Moderate	0	1	126	9	194	330
Extensive	0	48	0	0	26	74
Catastrophic	0	134	0	0	26	160

Percent	No Dmg	Limited	Moderate	Extensive	Catastrophic	Total
No Dmg	0.0	91.8	1.4	1.4	5.5	100
Limited	0.0	97.3	0.0	0.0	2.7	100
Moderate	0.0	0.3	38.2	2.7	58.8	100
Extensive	0.0	64.9	0.0	0.0	35.1	100
Catastrophic	0.0	83.8	0.0	0.0	16.3	100

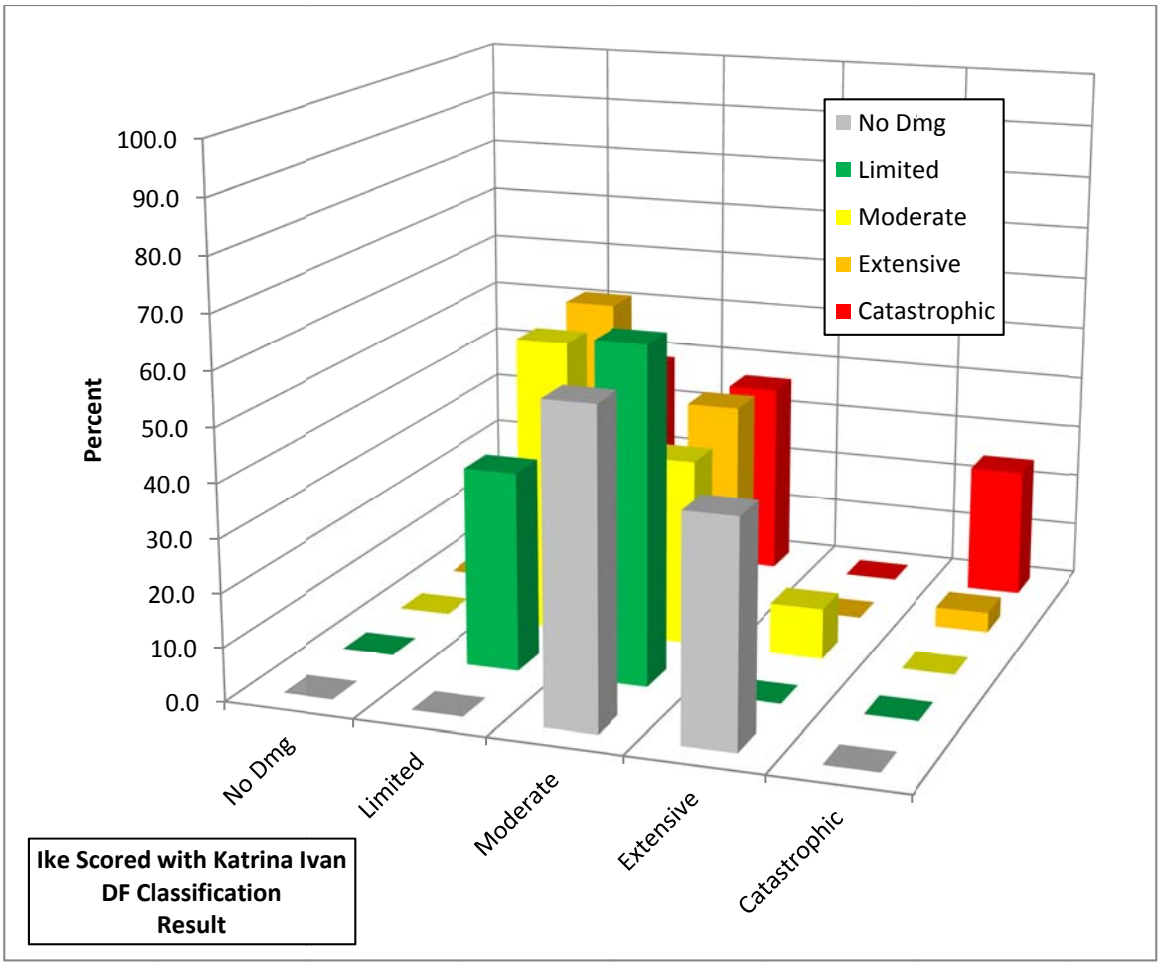

Classification accuracy bar chart of Ike samples scored with Katrina-Ivan discriminant function.

Classification accuracy table of Ike samples scored with Katrina-Ivan discriminant function.

Ike Scored with Katrina Ivan DF Classification Result – 17 percent correct classification

Count	**No Dmg**	**Limited**	**Moderate**	**Extensive**	**Catastrophic**	**Total**
No Dmg	0	0	160	114	0	274
Limited	0	32	54	0	0	86
Moderate	0	52	33	9	0	94
Extensive	0	60	41	0	4	105
Catastrophic	0	175	164	0	110	449

Percent	No Dmg	Limited	Moderate	Extensive	Catastrophic	Total
No Dmg	0.0	0.0	58.4	41.6	0.0	100
Limited	0.0	37.2	62.8	0.0	0.0	100
Moderate	0.0	55.3	35.1	9.6	0.0	100
Extensive	0.0	57.1	39.0	0.0	3.8	100
Catastrophic	0.0	39.0	36.5	0.0	24.5	100

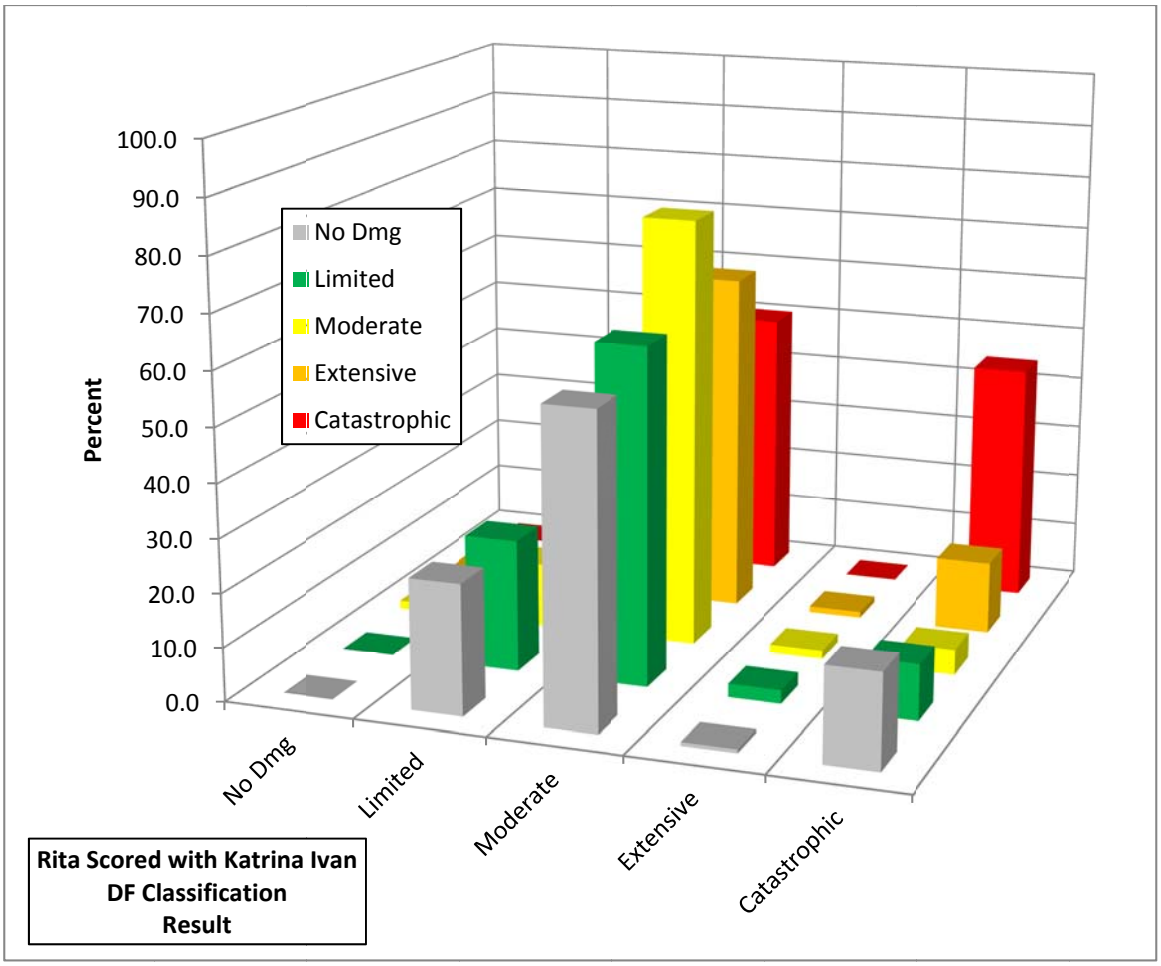

Classification accuracy bar chart of Rita samples scored with Katrina-Ivan discriminant function.

Classification accuracy table of Rita samples scored with Katrina-Ivan discriminant function.

Rita Scored with Katrina Ivan DF Classification Result – 30 percent correct classification

Count	**No Dmg**	**Limited**	**Moderate**	**Extensive**	**Catastrophic**	**Total**
No Dmg	0	69	164	2	50	285
Limited	0	59	150	6	25	240
Moderate	3	23	152	3	9	190
Extensive	2	36	113	2	24	177
Catastrophic	0	20	205	0	181	406

Percent	No Dmg	Limited	Moderate	Extensive	Catastrophic	Total
No Dmg	0.0	24.2	57.5	0.7	17.5	100
Limited	0.0	24.6	62.5	2.5	10.4	100
Moderate	1.6	12.1	80.0	1.6	4.7	100
Extensive	1.1	20.3	63.8	1.1	13.6	100
Catastrophic	0.0	4.9	50.5	0.0	44.6	100

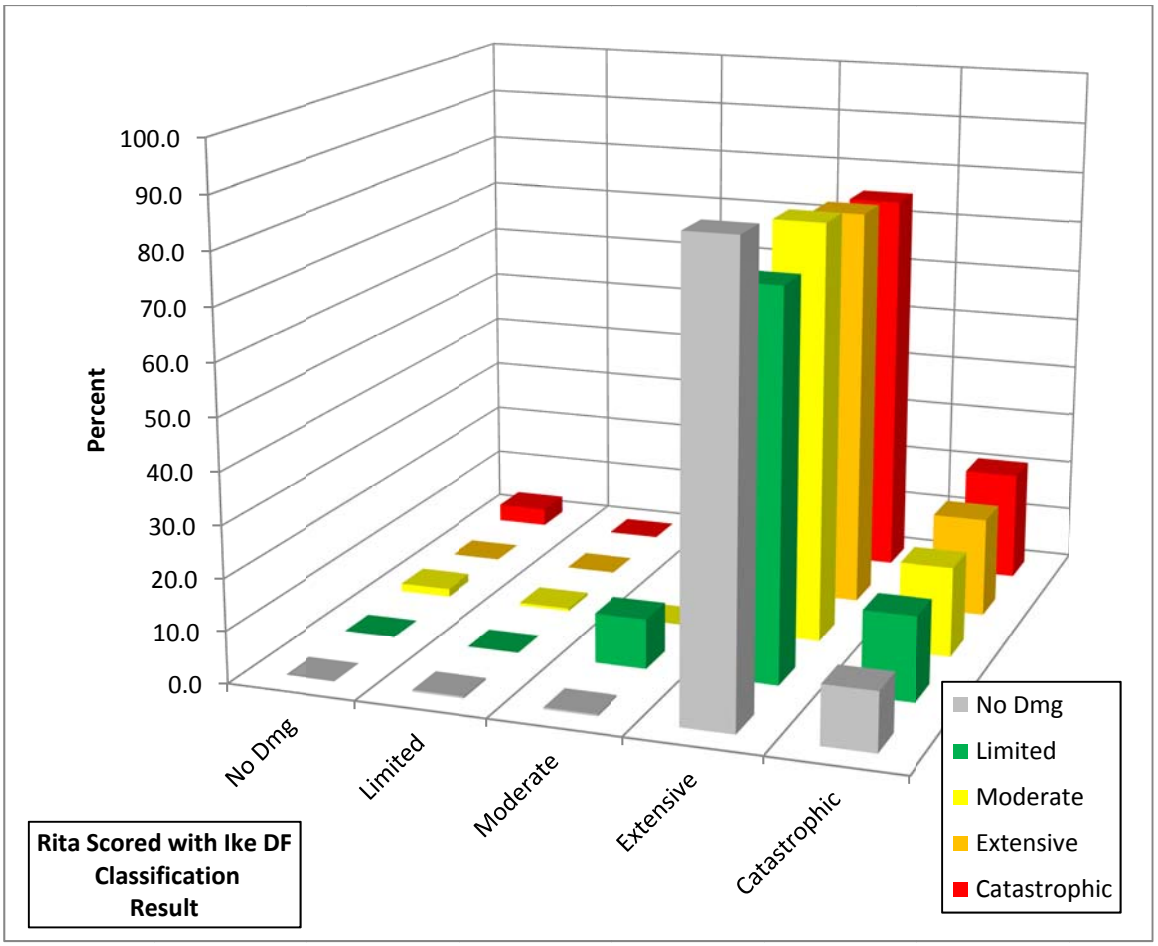

Classification accuracy bar chart of Rita samples scored with Ike discriminant function.

Classification accuracy table of Rita samples scored with Ike discriminant function.

Rita Scored with Ike DF - 17.2 percent correct classification

Count	**No Dmg**	**Limited**	**Moderate**	**Extensive**	**Catastrophic**	**Total**
No Dmg	0	1	1	251	32	285
Limited	0	0	23	178	39	240
Moderate	3	1	0	153	33	190
Extensive	0	0	6	137	34	177
Catastrophic	14	0	1	305	86	406

Percent	No Dmg	Limited	Moderate	Extensive	Catastrophic	Total
No Dmg	0.0	0.4	0.4	88.1	11.2	100
Limited	0.0	0.0	9.6	74.2	16.3	100
Moderate	1.6	0.5	0.0	80.5	17.4	100
Extensive	0.0	0.0	3.4	77.4	19.2	100
Catastrophic	3.4	0.0	0.2	75.1	21.2	100

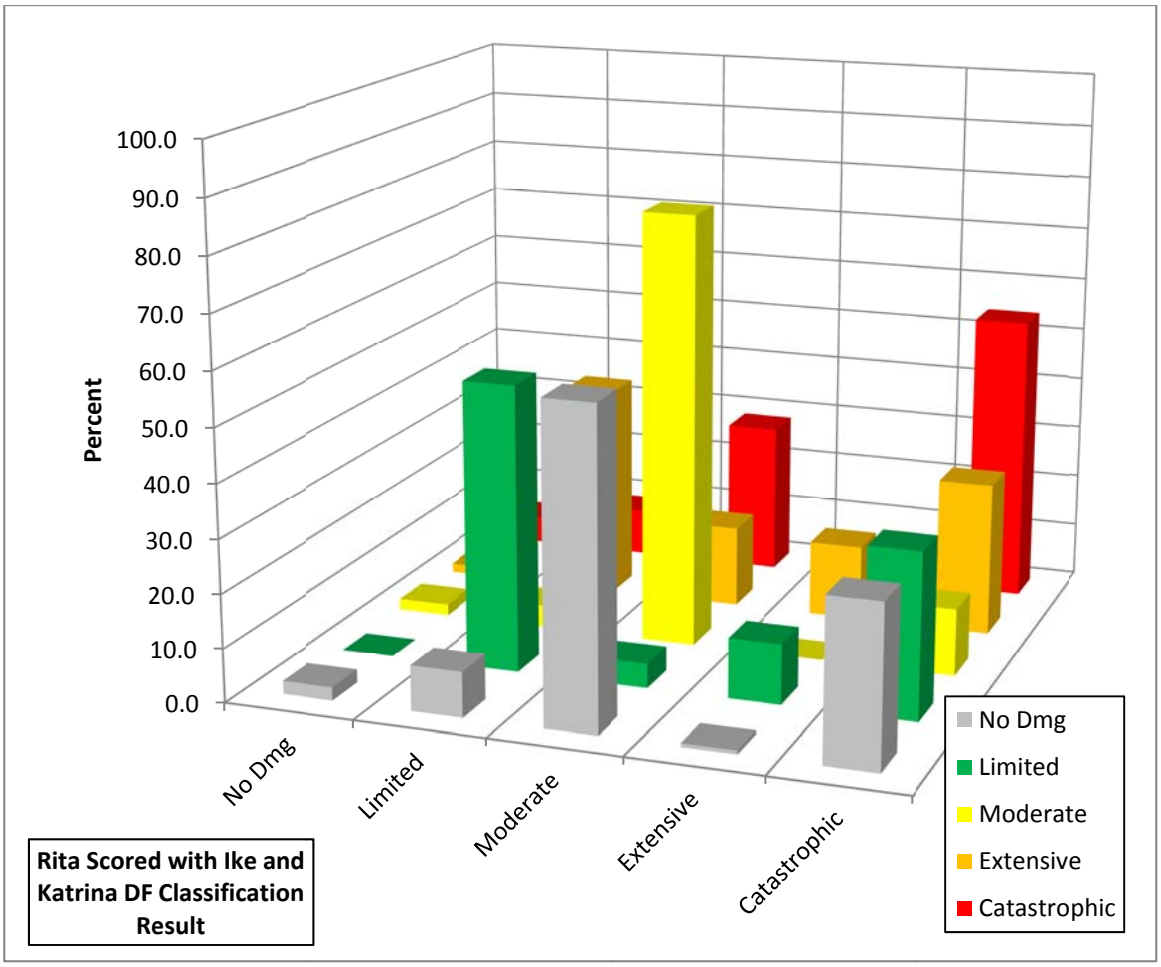

Classification accuracy bar chart of Rita samples scored with Ike-Katrina discriminant function.

Classification accuracy table of Rita samples scored with Ike-Katrina discriminant function.

Rita Scored with Ike and Katrina DF - 41.4 percent correct classification

Count	**No Dmg**	**Limited**	**Moderate**	**Extensive**	**Catastrophic**	**Total**
No Dmg	7	24	167	2	85	285
Limited	0	128	11	27	74	240
Moderate	4	8	154	0	24	190
Extensive	3	71	27	25	51	177
Catastrophic	21	36	116	13	220	406

Percent	No Dmg	Limited	Moderate	Extensive	Catastrophic	Total
No Dmg	2.5	8.4	58.6	0.7	29.8	100
Limited	0.0	53.3	4.6	11.3	30.8	100
Moderate	2.1	4.2	81.1	0.0	12.6	100
Extensive	1.7	40.1	15.3	14.1	28.8	100
Catastrophic	5.2	8.9	28.6	3.2	54.2	100

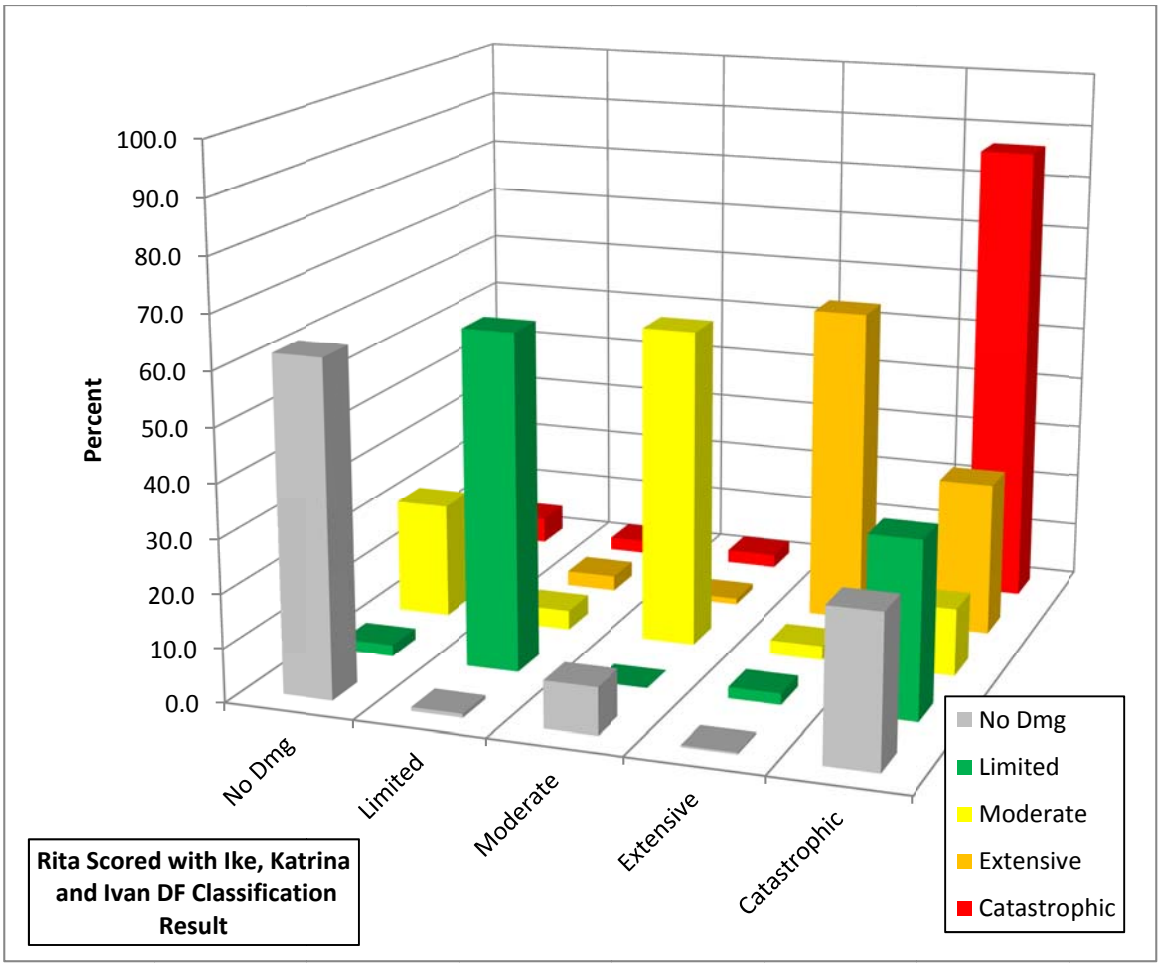

Classification accuracy bar chart of Rita samples scored with Ike-Katrina-Ivan discriminant function.

Classification accuracy table of Rita samples scored with Ike-Katrina-Ivan discriminant function.

Rita Scored with Ike, Katrina and Ivan DF - 69.3 percent correct classification

Count	**No Dmg**	**Limited**	**Moderate**	**Extensive**	**Catastrophic**	**Total**
No Dmg	177	2	25	1	80	285
Limited	5	151	0	5	79	240
Moderate	41	7	113	5	24	190
Extensive	14	5	2	105	51	177
Catastrophic	20	10	10	13	353	406

Percent	No Dmg	Limited	Moderate	Extensive	Catastrophic	Total
No Dmg	62.1	0.7	8.8	0.4	28.1	100
Limited	2.1	62.9	0.0	2.1	32.9	100
Moderate	21.6	3.7	59.5	2.6	12.6	100
Extensive	7.9	2.8	1.1	59.3	28.8	100
Catastrophic	4.9	2.5	2.5	3.2	86.9	100

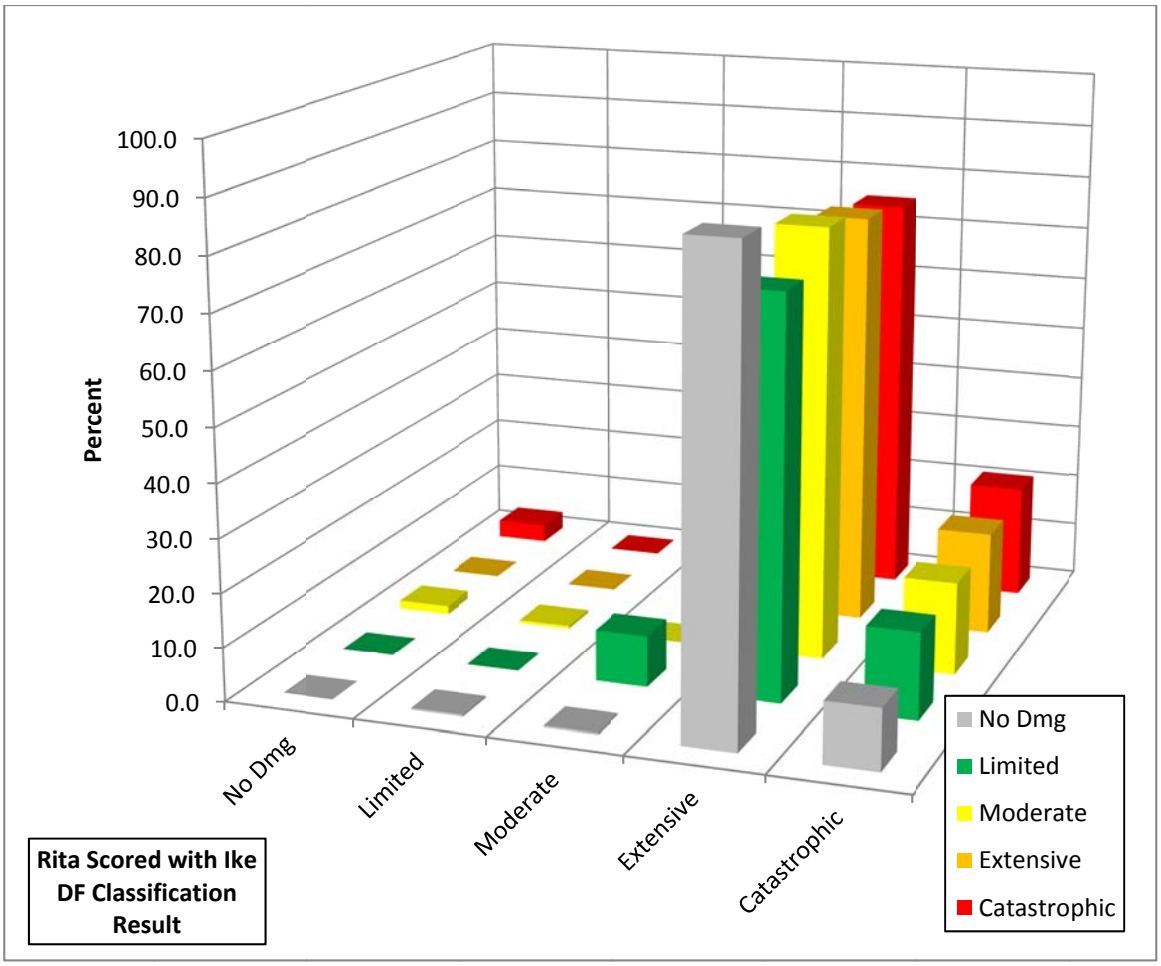

Classification accuracy bar chart of Rita samples with Ike discriminant function.

Classification accuracy table of Rita samples with Ike discriminant function.

Rita Scored with Ike DF - 17.2 percent correct classification

Count	**No Dmg**	**Limited**	**Moderate**	**Extensive**	**Catastrophic**	**Total**
No Dmg	0	1	1	251	32	285
Limited	0	0	23	178	39	240
Moderate	3	1	0	153	33	190
Extensive	0	0	6	137	34	177
Catastrophic	14	0	1	305	86	406

Percent	No Dmg	Limited	Moderate	Extensive	Catastrophic	Total
No Dmg	0.0	0.4	0.4	88.1	11.2	100
Limited	0.0	0.0	9.6	74.2	16.3	100
Moderate	1.6	0.5	0.0	80.5	17.4	100
Extensive	0.0	0.0	3.4	77.4	19.2	100
Catastrophic	3.4	0.0	0.2	75.1	21.2	100

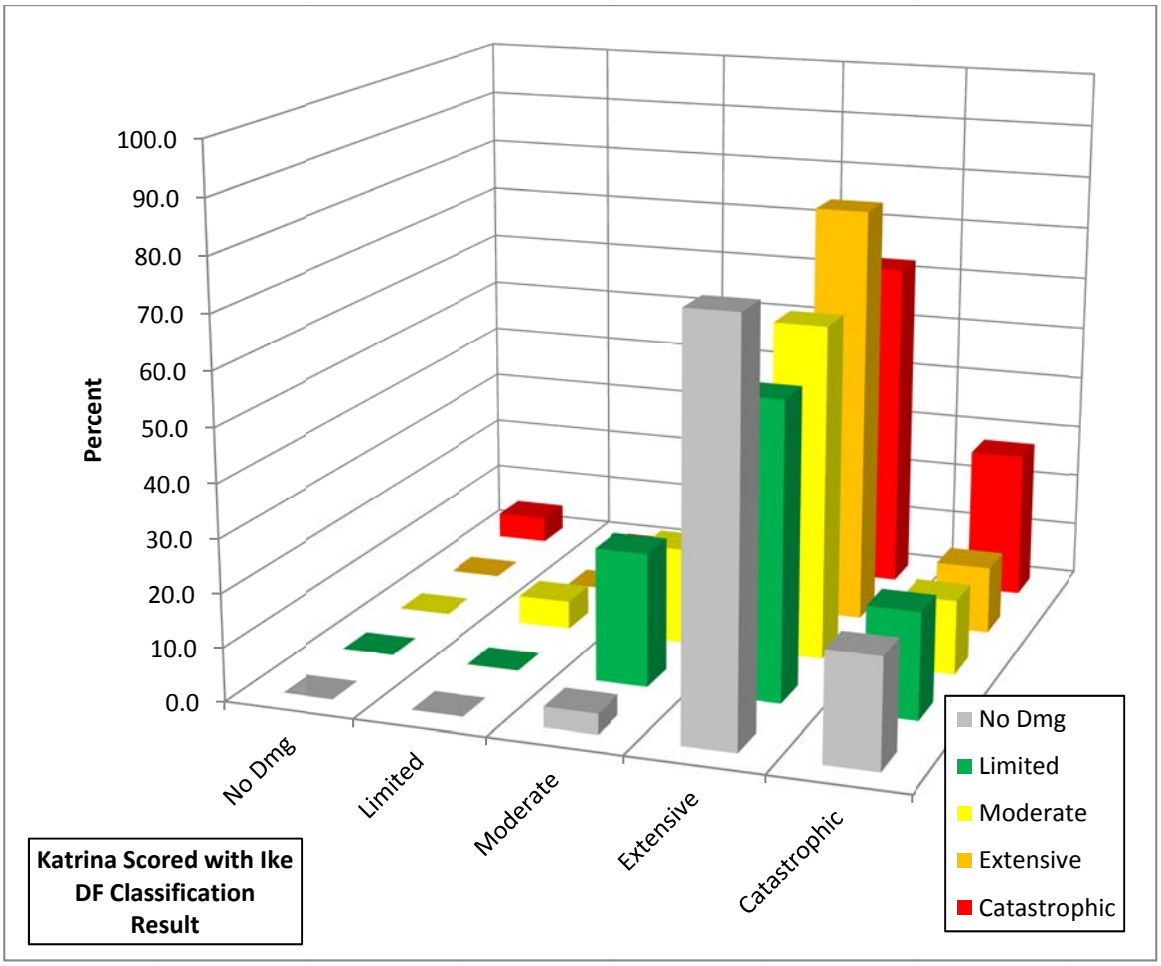

Classification accuracy bar chart of Katrina samples scored with Ike discriminant function.

Classification accuracy table of Katrina samples scored with Ike discriminant function.

Katrina Scored with Ike DF - 25.1 percent correct classification

Count	**No Dmg**	**Limited**	**Moderate**	**Extensive**	**Catastrophic**	**Total**
No Dmg	0	0	3	60	16	79
Limited	0	0	50	111	40	201
Moderate	0	25	85	294	66	470
Extensive	0	0	15	137	22	174
Catastrophic	18	1	16	231	102	368

Percent	No Dmg	Limited	Moderate	Extensive	Catastrophic	Total
No Dmg	0.0	0.0	3.8	75.9	20.3	100
Limited	0.0	0.0	24.9	55.2	19.9	100
Moderate	0.0	5.3	18.1	62.6	14.0	100
Extensive	0.0	0.0	8.6	78.7	12.6	100
Catastrophic	4.9	0.3	4.3	62.8	27.7	100

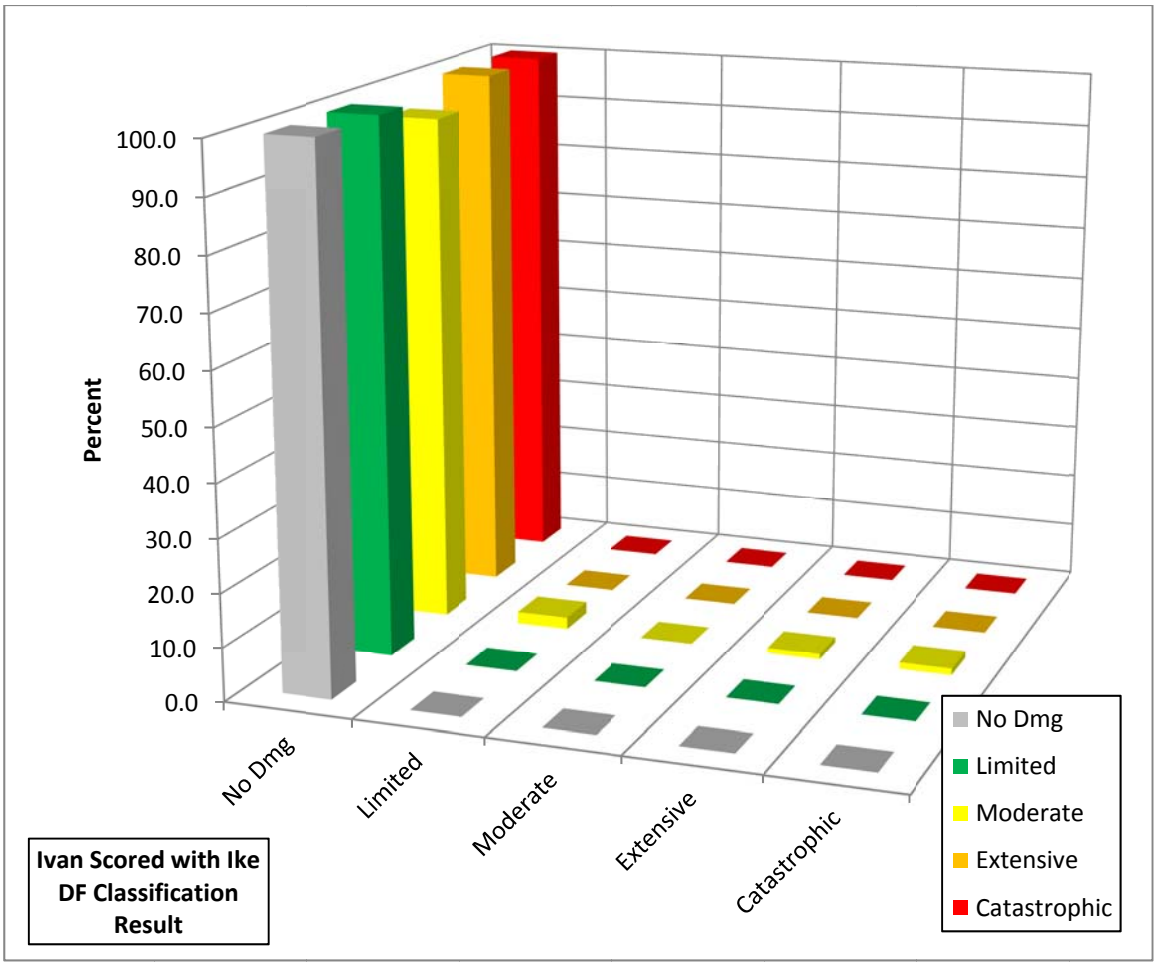

Classification accuracy bar chart of Ivan samples scored with Ike discriminant function.

Classification accuracy table of Ivan samples scored with Ike discriminant function.

Ivan Scored with Ike DF - 10.2 percent correct classification

Count	**No Dmg**	**Limited**	**Moderate**	**Extensive**	**Catastrophic**	**Total**
No Dmg	73	0	0	0	0	73
Limited	150	0	0	0	0	150
Moderate	383	9	0	4	5	401
Extensive	83	0	0	0	0	83
Catastrophic	9	0	0	0	0	9

Percent	No Dmg	Limited	Moderate	Extensive	Catastrophic	Total
No Dmg	100.0	0.0	0.0	0.0	0.0	100
Limited	100.0	0.0	0.0	0.0	0.0	100
Moderate	95.5	2.2	0.0	1.0	1.2	100
Extensive	100.0	0.0	0.0	0.0	0.0	100
Catastrophic	100.0	0.0	0.0	0.0	0.0	100

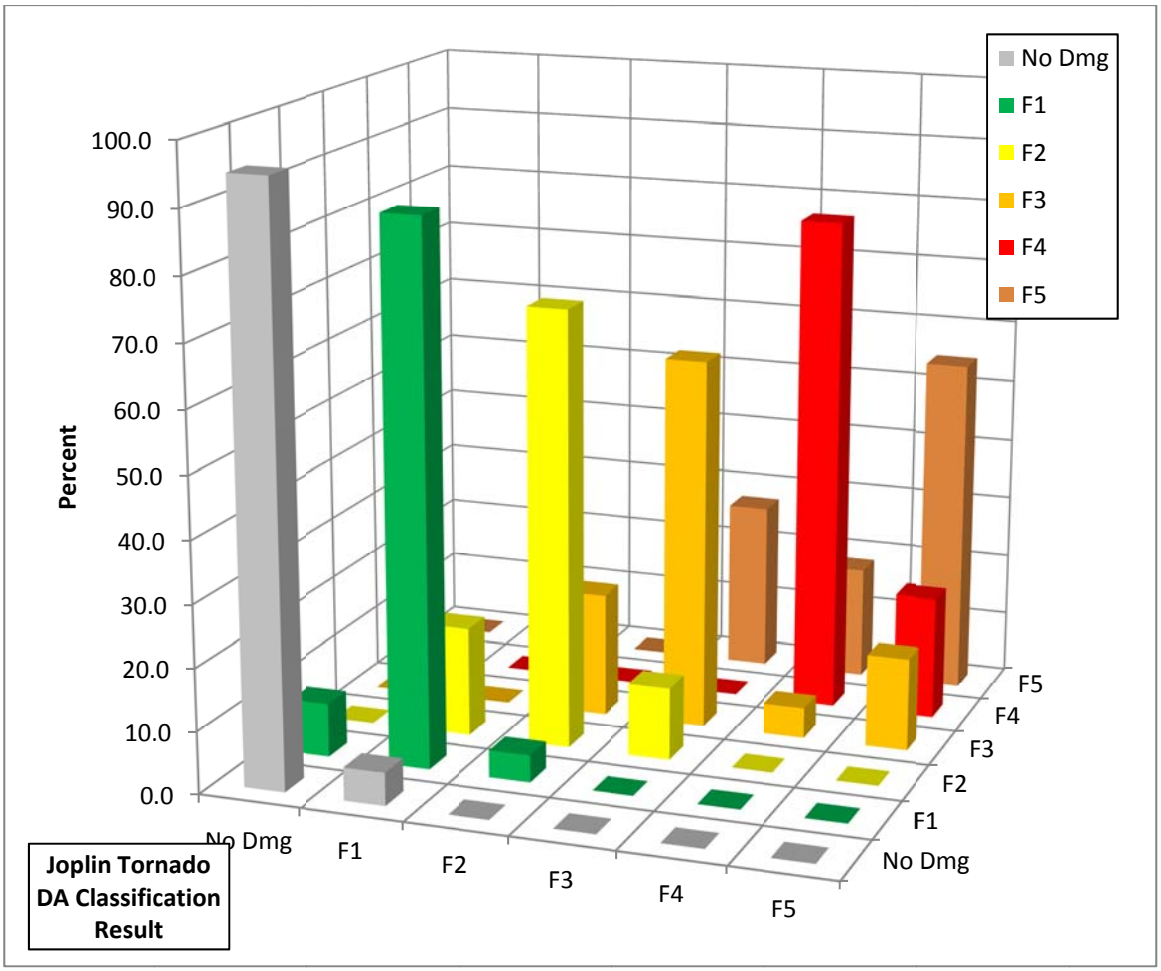

Classification accuracy bar chart of Joplin tornado samples informing discriminant function.

Classification accuracy table of Joplin tornado samples informing discriminant function.

Joplin DA Classification Result - 81.2 percent correct classification

Count	No Dmg	F1	F2	F3	F4	F5	Total
No Dmg	54	3	0	0	0	0	57
F1	2	20	1	0	0	0	23
F2	0	3	12	2	0	0	17
F3	0	0	4	12	1	3	20
F4	0	0	0	0	8	2	10
F5	0	0	0	3	2	6	11

Percent	No Dmg	F1	F2	F3	F4	F5	Total
No Dmg	94.7	5.3	0.0	0.0	0.0	0.0	100
F1	8.7	87.0	4.3	0.0	0.0	0.0	100
F2	0.0	17.6	70.6	11.8	0.0	0.0	100
F3	0.0	0.0	20.0	60.0	5.0	15.0	100
F4	0.0	0.0	0.0	0.0	80.0	20.0	100
F5	0.0	0.0	0.0	27.3	18.2	54.5	100

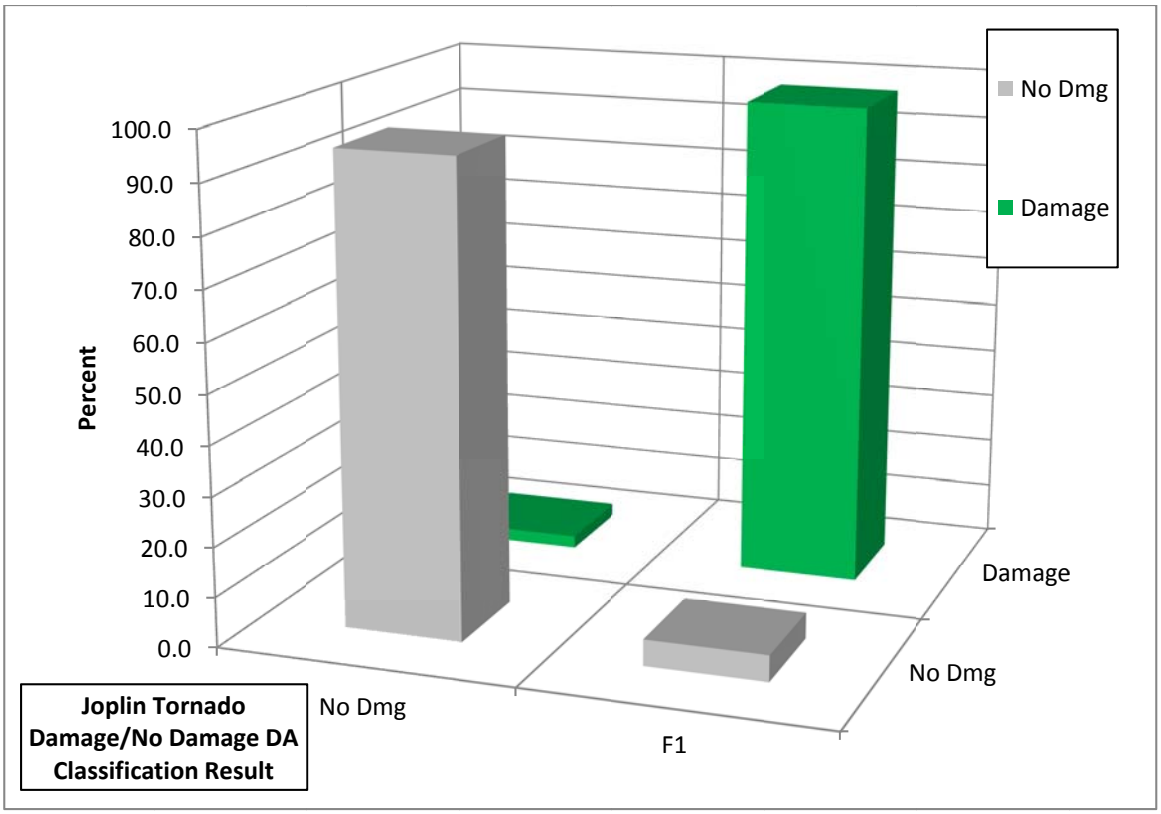

Classification accuracy bar chart of Joplin tornado samples informing discriminant function collapsed to two categories.

Classification accuracy table of Joplin tornado samples informing discriminant function collapsed to two categories.

Joplin DA Classification Result - Collapsed to Damage/No Damage - 81.2 percent correct classification

Count	No Dmg	Damage	Total
No Dmg	54	3	57
Damage	2	79	81

Percent	No Dmg	Damage	Total
No Dmg	94.7	5.3	100
Damage	2.5	97.5	100

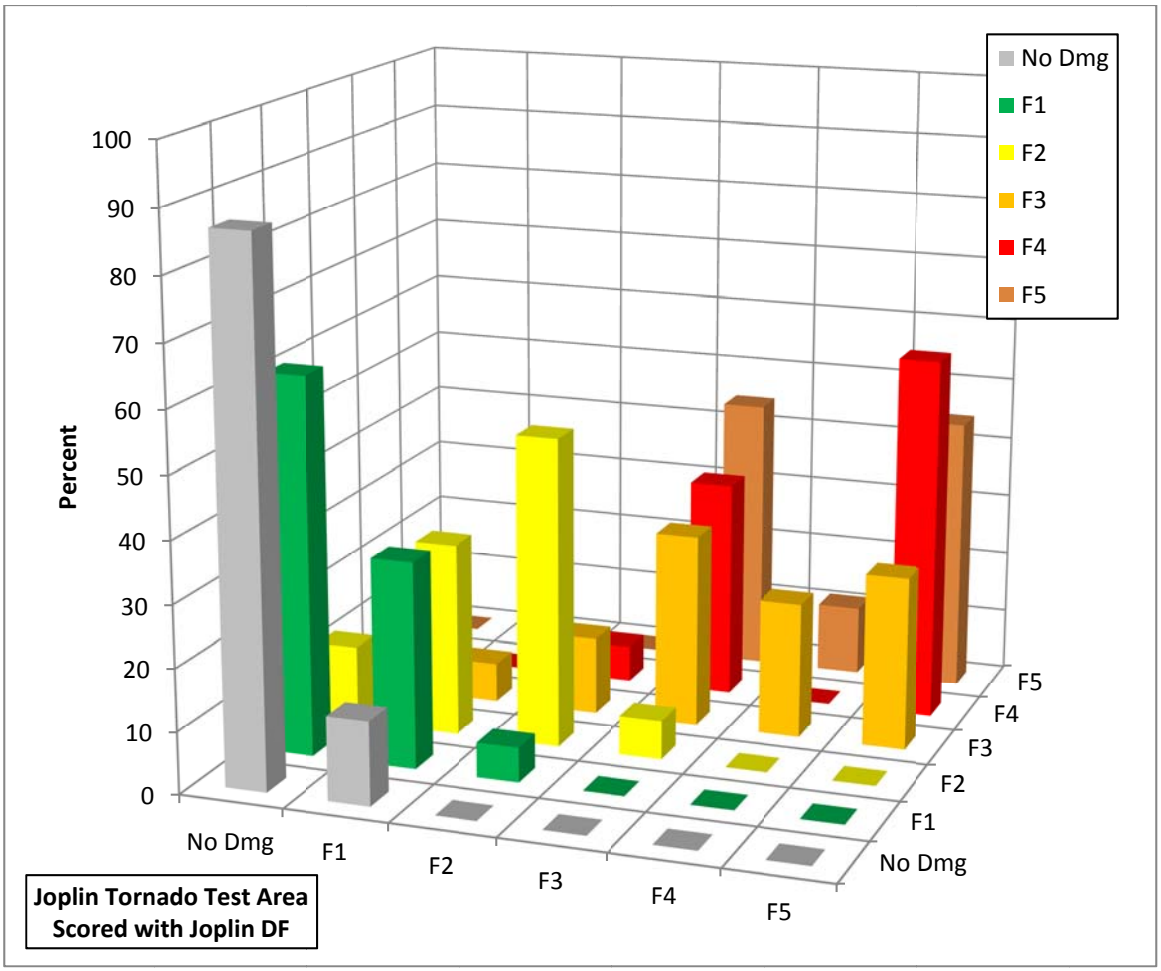

Classification accuracy bar chart of Joplin tornado samples not informing discriminant function scored with Joplin discriminant function.

Classification accuracy table of Joplin tornado samples not informing discriminant function scored with Joplin discriminant function.

Joplin test area scored with Joplin DF Classification Result - 81.2 percent correct classification

Percent	No Dmg	F1	F2	F3	F4	F5	Total
No Dmg	86.5	13.5	0	0	0	0	100
F1	61.1	33.3	5.6	0	0	0	100
F2	12.5	31.2	50	6.3	0	0	100
F3	0	6.3	12.5	31.3	21.9	28	100
F4	0	0	5.9	35.3	0	58.8	100
F5	0	0	0	44.4	11.1	44.5	100

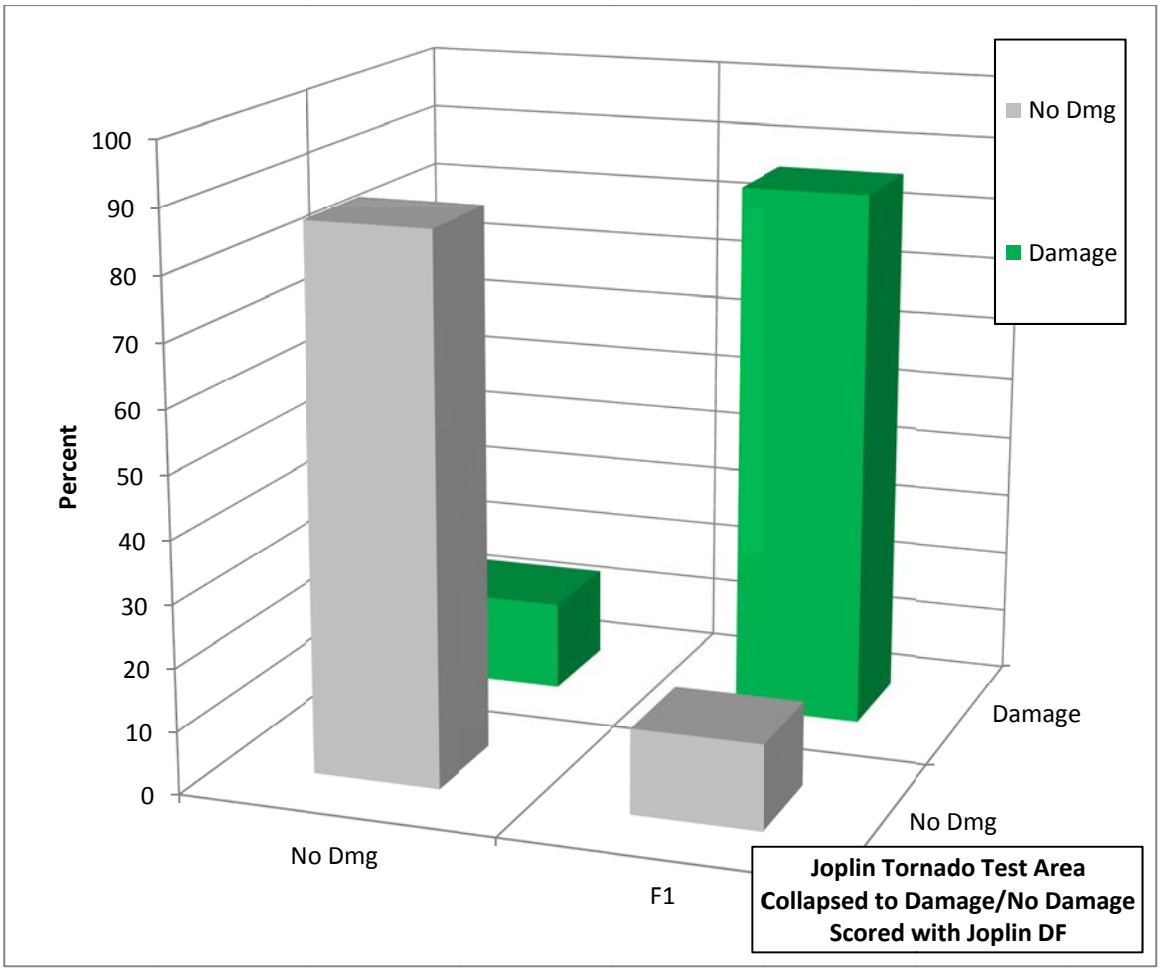

Classification accuracy bar chart of Joplin tornado samples not informing discriminant function scored with Joplin discriminant function collapsed to two categories.

Classification accuracy table of Joplin tornado samples not informing discriminant function scored with Joplin discriminant function collapsed to two categories.

Joplin test area scored with Joplin DF Classification Result Collapsed to Damage/No Damage - 89.9 percent correct classification

Percent	No Dmg	F1	Total
No Dmg	86.5	13.5	100
Damage	14.1	85.9	100

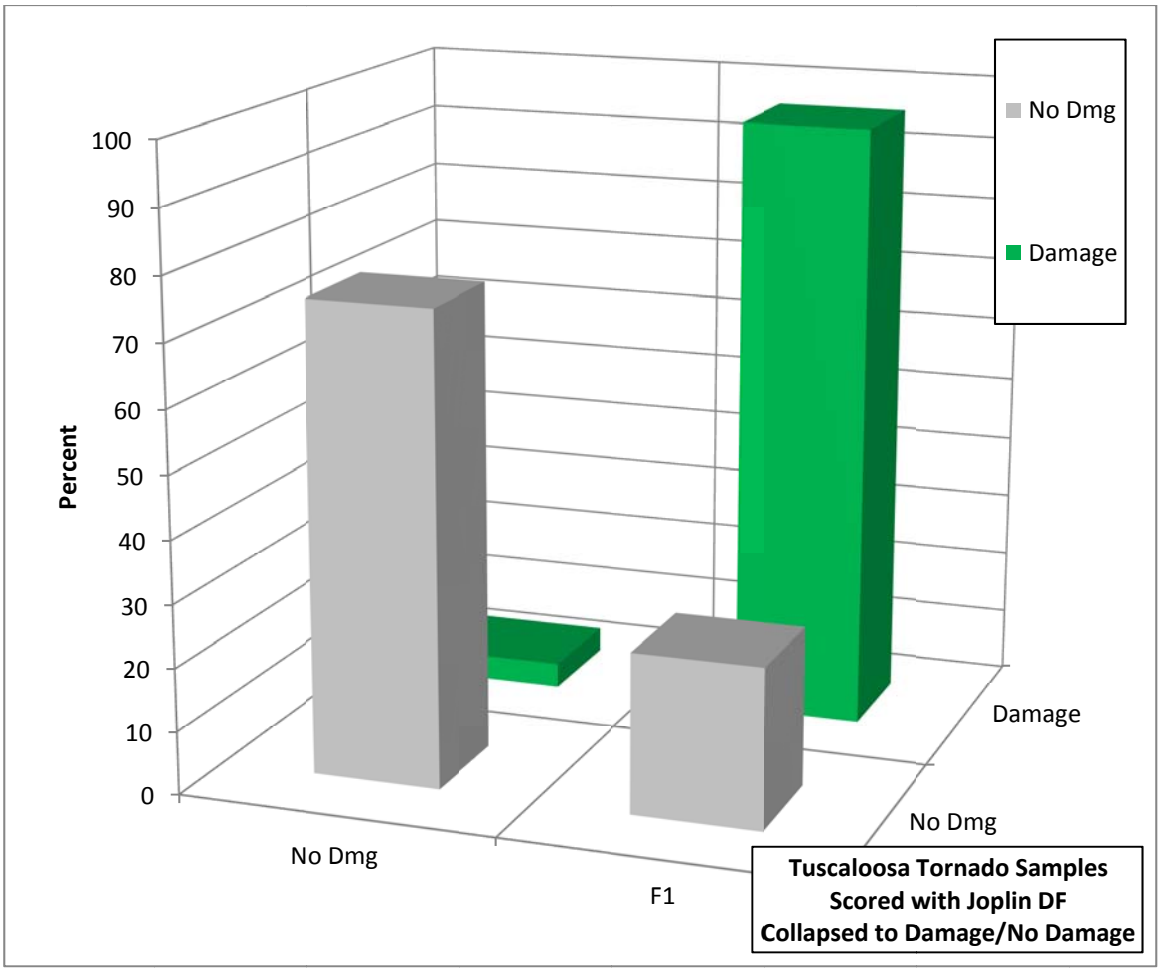

Classification accuracy bar chart of Tuscaloosa tornado samples scored with Joplin discriminant function collapsed to two categories.

Classification accuracy table of Tuscaloosa tornado samples scored with Joplin discriminant function collapsed to two categories.

Tuscaloosa samples scored with Joplin DF Classification Result Collapsed to Damage/No Damage - 85.2 percent correct classification

Percent	No Dmg	F1	Total
No Dmg	74.7	25.3	100
Damage	3.9	96.1	100

REFERENCES

Acharyya, M. and M. K. Kundu. 2001. An Adaptive Approach to Unsupervised Texture Segmentation Using M-band Wavelet Transform. *Signal Processing,* 81**:** 20.

Al-amri, S. S., N. V. Kalyankar and S. D. Khamitkar. 2010. Linear and Non-linear Contrast Enhancement Image. *International Journal of Computer Science and Network Security,* 10**:** 139-143.

Arellano, P. 2003. Missing Information In Remote Sensing: Wavelet Approach To Detect and Remove Clouds and Their Shadows. 76. Enschede, The Netherlands: Interternational Institute for Geo-information Science and Earth Observation.

Arivazhagan, S. and L. Ganesan. 2003a. Texture Classification Using Wavelet Transform. *Pattern Recognition Letters,* 24**:** 9.

---. 2003b. Texture Segmentation Using Wavelet Transform. *Pattern Recognition Letters,* 24**:** 7.

---. 2004. Automatic Target Detection Using Wavelet Transform. *Journal on Applied Signal Processing,* 17**:** 2663-2674.

Aslaksen, M. 2010. National Geodetic Survey Emergency Response Imagery. Silver Spring, MD: NOAA. http://ngs.woc.noaa.gov/eri_page/index.html (last accessed 17 July 2010).

---. 2011a. Joplin, MO Tornado Imagery Viewer. Silver Spring, MD: NOAA. http://ngs.woc.noaa.gov/storms/joplin/ (last accessed 16 December 2011).

---. 2011b. April 2011 Tornado Response Imagery Viewer. Silver Spring, MD: NOAA. http://ngs.woc.noaa.gov/storms/apr11_tornado/ (last accessed 19 December 2011).

Bailey, T. C., T. Sapatinas, K. J. Powell and W. J. Krzanowski. 1998. Signal Detection in Underwater Sound Using Wavelets. *Journal of the American Statistical Association,* 93**:** 11.

Barnett, M. R. 2004. Hurricane Ivan - Beach and Dune Erosion and Structural Damage Assessment and Post-Storm Recovery Plan for the Panhandle Coast of Florida. 64. Tallahassee, Florida: Florida Department of Environmental Protection.

Blackmun, H. A. 1993. William Daubert, et ux., etc., et al., Petitioners v. Merrell Dow Pharmaceuticals, Inc.*,* ed. U. S. S. Court. Washington, D.C.: U.S. Supreme Court.

Boruff, B. J., J. A. Easoz, S. D. Jones, H. R. Landry, J. D. Mitchem and S. L. Cutter. 2003. Tornado Hazards in the United States. *Climate Research,* 24**:** 103-117.

Bruce, L. M., A. Mathur and J. D. Byrd Jr. 2006. Denoising and Wavelet-Based Feature Extraction of MODIS Multi-Temporal Vegetation Signatures. *GIScience & Remote Sensing,* 43**:** 170-180.

Burns, R. B. & R. A. Burns. 2008. *Business Research Methods and Statistics Using SPSS*. Sage Publications Ltd.

Cai, H. 2007. Wavelet Structure Based Transform: Information Extraction and Analysis. In *Department of Electrical and Computer Engineering, College of Engineering*, 180. San Antonio, Texas: University of Texas at San Antonio.

Chen, F. and W. Wang. 2009. Target Recognition in Clutter Scene Based on Wavelet Transform. *Optics Communication,* 282**:** 523-526.

Chen, G. and T. D. Bui. 1999. Invariant Fourier-wavelet Descriptor for Pattern Recognition. *Pattern Recognition,* 32**:** 6.

Chou, J. J., C. P. Chen and J. T. Yeh. 2007. Crop Identification with Wavelet Packet Analysis and Weighted Bayesian Distance. *Computers and Electronics in Agriculture,* 57**:** 88-98.

Clarke, K. C., I. F. Cruz, R. P. Denaro, S. Elhami, D. R. Fletcher, J. Geringer, J. R. Jensen, N. S.-N. Lam, M. L. Larsgaard, D. R. Maidment, R. B. McMaster, S. Shekhar, N. Tosta and E. Trobia. 2007. *Successful Response Starts with a Map: Improving Geospatial Support for Disaster Management*. Washington, D.C.: National Academies Press.

Congalton, R. G. 1991. A Review of Assessing the Accuracy of Classifications of Remotely Sensed Data. *Remote Sensing of the Environment,* 37**:** 35-46.

Congalton, R. G. and K. Green. 2009. *Assessing the Accuracy of remotely Sensed Data - Principles and Practices*. Boca Raton, Florida: CRC Press, Taylor and Francis Group.

Croisier, A., D. Esteban and C. Galand. 1977. Perfect Channel Splitting by Use of Interpolation, Decimation, Tree Decomposition Techniques. In *First International Conference on Information Sciences and Systems,* eds. D. G. Lainiotis and N. S. Tzannes, 443-446. University of Patras, Patras: Hemisphere Publishing Corporation, Washington, D.C.-London.

Curran, P. J. 2001. Remote Sensing: Using the Spatial Domain. *Environmental and Ecological Statistics,* 8**:** 14.

Dale, M. R. T. and M. Mah. 1998. The Use of Wavelets for Spatial Pattern Analysis in Ecology. *Journal of Vegetation Science,* 9**:** 805-814.

Daubechies, I. 1992. *Ten Lectures on Wavelets*. Philadelphia, Pennsylvania: Society for Industrial and Applied Mathematics.

DeBlasio, S., Stephen M. 2008. Hurricane Ike Impact Report - December 2008. 64. Federal Emergency Management Agency.

Dunlop, J. D., G. H. Holder and E. F. LeDrew. 1989. Image Matching Using Spatial Frequency Signatures. In *Geoscience and Remote Sensing Symposium, 1989. IGARSS'89. 12th Canadian Symposium on Remote Sensing*, 1273-1276. Vancouver, B.C.: IEEE International Geoscience & Remote Sensing Symposium.

Elsayed, M. A. K. 2007. The Use of Wavelet Analysis in Detecting Dispersion and Groupings of Waves during a Mistral Event. *Journal of Coastal Research,* 23**:** 417-420.

Falkowski, M. J., A. M. S. Smith, A. T. Hudak, P. E. Gessler, L. A. Vlerling and N. L. Crookston. 2006. Automated estimation of individual conifer tree height and crown diameter via two-dimensional spatial wavelet analysis of lidar data. *Canadian Journal of Remote Sensing,* 32**:** 153-161.

Fourier, J. B. J. 1878. *The Analytical Theory of Heat, Translated with Notes by Alexander Freeman*. London: University Press.

Franklin, J. 2011. National Weather Service National Hurricane Center GIS Data and Products. Miami, FL: NOAA. http://www.nhc.noaa.gov/gis/ (last accessed 11 August 2011).

Gabe, T., G. Falk, M. McCarty and V. W. Mason. 2005. Hurricane Katrina: Social-Demographic Characteristics of Impacted Areas. 1-35. Washington, DC: Congressional Research Service.

Gabor, D. 1946. Theory of Communication. *Journal of the Institute of Electrical Engineers,* 93**:** 429-457.

Ghazvini, M., S. A. Monadjemi, N. Movahhedinia and K. Jamshidi. 2009. Defect Detection of Tiles Using 2D-Wavelet Transform and Statistical Features. *World Academy of Science, Engineering and Technology,* 49.

He, L. X. 1996. Pattern Recognition and Image Processing of Infrared Astronomical Satellite Images. In *Electrical and Computer Engineering*, 201. Ames, Iowa: Iowa State University.

Hodgson, M. E. 1998. What Size Window for Image Classification? A Cognitive Perspective. *Photogrammetric Engineering & Remote Sensing,* 64**:** 797-807.

Hong, G. and Y. Zhang. 2004. The Effects of Different Types fo Wavelets on Image Fusion. *International Archives of Photogrammetry and Remote Sensing,* 35**:** 915-920.

Huang, J. and H. Wechsler. 1999. Eye Detection Using Optimal Wavelet Packets and Radial Basis Functions (RBFs). *International Journal of Pattern Recognition and Artificial Intelligence,* 13.

Hubbard, B. B. 1998. *The World According to Wavelets: The Story of a Mathematical Technique in the Making*. Natick, MA: A K Peters, Ltd.

Jensen, J. R. 1986. *Introductory Digital Image Processing: A Remote Sensing Perspective*. Englewood Cliffs, New Jersey: Prentice-Hall.

Keitt, T. H. and J. Fischer. 2006. Detection of Scale-Specific Community Dynamics Using Wavelets. *Ecology,* 87**:** 2895-2904.

Keitt, T. H. and D. L. Urban. 2005. Scale-Specific Inference Using Wavelets. *Ecology,* 86**:** 2497-2504.

Kim, S. C. and T. J. Kang. 2007. Texture Classification and Segmentation Using Wavelet Packet Frame and Gaussian Mixture Model. *Pattern Recognition,* 40**:** 15.

Knabb, R. D., D. P. Brown and J. R. Rhome. 2006. Tropical Cyclone Report - Hurricane Rita. 33. Washington, D.C.: National Hurricane Center.

Knabb, R. D., J. R. Rhome and D. P. Brown. 2005, Updated 2006. Tropical Cyclone Report, Hurricane Katrina 23-30 August 2005. Washington, D.C.: National Hurricane Center.

Kurth, M. M. and D. V. Burckel. 2006. The Rita Report: A Summary of the Social and Economic Impact and Recovery of Southwest Louisiana One Year After Hurricane Rita. 58. New Orleans, Louisiana: Louisiana Recovery Authority.

Li, J. 2004. Wavelet-Based Feature Extraction for Improved Endmember Abundance Estimation in Linear Unmixing of Hyperspectral Signals. *IEEE Transactions on Geoscience and Remote Sensing,* 42**:** 644-649.

Mallat, S. G. 1989. A Theory for Multiresolution Signal Decomposition: The Wavelet Representation. *IEEE Transactions on Pattern Analysis and Machine Intelligence,* 11**:** 674-693.

Marcelja, S. 1980. Mathematical Description of the Responses of Simple Cortical Cells. *Journal of the Optical Society of American,* 70**:** 1297-1300.

Maximuk, L. P. 2011. NWS Central Region Service Assessment Joplin Missouri Tornado May 22 2011. 40. Kansas City, MO: National Weather Service Central Region Service Assessment.

Mi, X., H. Ren, Z. Ouyang, W. Wei and K. Ma. 2005. The Use of the Mexican Hat and the Morlet Wavelets for Detection of Ecological Patterns. *Plant Ecology,* 179**:** 1-19.

Misiti, M., Y. Misiti, G. Oppenheim and J.-M. Poggi. 2011. *Wavelet Toolbox 4 User's Guide*. Mathworks.

Myint, S. W. 2001. Wavelet Analysis and Classification of Urban Environment Using High-Resolution Multispectral Image Data. In *The Department of Geography and Anthropology*, 351. Baton Rouge, Louisiana: Louisiana State University and Agricultural and Mechanical College.

---. 2003. Fractal Approaches in Texture Analysis and Classification of Remotely Sensed Data: Comparisons with Spatial Autocorrelation Techniques and Simple Descriptive Statistics. *International Journal of Remote Sensing,* 24**:** 1925-1947.

---. 2006. A New Framework for Effective Urban Land Use and Land Cover Classification: A Wavelet Approach. *GIScience & Remote Sensing,* 43**:** 155-178.

---. 2010. Multi-Reolution Decomposition in Relation to Characteristic Scales and Local Window Sizes Using an Operational Wavelet Algorithm. *International Journal of Remote Sensing,* 31**:** 2551-2572.

Myint, S. W., N. S.-N. Lam and J. Tyler. 2002. An Evaluation of Four Different Wavelet Decomposition Procedures for Spatial Feature Discrimination in Urban Areas. *Transactions in GIS,* 6**:** 403-429.

Myint, S. W., N. S.-N. Lam and J. M. Tyler. 2004. Wavelets for Urban Spatial Feature Discrimination: Comparisons with Fractal, Spatial Autocorrelation, and Spatial Co-Occurrence Approaches. *Photogrammetric Engineering & Remote Sensing,* 70**:** 10.

Myint, S. W. and V. Mesev. 2012. A Comparative Analylsis of Spatial Indices and Wavelet-based Classification. *Remote Sensing Letters,* 3**:** 141-150.

Osicka, T. 2008. Wavelet-based Pulmonary Nodules Features Characterization on Computed Tomography (CT) Scans. In *Department of Electrical Engineering & Computer Science, School of Engineering*, 307. District of Columbia: The Catholic University of America.

Pajares, G. and J. M. de la Cruz. 2004. A Wavelet-based Image Fusion Tutorial. *Pattern Recognition,* 37**:** 1855-1872.

Pielke, J., Roger A. 2009. United States Hurricane Landfalls and Damages: Can One-to-Five-Year Predictions Beat Climatology? *Environmental Hazards,* 8**:** 187-200.

Pielke, J., Roger A., J. Gratz, C. W. Landsea, D. Collins, M. A. Saunders and R. Musulin. 2008. Normalized Hurricane Damage in the United States: 1900-2005. *Natural Hazards Review,* 9**:** 29-42.

Pokhriyal, A. and S. Lehri. 2010. A New Method of Fingerprint Authentication Using 2D Wavelets. *Journal of Theoretical and Applied Information Technology,* 13**:** 131-138.

Pouncey, R., K. Swanson and K. Hart. 1999. *ERDAS Field Guide: Fifth Edition, Revised and Expanded*. ERDAS, Inc.

Proenza, B. 2011a. Joplin Tornado Event Summary. Joplin Tornado Event Summary - May 22, 2011. Springfield, MO: National Weather Service Weather Forecast Office.

---. 2011b. Tuscaloosa-Birmingham EF-4 Tornado April 27, 2011. Description of April 27, 2011 Tuscaloosa-Birmingham EF-4 Tornado. Birmingham, AL: National Weather Service Weather Forecast Office.

Ramsdell Jr., J. V., J. P. Rishel and A. J. Buslik. 2007. Tornado Climatology of the Contiguous United States. ed. U. S. N. R. Commission, 246. Washington, D.C.: U.S. Nuclear Regulatory Commission.

Rao, R. M. and A. S. Bopardikar. 1998. *Wavelet Transforms: Introduction to Theory and Applications*. Delhi, India: Pearson Education.

Richard, B. 2005. Initial Estimate of the Impacts of Hurricane Katrina. 12. Hattiesburg, MS: University of Southern Mississippi.

Richards, J. A. and X. Jia. 2006. *Remote Sensing Digital Image Analysis: An Introduction*. Berlin, Germany: Springer.

Ruiz, L. A., A. Fdez-Sarria and J. A. Recio. 2004. Texture Feature Extraction for Classification of Remote Sensing Data Using Wavelet Decomposition: A Comparative Study. In *ISPRS XXth Congress, Commission 4*. Istanbul, Turkey: ISPRS.

Smith, C., N. Pyden and P. Cole. 1995. ERDAS Field Guide. 628. Atlanta, Georgia: ERDAS, Inc.

Strand, E. K., A. M. S. Smith, S. C. Bunting, L. A. Vierling, D. B. Hann and P. E. Gessler. 2006. Wavelet Estimation of Plant Spatial Patterns In Multitemporal Aerial Photography. *International Journal of Remote Sensing,* 27**:** 2049-2054.

Tang, X. and W. K. Stewart. 2000. Optical and Sonar Image Classification: Wavelet Packet Transform vs Fourier Transform. *Computer Vision and Image Understanding,* 79**:** 25-46.

Tello, M., C. Lopez-Martinex and J. J. Mallorqui. 2005. A Novel Algorithm for Ship Detection in SAR Imagery Based on the Wavelet Transform. *IEEE Geoscience and Remote Sensing Letters,* 2**:** 201-205.

Townshend, J. R. G. 1981. Terrain Analysis and Remote Sensing. London: George Allen and Unwin.

Ulfarsson, M. O., J. A. Benediktsson and J. R. Sveinsson. 2003. Data Fusion and Feature Extraction in the Wavelet Domain. *International Journal of Remote Sensing,* 24**:** 3933-3945.

Verbeke, L. P. C., F. M. B. Van Coillie and R. R. De Wulf. 2006. Object Based Forest Stand Density Estimation from Very High Resolution Optical Imagery Using Wavelet Based Texture Measures. 6. Ghent, Belgium: Laboratory of Forest Management and Spatial Information Techniques, Ghent University.

Wang, L. and J. Liu. 1999. Texture Classification Using Multiresolution Markov Random Field Models. *Pattern Recognition Letters,* 20**:** 12.

Watson, G. H. 1999. Introduction to Wavelet Analysis. In *Application of Mathematical Signal Processing Techniques to Mission Systems*, 12. Koln, Germany: RTO EN-7.

Zhou, G. 2006. Detecting the Socioeconomic Conditions of Urban Neighborhoods Through Wavelet Analysis of Remotely Sensed Imagery. In *The Department of Geography and Anthropology*, 171. Baton Rouge, Louisiana: Louisiana State University and Agricultural & Mechanical College.

Zhu, C. and X. Yang. 1998. Study of Remote Sensing Image Texture Analysis and Classification Using Wavelet. *International Journal of Remote Sensing,* 19**:** 3197-3203.

Zweig, G., R. Lipes and J. R. Pierce. 1976. The Cochlear Compromise. *Journal of Acoustical Society of America,* 59**:** 975-982.